Preprint

NASA TECHNICAL MEMORANDUM

NASA TM X-62,307

NASA TM X-62,307

(NASA-TM-X-62307) WIND SENSITIVITY STUDIES OF A NON-RETURN WIND TUNNEL WITH A 216- BY 432-mm (8 5- BY 17 0-INCHES) TEST SECTION, PHASE 2 (NASA) 123 p HC $8 25

N74-13949

CSCL 14B G3/11

Unclas 25721

WIND SENSITIVITY STUDIES OF A NON-RETURN WIND TUNNEL WITH A 216- BY 432-MM (8.5- BY 17.0-IN) TEST SECTION – PHASE II

William T. Eckert, Kenneth W. Mort, and J. E. Piazza

Ames Research Center
and
U.S. Army Air Mobility Research & Development Laboratory
Moffett Field, California 94035

August 1973

NOTATION

B	semiwidth of model test section, mm
C	center direction probe
C_P,CP	test-section local pressure coefficient, $\frac{P_{T_o} \text{ or } P_{S_o} - P_{S_w}}{Q_o}$
H	semiheight of model test section, mm
L,ℓ	length of flow-straightener cell
P	port direction probe
P_{S_o}	test-section local static pressure, mm of water
P_{S_w}	wind static pressure, mm of water
P_{T_o}	test-section local total pressure, mm of water
P_{T_w}	wind total pressure, mm of water
Q_o,QO	test-section dynamic pressure, (average P_{T_o}) - (average P_{S_o}), mm of water
Q_w,QW	wind dynamic pressure, $P_{T_w} - P_{S_w}$, mm of water
R	radius
S	starboard direction probe
V	test-section velocity, knots
V_w	wind velocity, knots
W	width of flow-straightener cell
Y	horizontal distance from test-section centerline (positive starboard), mm
Z	vertical distance from test-section centerline (positive up), mm
ΔP	total tunnel pressure loss, average static pressure rise across the fans; increment from no-wind condition, mm of water

ΔP_I inlet pressure loss, (P_{S_w}) - (average P_{T_o}); mm of water

$\frac{\Delta Q}{Q_o}$ maximum difference in local test-section dynamic pressure over 75% of B and H;

$$\left[\left(C_{P_{total}} - C_{P_{static}}\right)_{\substack{\text{local maximum} \\ Q_w \neq 0}} - \left(C_{P_{total}} - C_{P_{static}}\right)_{Q_w = 0}\right]$$

$\frac{\Delta Q_*}{Q_o}$ maximum test-section local dynamic pressure variation, increment from the no-wind condition;

$$\left(\frac{\Delta Q}{Q_o}\right)_{Q_w \neq 0} - \left(\frac{\Delta Q}{Q_o}\right)_{Q_w = 0}$$

Δu maximum deviation from the mean axial velocity over 75% of the width on the horizontal centerline and of the height on the vertical centerline of the test section; increment from no-wind condition,

$\frac{V}{2} \frac{\Delta Q_*}{Q_o}$, knots

Δv maximum lateral velocity deviation on the centerline; increment from the no-wind condition (positive to the starboard),

$V \frac{\theta_s}{57.3}$, knots

Δw maximum vertical velocity deviation on the centerline; increment from the no-wind condition (positive up),

$V \frac{\theta_u}{57.3}$, knots

θ_s test-section sideflow angle; increment from the no-wind condition (positive for air from port), deg

θ_u test-section upflow angle; increment from the no-wind condition, deg

ψ azimuth angle of model centerline with respect to wind axis; (positive for wind from port), deg

WIND-SENSITIVITY STUDIES OF A NON-RETURN WIND TUNNEL WITH A 216- BY 432-MM (8.5- BY 17.0-IN) TEST SECTION - PHASE II

William T. Eckert, Kenneth W. Mort, and J. E. Piazza

Ames Research Center

and

U.S. Army Air Mobility and Research & Development Laboratory

SUMMARY

The purpose of this study was to refine inlet and exit treatments which would minimize the effect of external wind on the test-section flow quality of a non-return wind tunnel. The investigation was conducted in the Ames Research Center 40- by 80-Foot Wind Tunnel which served as the wind source. Several inlets and two exits were tested at wind directions ranging from 0 to 180 degrees and at wind-to-test-section velocity ratios from zero to somewhat greater than one.

For the best inlet configuration the flow quality was good, with a velocity deviation in each of the three component directions generally less than 0.26m/sec (1/2 knot) for wind velocities of 7.7 m/sec (15 knots) or less. The loss in total pressure due to the inlet treatment was low: about 0.035 of the test-section dynamic pressure for the no-wind case.

INTRODUCTION

The NASA has been investigating the usefulness and practicability of a new full-scale V/STOL wind tunnel. During these studies the feasibility of using a non-return wind tunnel configuration was established.

There are two advantages that a non-return wind tunnel has over a closed-circuit tunnel: (1) no purging of contaminants such as

engine exhaust gases and heated tunnel air is required; and (2) the structural cost is potentially less.

Non-return tunnels can be made to have good power efficiency (ref. 1). However, because of the open ends, the flow quality may be adversely affected by external winds. It has been generally found that although shielding can be used at the ends to significantly reduce the effects of winds, this treatment caused large losses in power (refs. 2 through 4).

The first phase of the current study (ref. 5) was begun in an attempt to develop effective wind shielding with an emphasis on minimizing the power losses. The efforts of this, the second phase, were directed at refinement of the wind treatment for two selected inlets in order to further improve the test section flow quality.

The authors wish to acknowledge the valuable assistance of Mrs. Margaret Campbell in the development and preparation of the data presentation formats.

MODEL DESCRIPTION

General

The model installed in the Ames 40- by 80-Foot Wind Tunnel is shown in figure 1, and dimensions and geometry are given in figures 2 and 3 and in table I.

The basic inlet protection consisted of an area with a flat-oval planform enclosed by a peripheral screen of perforated plate (figures 3(a) and 3(b)), flow straighteners inside at the front part of the screen (figures 3(a) and 3(c) top), a solid roof with streamlined vertical posts (figures 3(a) and 3(c)), and an additional flow straightener grating (figure 3(a) and 3(d)) at the entrance to a large area-ratio contraction cone (figure 3(e)). Two inlet screen sizes (figure 3(c)) were studied along with alternate contraction flow straighteners (listed on figure 3(d)).

The basic, area-ratio 20 vertical-exhaust exit is shown at the top of figure 4. An alternate area-ratio 8 vertical-exhaust section (identical to the basic exit of reference 5) is shown at the bottom of figure 4.

Instrumentation

The vertical and transverse locations of the total and static pressure probes and the direction rake in the test section are shown in figure 5. The pressure probes were located in a plane 63.5 mm (2.5 in), or 14.7 percent of the test-section length, downstream of the test-section entrance. The static pressure rise across the fans was measured by orifices located 0.3 fan diameters ahead of and behind the fan in each nacelle.

TEST PROCEDURE

The test program was conducted with the model elevated from the 40- by 80-Foot Wind Tunnel test-section floor (out of the boundary layer) on legs as shown in figure 1(b). The centerline of the model was set at selected azimuth angles, measured from the wind axis, to simulate various wind directions.

The model test-section dynamic pressure was set initially at about 254 mm (ten inches) of water with the external wind at zero dynamic pressure. The subsequent measurements were made with the wind held steady according to the following schedule.

Approximate test section dynamic pressure Q_o, mm (in) of water	Approximate wind dynamic pressure Q_w, mm (in) of water	Nominal Q_w/Q_o
254.0 (10)	0 (0)	0
254.0 (10)	2.5 (0.1)	0.01
254.0 (10)	6.4 (0.25)	0.025
254.0 (10)	12.7 (0.5)	0.05
254.0 (10)	25.4 (1.0)	0.1
101.6 (4)	25.4 (1.0)	0.25
50.8 (2)	25.4 (1.0)	0.5
50.8 (2)	35.6 (1.4)	0.7
50.8 (2)	43.2 (1.7)	0.85
50.8 (2)	50.8 (2.0)	1.0
101.6 (4)	50.8 (2.0)	0.5
127.0 (5)	50.8 (2.0)	0.4
254.0 (10)	50.8 (2.0)	0.2
0 (0)	50.8 (2.0)	∞

Reduction of Data

The pressure data were measured using multiple-tube manometers and recorded photographically. Flow-angularities, total-pressure losses and test-section dynamic-pressure variations were determined by subtracting the zero-wind values from the wind-on values and hence represent the effects due only to external winds.

The local dynamic pressures used to determine $\Delta Q_*/Q_o$ were found by linear interpolation of local pressure coefficient values.

Accuracy of Measurements

The azimuth angles were set with an accuracy of about ±1 degree.

The pressure readings which were used to determine the pressure coefficients, pressure ratios, and angularities, were accurate to about ± 1.27 mm (± 0.05 in) of water. The effect of this on the accuracy of data presented in the figures was determined for the values of Q_o corresponding to the schedule of Q_w/Q_o values shown in the section on TEST PROCEDURE. For convenience, these accuracies are shown as functions of Q_w/Q_o in sketch (a).

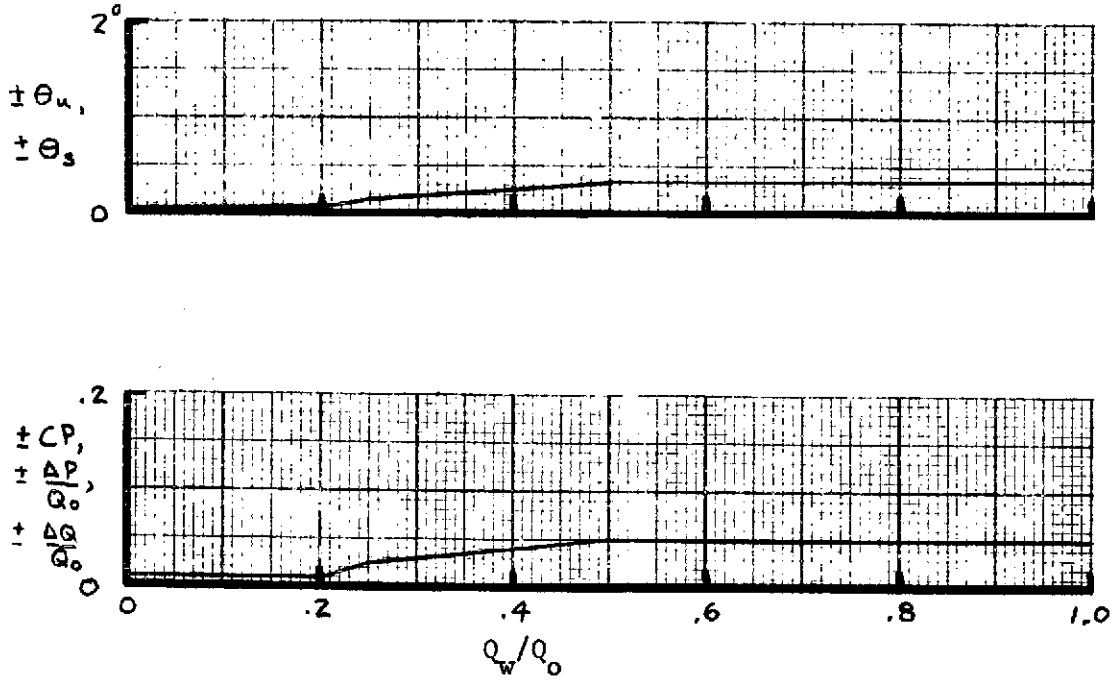

Sketch (a)

RESULTS

The plotted data are indexed in table II by configuration. In most of the component-effect plots the flow angularities, dynamic pressure variations and pressure losses are plotted against dynamic pressure ratio at various azimuth angles. The one exception was the exit effects. In this case only the pressure loss data are presented since the exits studied had no effect on the test-section flow quality.

The plotted data are indexed in table II by configuration. The basic data are presented in figure 6: test section flow angularities, dynamic pressure variations, and pressure losses are presented as functions of dynamic pressure ratio; and local pressure coefficients (note carefully the sliding ordinate scale) are presented as functions of test-section location for various dynamic pressure ratios. The following results are shown in summary plots: the effect of inlet system size (figure 7); the effect of peripheral flow straightener position with small inlet and posts (figure 8), with large inlet and posts (figure 9), and with large inlet and posts removed (figure 10); the effect of inlet roof posts with small inlet and peripheral flow straighteners inside (figure 11), with large inlet and peripheral flow straighteners inside (figure 12), and with large inlet and peripheral flow straighteners removed (figure 13); the effect of contraction flow straighteners (figure 14); the effect of exit area ratio (figure 15); and the comparison of the test-section flow characteristics of the basic configuration with the previously-established flow quality criteria of reference 6 (figure 16).

To evaluate the flow quality of the basic configuration the flow quality criteria of reference 6 were used. Figure 16 compares the experimental results with these criteria at several wind conditions. It is evident from figure 16(a) that for the basic configuration the test section velocity deviation in each of the three directions was generally less than 0.26 m/sec (1/2 knot) for wind velocities of 7.7 m/sec (15 knots) or less. At more severe wind conditions the test-section flow characteristics exceeded the criteria. Figure 16(b) shows that the flow quality is affected by wind direction. The axial velocity component appears to be the most critical aspect of external winds since this criterion is exceeded in some cases.

REFERENCES

1. Krishnaswamy, T. N.; Ramachandra, S. M.; and Krishnamoorthy, V.: Design and Characteristics of 14- by 9-Foot Open Circuit Wind Tunnel, Proc. of Seminar on Aeronautical Sciences, N.A.L., Bangalore, 1961.

2. Anderson, C. F.; and Carleton, W. E.: Effects of External Winds on a 1/40-Scale Model of the Open-Circuit Configuration of the Proposed AEDC Multipurpose Low-Speed Wind Tunnel. AEDC-TR-69-231, 1970.

3. Kirk, J. A.: Experience With a V/STOL Tunnel. Journal of the Royal Aeronautical Society, Vol. 71, No. 681, September, 1967, pp 606-622.

4. Leef, C. R.; and Hendry, R. G.: Development of a Nonrecirculating Wind Tunnel Configuration Insensitive to External Winds. Journal of Aircraft, Vol. 6, No. 3, May-June 1969, pp 221-227.

5. Eckert, William T.; Mort, Kenneth W.; Piazza, J. E.: Wind Sensitivity Studies of a Non-Return Wind Tunnel With a 216- By 432-mm (8.5- By 17.0- in) Test Section - Phase I. NASA TM X-62,171, September 1972.

6. Mort, K. W.; Eckert, W. T.; and Kelly, M. W.: The Steady-State Flow Quality of an Open Return Wind Tunnel Model. Canadian Aeronautics and Space Journal, Volume 18, Number 9, November 1972, pp 285-289. (Also NASA TM X-62, 170, 1972)

TABLE I. - MODEL DIMENSIONS FOR THE BASIC CONFIGURATION

Test section area, sq m (sq in)	0.083 (128.8)
Inlet screen (perforated plate)	
Porosity, percent	40
Hole diameter, mm (in)	3.175 (0.125)
Thickness, mm (in)	1.016 (0.040)
Flow area at start of fan nacelle contraction, sq m (sq in)	0.402 (623.0)
Flow area at fans, sq m (sq in)	0.224 (347.0)
Fan diameter, mm (in)	213.4 (8.4)
Number of fans	8
Vertical exit	
Area ratio	20:1

TABLE II - INDEX TO DATA FIGURES.

Figure Number	Effect Shown	Azimuth Angle, $-\psi$ (deg)	Configuration				
			Inlet				Exit Area Ratio
			Screen		Flow Straighteners		
			Size[1]	Roof Posts	Peripheral (Position)	In Contraction (Size[1])	
6	Basic Configuration	0 → -157-1/2	58×203 (23×80)	in	Front	2.54×2.54(1×1)	20
7	Inlet Size	0 → 180	58×203 (23×80) 107×254 (42×100)	in	Inside	2.54×2.54(1×1)	20
8	Peripheral Flow Straighteners: Small Inlet, Posts in	0 → 180	58×203 (23×80)	in	Front Inside	2.54×2.54(1×1)	20
9	Large Inlet, Posts in	0	107×254 (42×100)	in	Front Inside Removed	2.54×2.54(1×1)	20
		22-1/2 , 45			Front Inside		
		90			Front Inside Removed		
		112-1/2			Front Inside		
		180			Front Inside Removed		
10	Large Inlet, Posts Removed	0 , 90	107×254 (42×100)	out	Inside Outisde Removed	2.54×2.54(1×1)	20
11	Inlet Roof Posts: Small Inlet, Peripheral Flow Straighteners Inside	0, 90, 180	58×203 (23×80)	in out	Inside	2.54×2.54(1×1)	20

[1]All dimensions in cm (in).

TABLE II - CONCLUDED.

Figure Number	Effect Shown	Azimuth Angle. - ψ (DEG)	Configuration				
			Inlet				
			Screen		Flow Straighteners		Exit Area Ratio
			Size[1]	Roof Posts	Peripheral (Position)	In Contraction (Size[1])	
12	Inlet Roof Posts (concluded): Large Inlet, Peripheral Flow Straighteners Inside	0 , 90	107×254 (42×100)	in out	Inside	2.54×2.54(1×1)	20
13	Large Inlet, Peripheral Flow Straighteners Removed	0, 90, 180	107×254 (42×100)	in out	Removed	2.54×2.54(1×1)	20
14	Contraction Flow Straighteners	0 → 157-1/2	58×203 (23×80)	in	Front	2.54×2.54(1×1) .32×.32(1/8×1/8) 5.1×5.1(2×2)	20
15	Exit Area Ratio	0, 90, 180	107×254 (42×100)	in	Removed	2.54×2.54(1×1)	20 8
16	Flow Quality Evaluation	0 → 157-1/2	58×203 (23×80)	in	Front	2.54×2.54(1×1)	20

[1]All dimensions in cm(in).

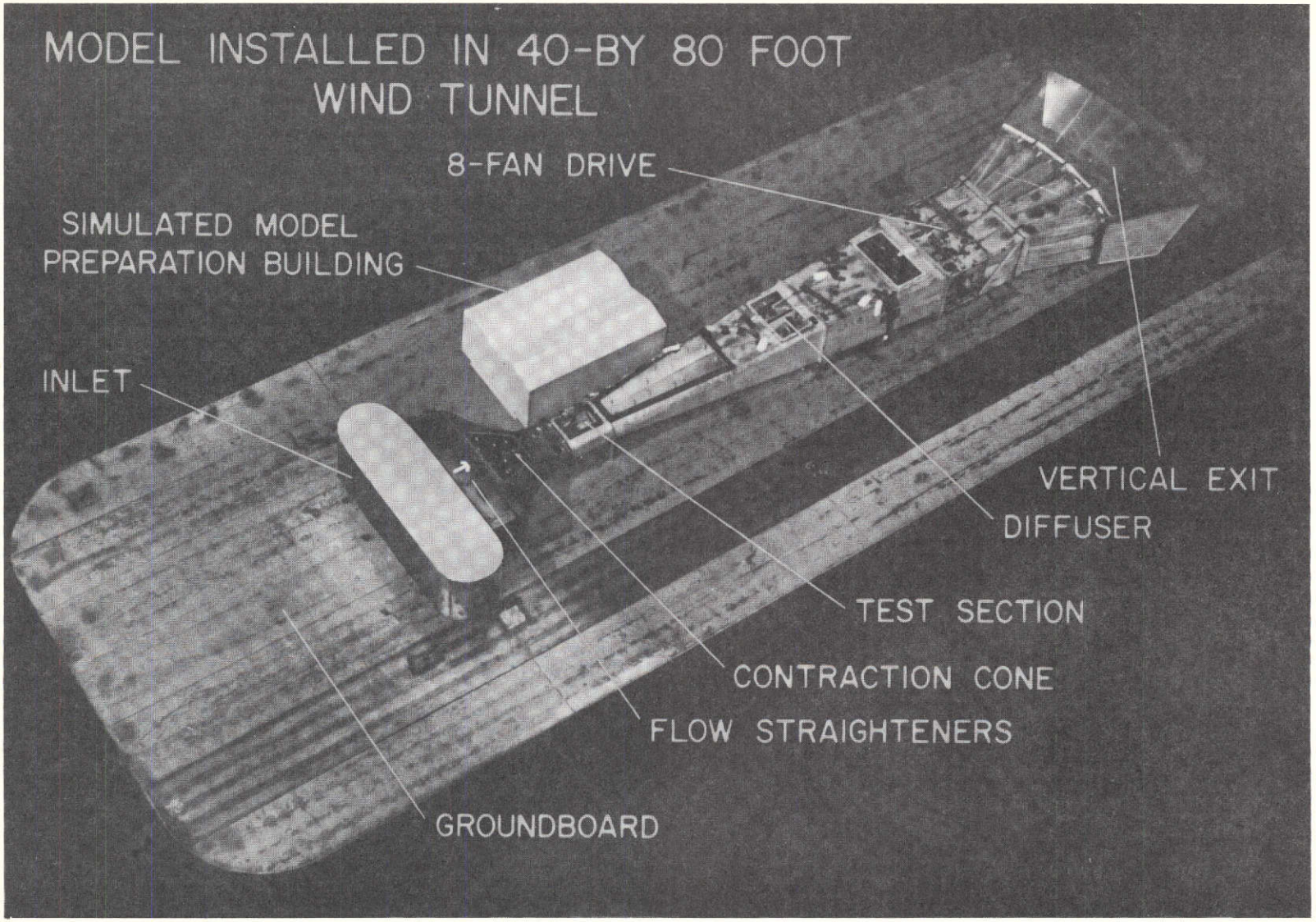

(a) Top view, with basic inlet system.

Figure 1. - Model installed in Ames 40- By 80-Foot Wind Tunnel.

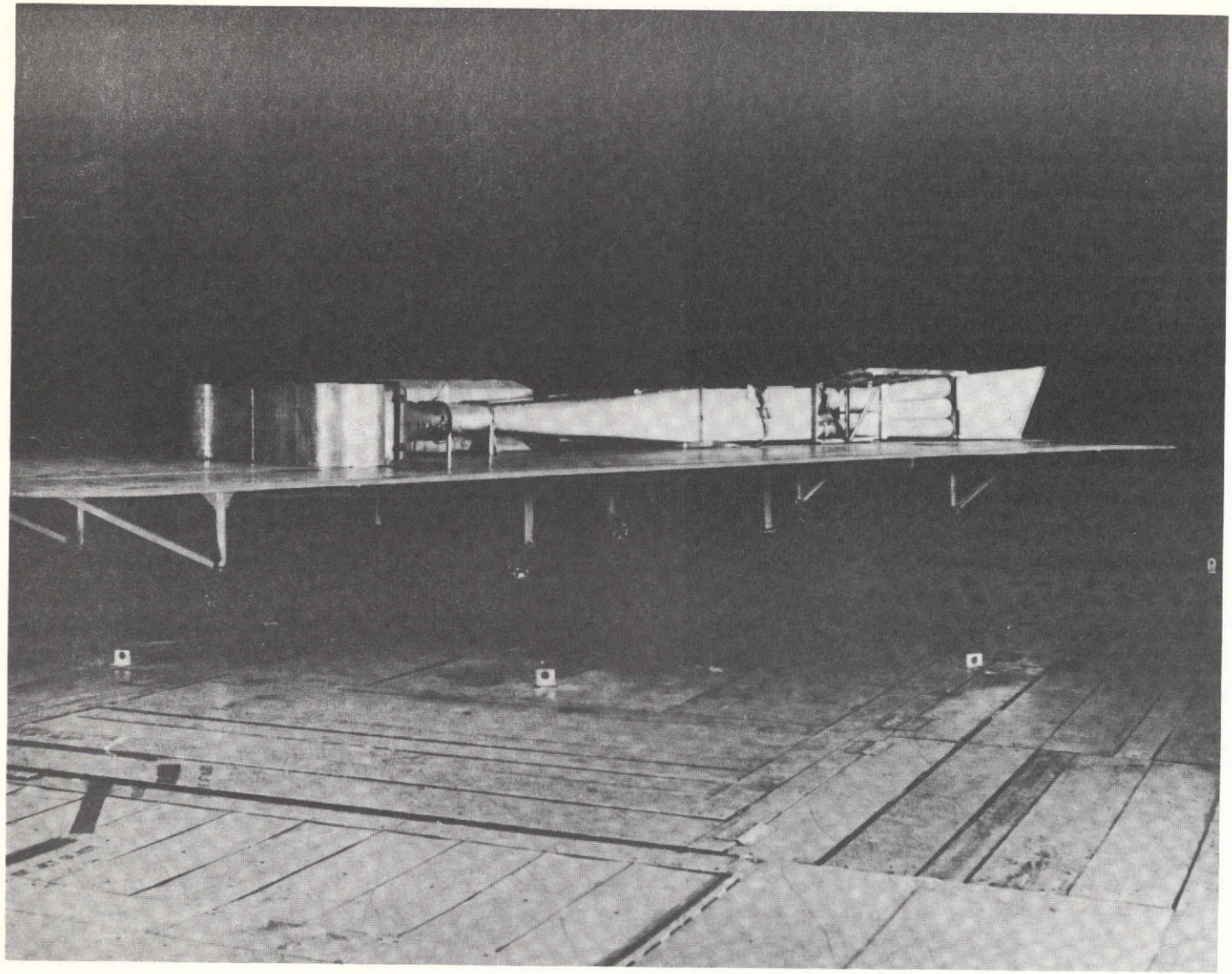

(b) Side view, with basic inlet system.

Figure 1. - Concluded.

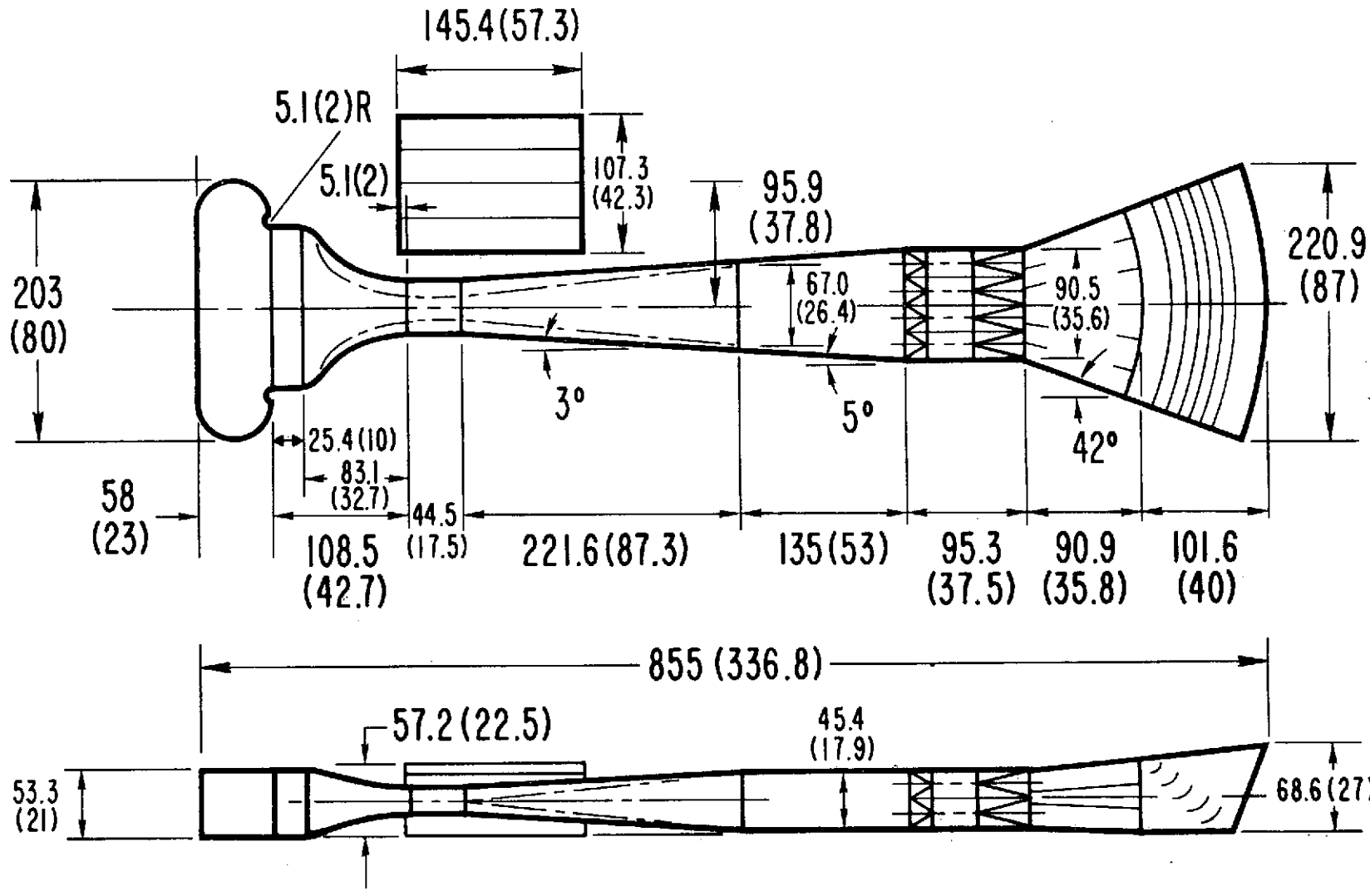

Figure 2.- Model dimensions for basic configuration.

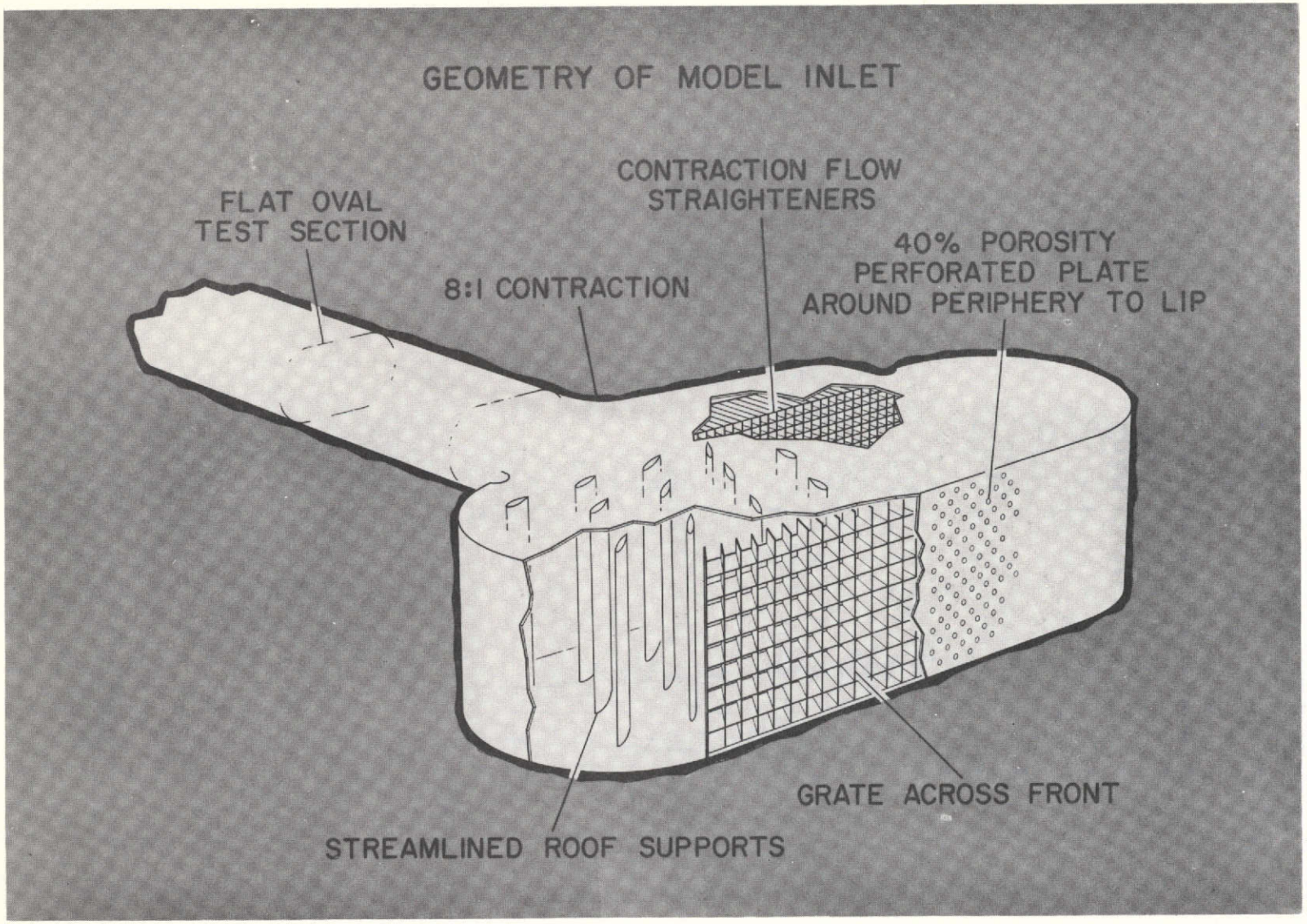

(a) Inlet geometry with front-only peripheral flow straighteners.

Figure 3. - Model inlet components.

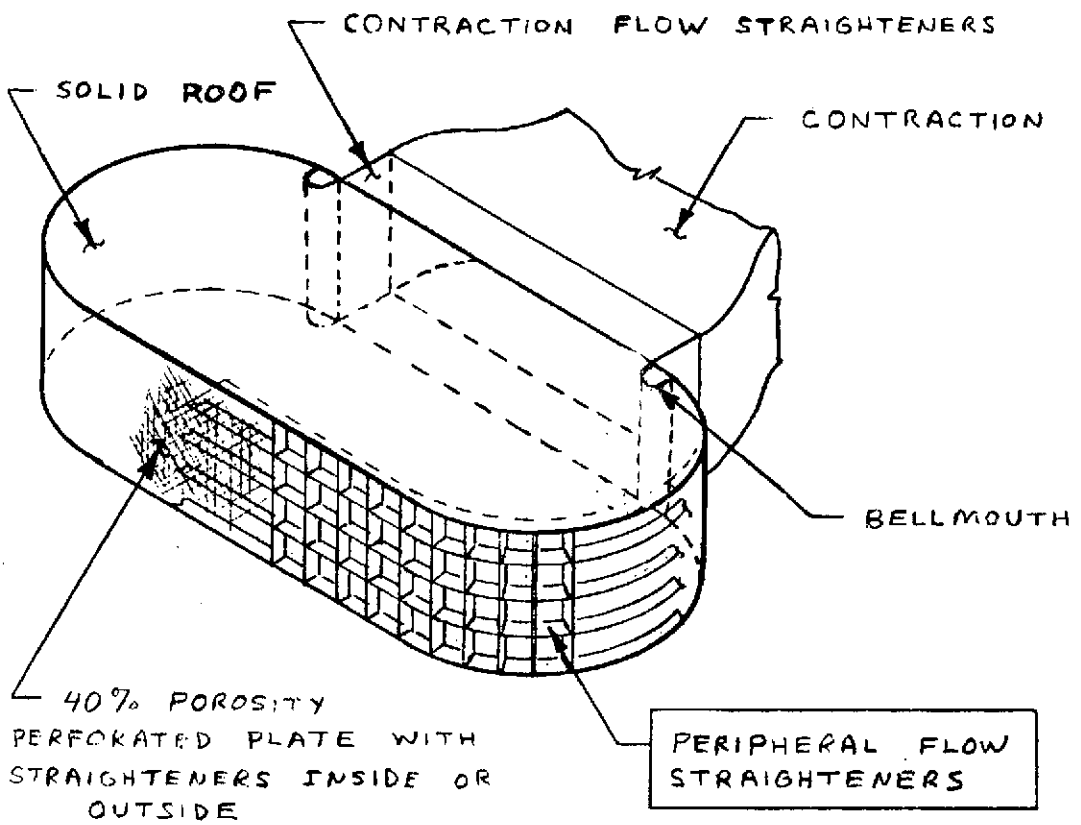

(b) Placement of peripheral flow straighteners.

Figure 3. - Continued.

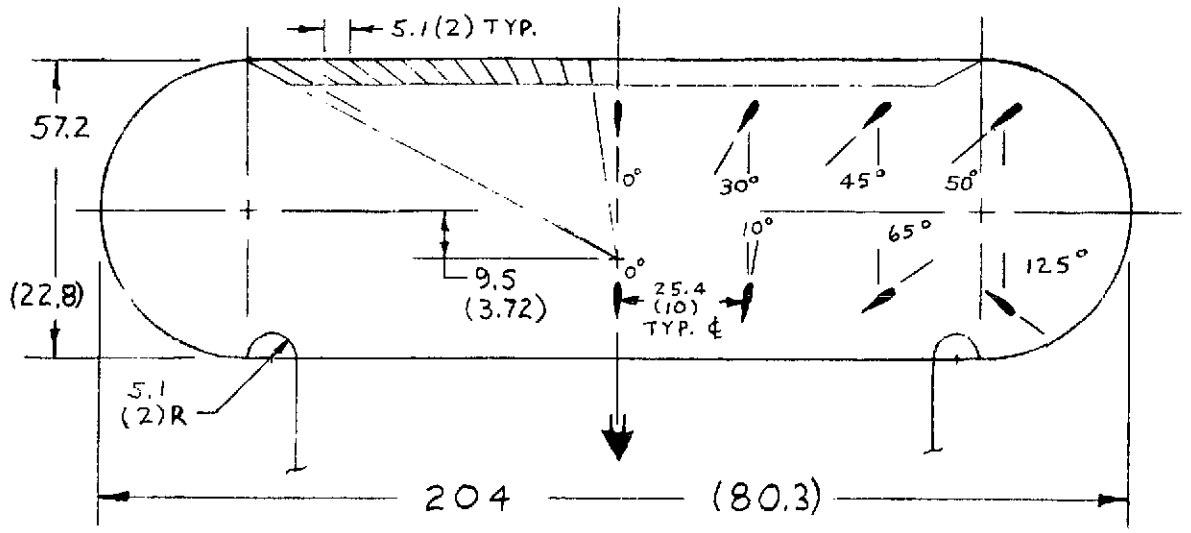

BASIC (SMALL) INLET
(WITH FRONT FLOW STRAIGHTENERS)

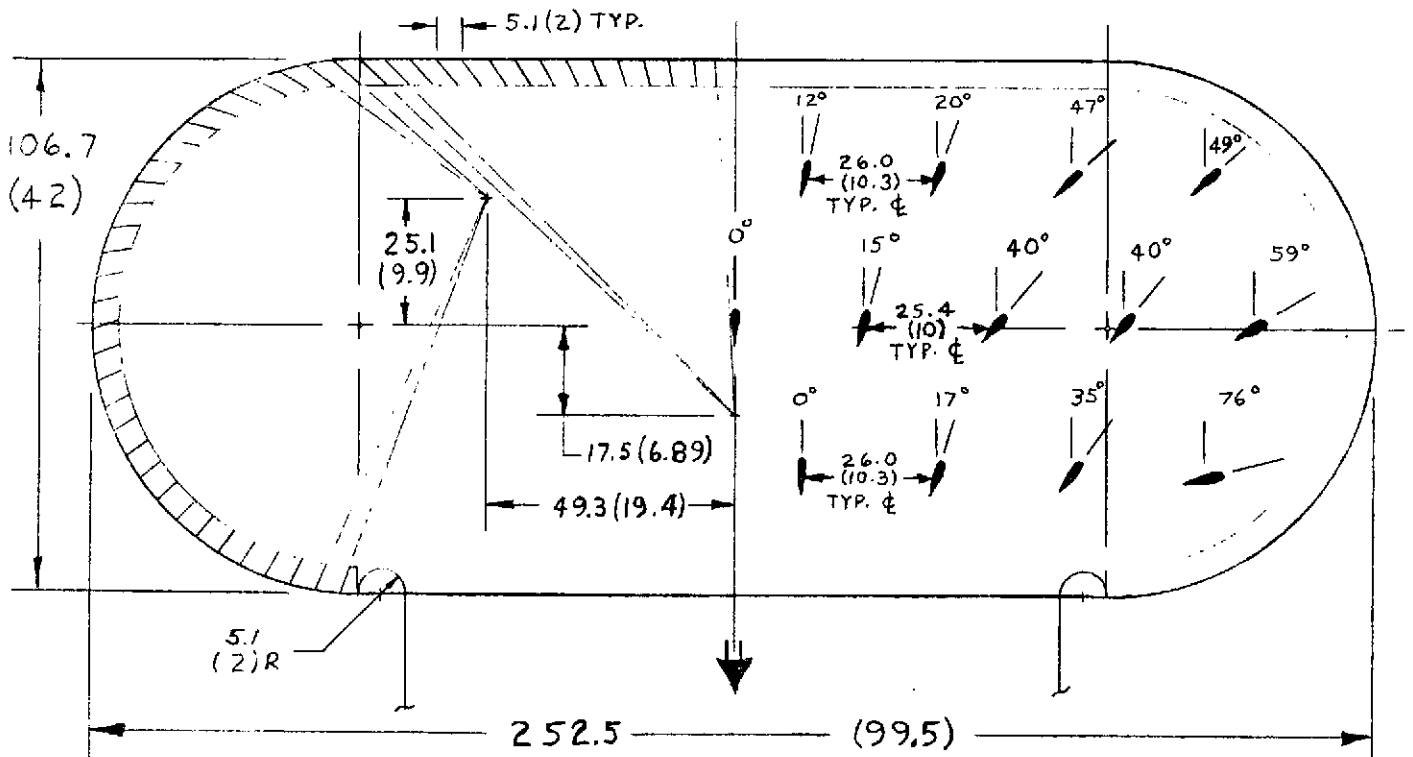

ALTERNATE (LARGE) INLET
(WITH PERIPHERAL FLOW STRAIGHTENERS)

ALL DIMENSIONS IN CM (IN).

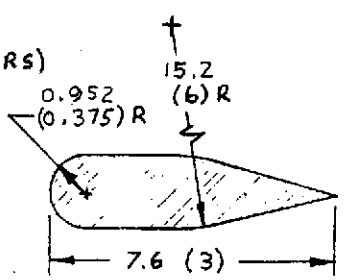

ROOF POST CROSS-SECTION

(c) Inlet area planform and post arrangement details.

Figure 3.- Continued.

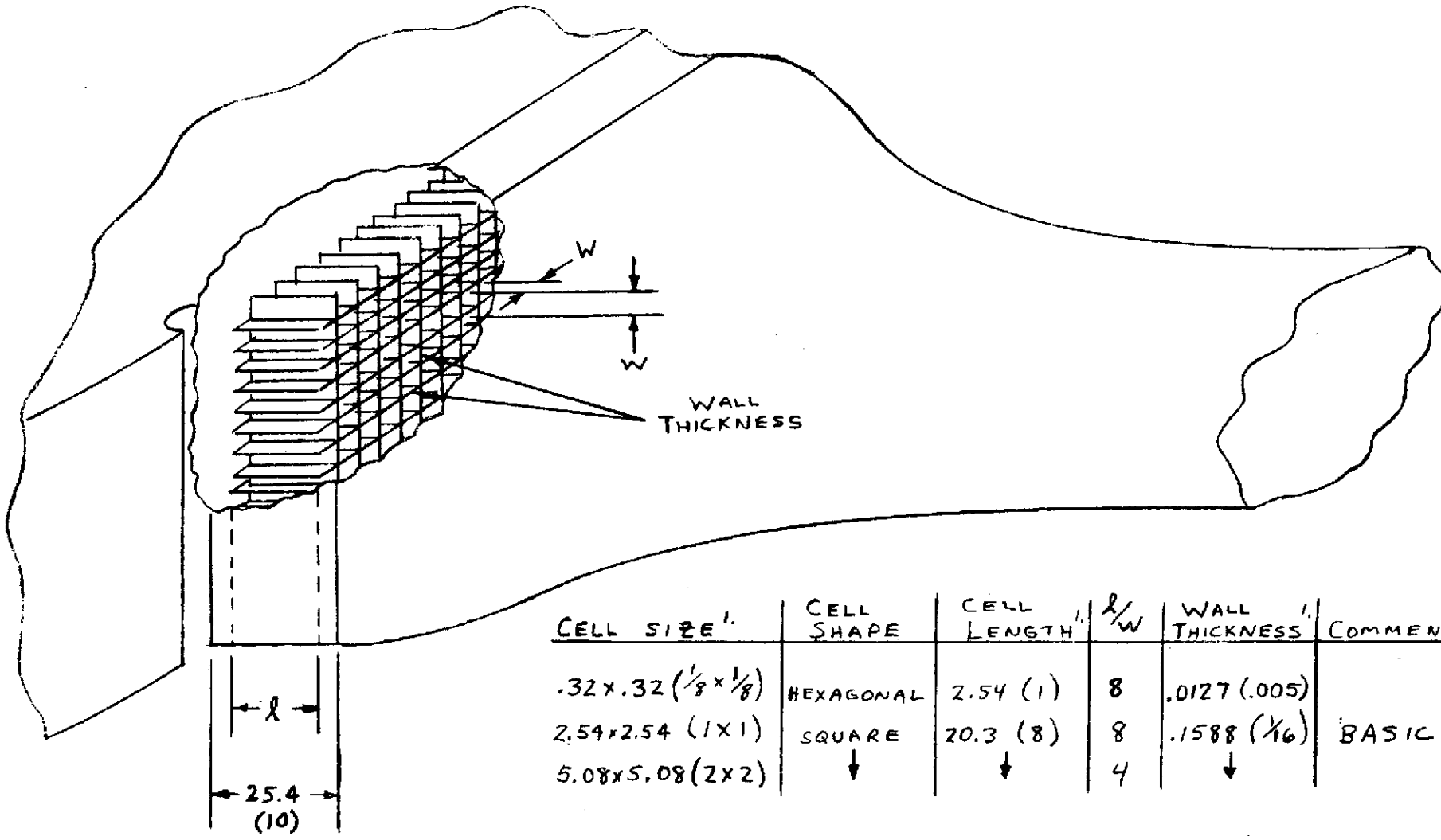

CELL SIZE [1]	CELL SHAPE	CELL LENGTH [1]	ℓ/W	WALL THICKNESS [1]	COMMENT
.32 x .32 (1/8 x 1/8)	HEXAGONAL	2.54 (1)	8	.0127 (.005)	
2.54 x 2.54 (1 x 1)	SQUARE	20.3 (8)	8	.1588 (1/16)	BASIC
5.08 x 5.08 (2 x 2)	↓	↓	4	↓	

[1] ALL DIMENSIONS IN CM (IN).

(d) Flow straighteners in contraction cone.

Figure 3.- Continued.

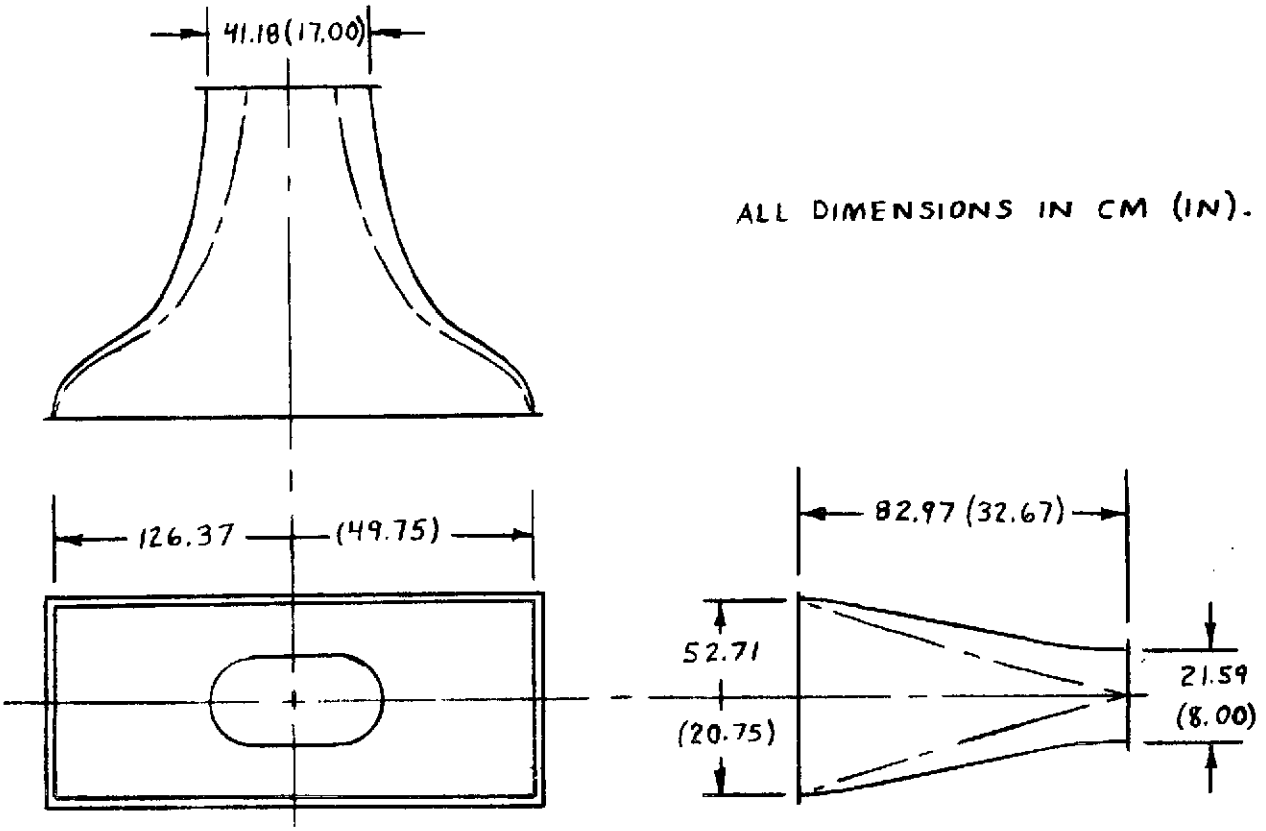

ALL DIMENSIONS IN CM (IN).

CONTRACTION WALL COORDINATES

X	Y	Z	R
0 (0)	63.20 (24.88)	26.37 (10.38)	0 (0)
2.54 (1)	63.14 (24.86)	26.31 (10.36)	
5.08 (2)	62.84 (24.74)	26.01 (10.24)	1.65 (0.65)
5.33 (2.1)	62.79 (24.72)	25.96 (10.22)	
10.16 (4)	60.43 (23.79)		3.30 (1.30)
13.82 (5.44)	56.24 (22.14)		
15.24 (6)	54.15 (21.32)		4.95 (1.95)
20.32 (8)	47.29 (18.62)		6.60 (2.60)
25.40 (10)	41.48 (16.33)		8.26 (3.25)
30.48 (12)	36.70 (14.45)		9.91 (3.90)
35.56 (14)			10.80 (4.25)
40.64 (16)	29.54 (11.63)		
45.72 (18)			
50.80 (20)	25.10 (9.88)		
54.10 (21.3)	24.10 (9.49)	13.31 (5.24)	
55.88 (22)			
60.96 (24)	22.71 (8.94)	11.91 (4.69)	
66.04 (26)			
71.12 (28)	21.77 (8.57)	10.97 (4.32)	
76.20 (30)	21.62 (8.51)	10.82 (4.26)	
82.98 (32.67)	21.59 (8.50)	10.80 (4.25)	10.80 (4.25)

LINEAR

CONSTANT

(e) Contraction cone.

Figure 3.- Concluded.

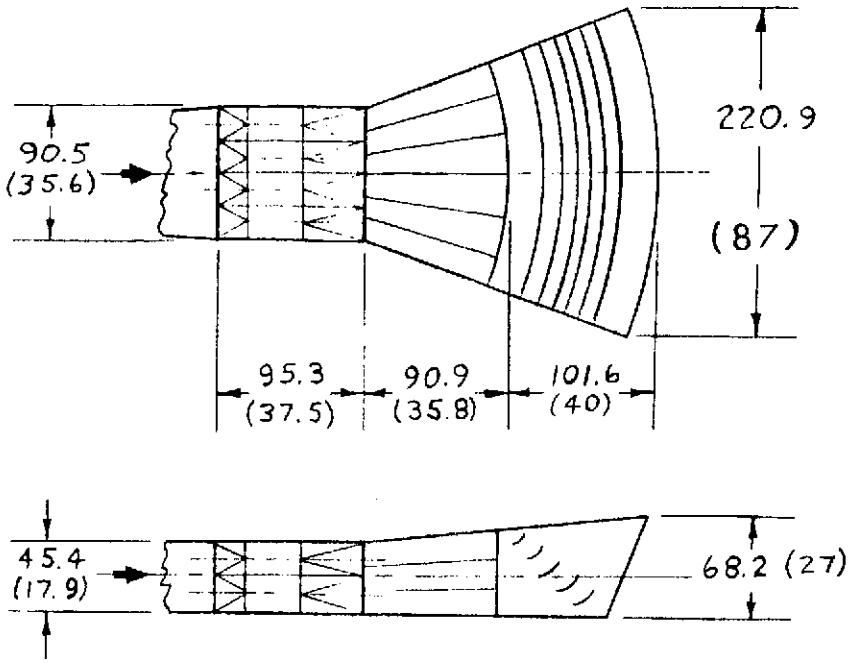

AREA RATIO 20:1 (BASIC) VERTICAL EXIT

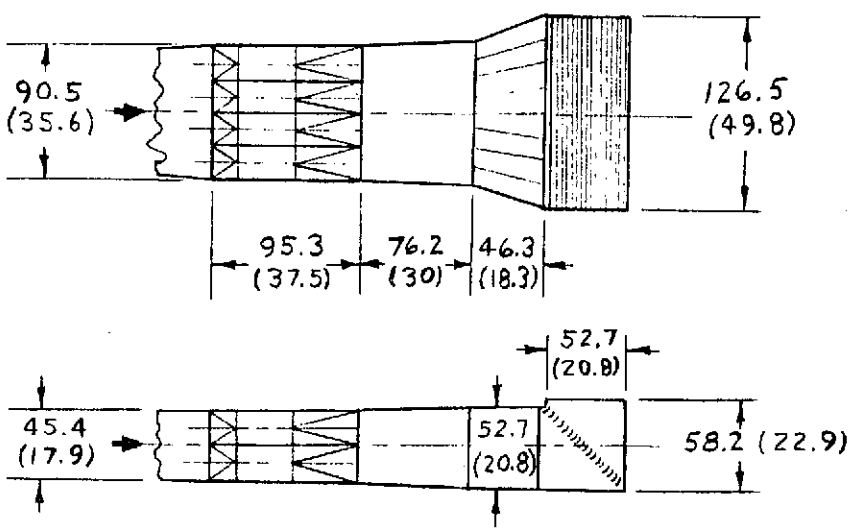

AREA RATIO 8:1 (ALTERNATE) VERTICAL EXIT

Figure 4.- Exit configurations.

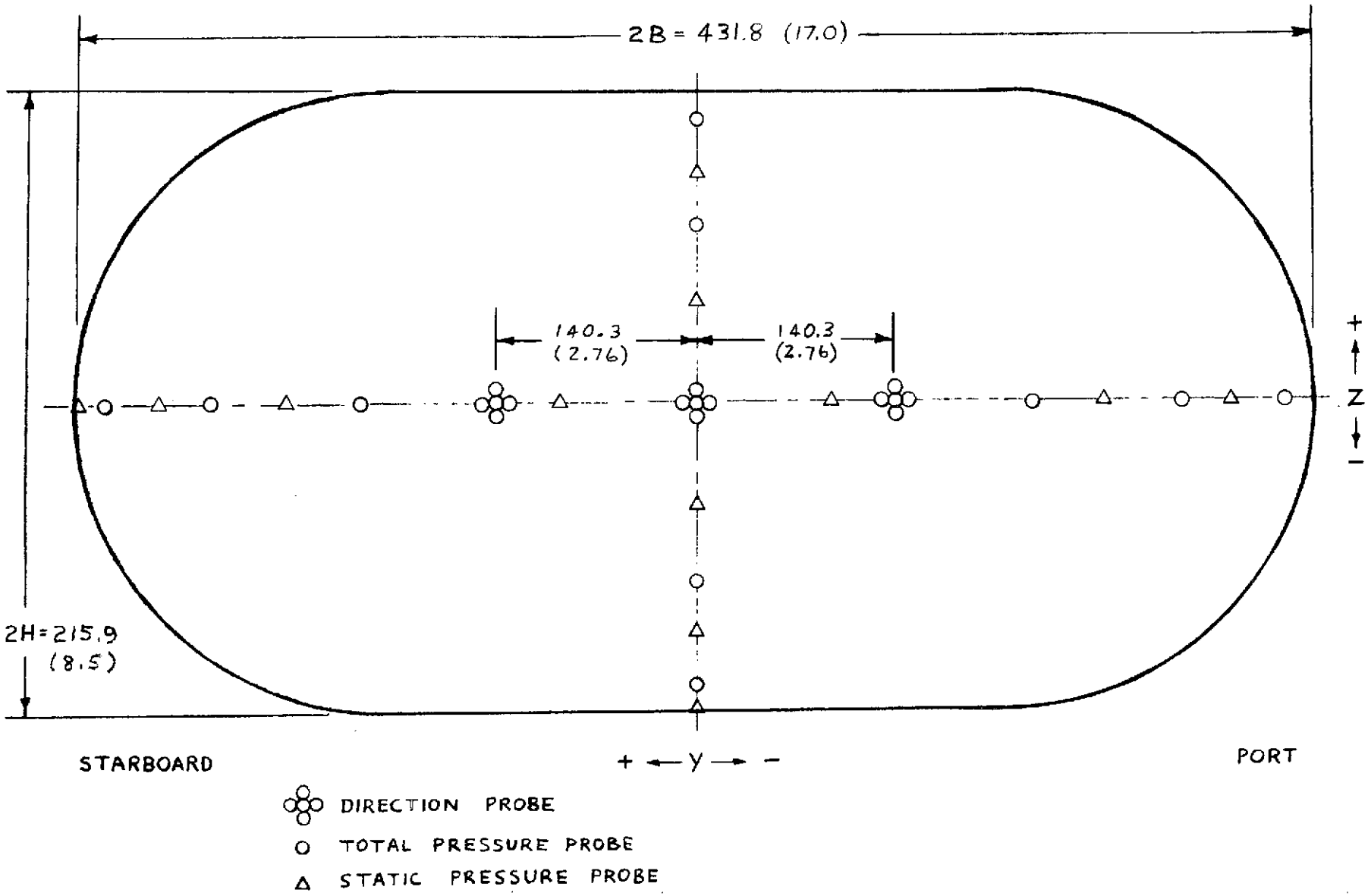

Figure 5.- Test section instrumentation.

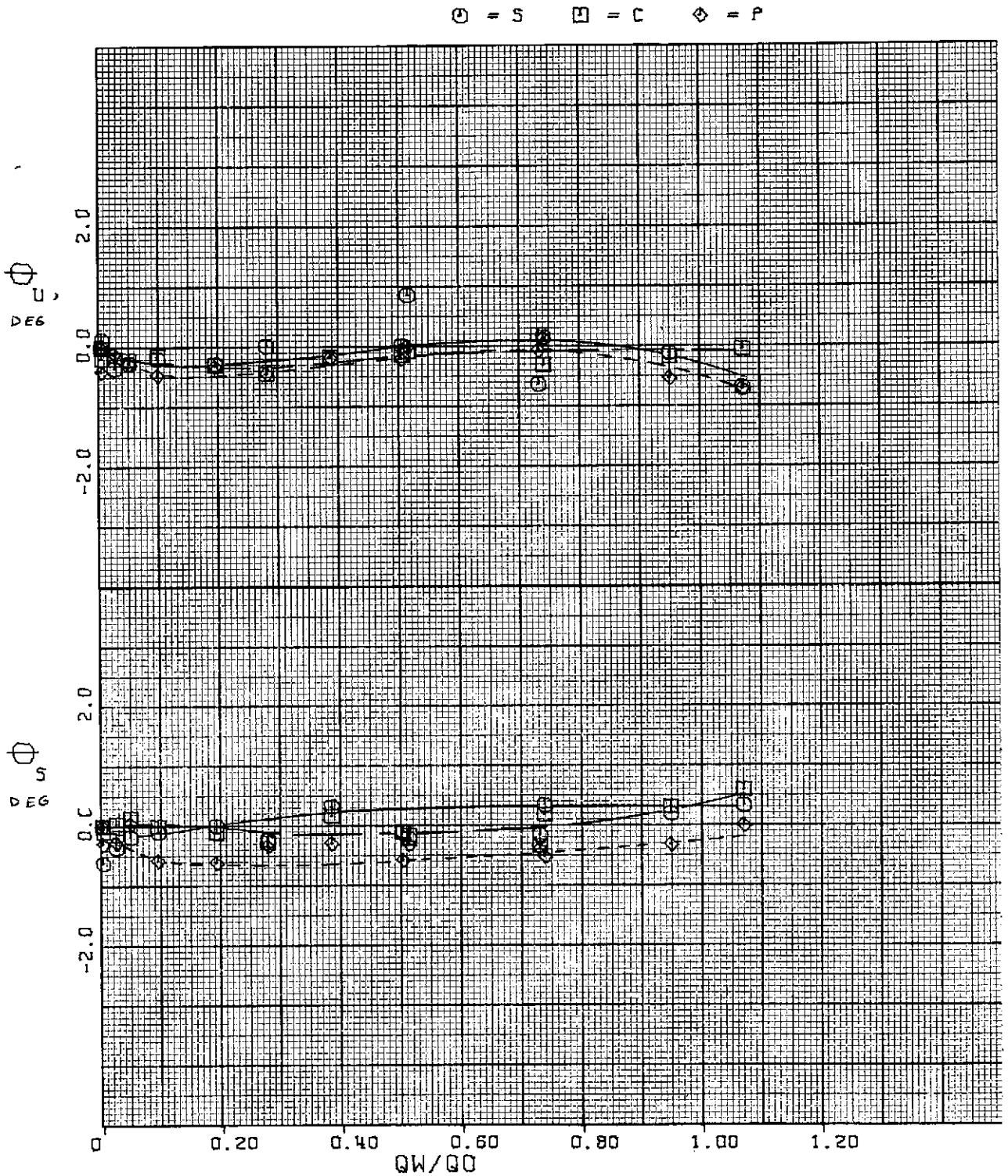

$\psi = 0°$.
(a) Test Section flow angularities.

Figure 6. - Results from basic configuration: 58×203 cm (23×80 in) inlet, roof posts in, front-only peripheral flow straighteners, 2.54×2.54 cm (1×1 in) contraction flow straighteners, area ratio 20 exit.

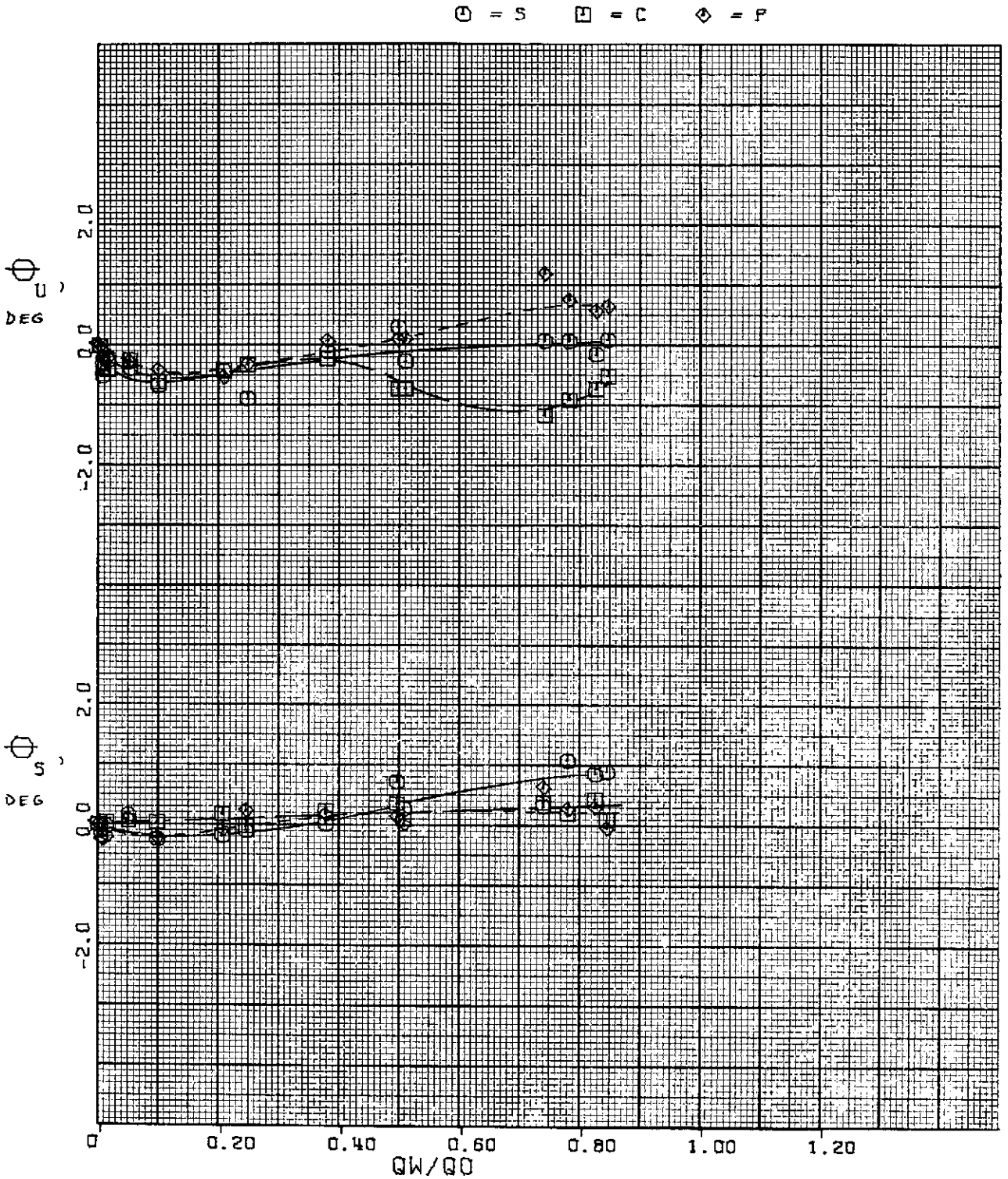

ψ = -22-1/2°.
(a) Test Section flow angularities - continued.

Figure 6. - Continued.

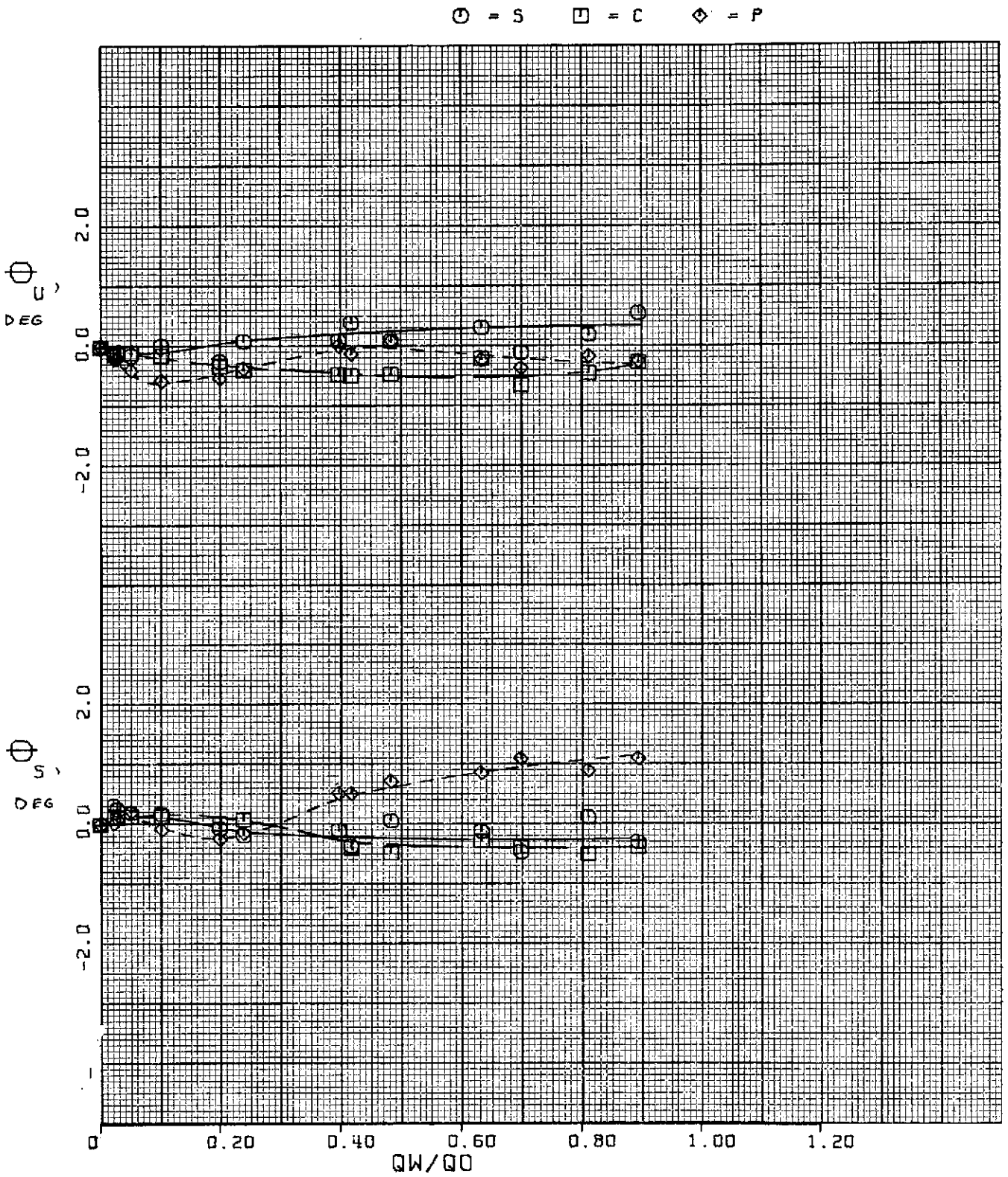

ψ = -45°.
(a) Test Section flow angularities - continued.

Figure 6. - Continued.

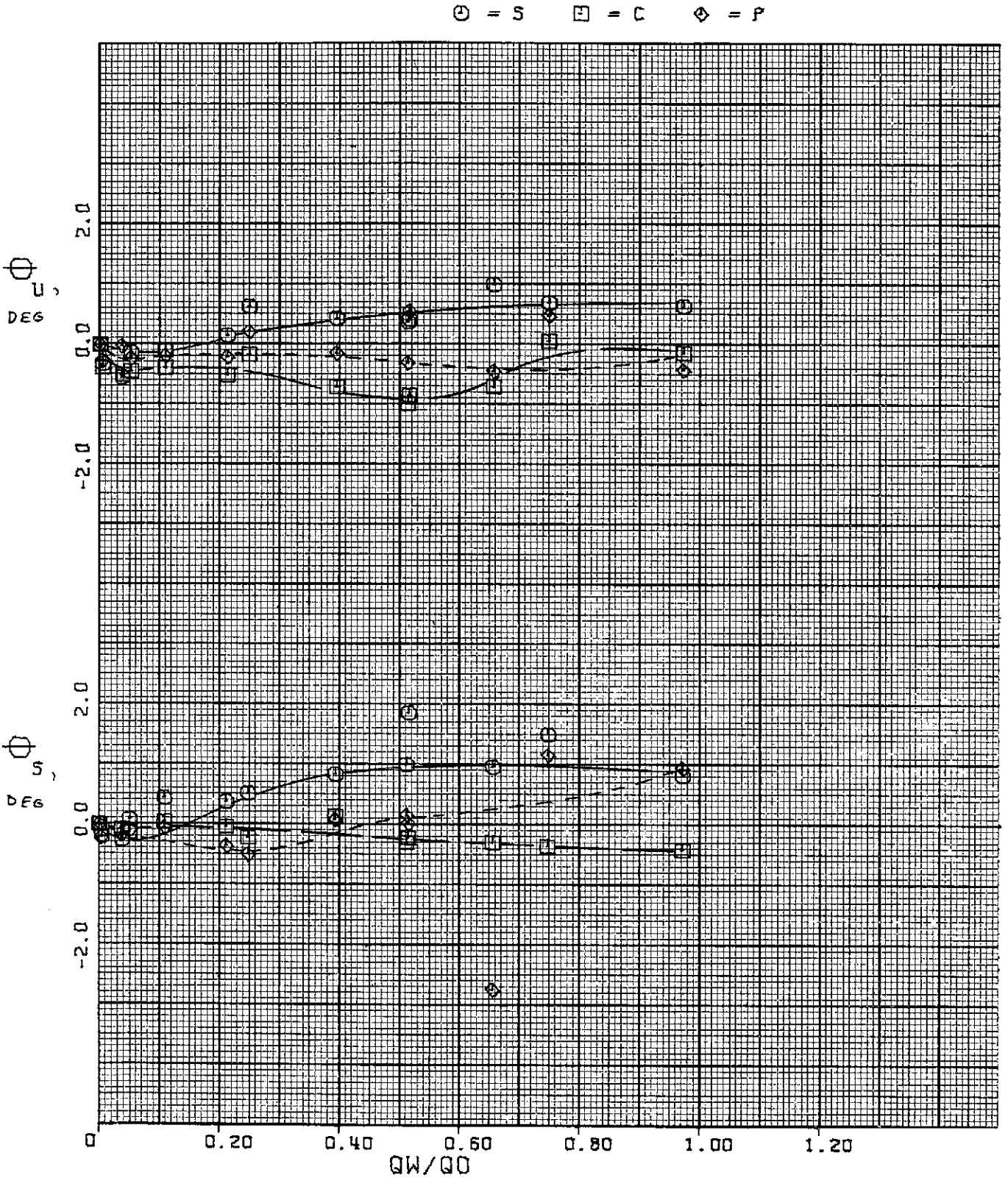

ψ = -67-1/2°.
(a) Test Section flow angularities - continued.

Figure 6. - Continued.

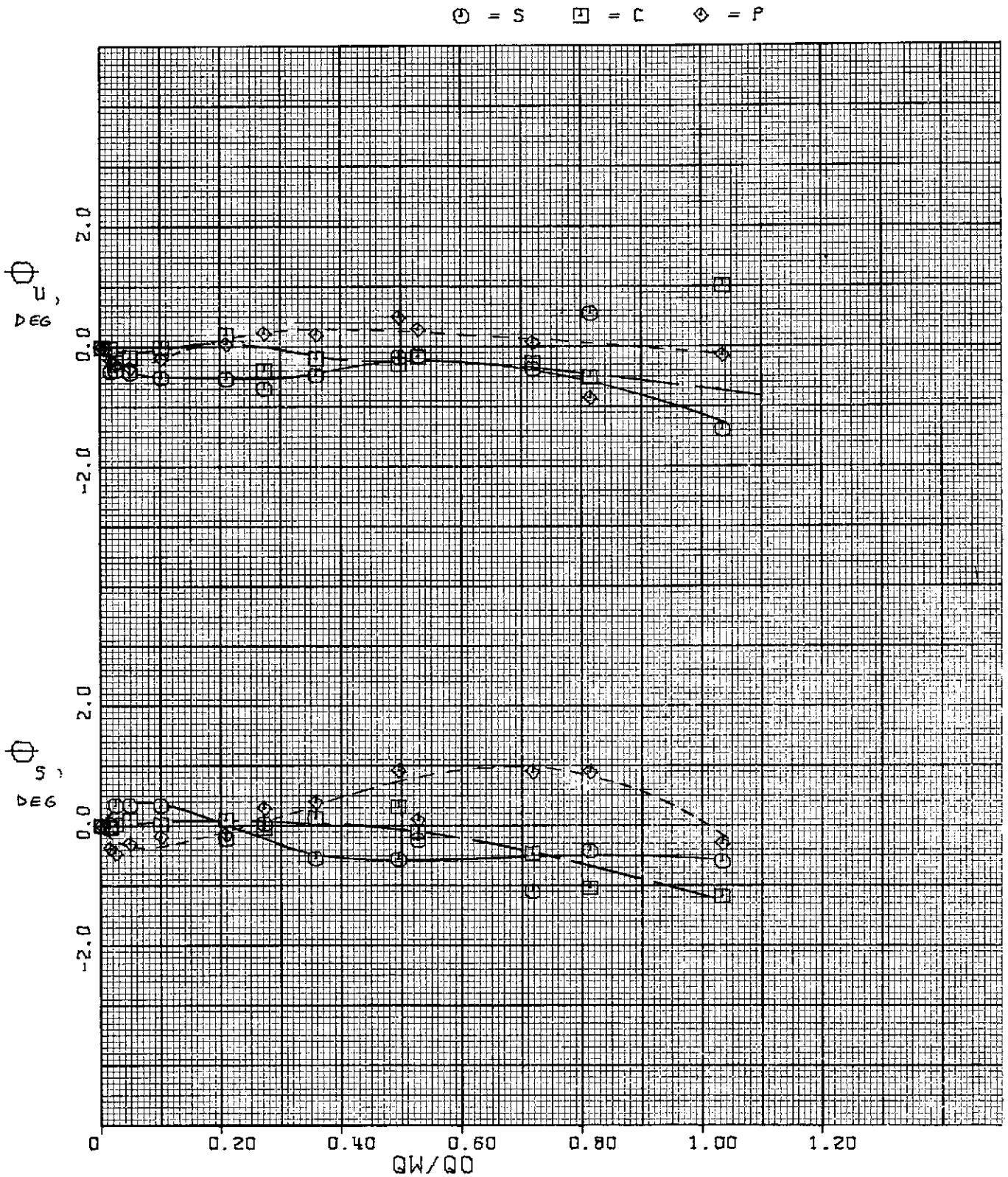

$\psi = -90°$.

(a) Test Section flow angularities - continued.

Figure 6. - Continued.

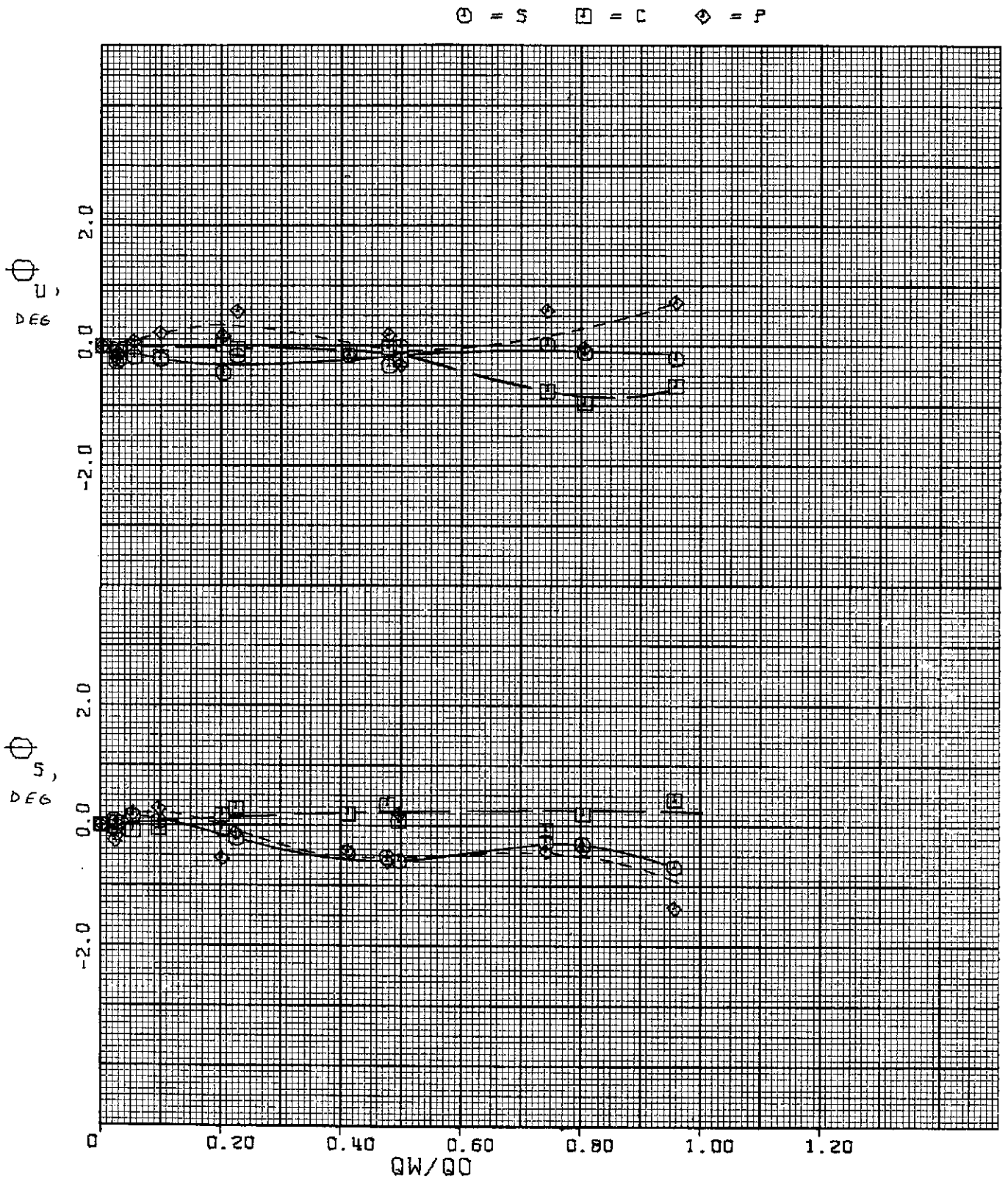

ψ = -112-1/2°.
(a) Test Section flow angularities - continued.

Figure 6. - Continued.

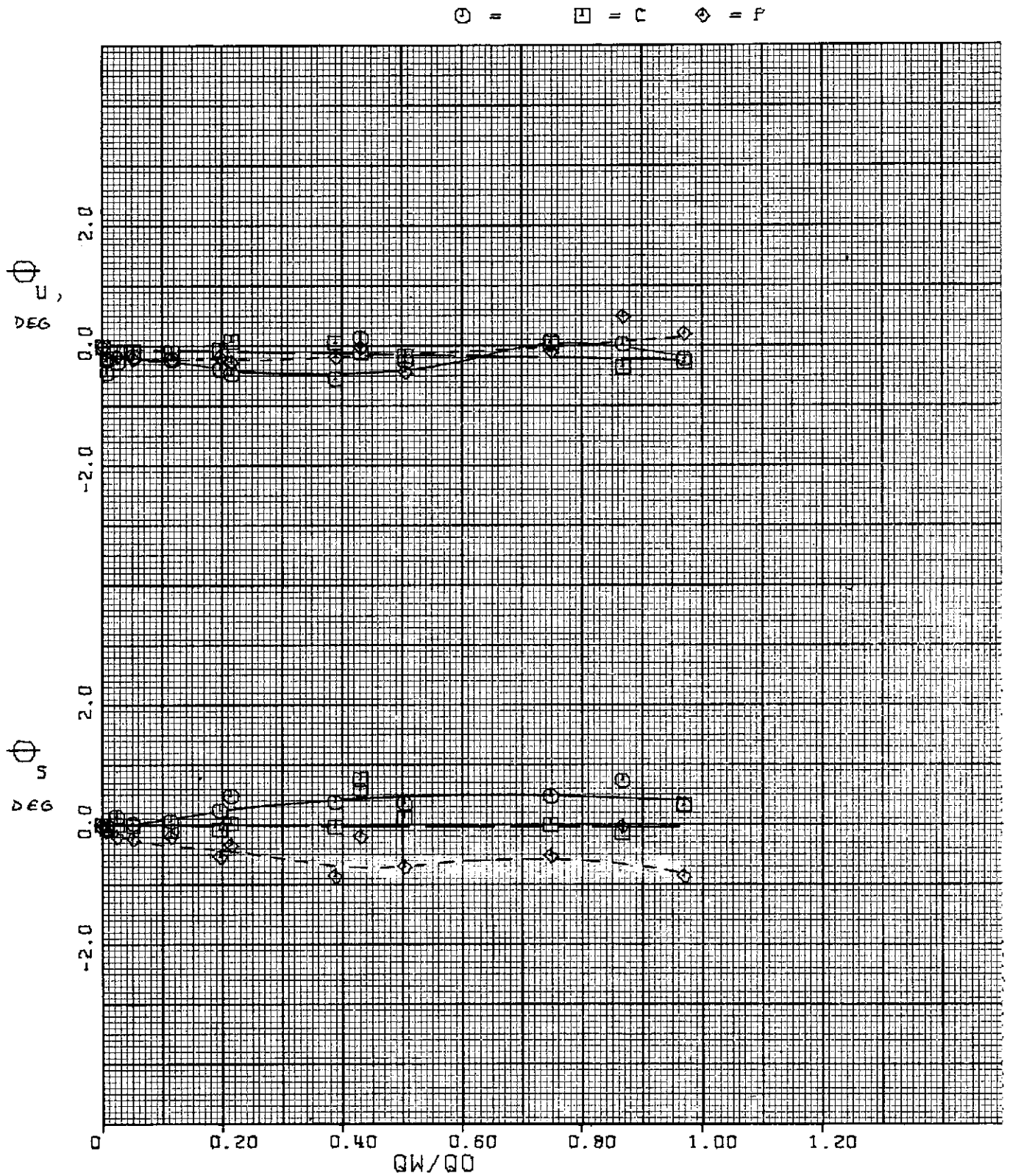

ψ = -135°.

(a) Test Section flow angularities - continued.

Figure 6. - Continued.

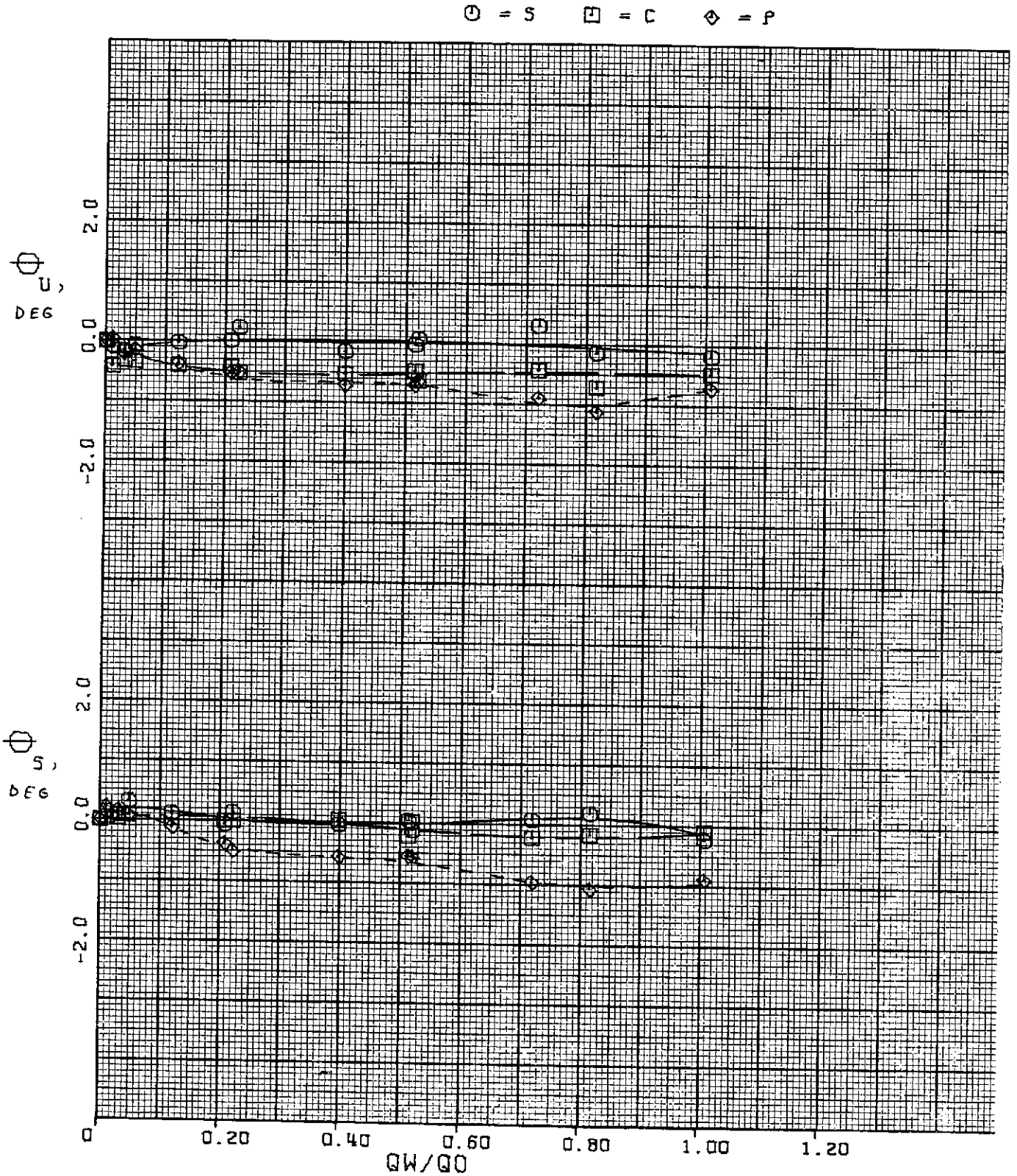

ψ = -157-1/2°.
(a) Test Section flow angularities - continued.

Figure 6. - Continued.

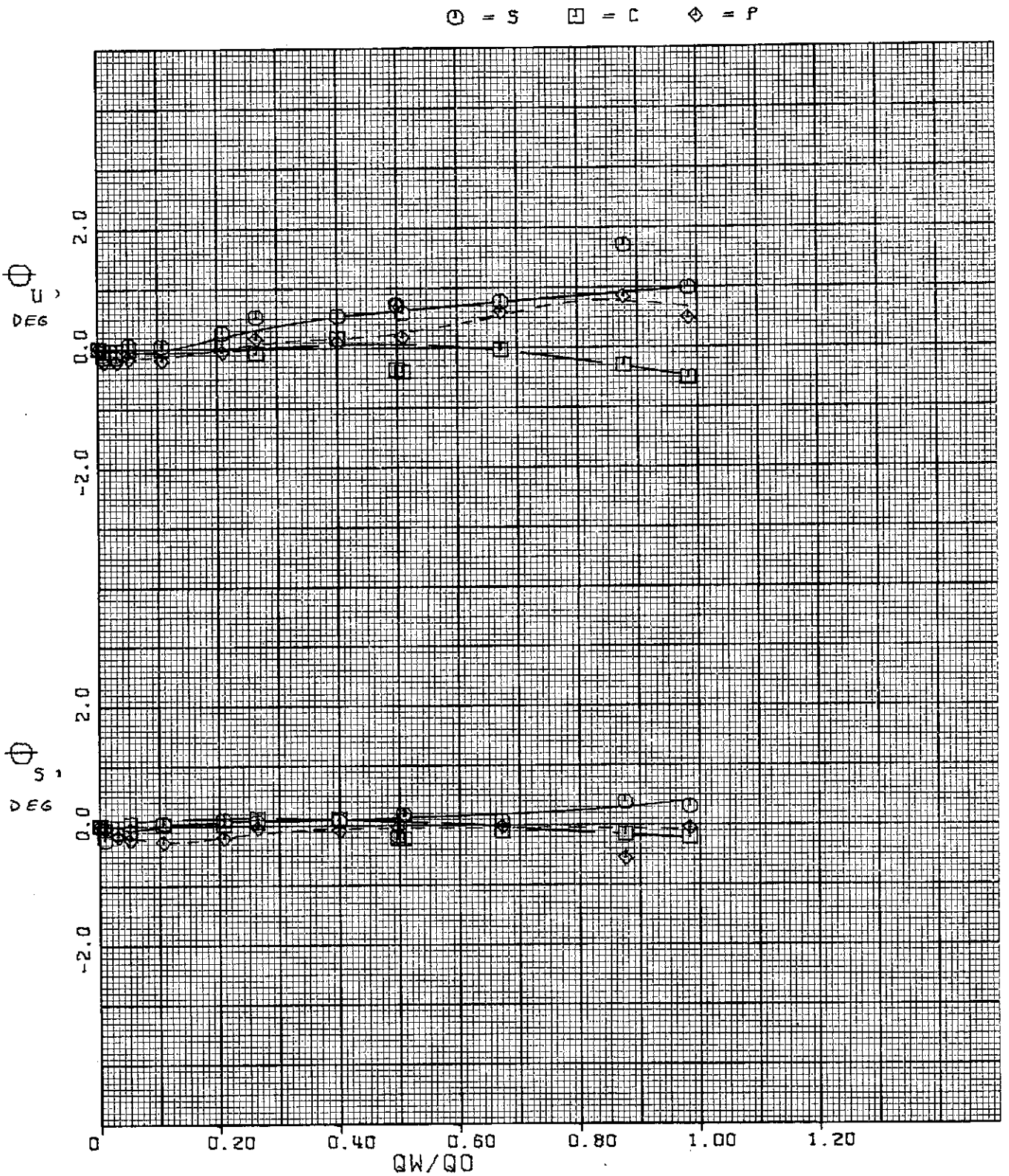

ψ = 180°.

(a) Test Section flow angularities - continued.

Figure 6. - Continued.

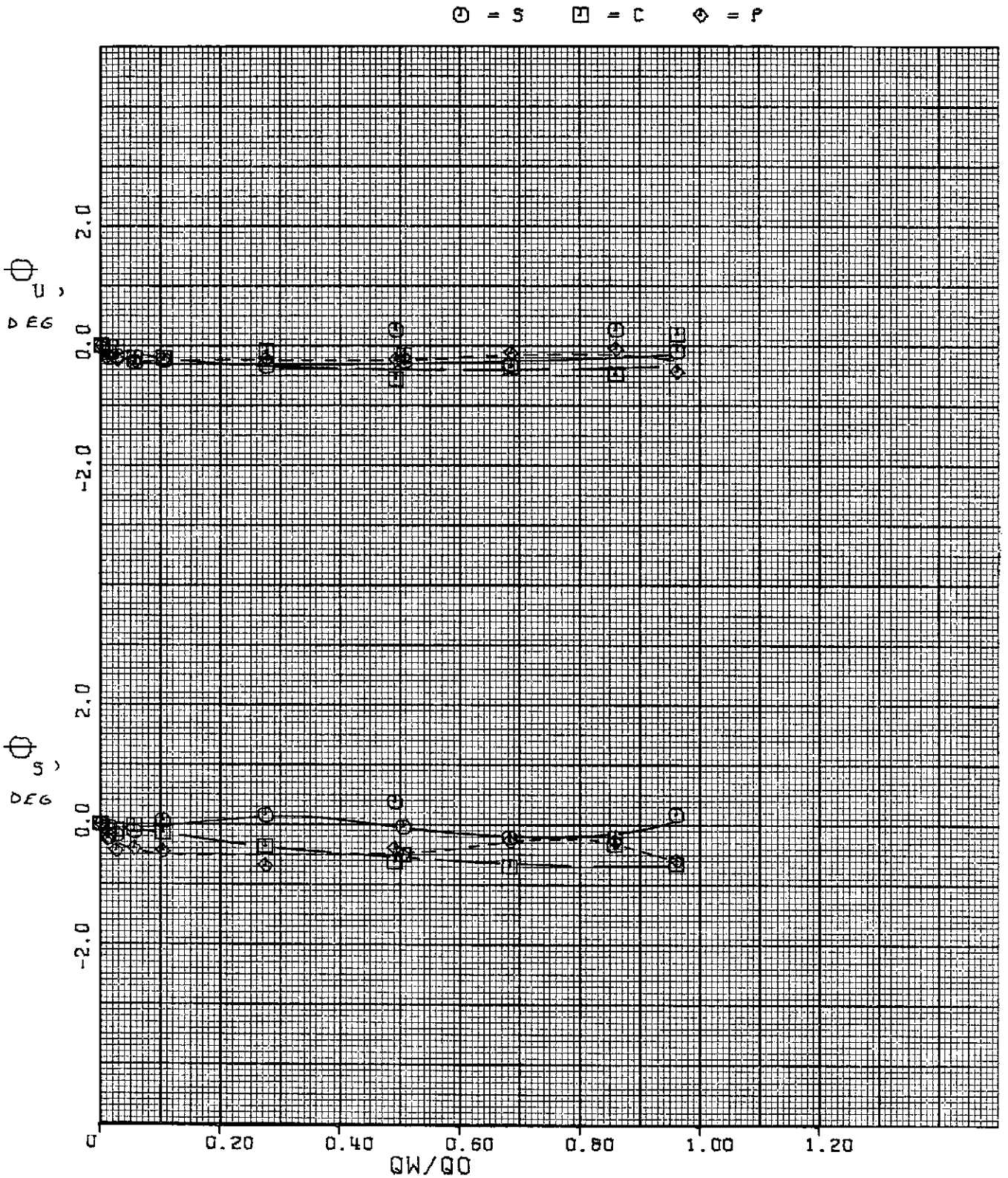

ψ = 157-1/2°.
(a) Test Section flow angularities - concluded.

Figure 6. - Continued.

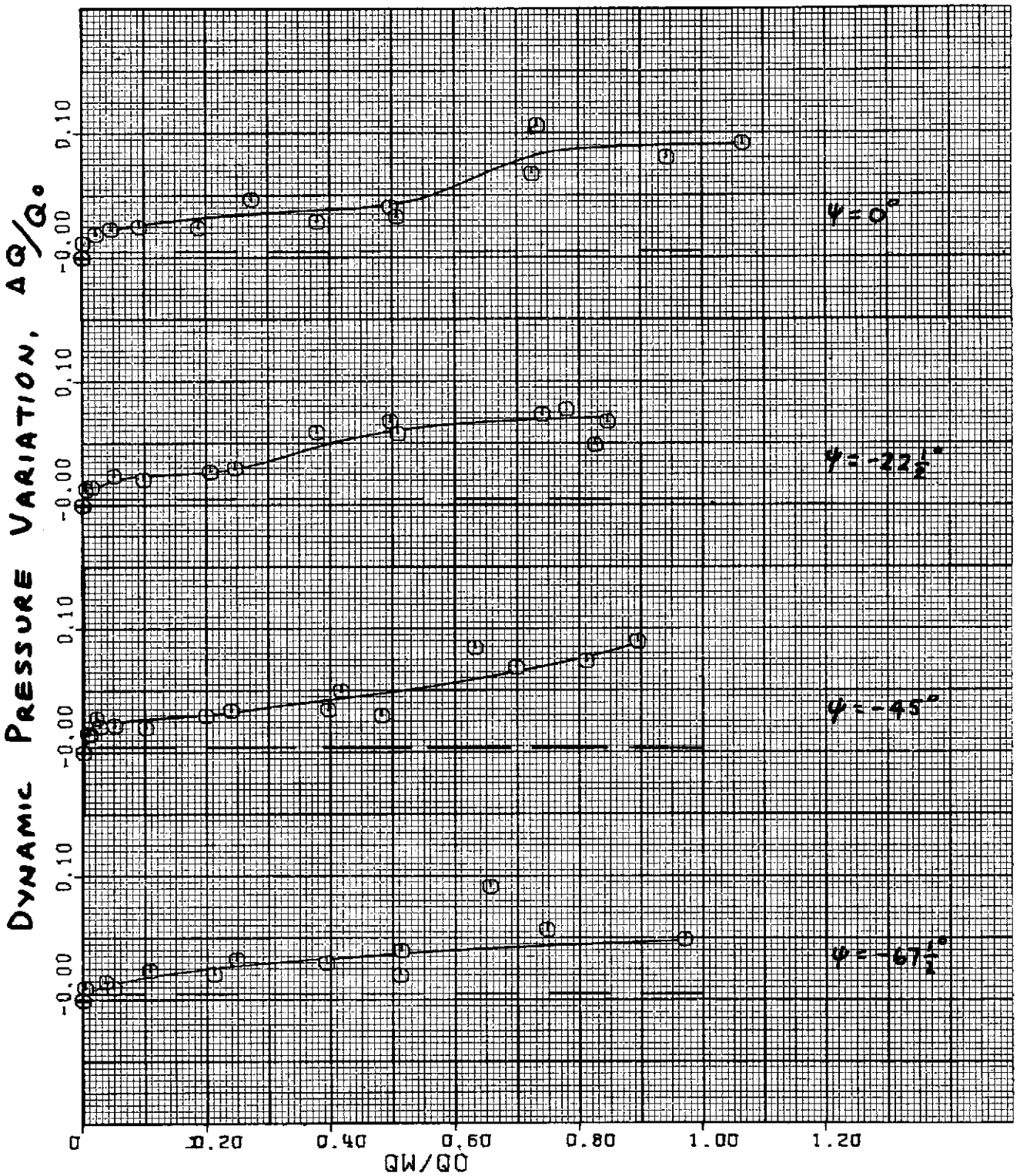

ψ = 0°, -22-1/2°, -45° and -67-1/2°.
(b) Dynamic pressure variation.

Figure 6. - Continued.

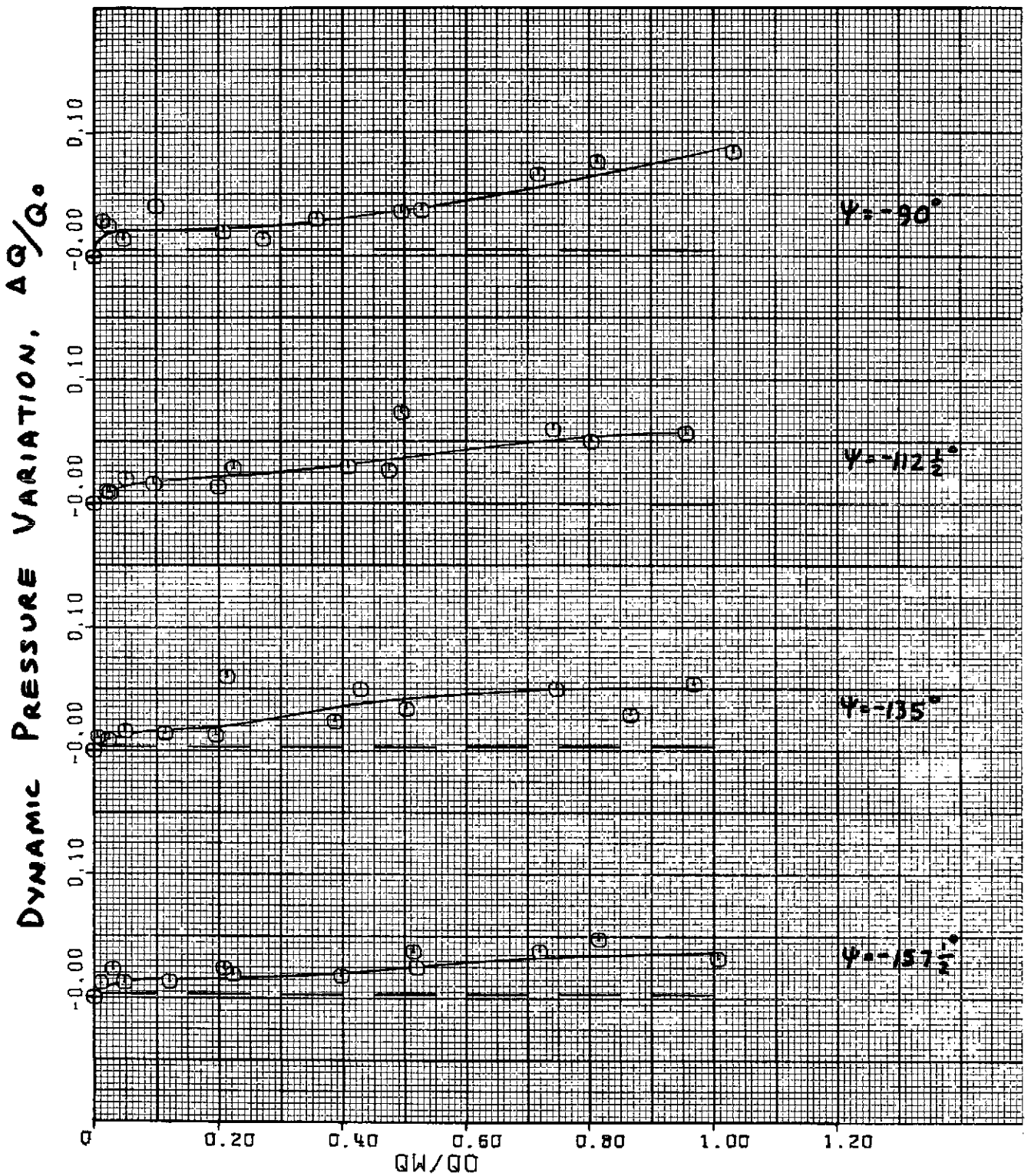

ψ = -90°, -112-1/2°, -135° and -157-1/2°
(b) Dynamic pressure variation - continued.

Figure 6. - Continued.

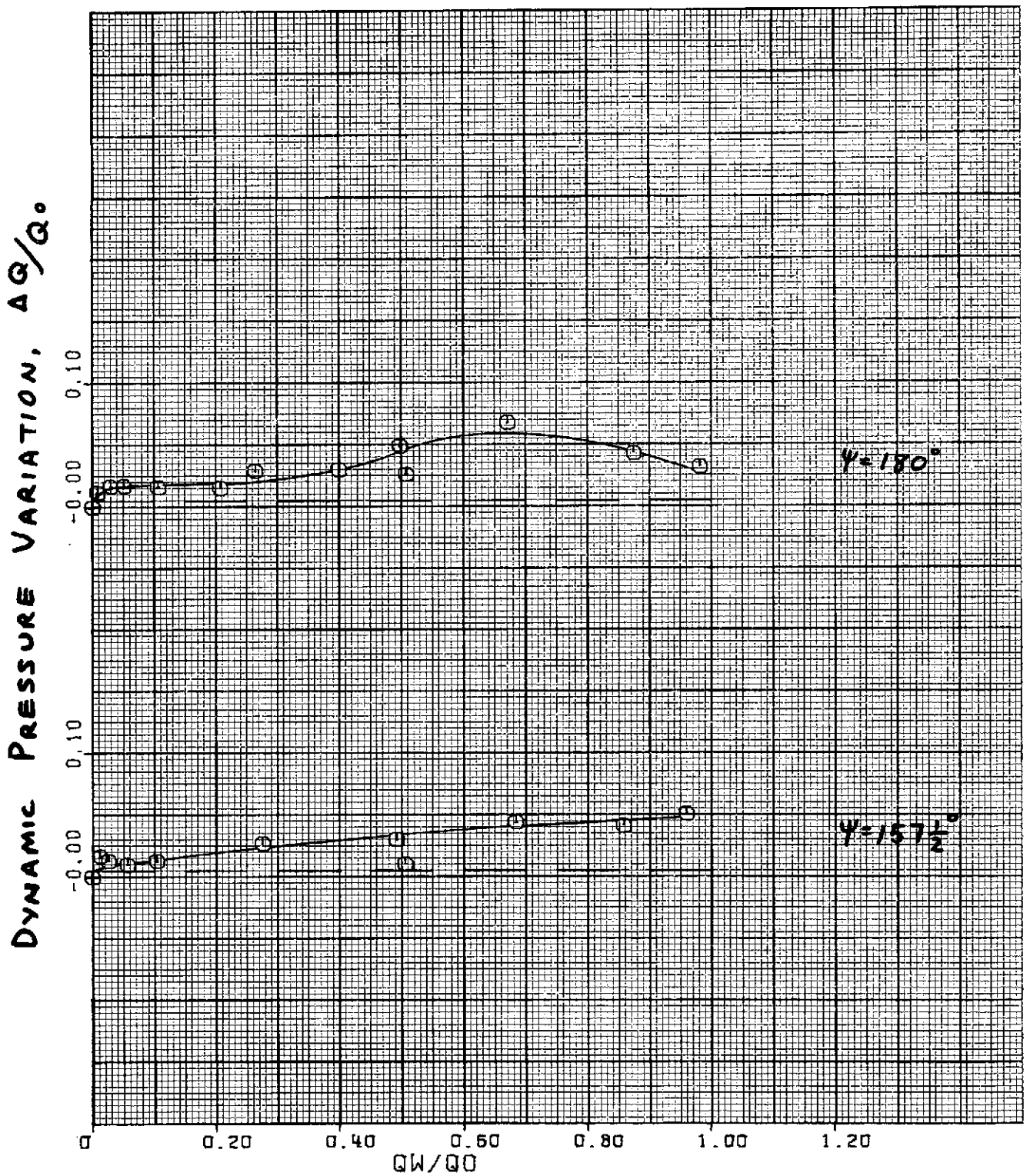

ψ = 180° and 157-1/2°.
(b) Dynamic pressure variation - concluded.

Figure 6. - Continued.

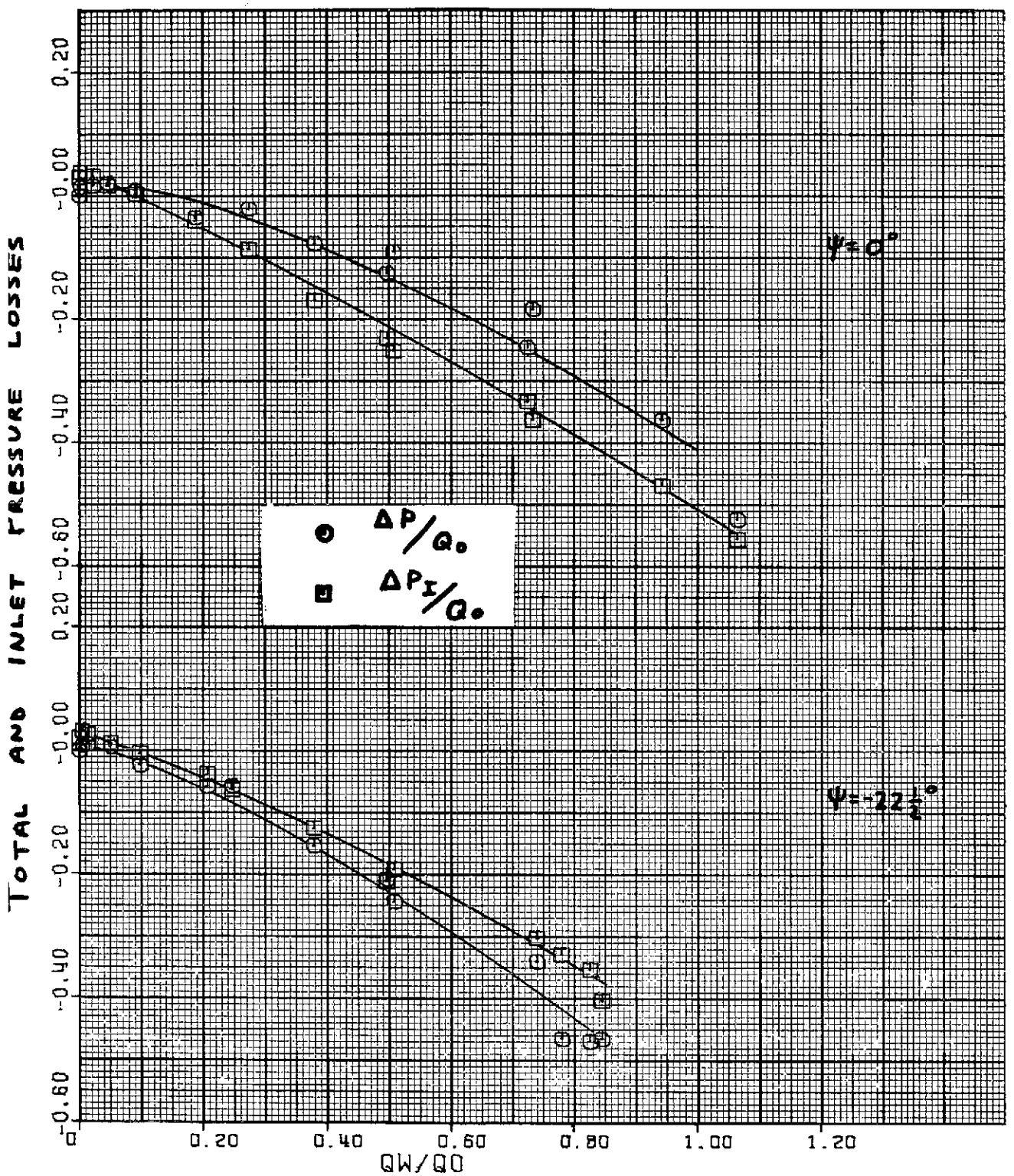

ψ = 0° and -22-1/2°.
(c) Pressure losses.

Figure 6. - Continued.

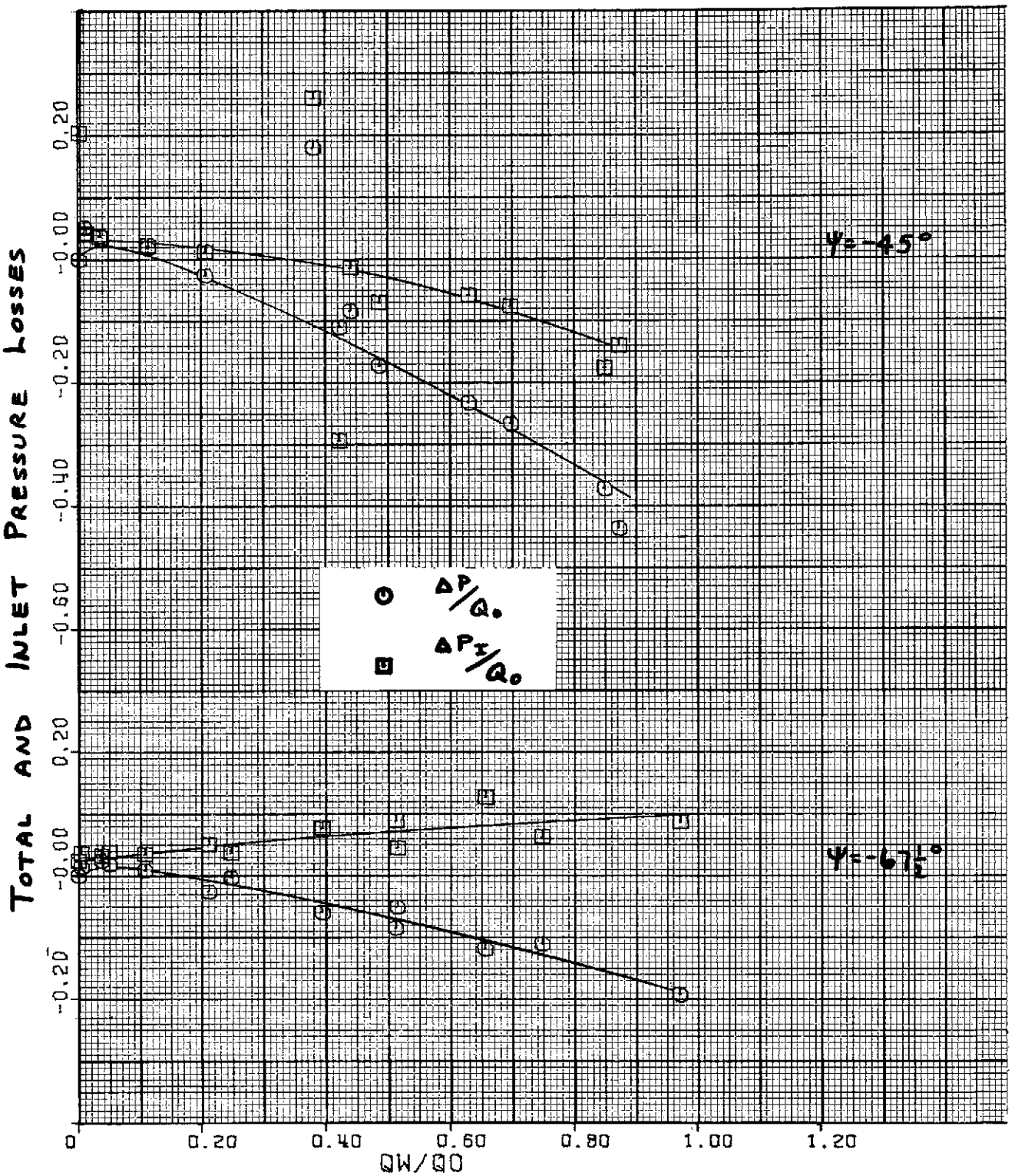

ψ = -45° and -67-1/2°.
(c) Pressure losses - continued.

Figure 6. - Continued.

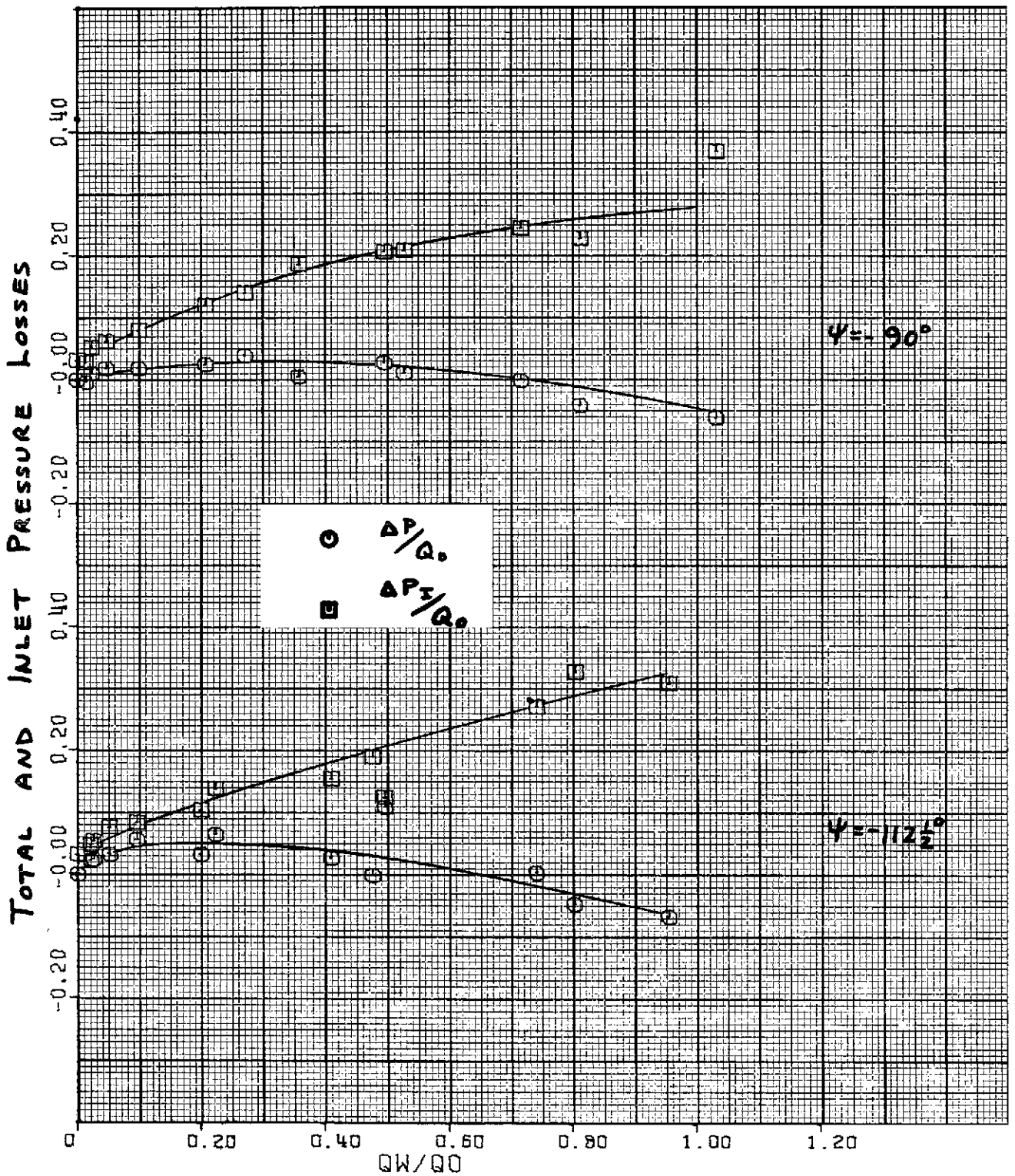

ψ =-90° and -112-1/2°.
(c) Pressure losses - continued.

Figure 6. - Continued.

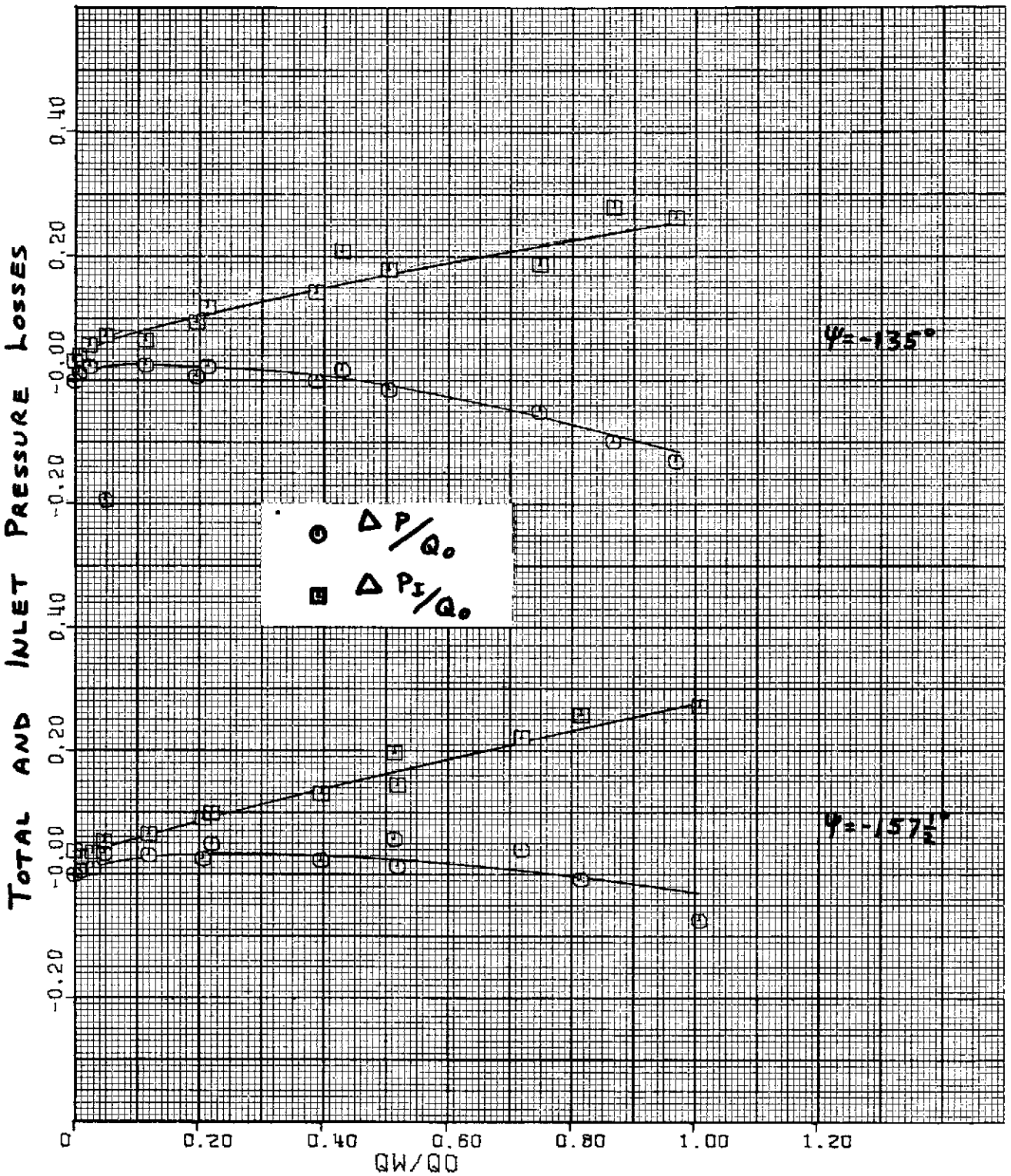

ψ = -135° and -157-1/2°.
(c) Pressure losses - continued.

Figure 6. - Continued.

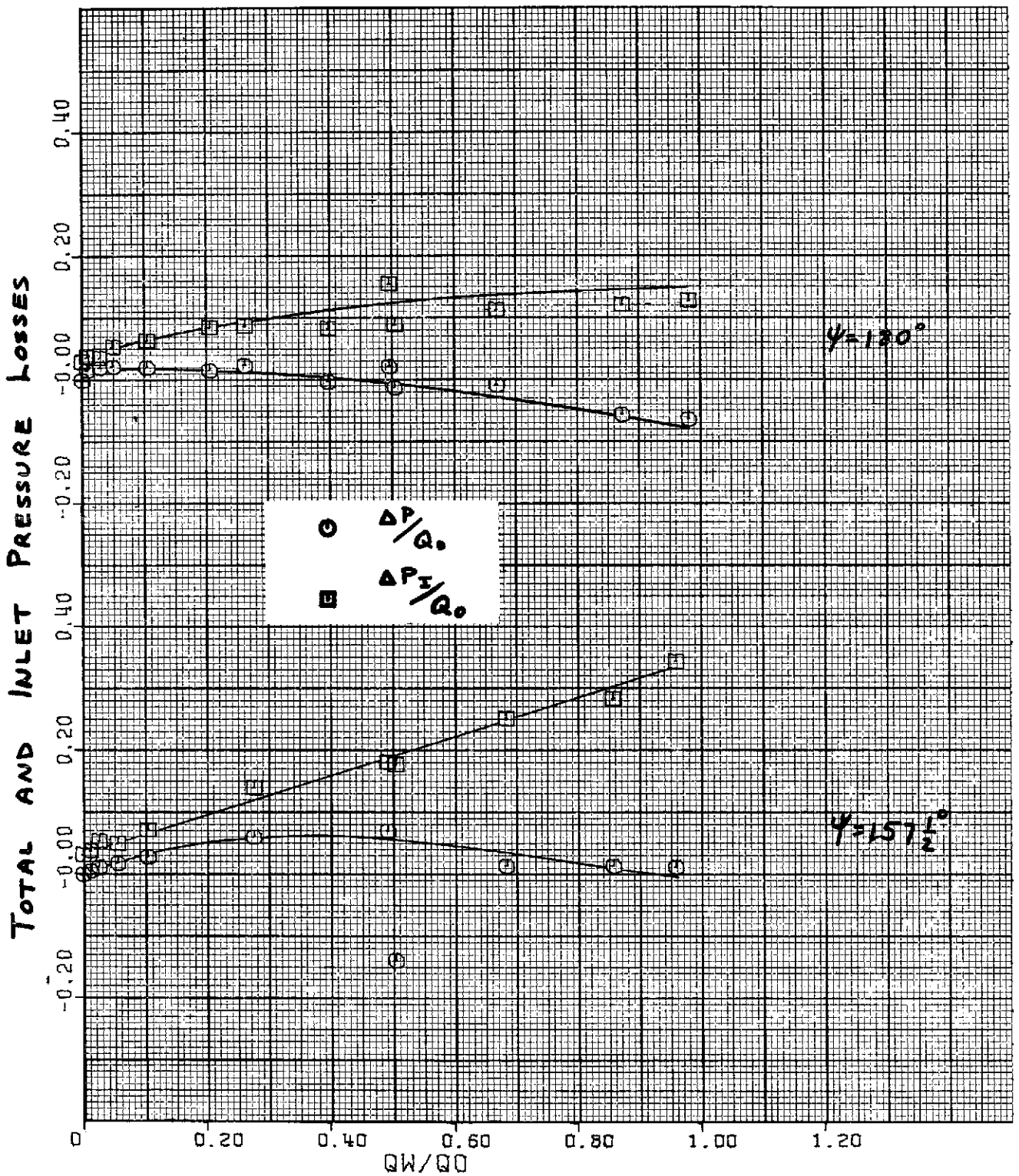

ψ = 180° and 157-1/2°.
(c) Pressure losses - concluded.

Figure 6. - Continued.

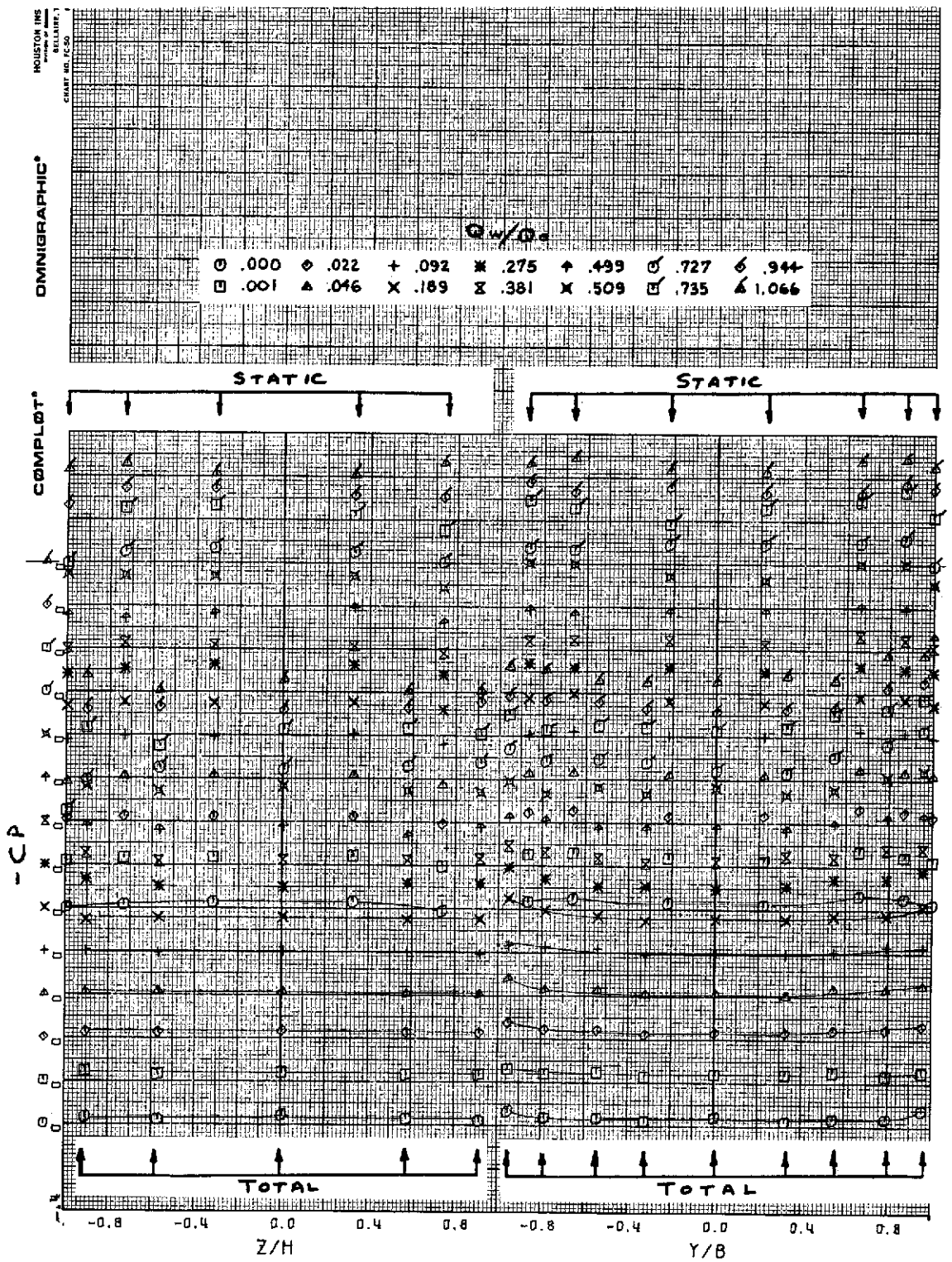

$\psi = 0°$.
(d) Local pressure coefficients.

Figure 6. - Continued.

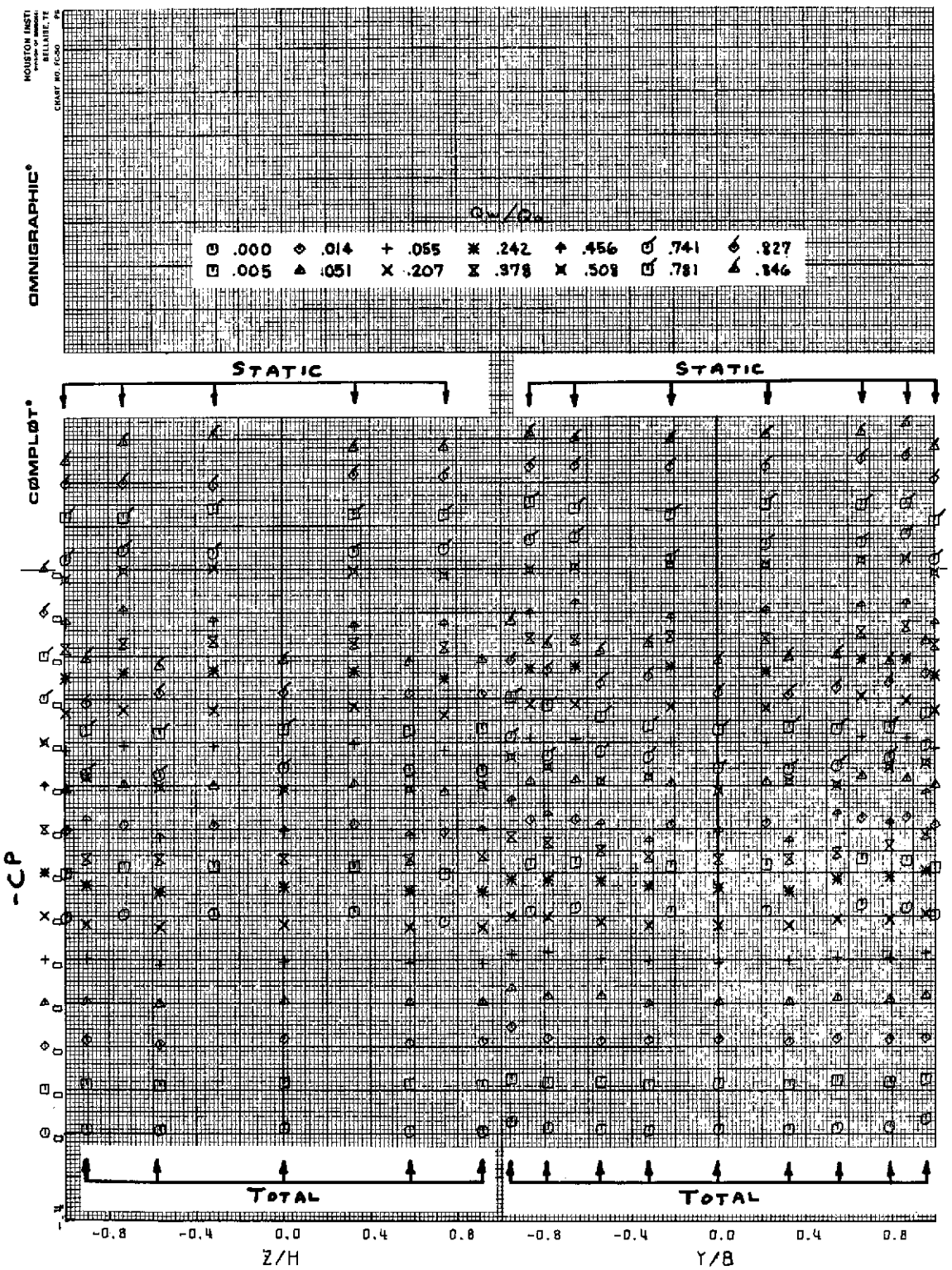

ψ = -22-1/2°.
(d) Local pressure coefficients - continued.

Figure 6. - Continued.

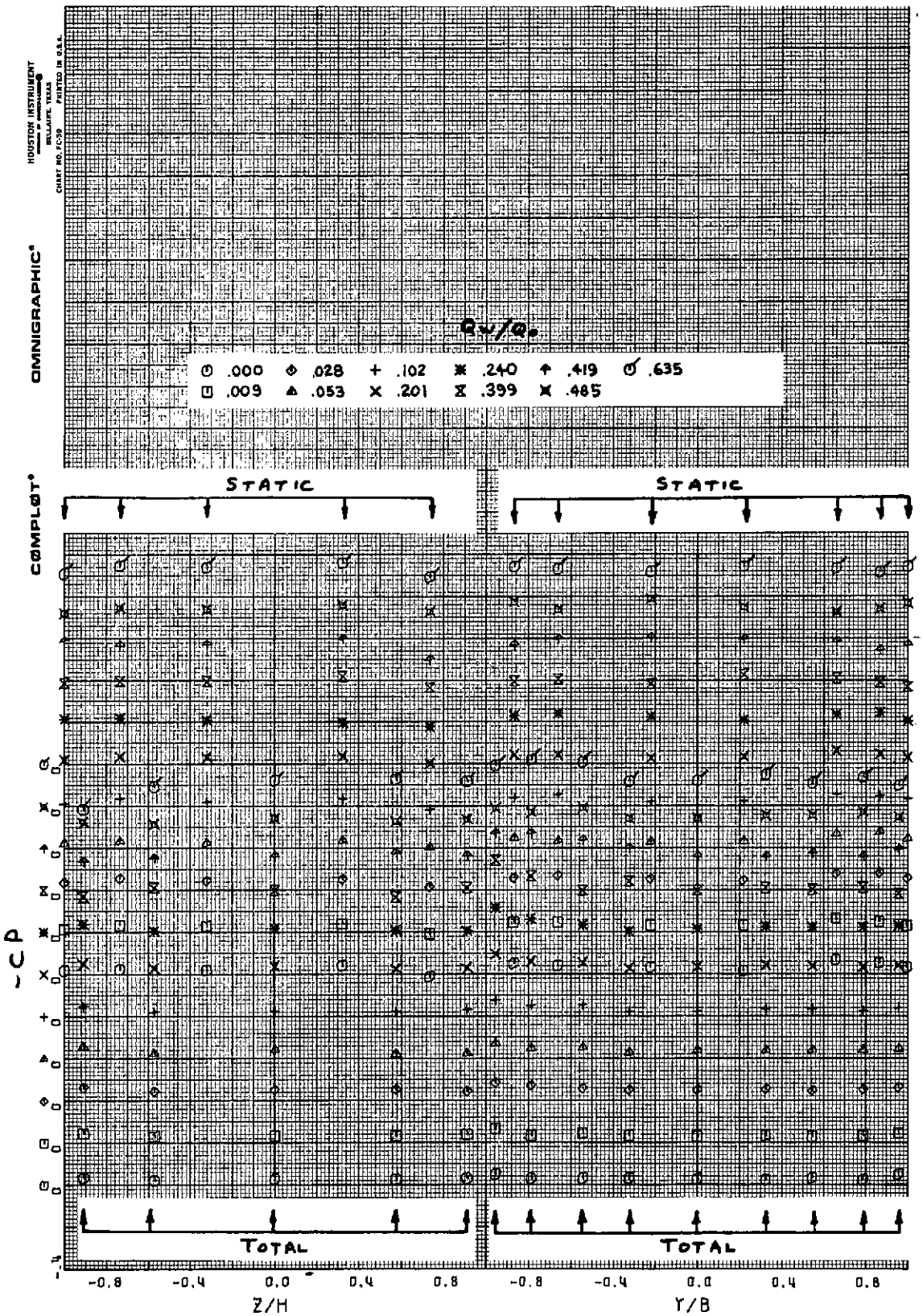

$\psi = -45°$.
(d) Local pressure coefficients - continued.

Figure 6. - Continued.

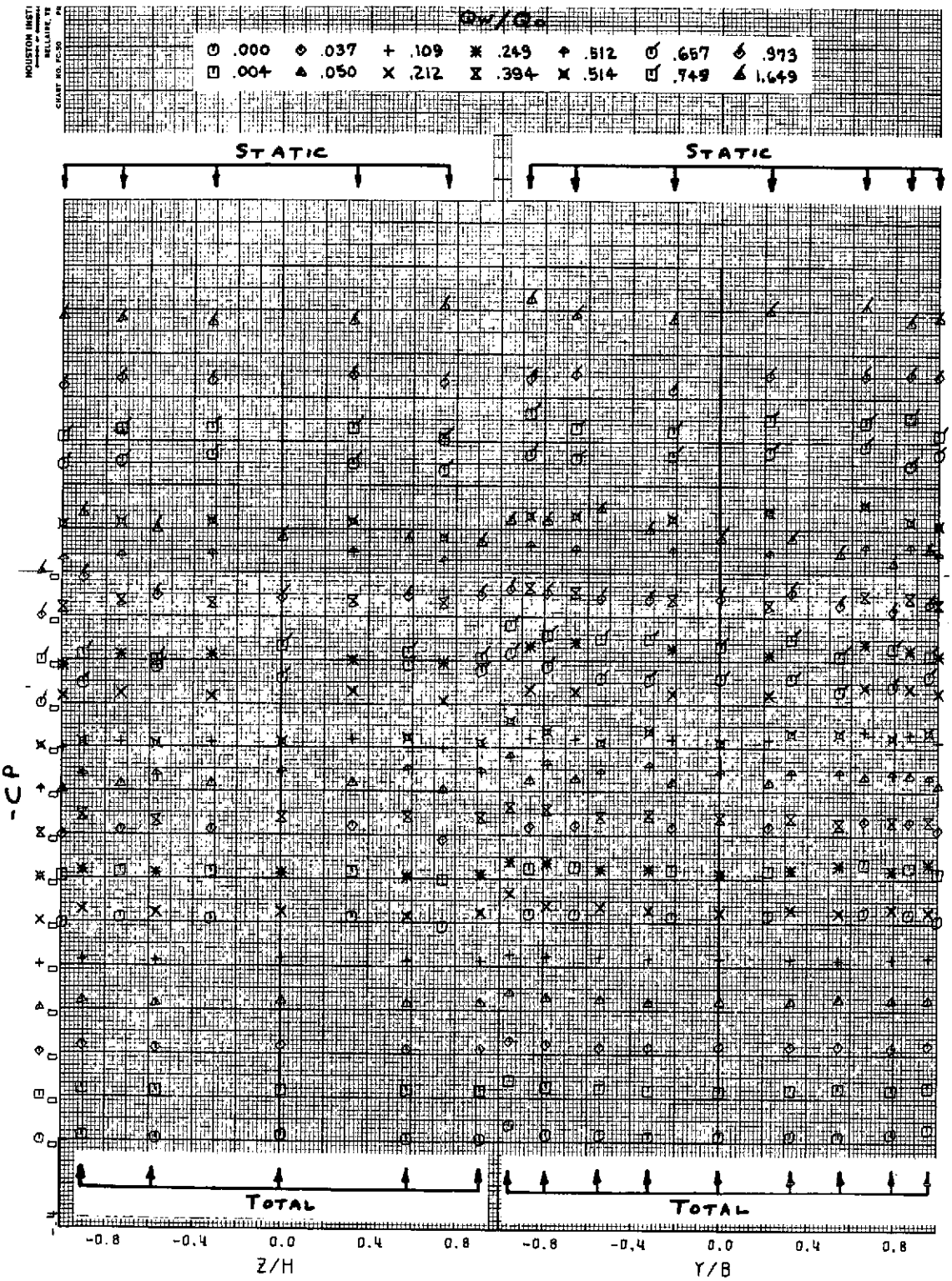

ψ = -67-1/2°.
(d) Local pressure coefficients - continued.

Figure 6. - Continued.

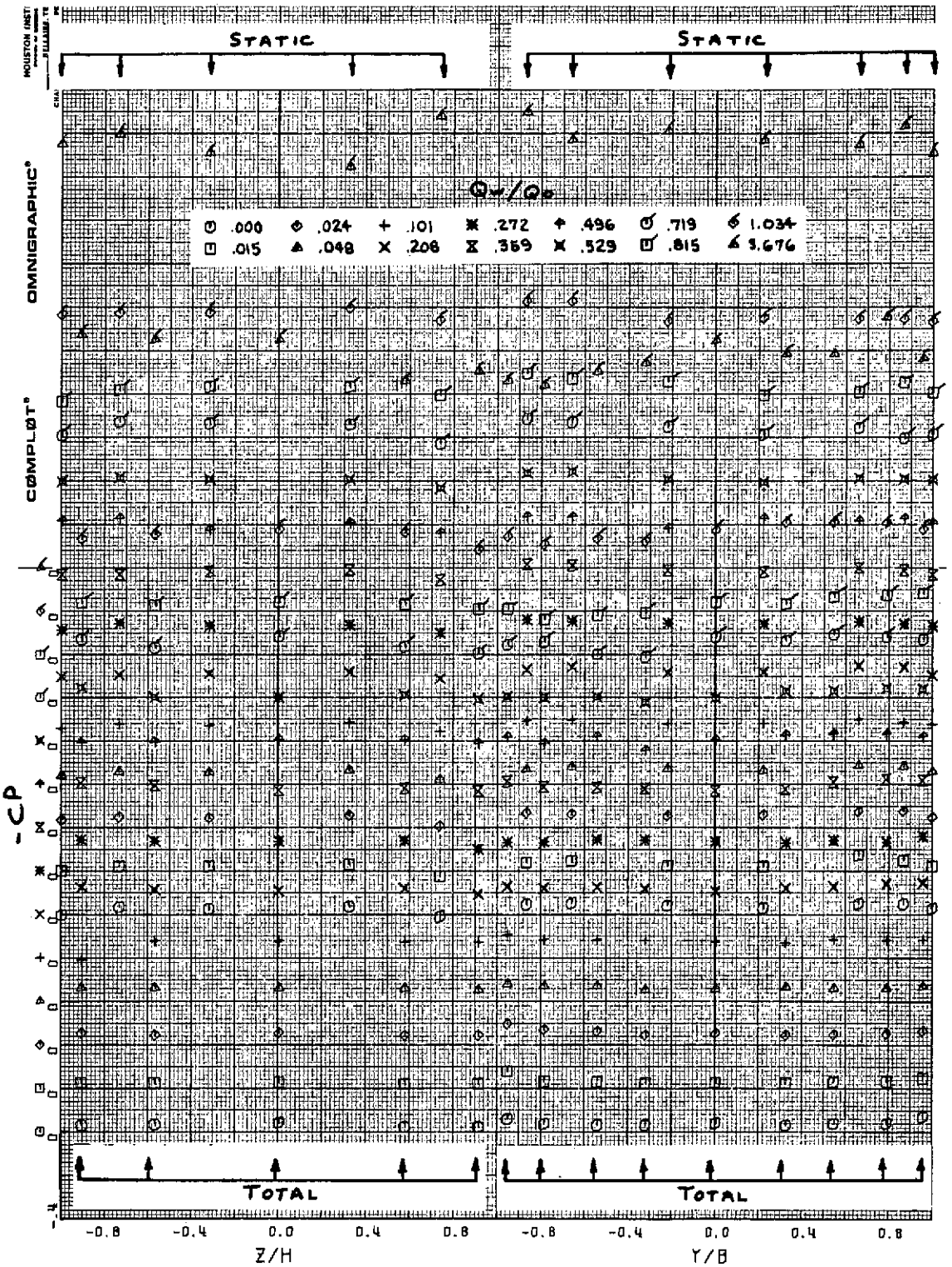

ψ = -90°.
(d) Local pressure coefficients - continued.

Figure 6. - Continued.

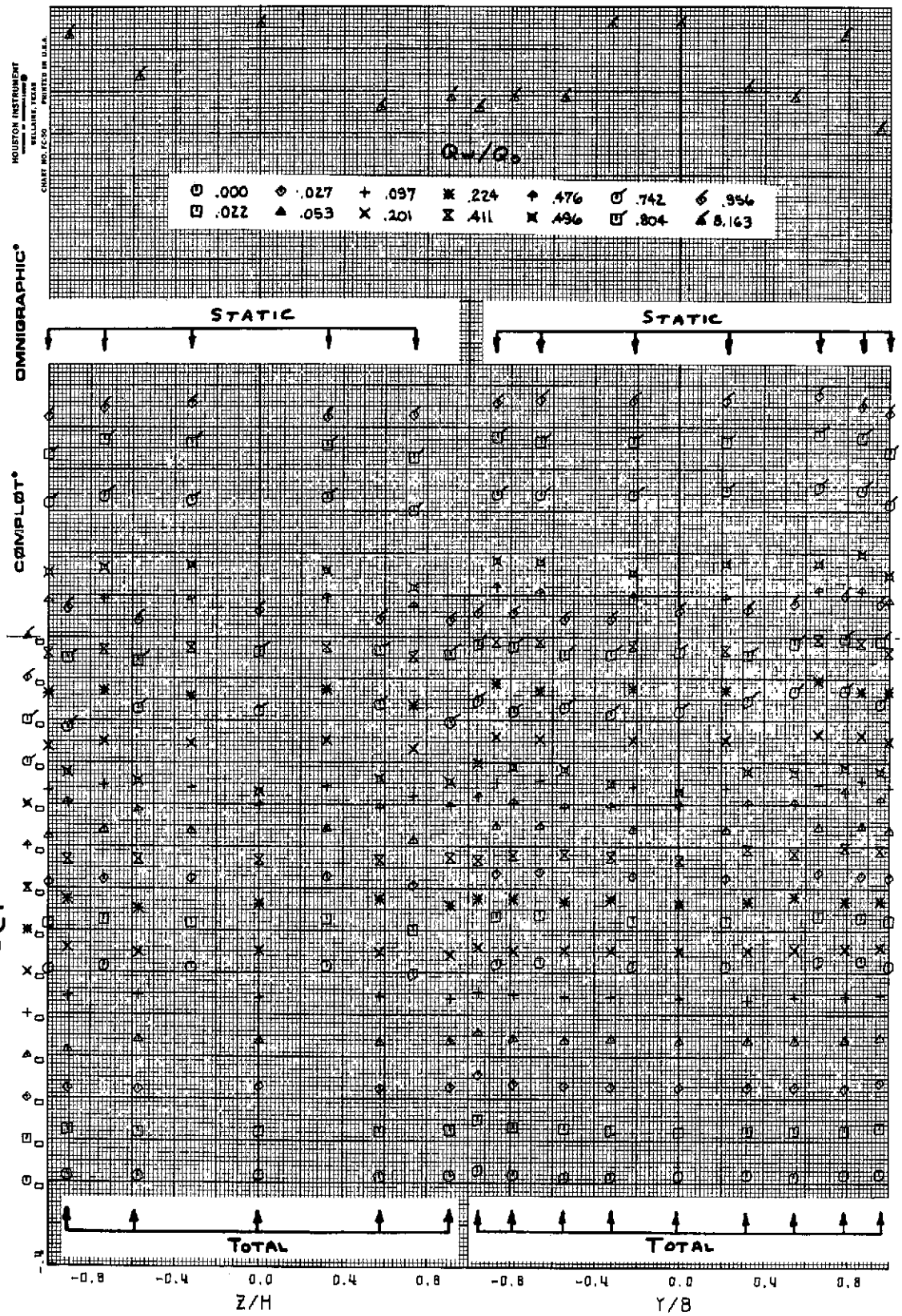

ψ = -112-1/2°.
(d) Local pressure coefficients - continued.

Figure 6. - Continued.

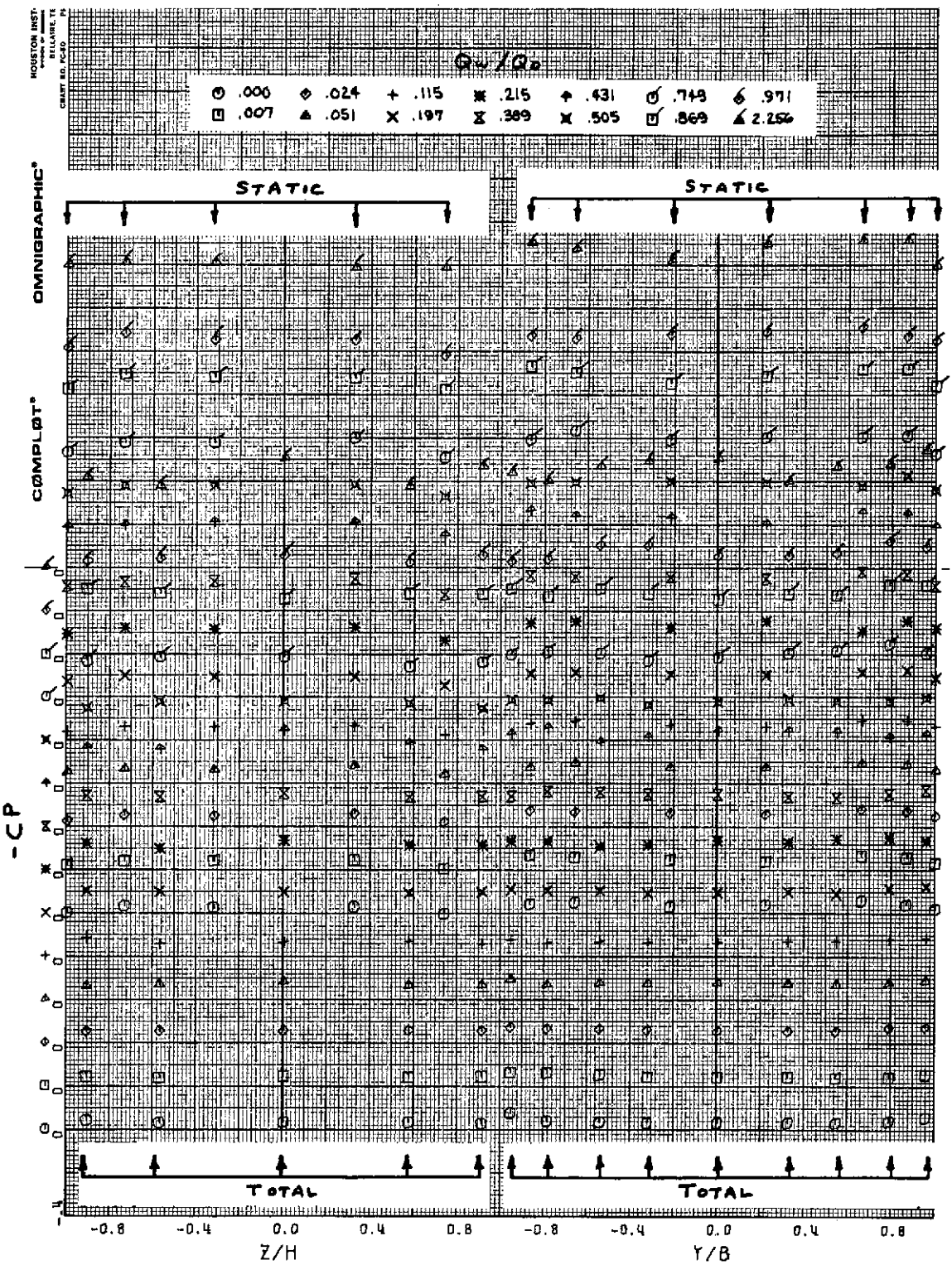

ψ = -135°.
(d) Local pressure coefficients - continued.

Figure 6. - Continued.

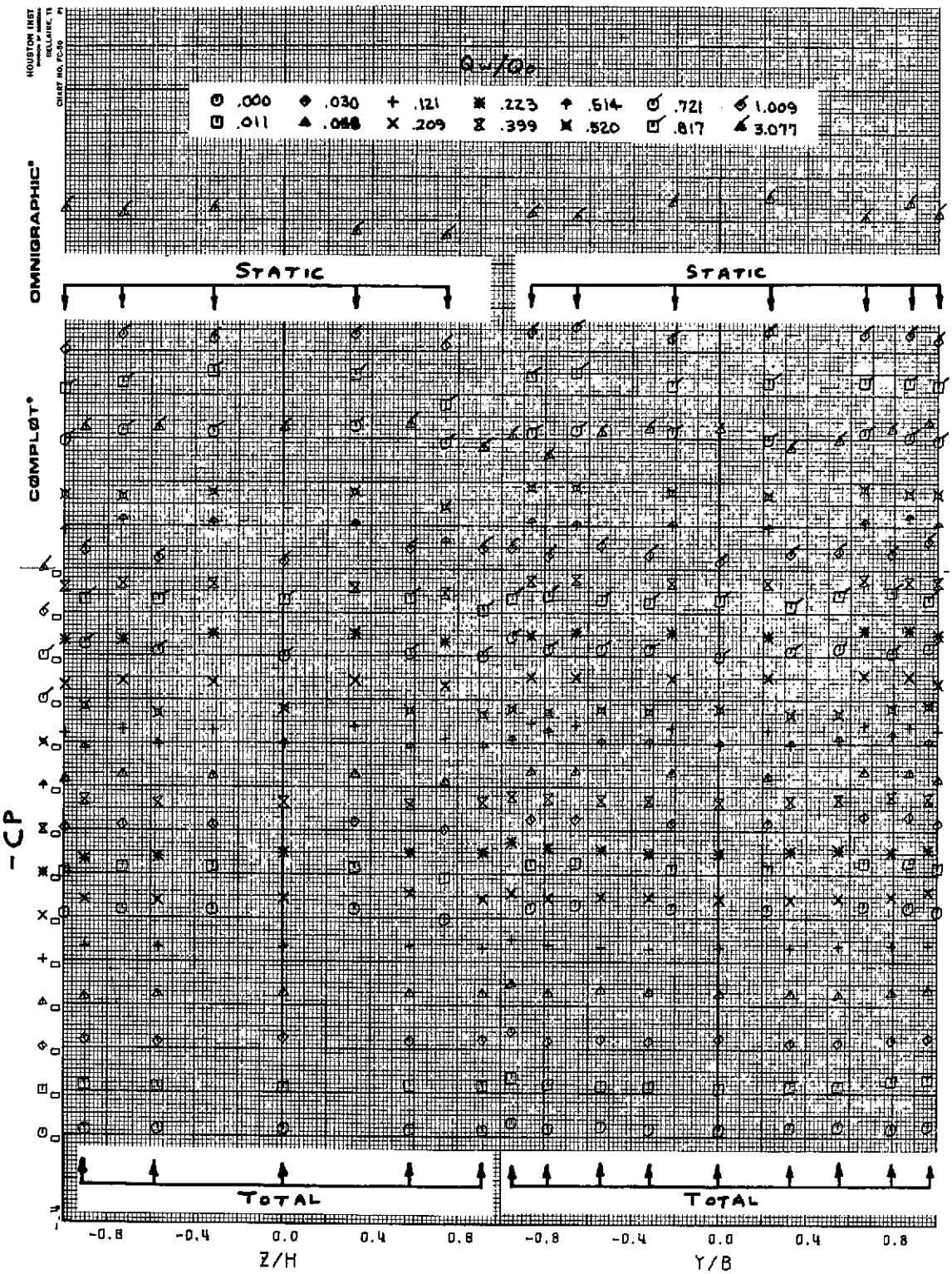

ψ = -157-1/2°.
(d) Local pressure coefficients - continued.

Figure 6. - Continued.

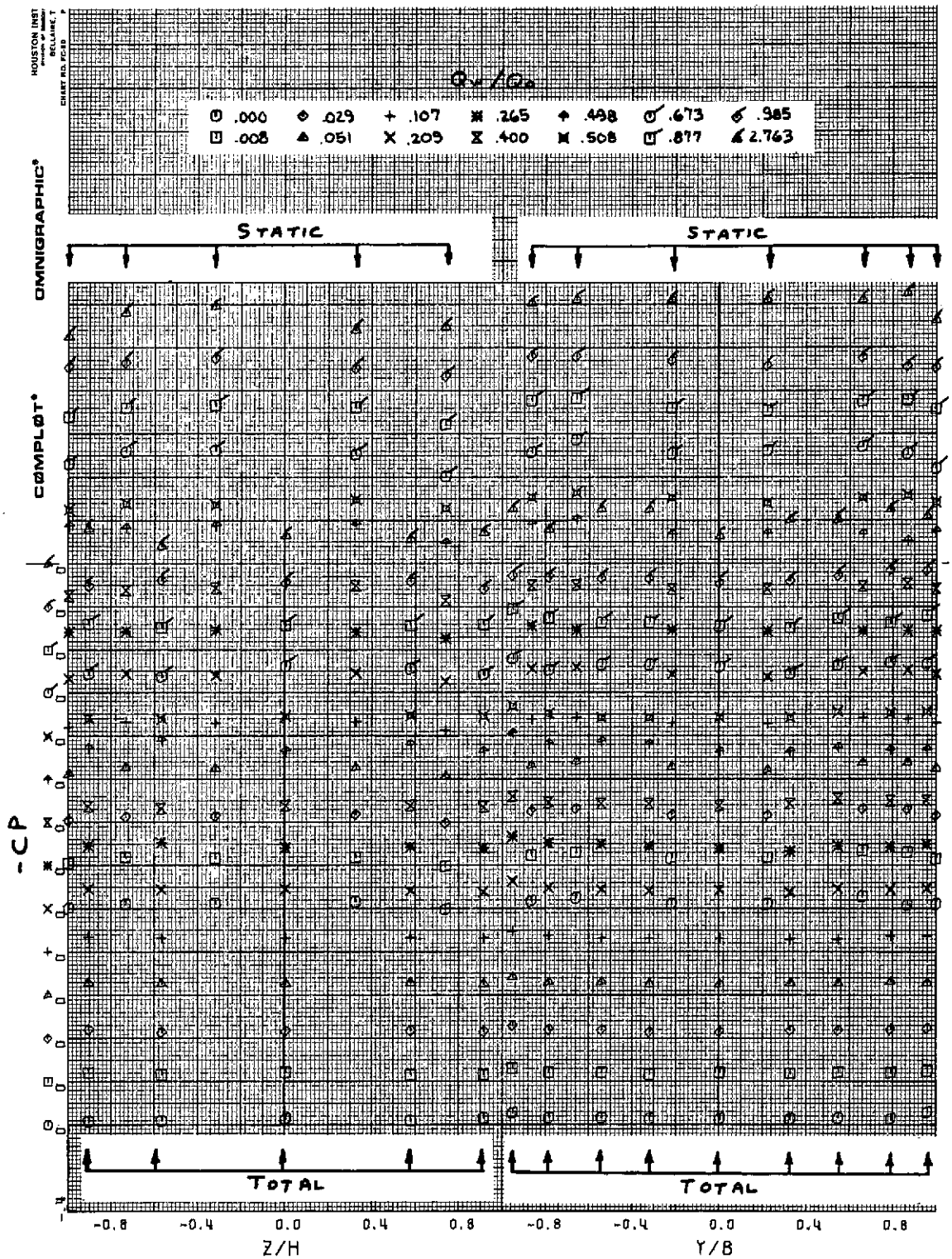

$\psi = 180°$.
(d) Local pressure coefficients - continued.

Figure 6. - Continued.

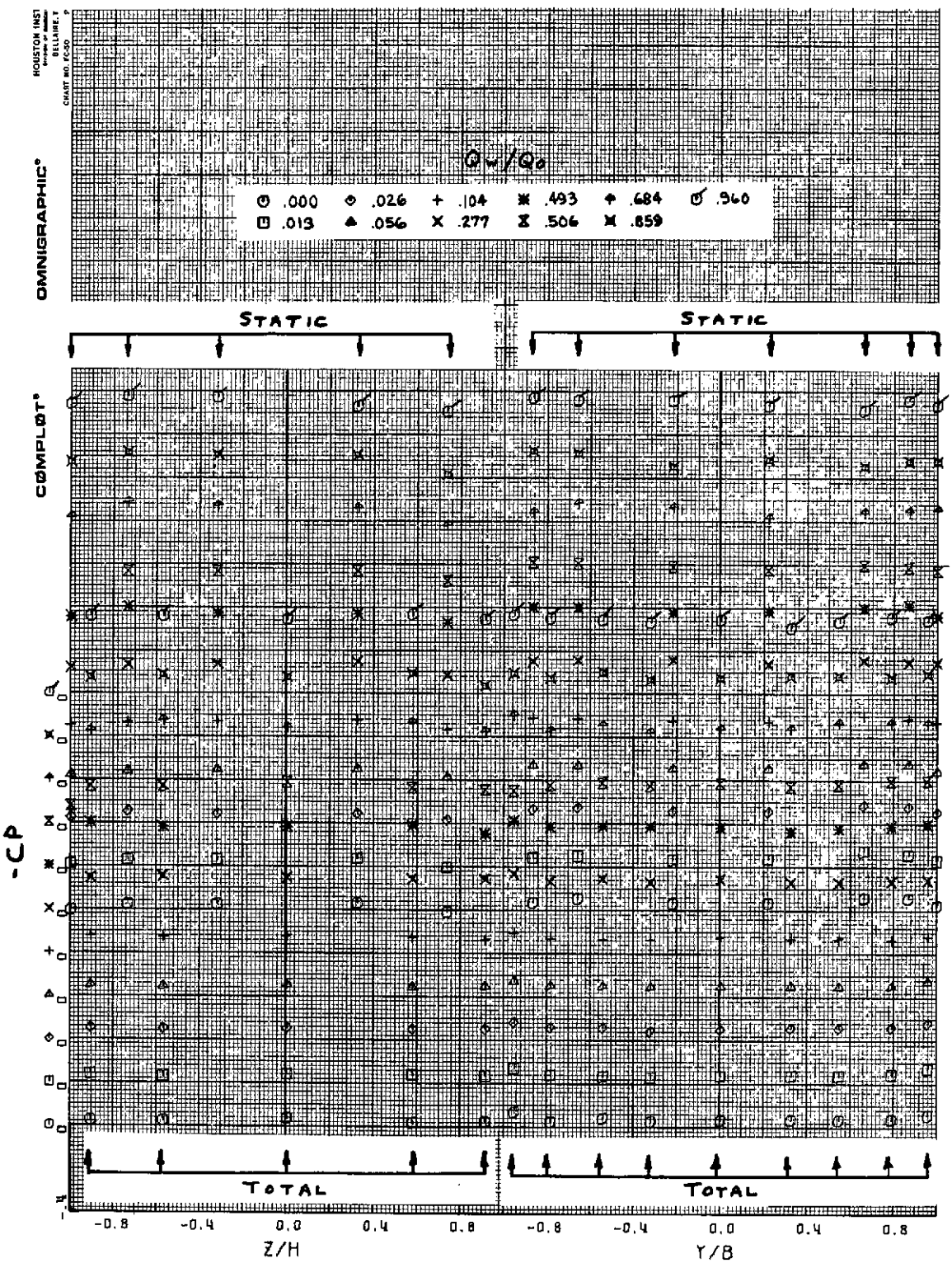

ψ = 157-1/2°.
(d) Local pressure coefficients - concluded.

Figure 6. - Concluded.

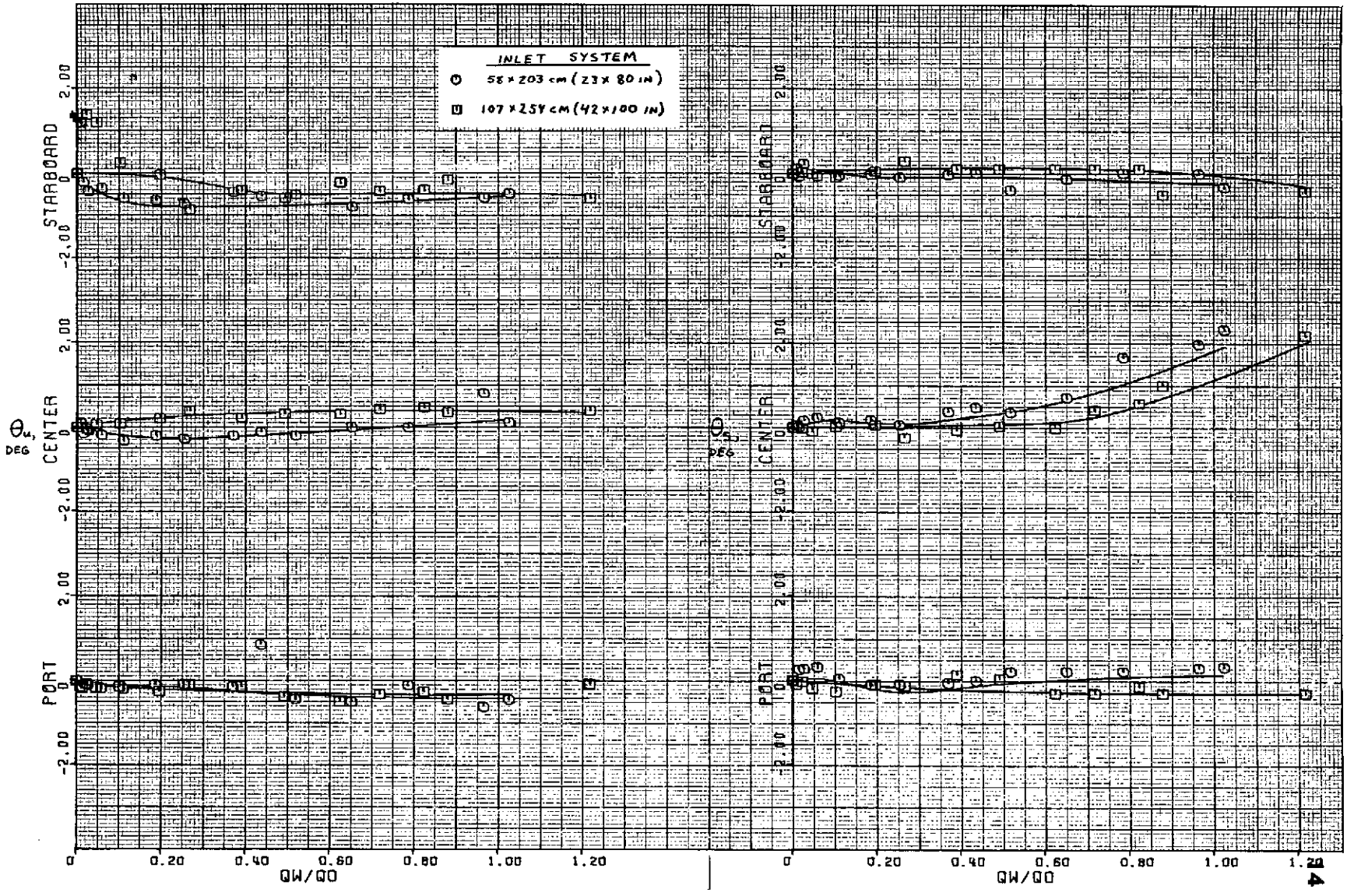

(a) Test section flow angularities.

Figure 7. - Effect of inlet size with roof posts in, peripheral flow straighteners inside, 2.54×2.54 cm (1×1 in) contraction flow straighteners, area ratio 20 exit.

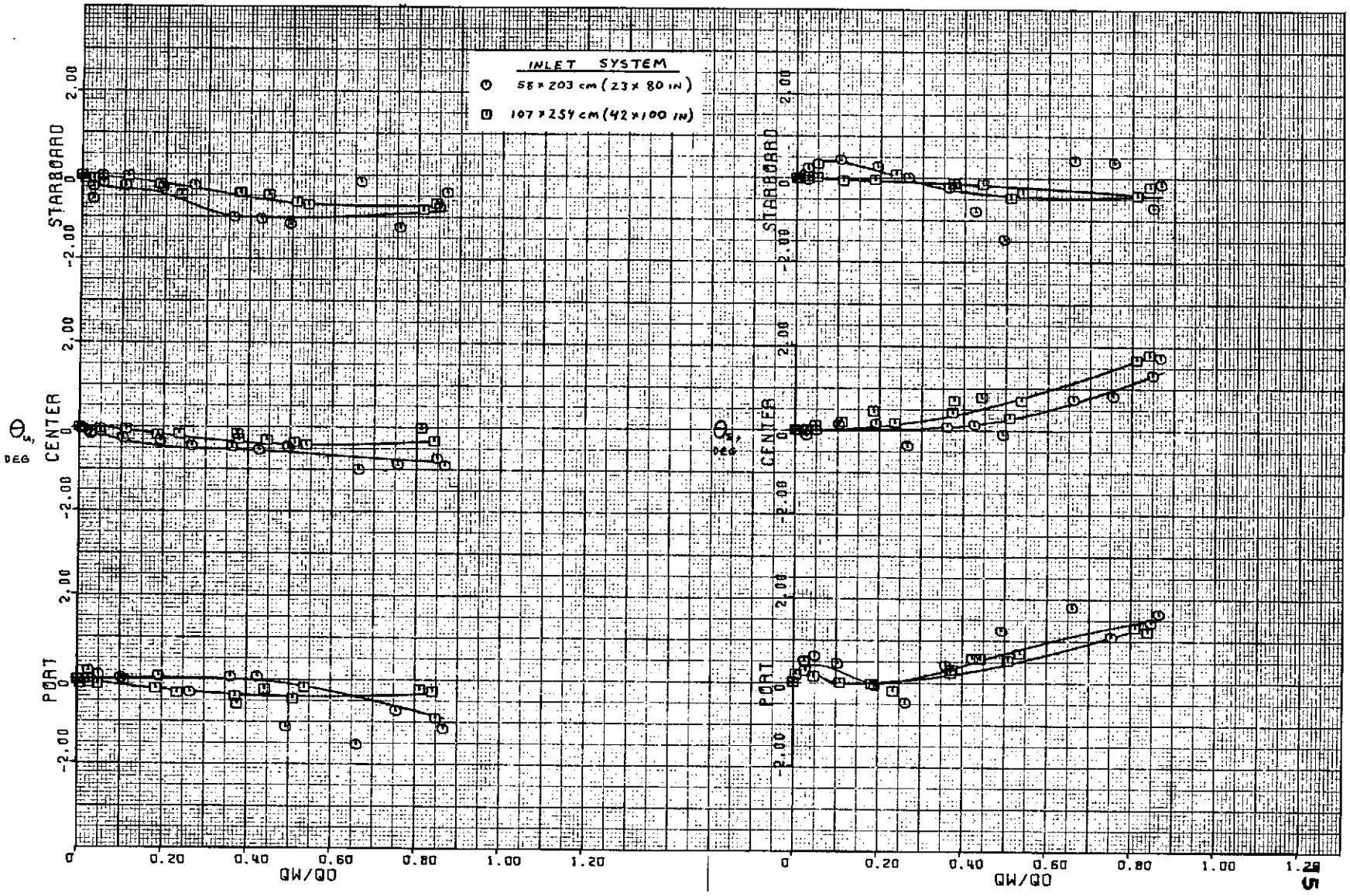

$\psi = -45°$.

(a) Test section flow angularities - continued.

Figure 7. - Continued.

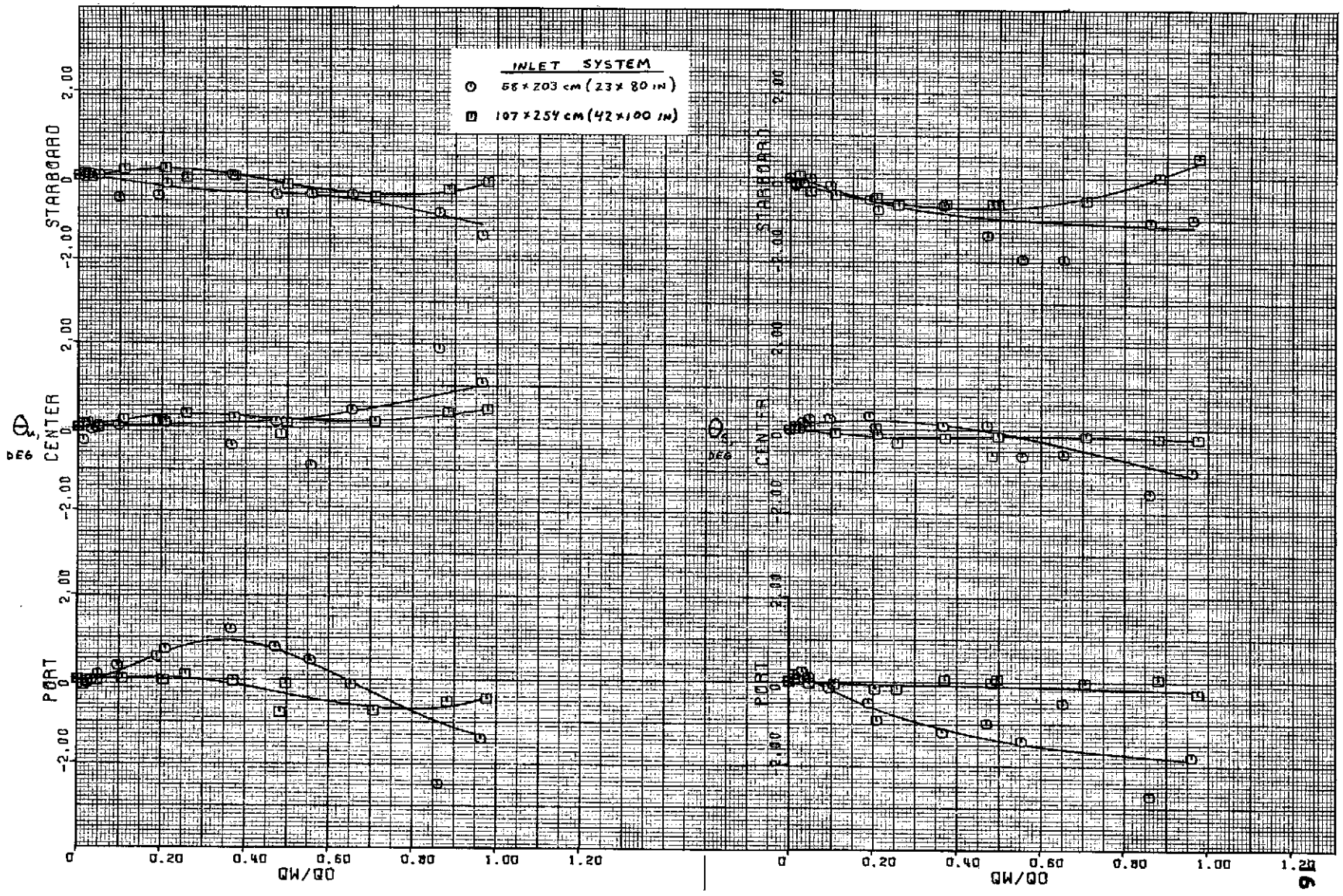

ψ = -90°.

(a) Test section flow angularities - continued.

Figure 7. - Continued.

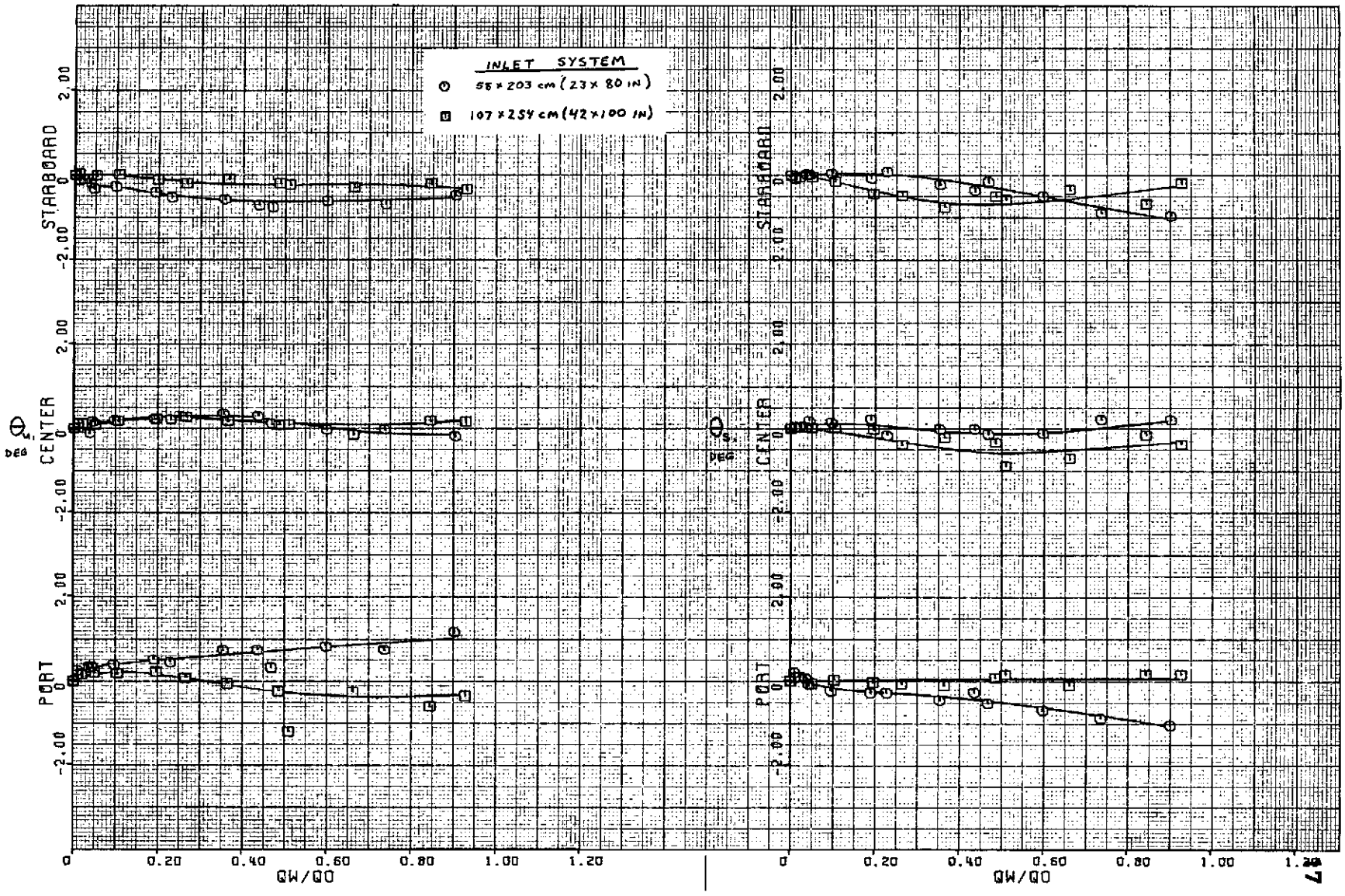

ψ = -135°.

(a) Test section flow angularities - continued.

Figure 7. - Continued.

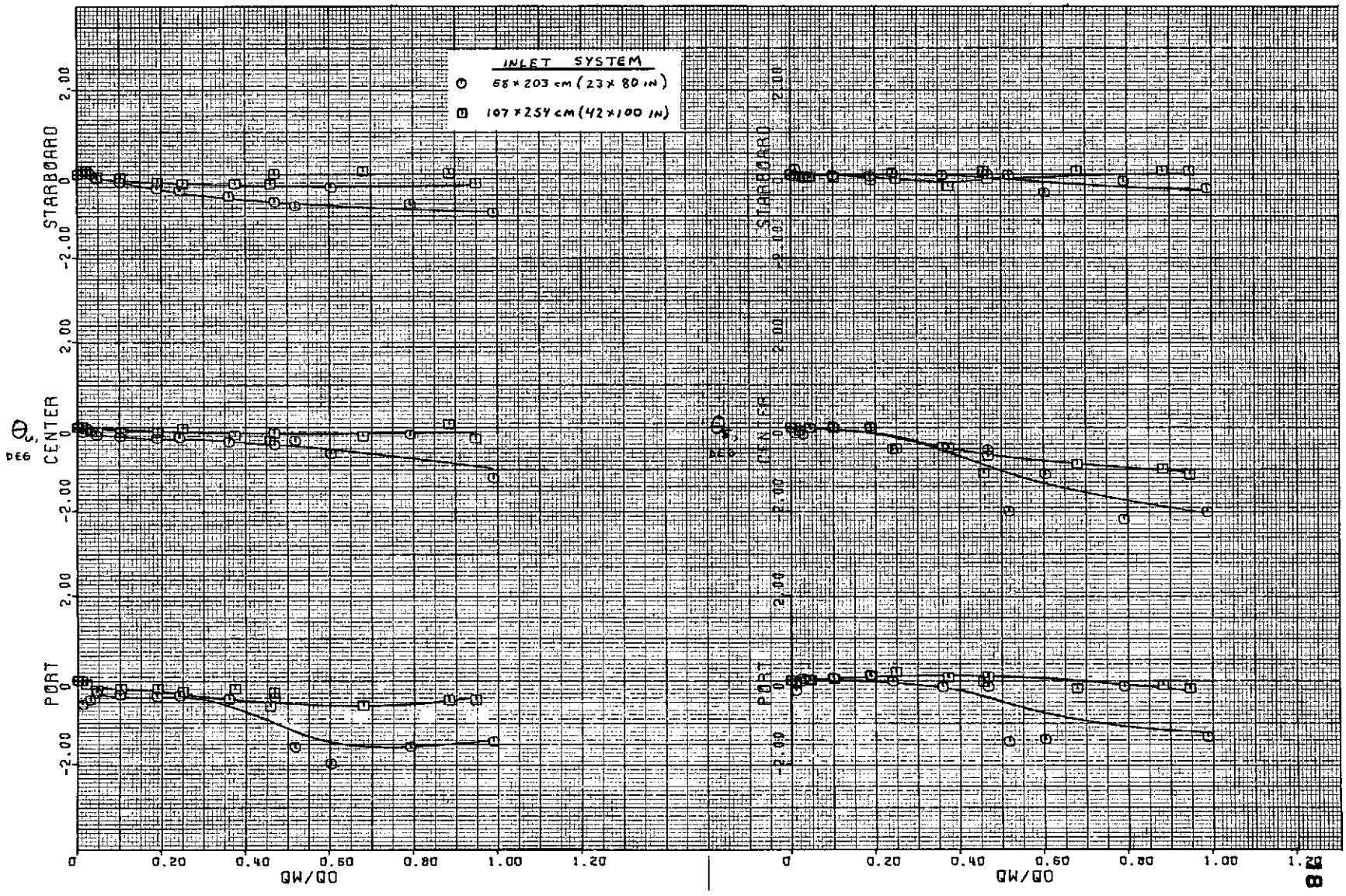

ψ = 180°.

(a) Test section flow angularities - concluded.

Figure 7. - Continued.

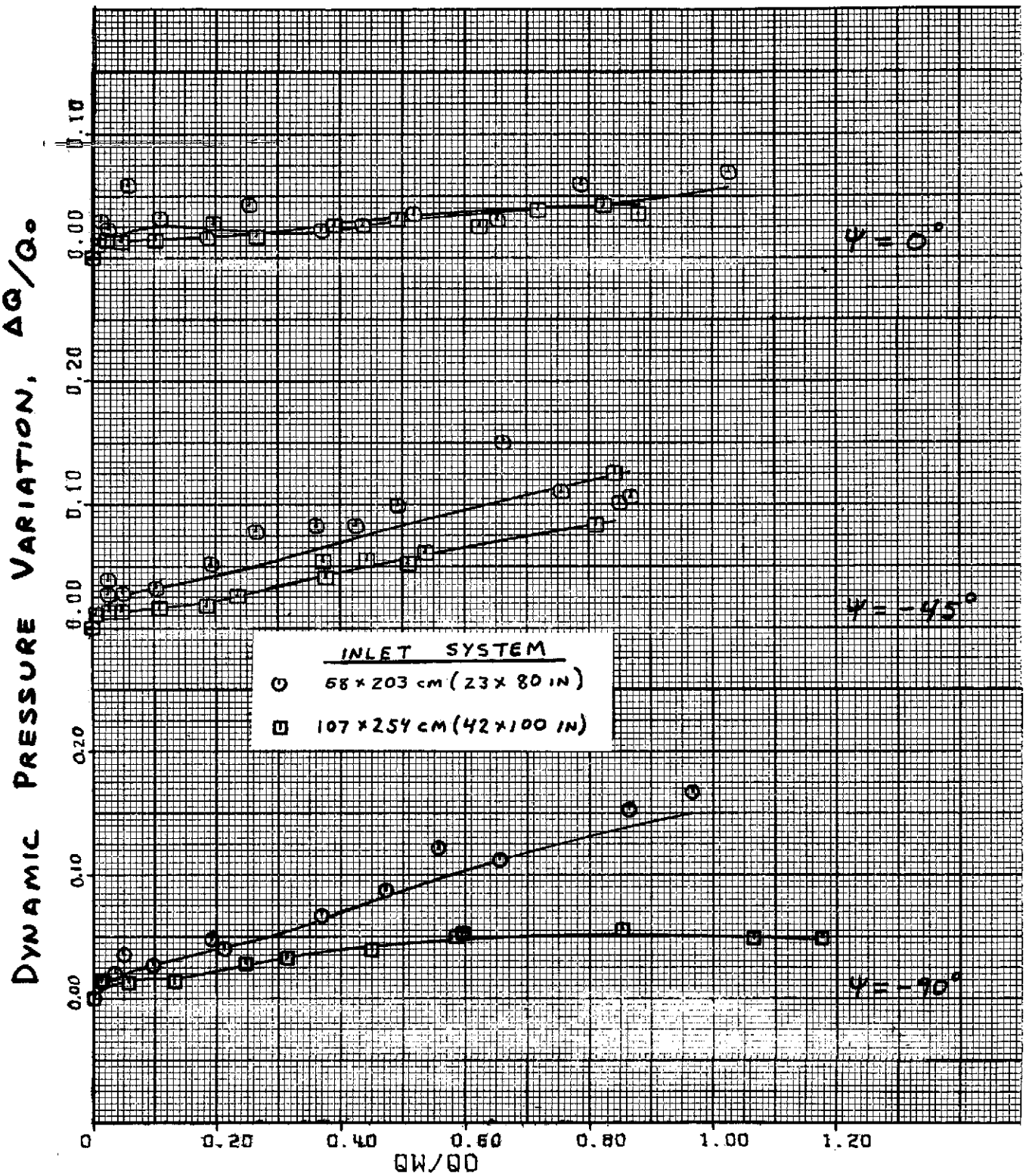

ψ = 0°, -45° and -90°.
(b) Dynamic pressure variation.

Figure 7. - Continued.

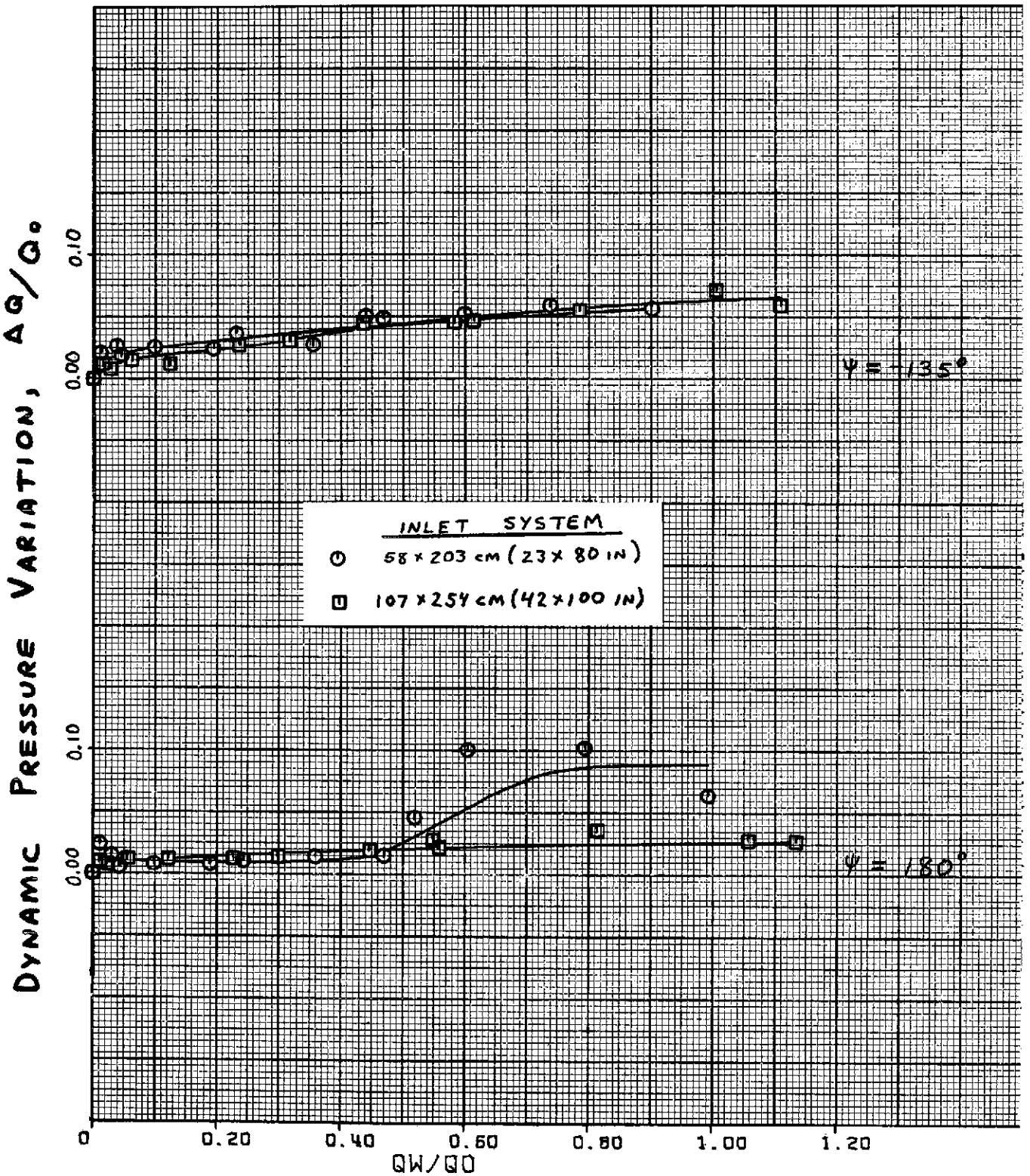

ψ = -135° and 180°.
(b) Dynamic pressure variation - concluded.

Figure 7. - Continued.

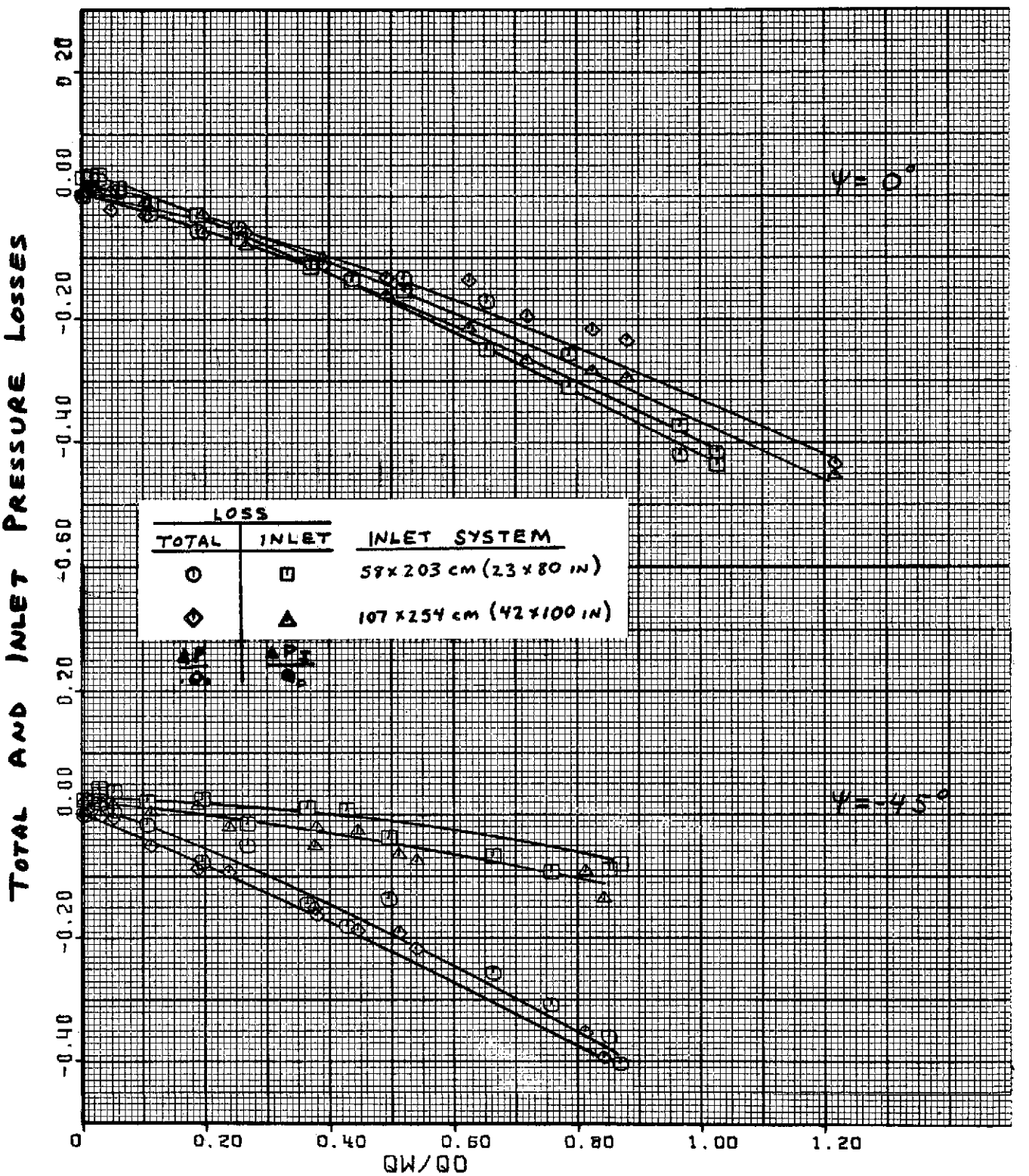

ψ = 0° and -45°.
(c) Pressure losses.

Figure 7. - Continued.

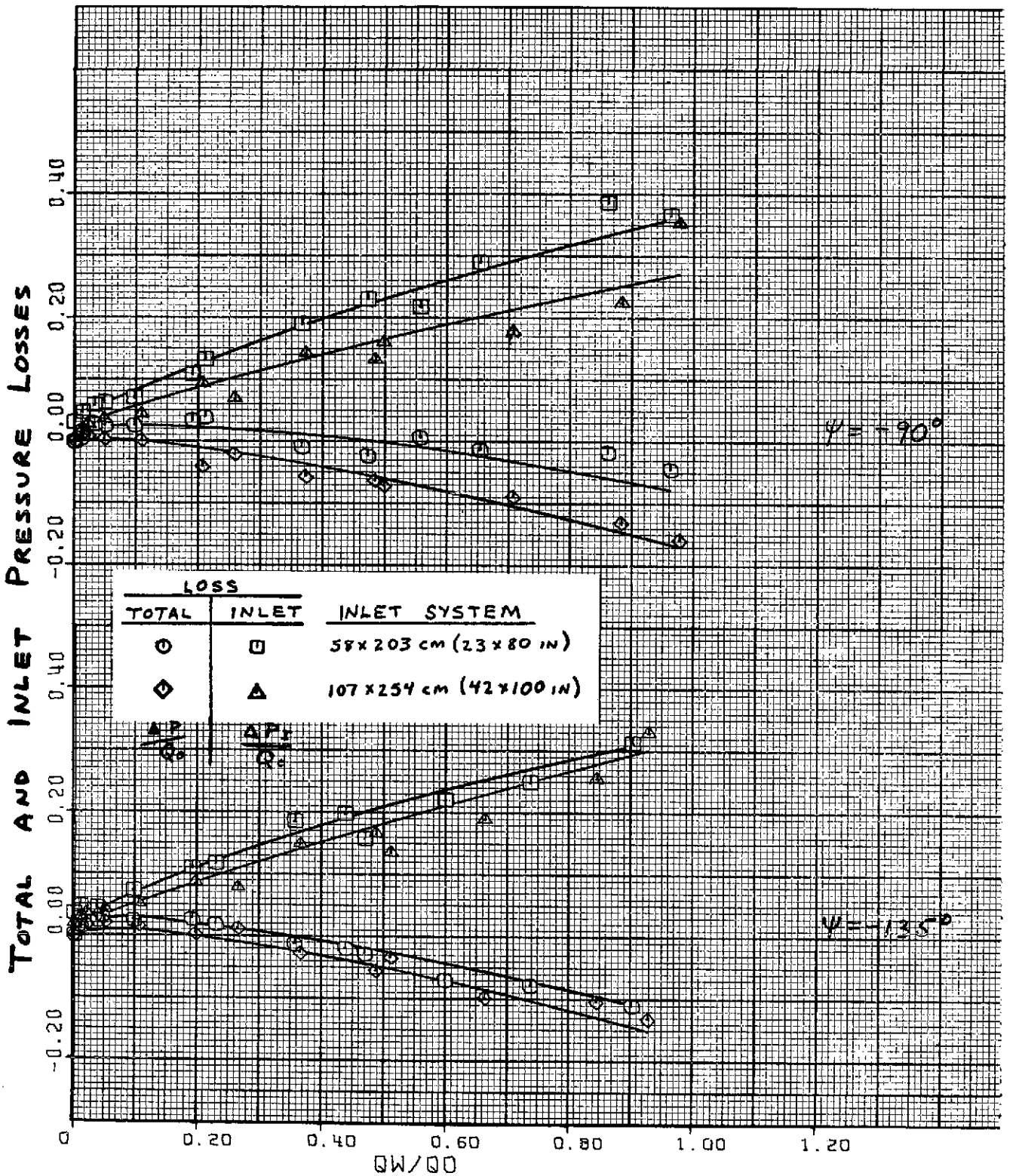

ψ = -90° and -135°.
(c) Pressure losses - continued.

Figure 7. - Continued.

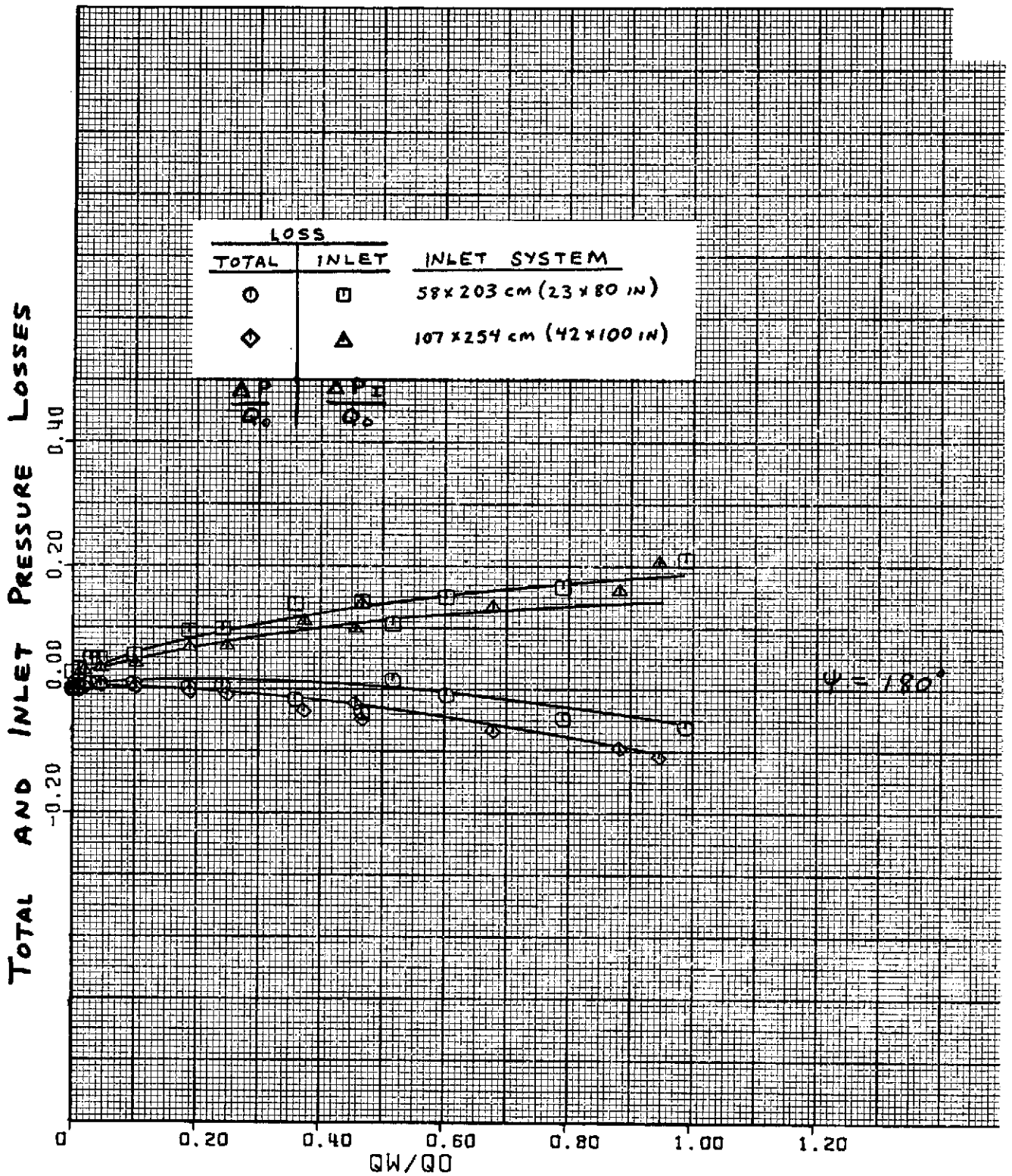

ψ = 180°.
(c) Pressure losses - concluded.

Figure 7. - Concluded.

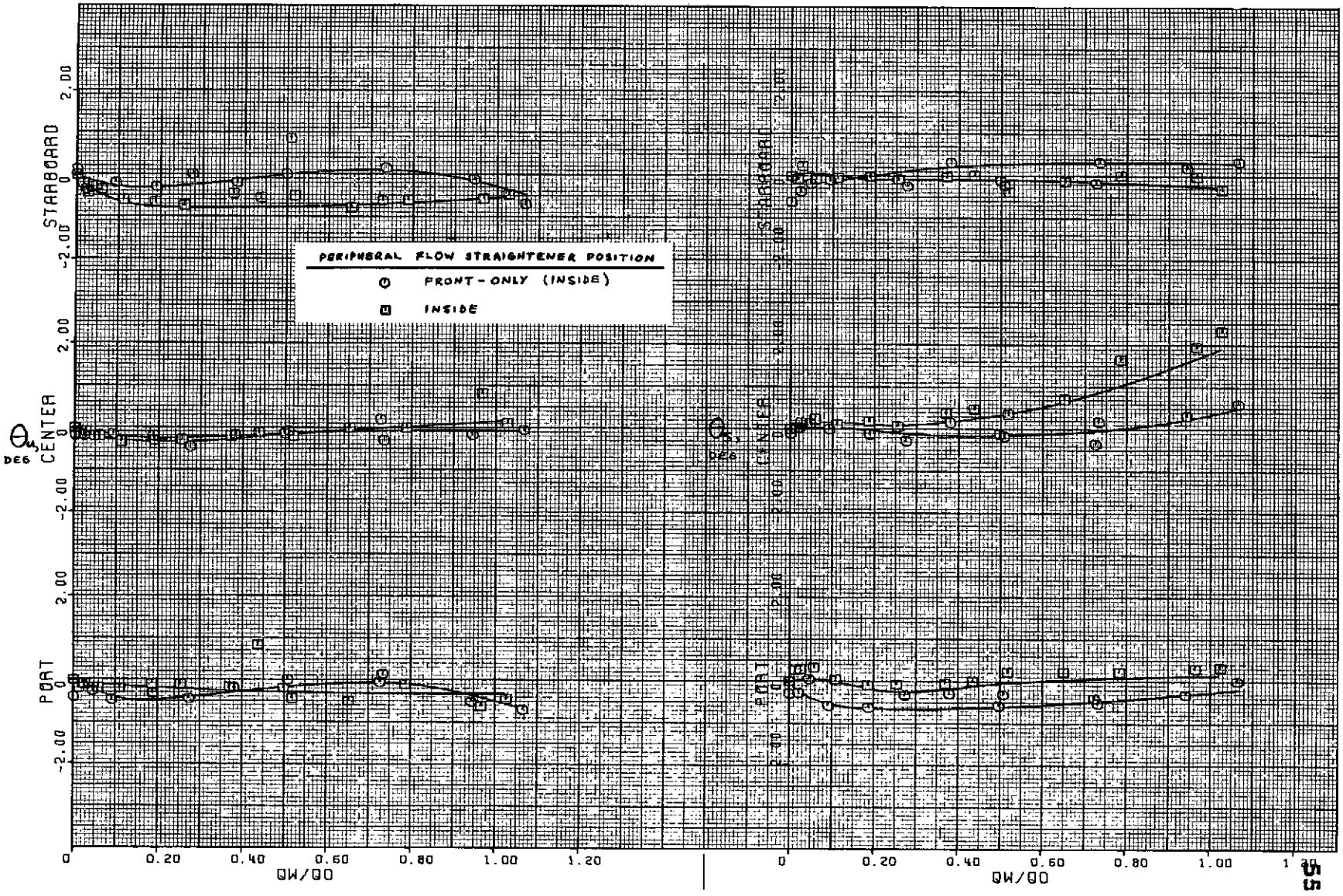

$\psi = 0°$.

(a) Test section flow angularities.

Figure 8. - Effect of peripheral flow straighteners with 58×203 cm (23×80 in) inlet, roof posts in, 2.54×2.54 cm (1×1 in) contraction flow straighteners, area ratio 20 exit.

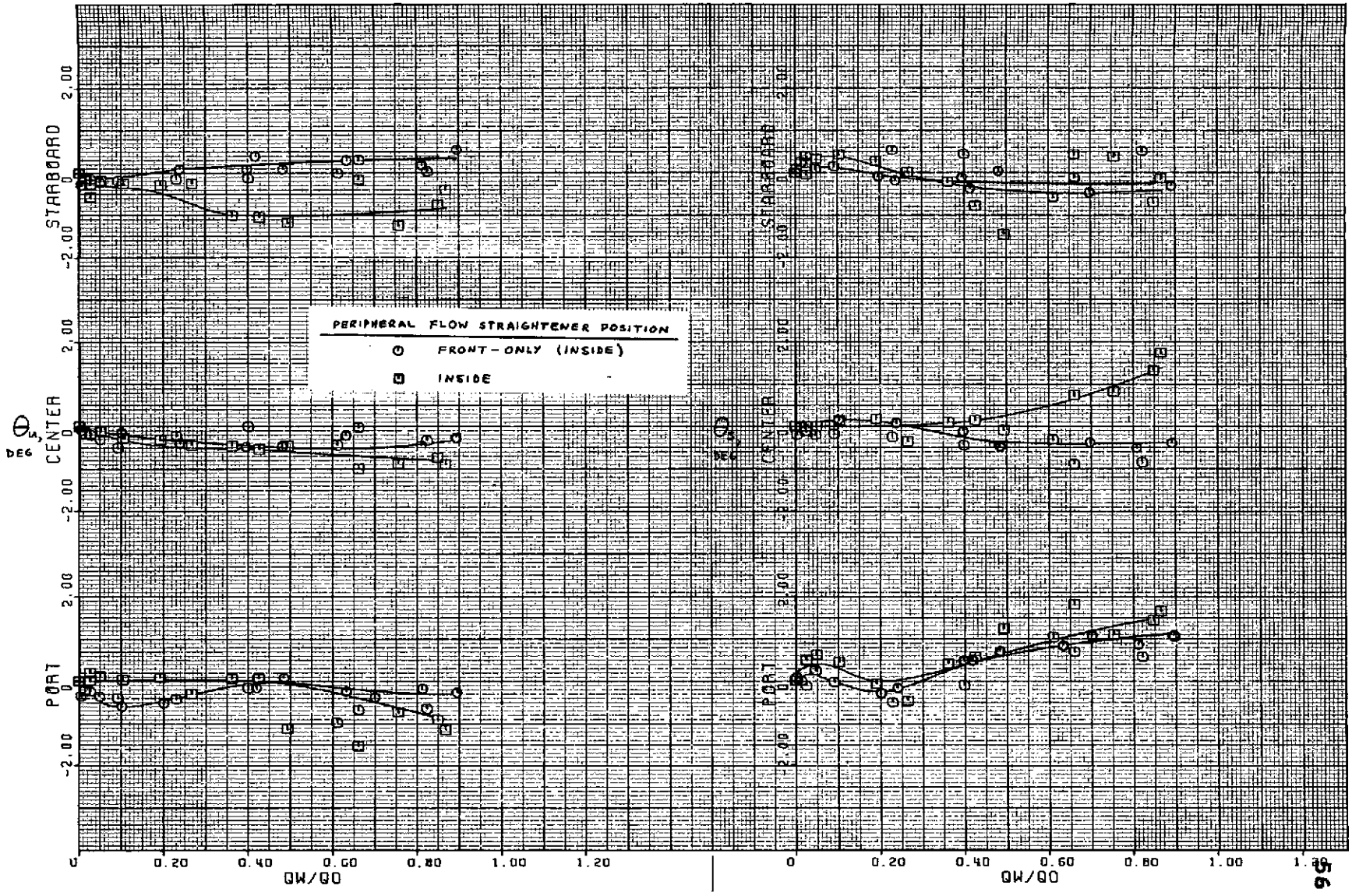

$\psi = -45°$.

(a) Test section flow angularities - continued.

Figure 8. - Continued.

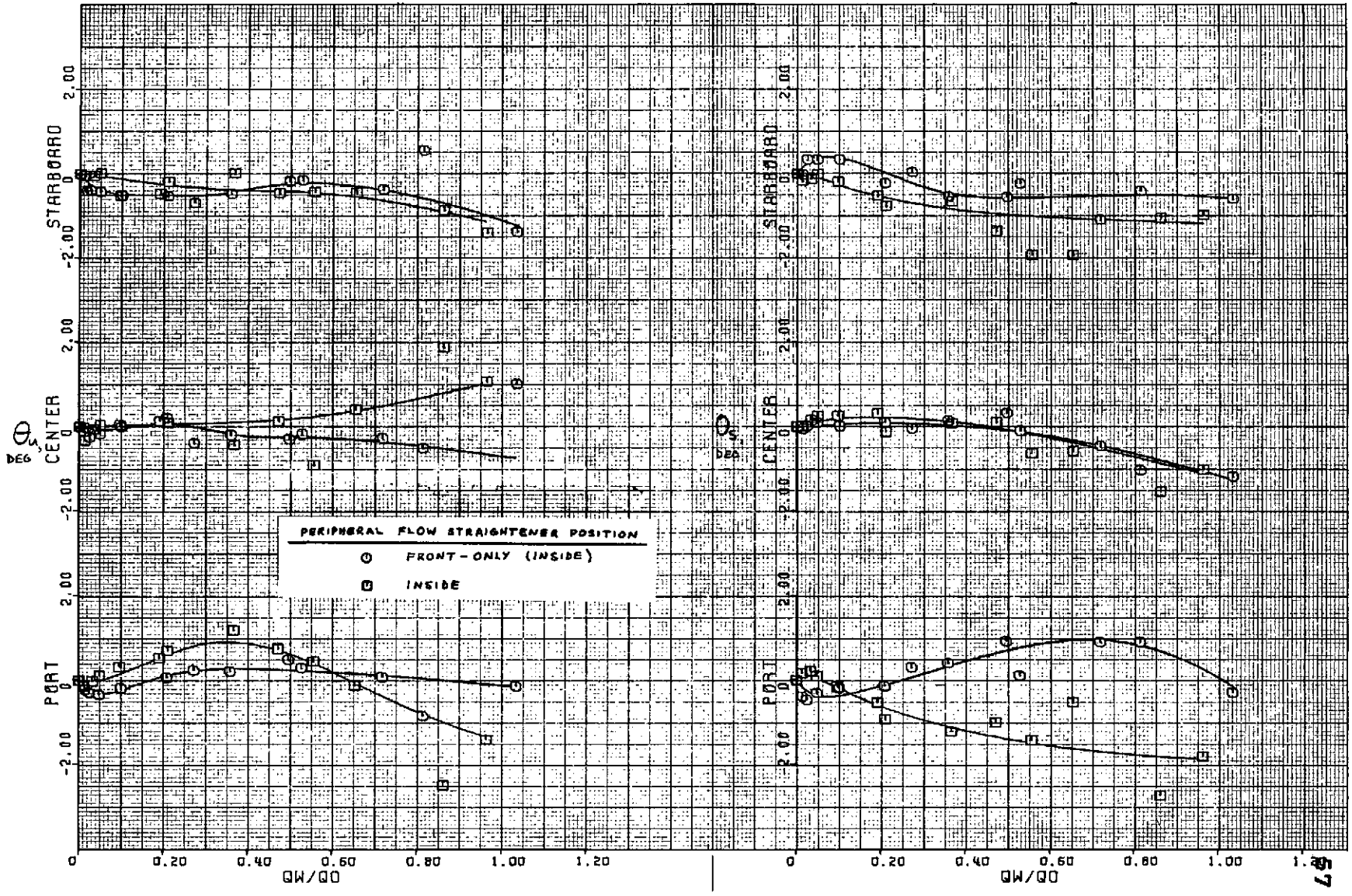

ϕ = -90°.
(a) Test section flow angularities - continued.

Figure 8. - Continued.

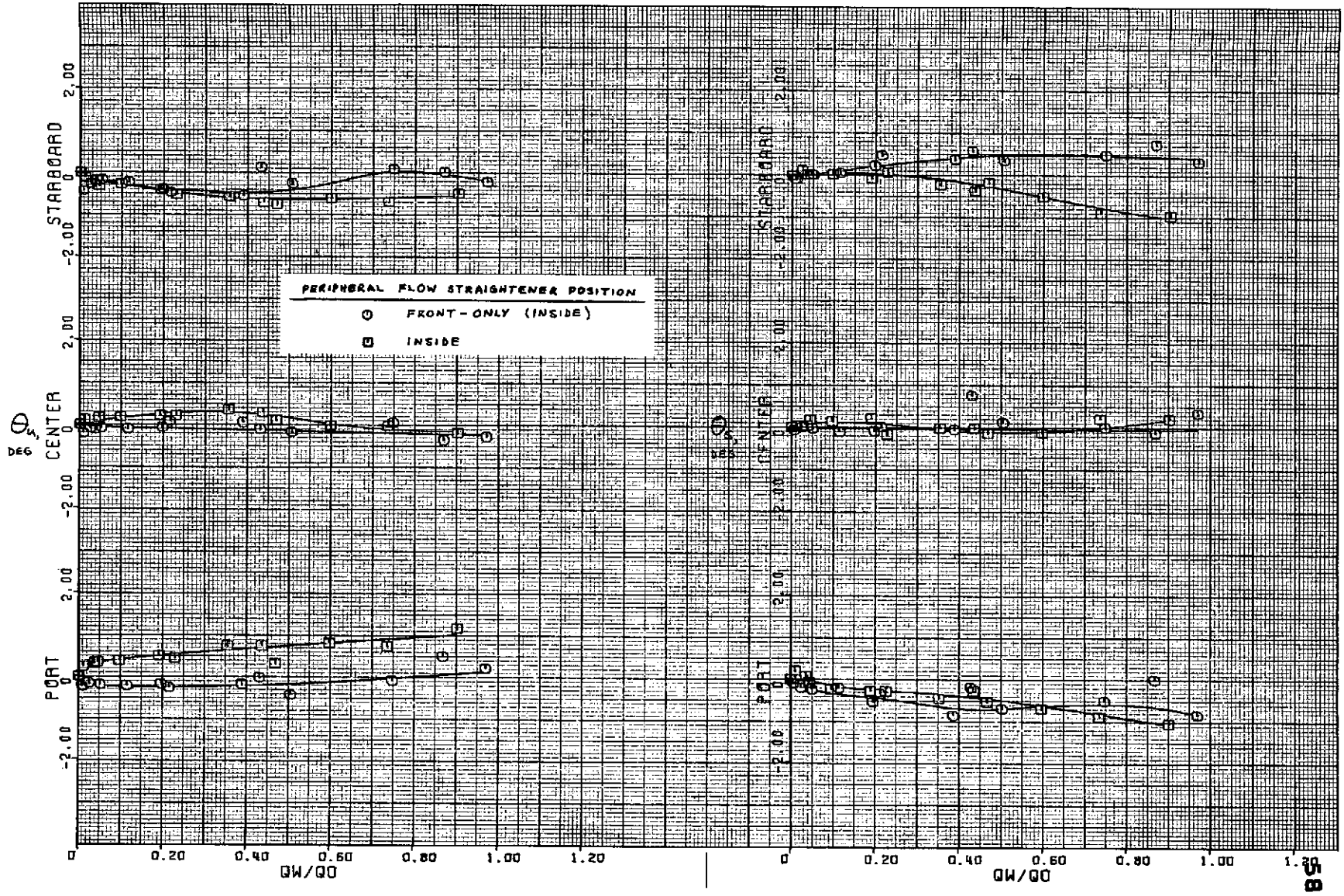

ϕ = -135°.

(a) Test section flow angularities - continued.

Figure 8. - Continued.

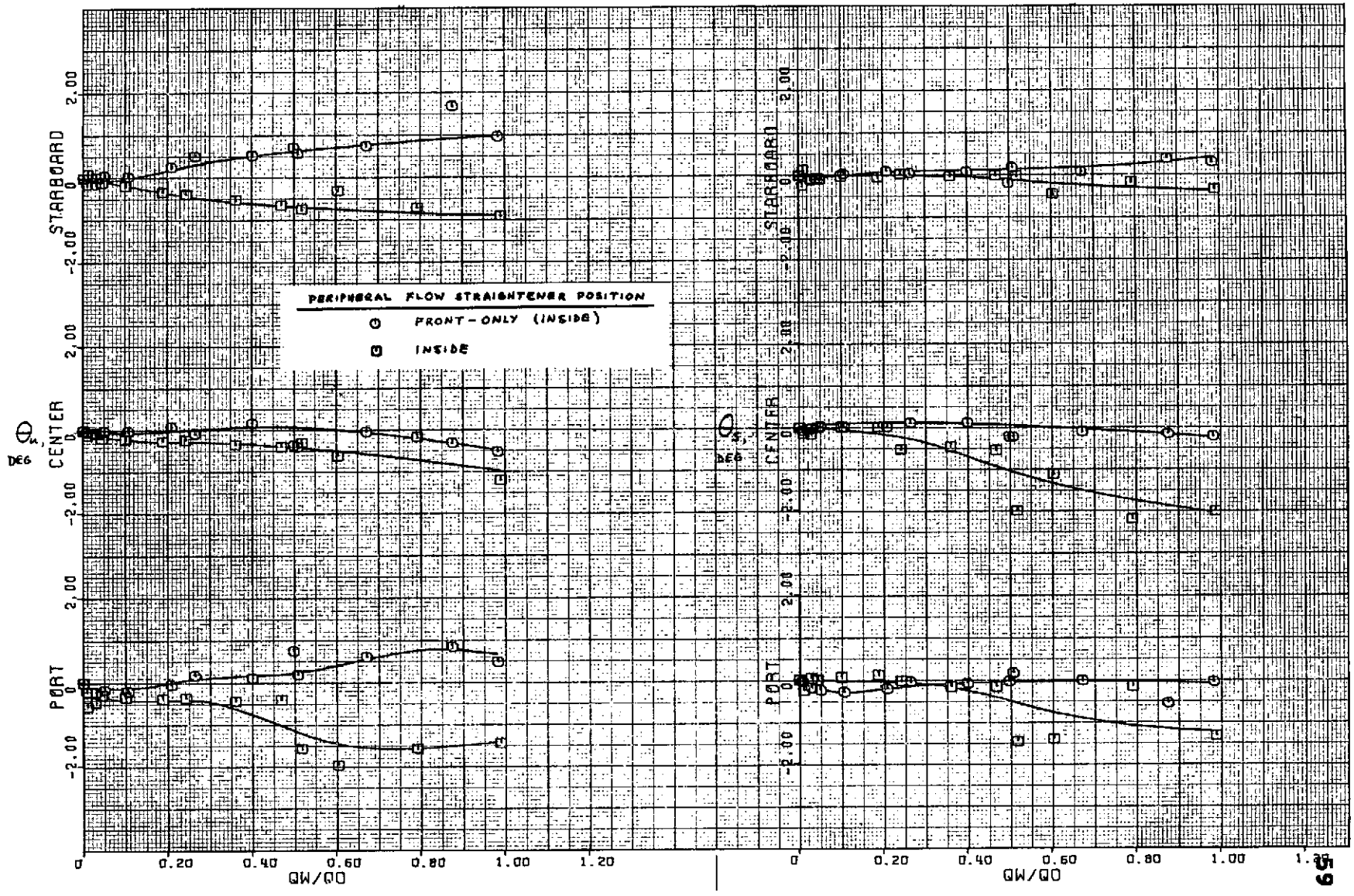

ψ = 180°.

(a) Test section flow angularities – concluded.

Figure 8. – Continued.

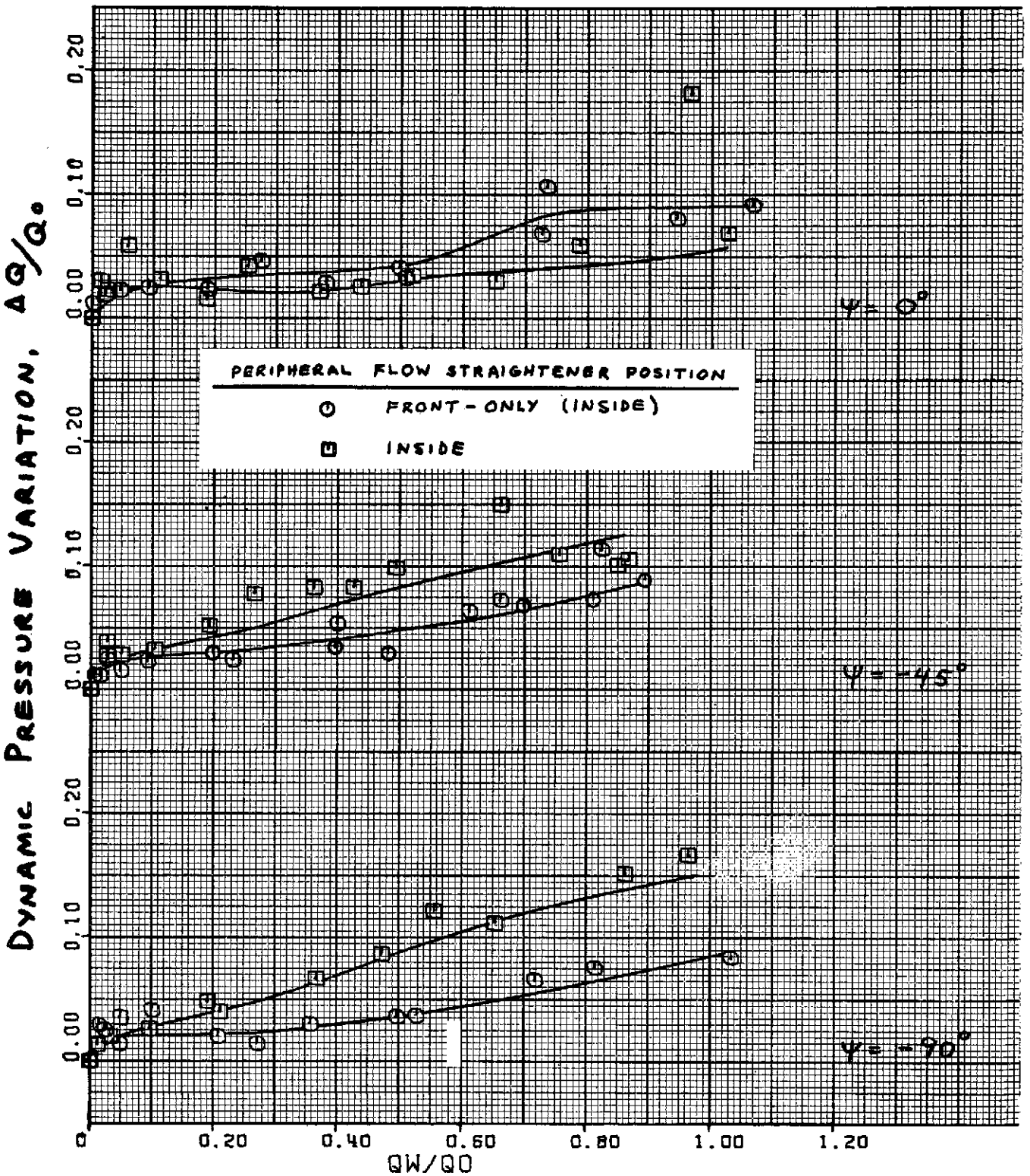

ψ = 0°, -45° and -90°.
(b) Dynamic pressure variation.

Figure 8. - Continued.

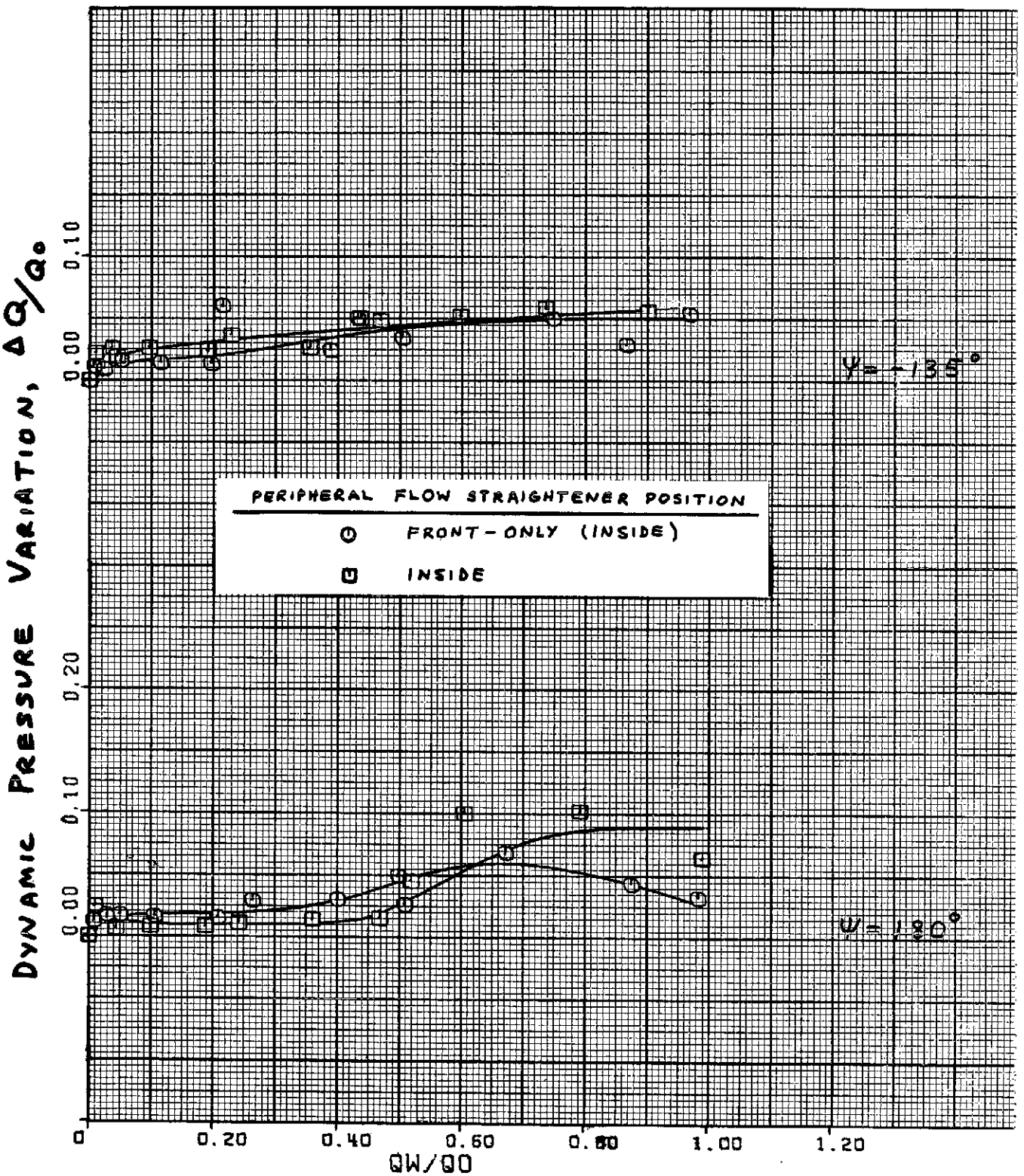

ψ = -135° and 180°.
(b) Dynamic pressure variation - concluded.

Figure 8. - Continued.

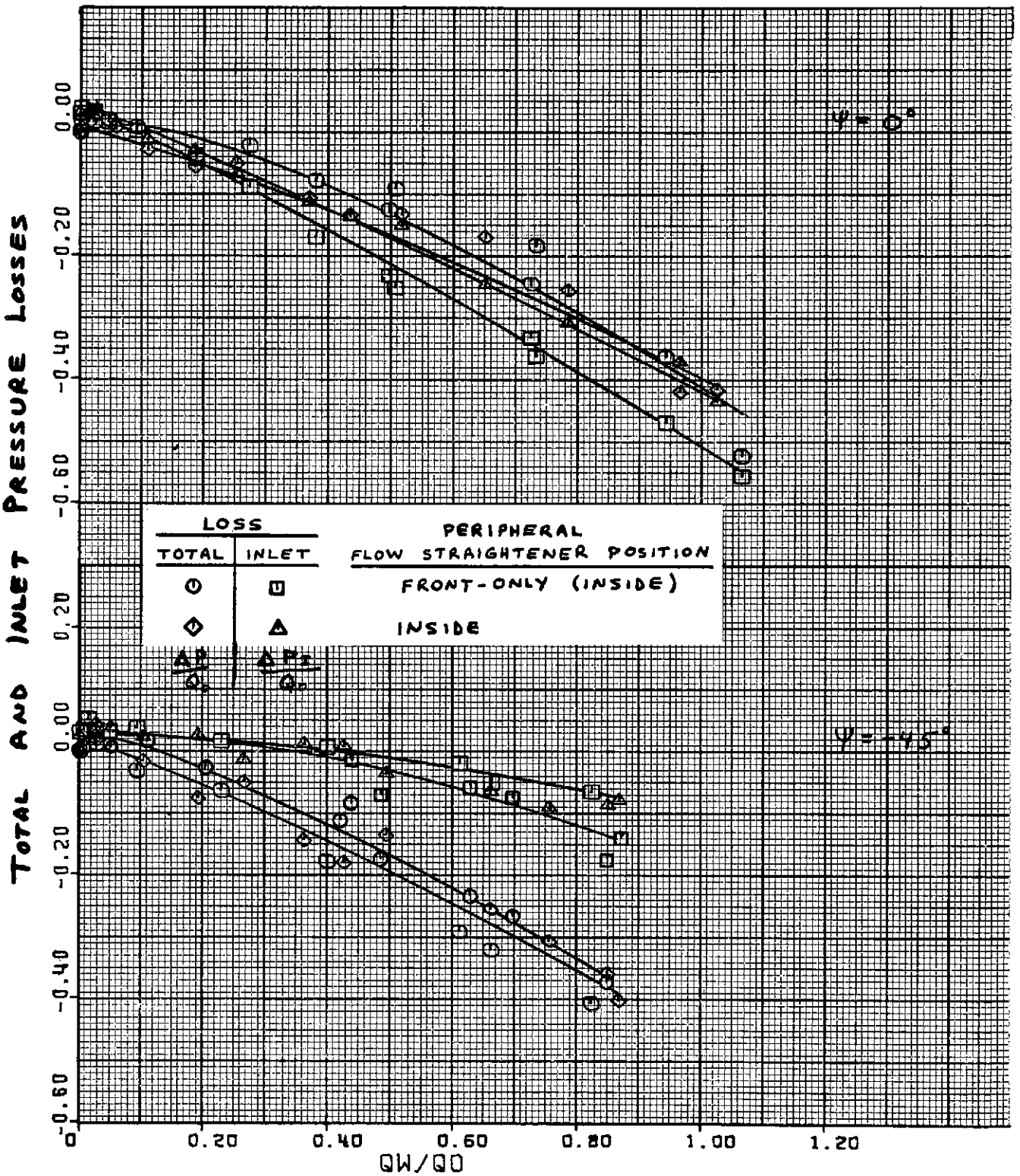

ψ = 0° and -45°.
(c) Pressure losses.

Figure 8. - Continued.

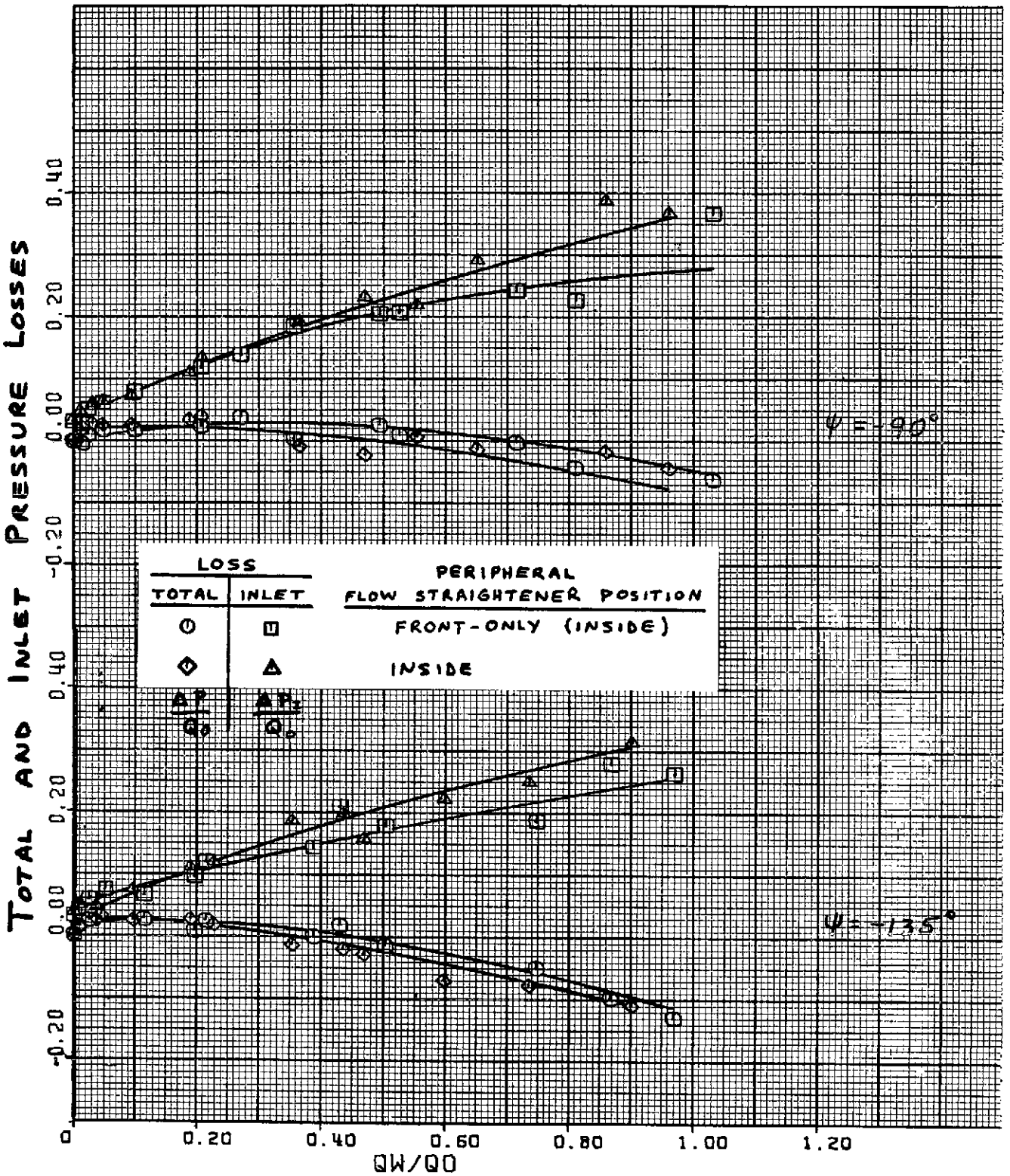

ψ = -90° and -135°.
(c) Pressure losses - continued.

Figure 8. - Continued.

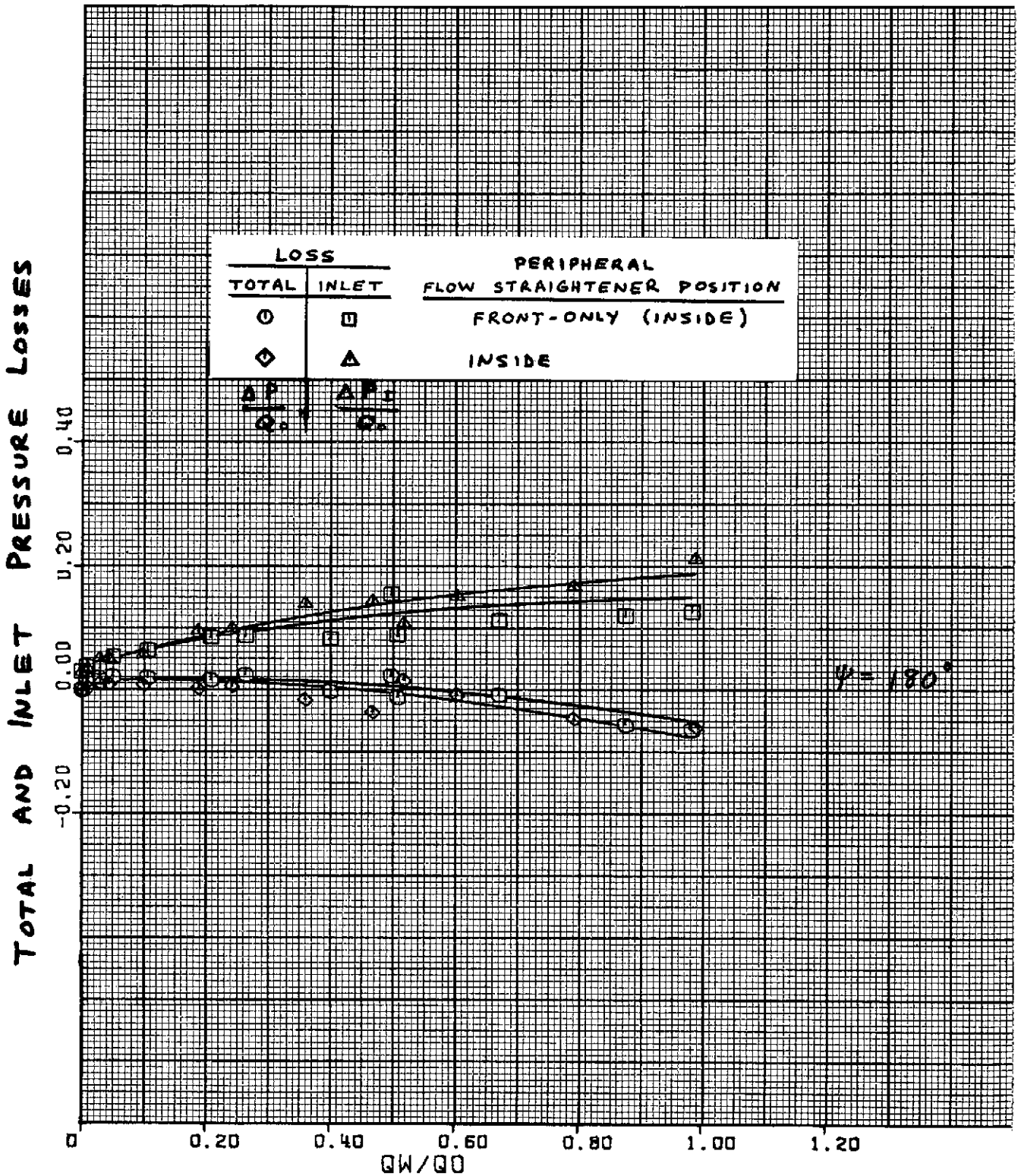

ψ = 180°.
(c) Pressure losses - concluded.

Figure 8. - Concluded.

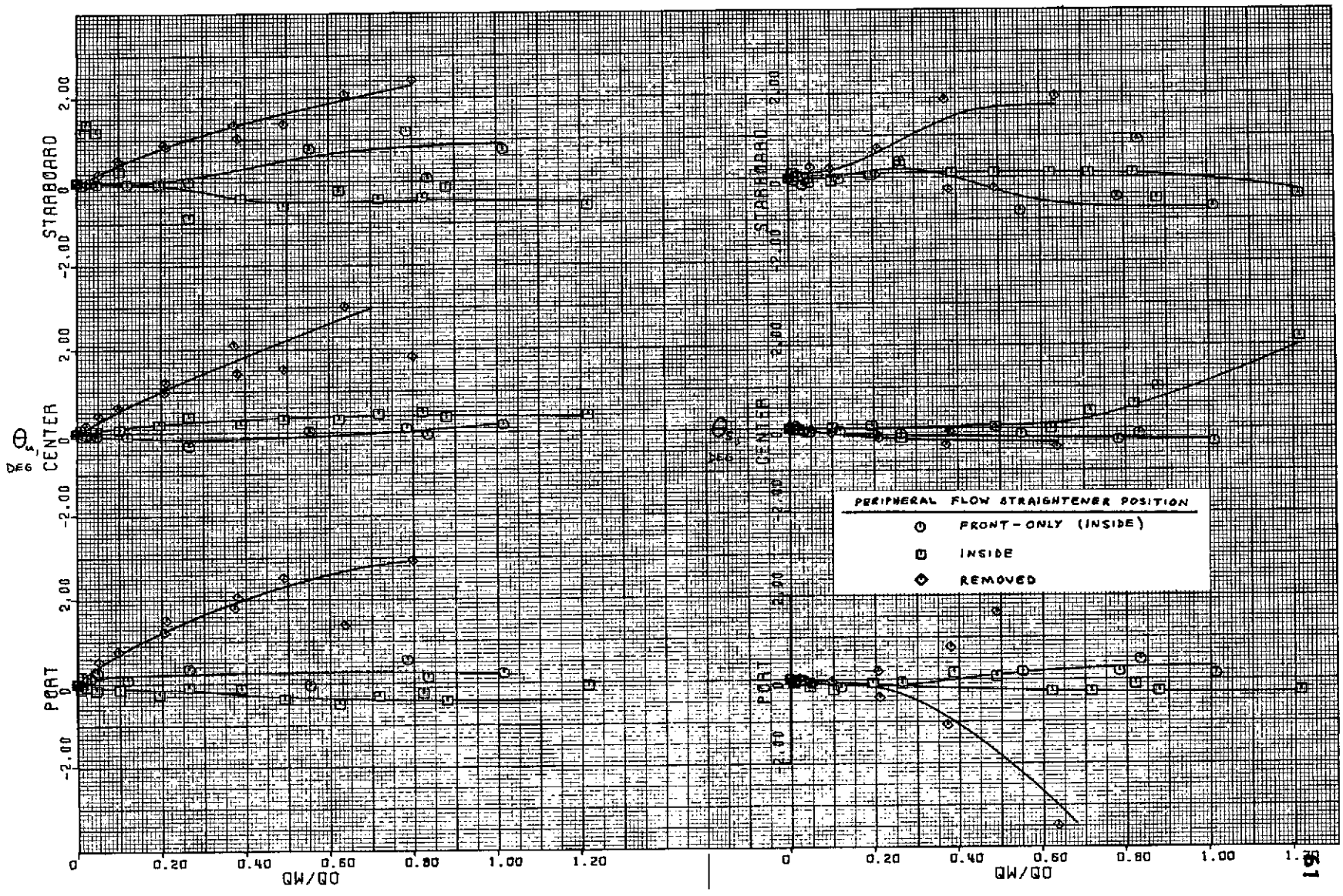

$\phi = 0°$.

(a) Test section flow angularities.

Figure 9. - Effect of peripheral flow straighteners with 107×254 cm (42×100 in) inlet, roof posts in, 2.54×2.54 cm (1×1 in) contraction flow straighteners, area ratio 20 exit.

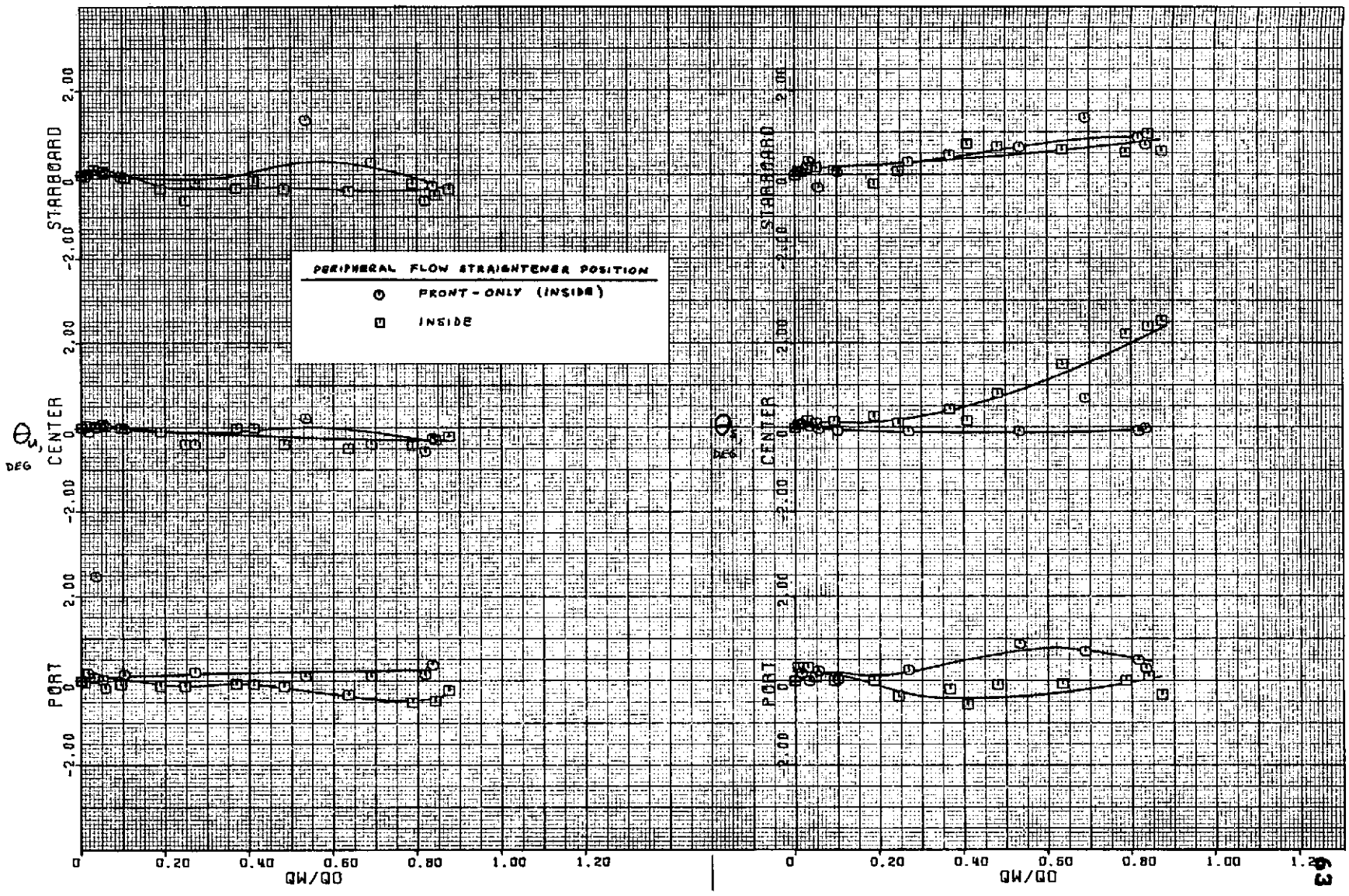

$\psi = -22\text{-}\frac{1}{2}/2°$.

(a) Test section flow angularities - continued.

Figure 9. - Continued.

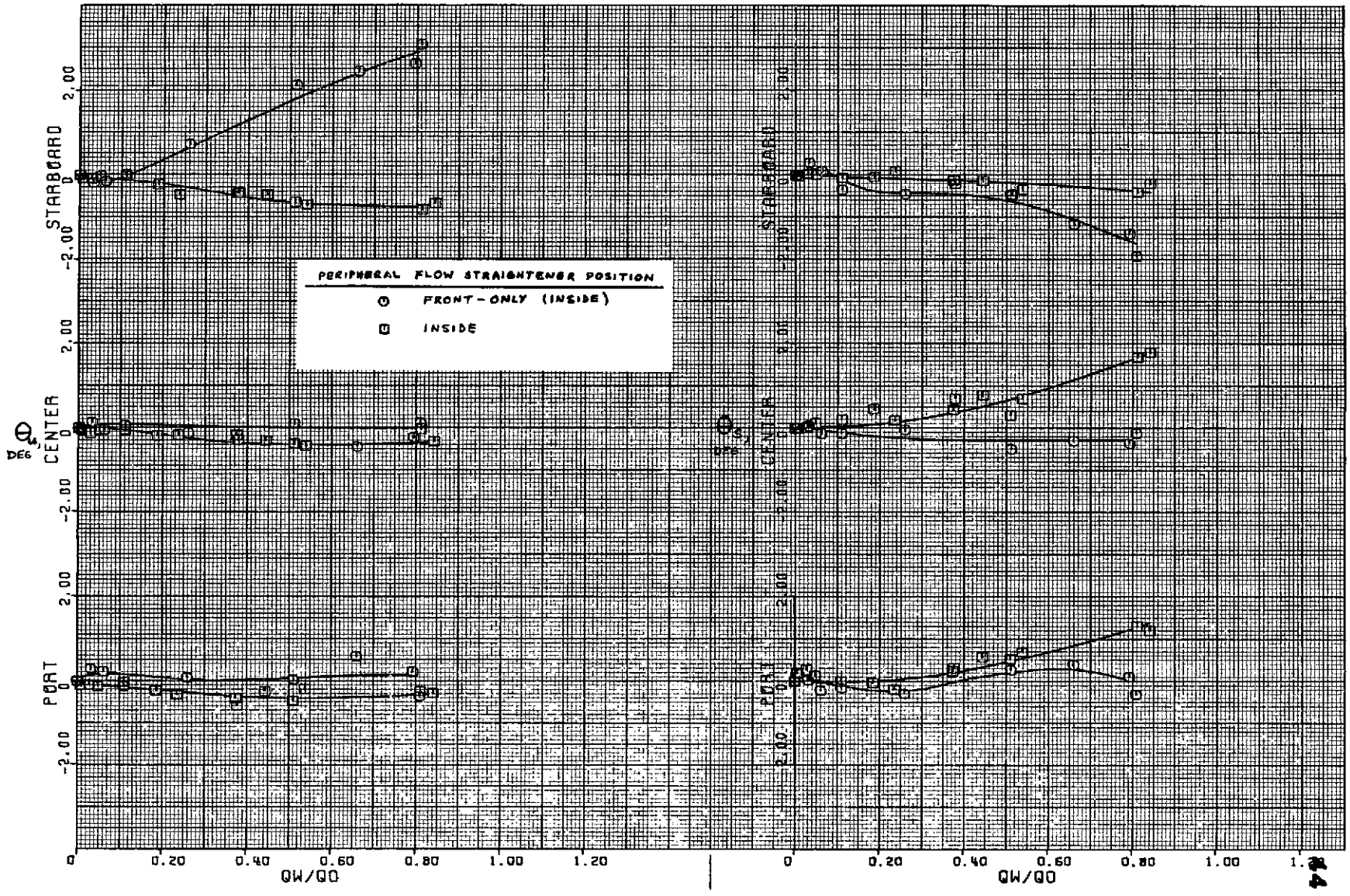

ψ = -45°.

(a) Test section flow angularities - continued.

Figure 9. - Continued.

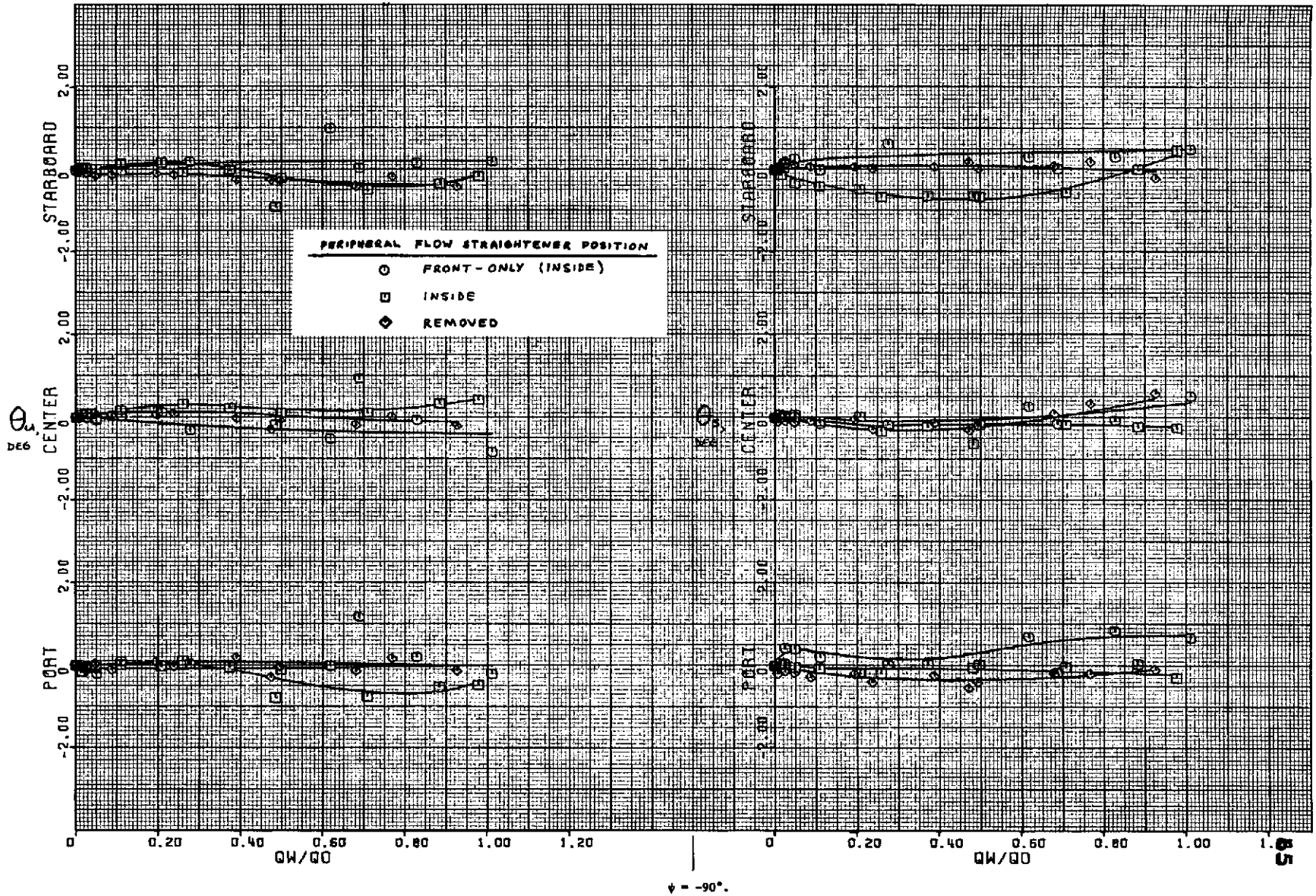

$\psi = -90°$.

(a) Test section flow angularities - continued.

Figure 9. - Continued.

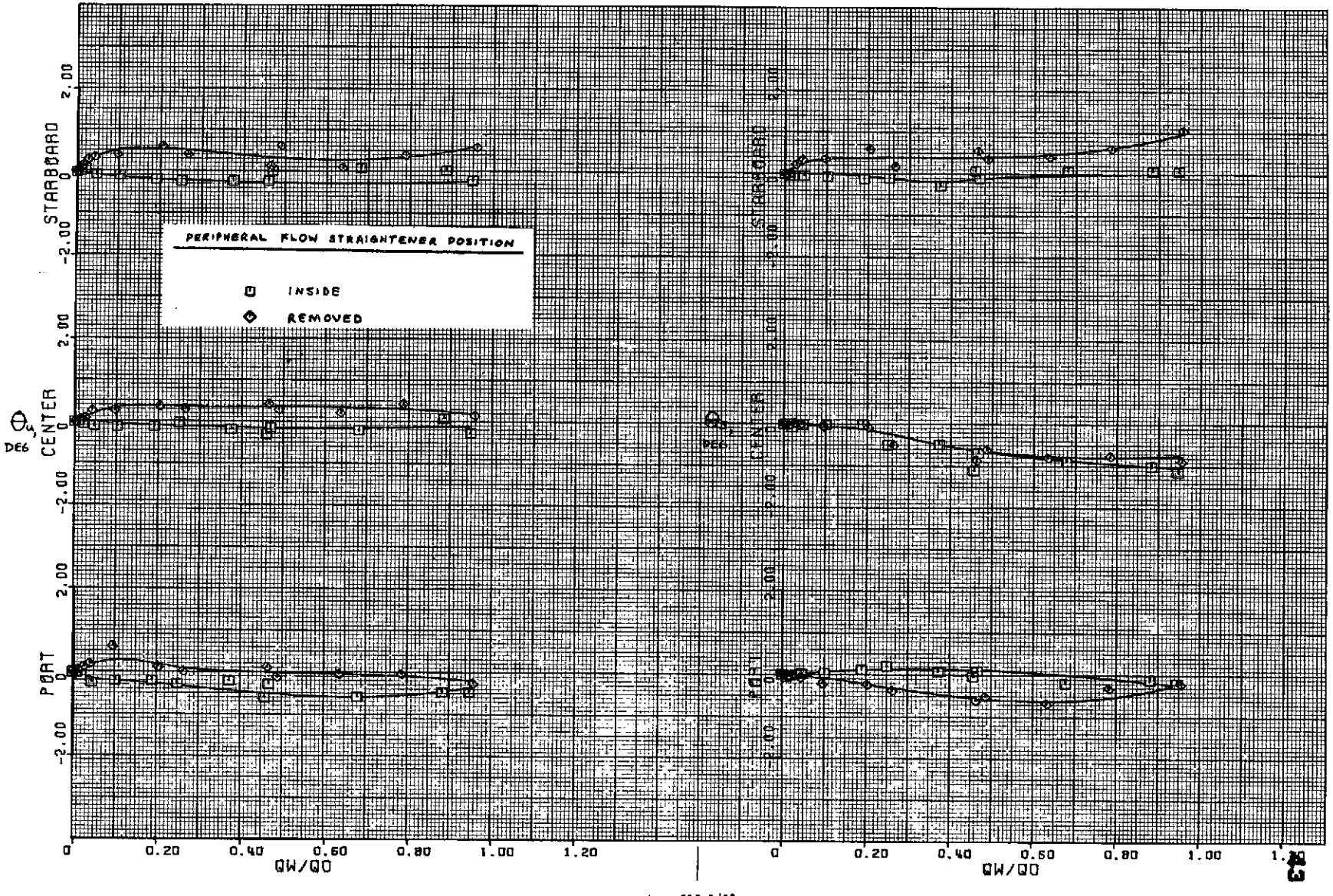

ψ = -112-1/2°.
(a) Test section flow angularities - continued.

Figure 9. - Continued.

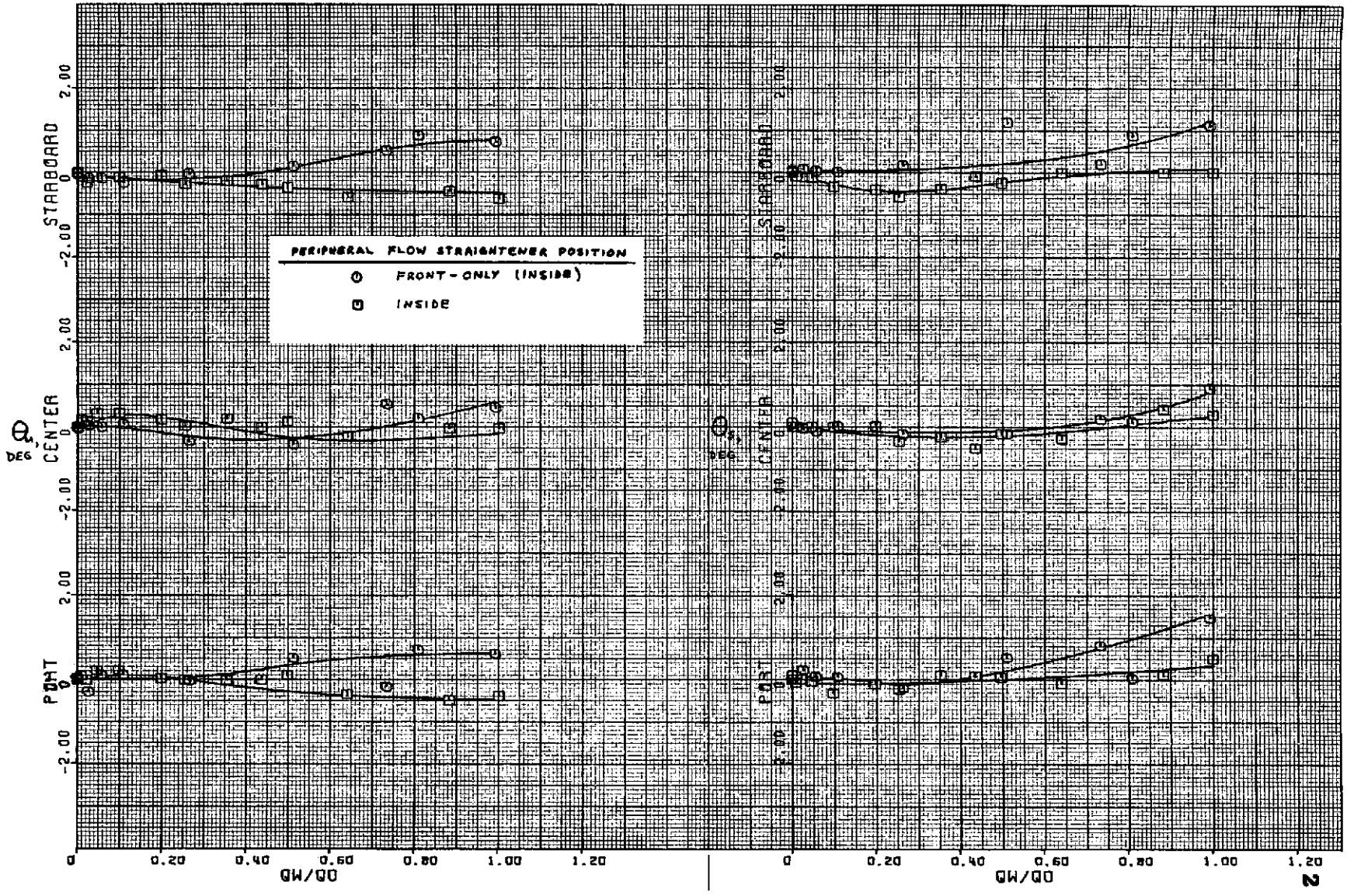

ϕ = 180°.
(a) Test section flow angularities - concluded.

Figure 9. - Continued.

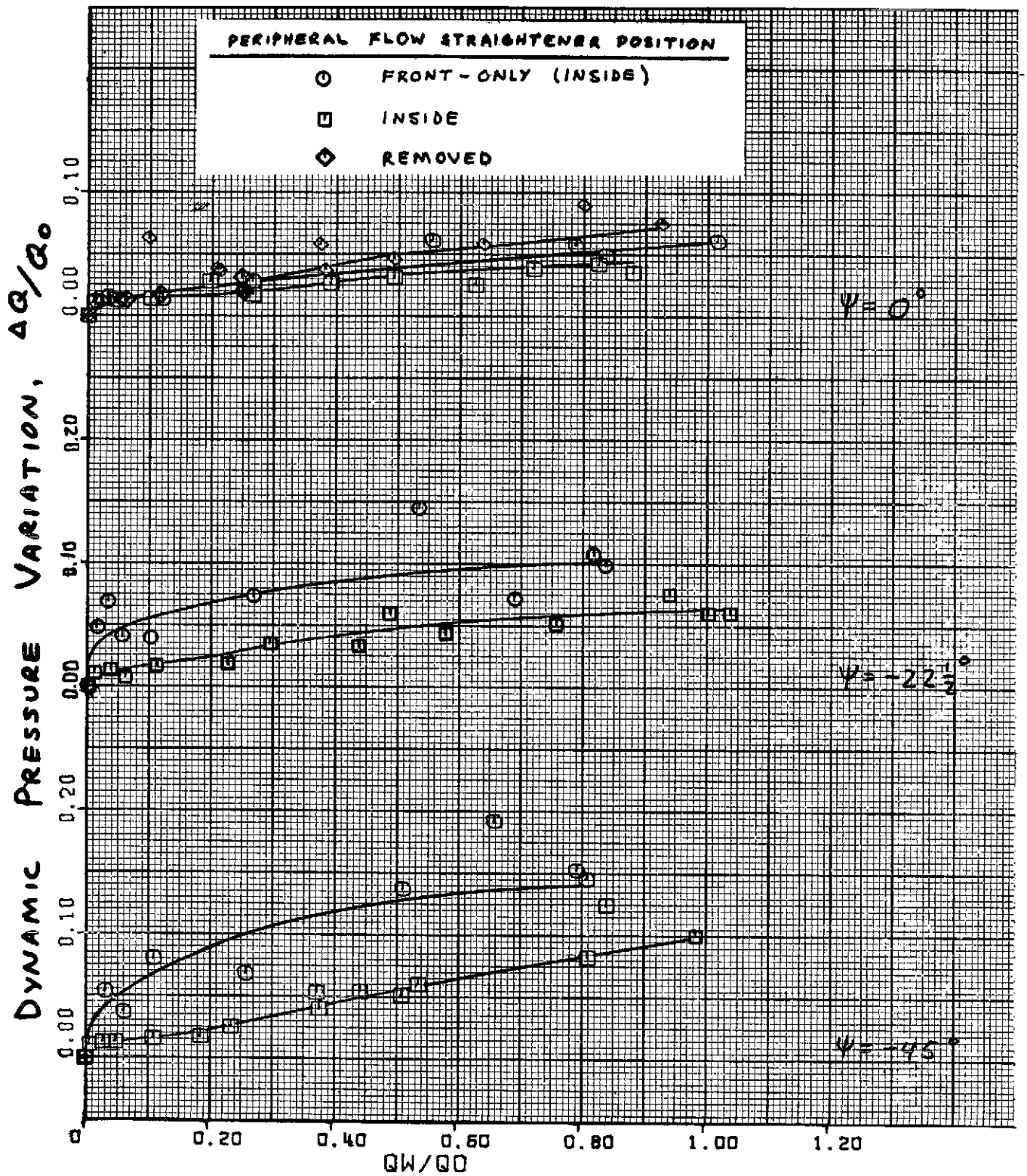

ψ = 0°, -22-1/2° and -45°.
(b) Dynamic pressure variation.

Figure 9. - Continued.

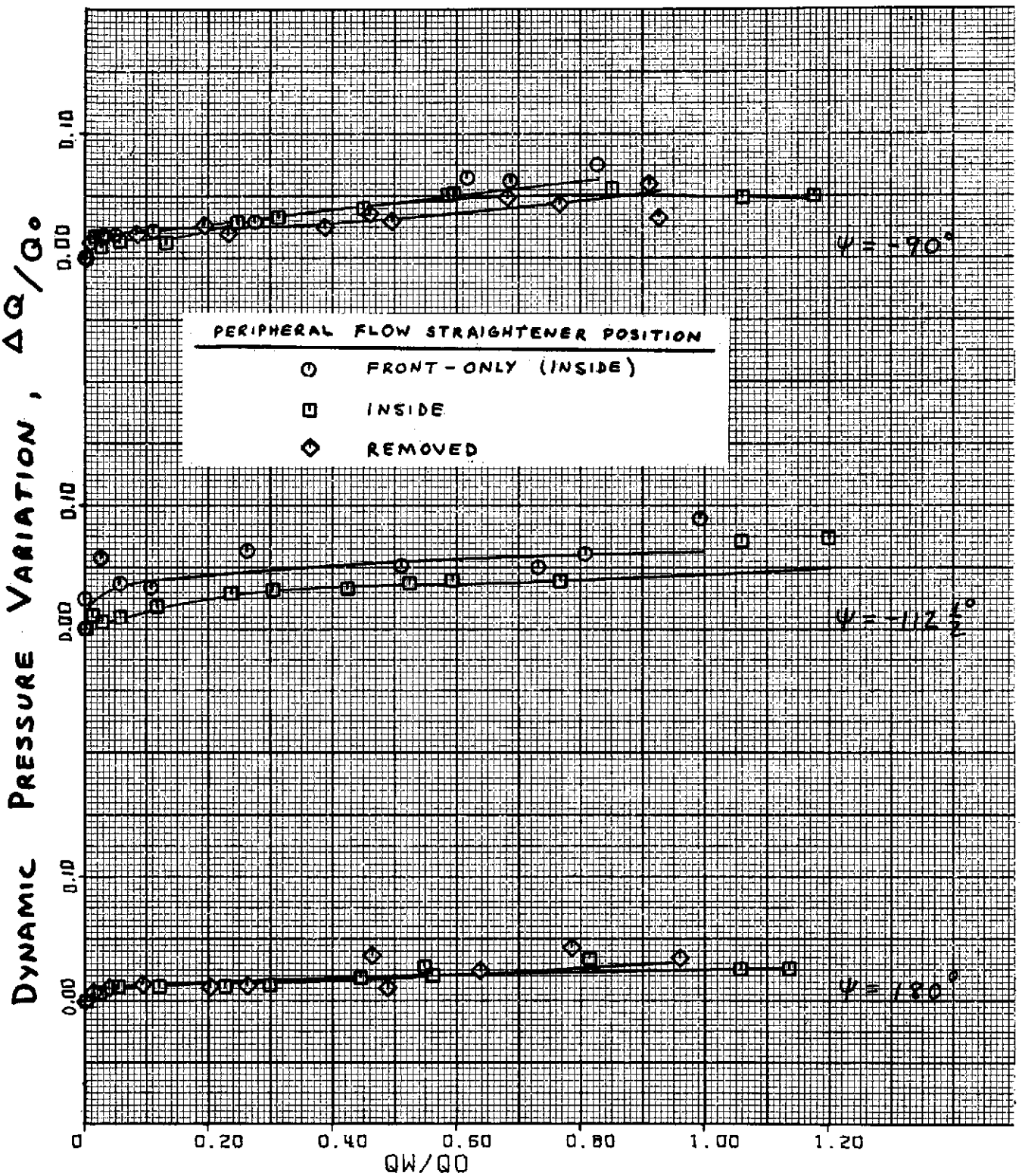

ψ = -90°, -112-1/2° and 180°.
(b) Dynamic pressure variation - concluded.

Figure 9. - Continued.

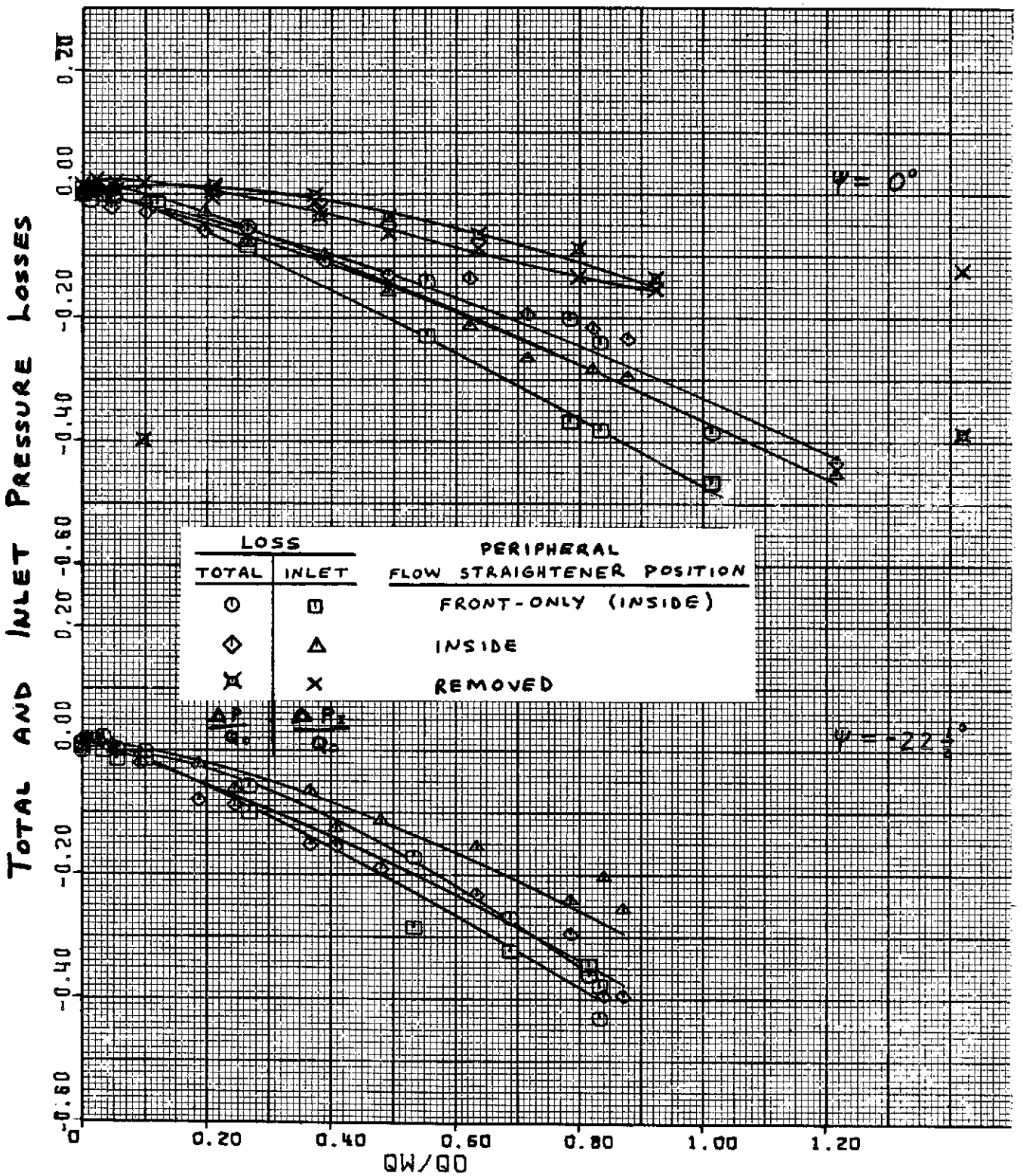

ψ = 0° and -22-1/2°.
(c) Pressure losses.

Figure 9. - Continued.

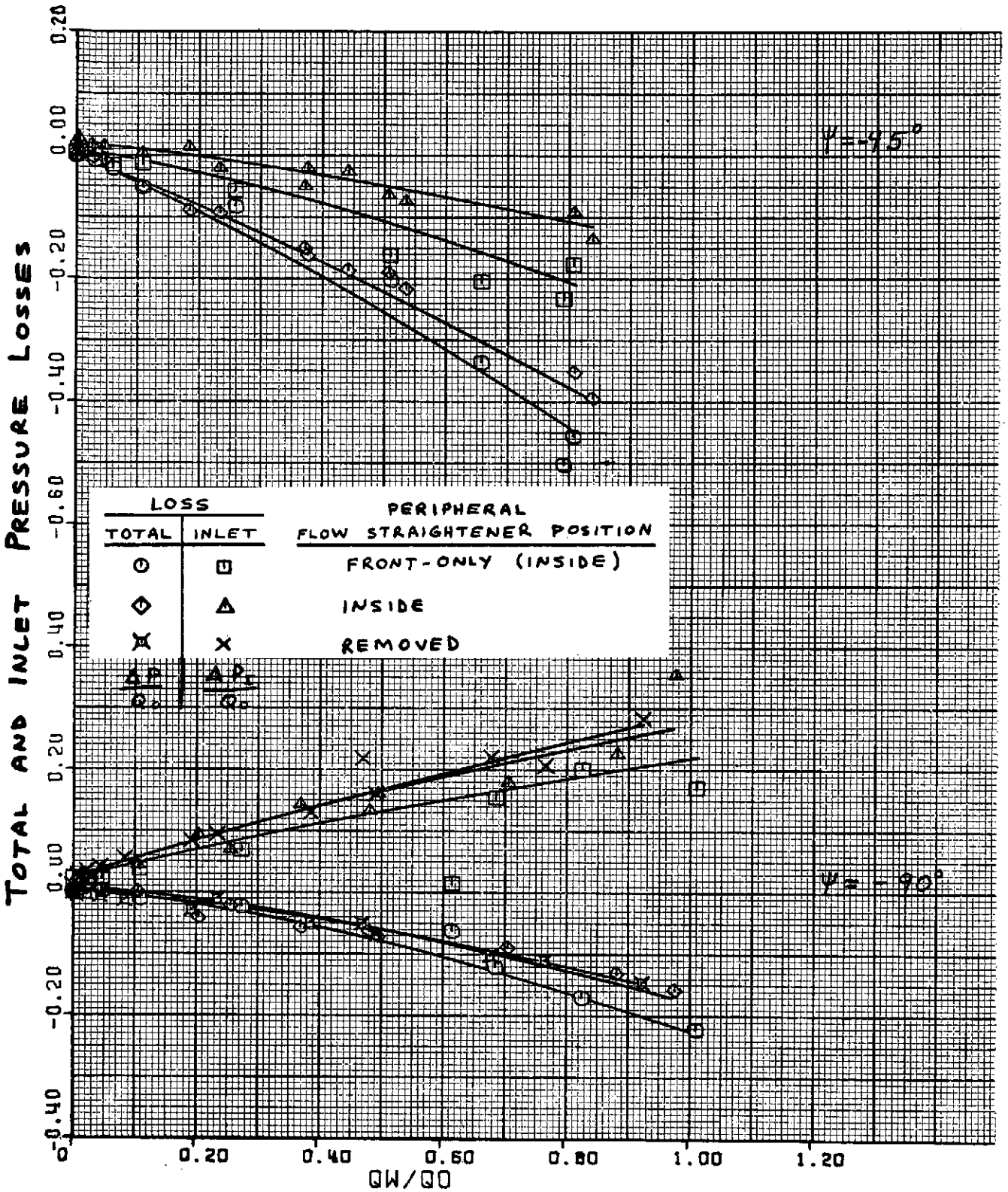

ψ = -45° and -90°.
(c) Pressure losses - continued.

Figure 9. - Continued.

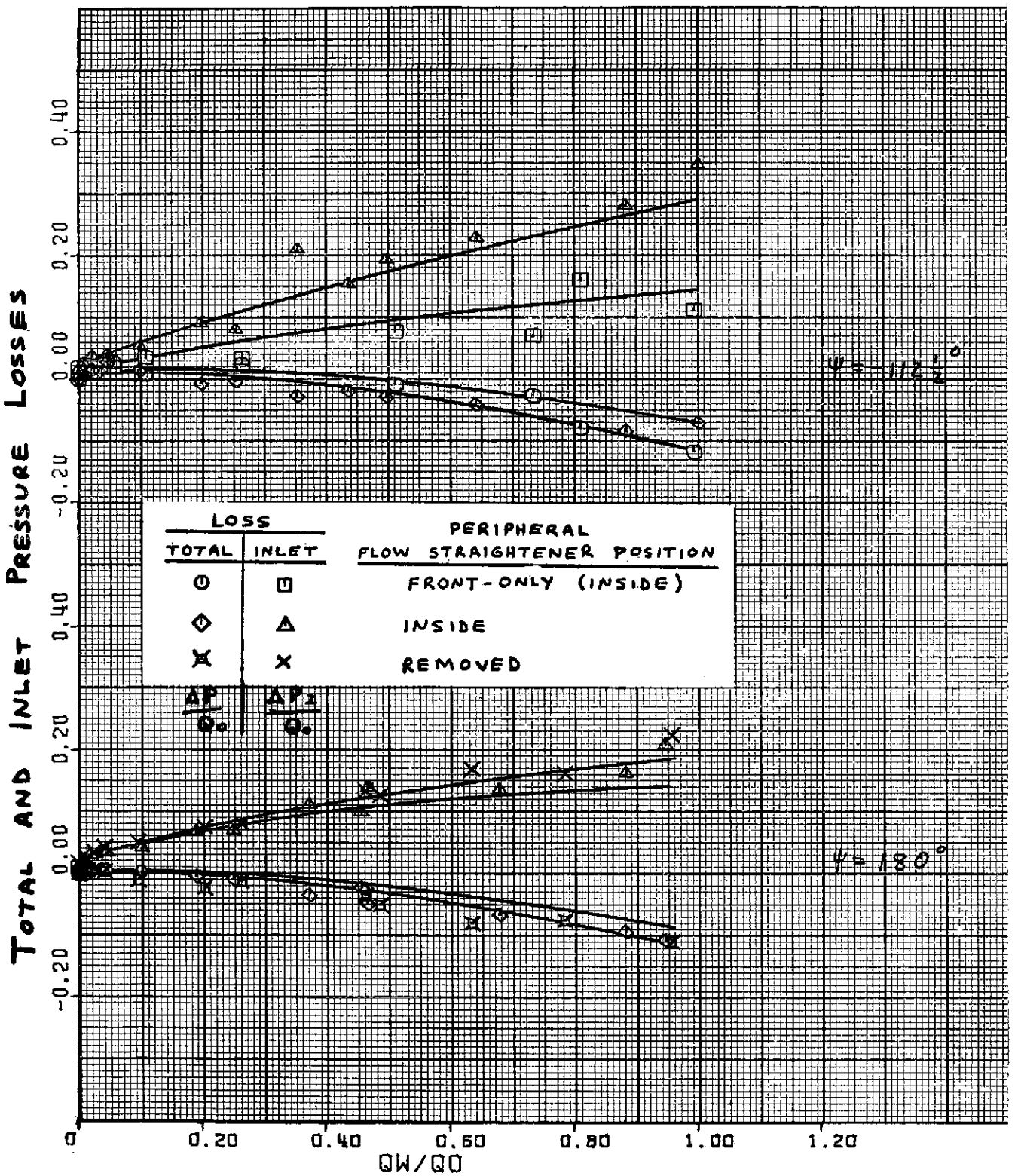

ψ = -112-1/2° and 180°.
(c) Pressure losses - concluded.

Figure 9. - Concluded.

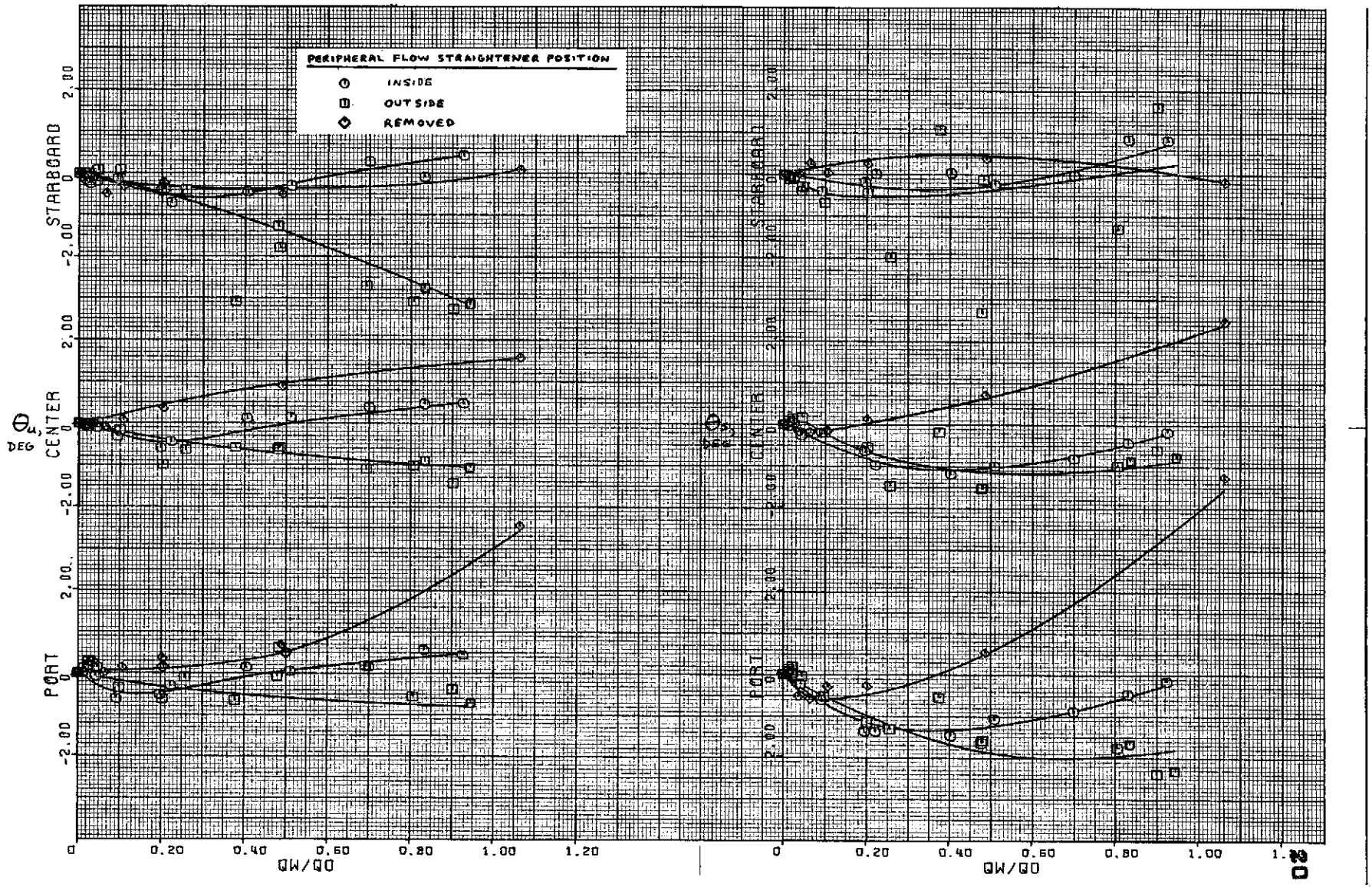

$\psi = 0°$.
(a) Test section flow angularities.

Figure 10. - Effect of peripheral flow straighteners with 107×254 cm (42×100 in) inlet, roof posts out, 2.54×2.54 cm (1×1 in) contraction flow straighteners, area ratio 20 exit.

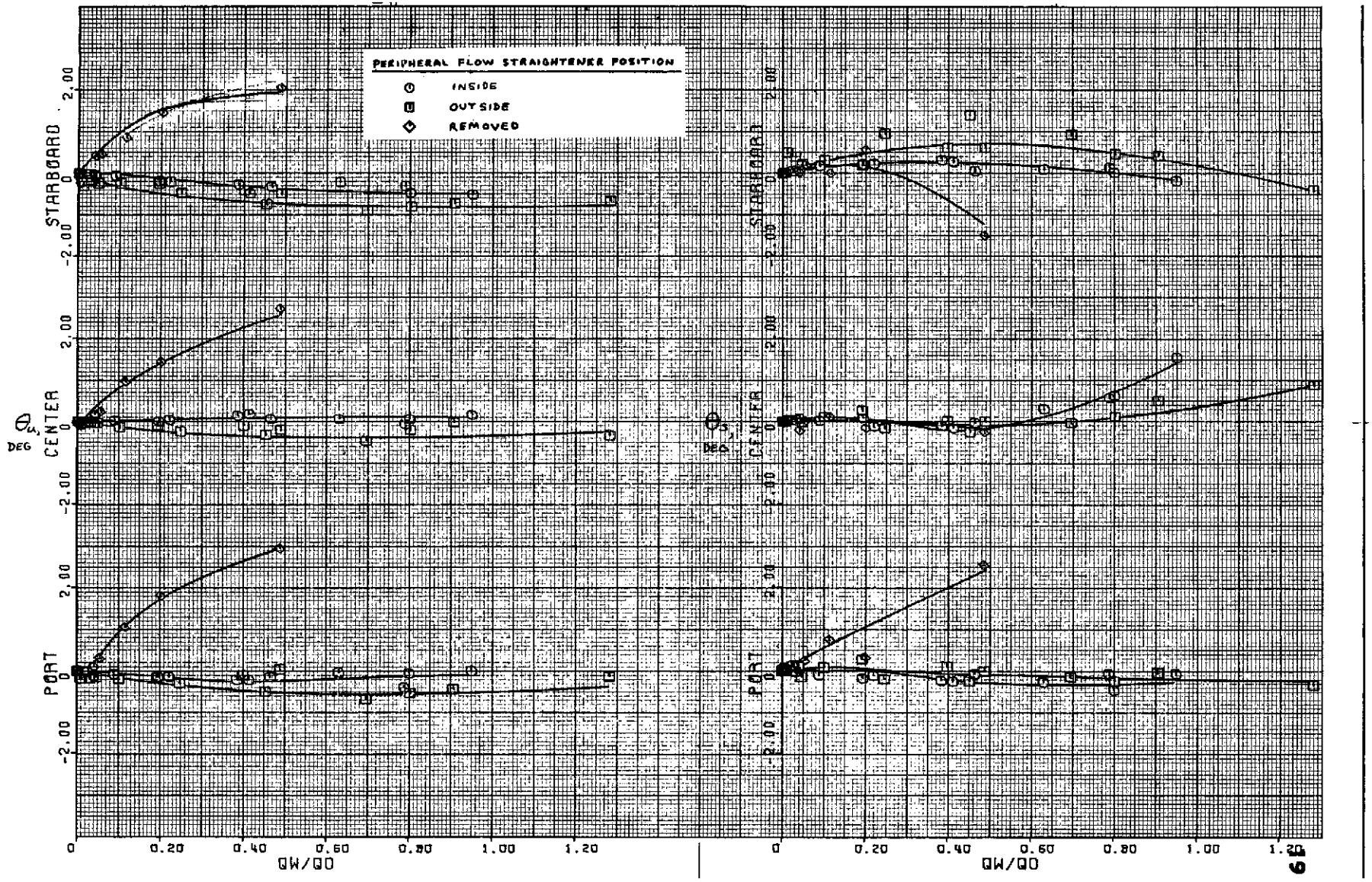

ψ = -90°.

(a) Test section flow angularities - concluded.

Figure 10. - Continued.

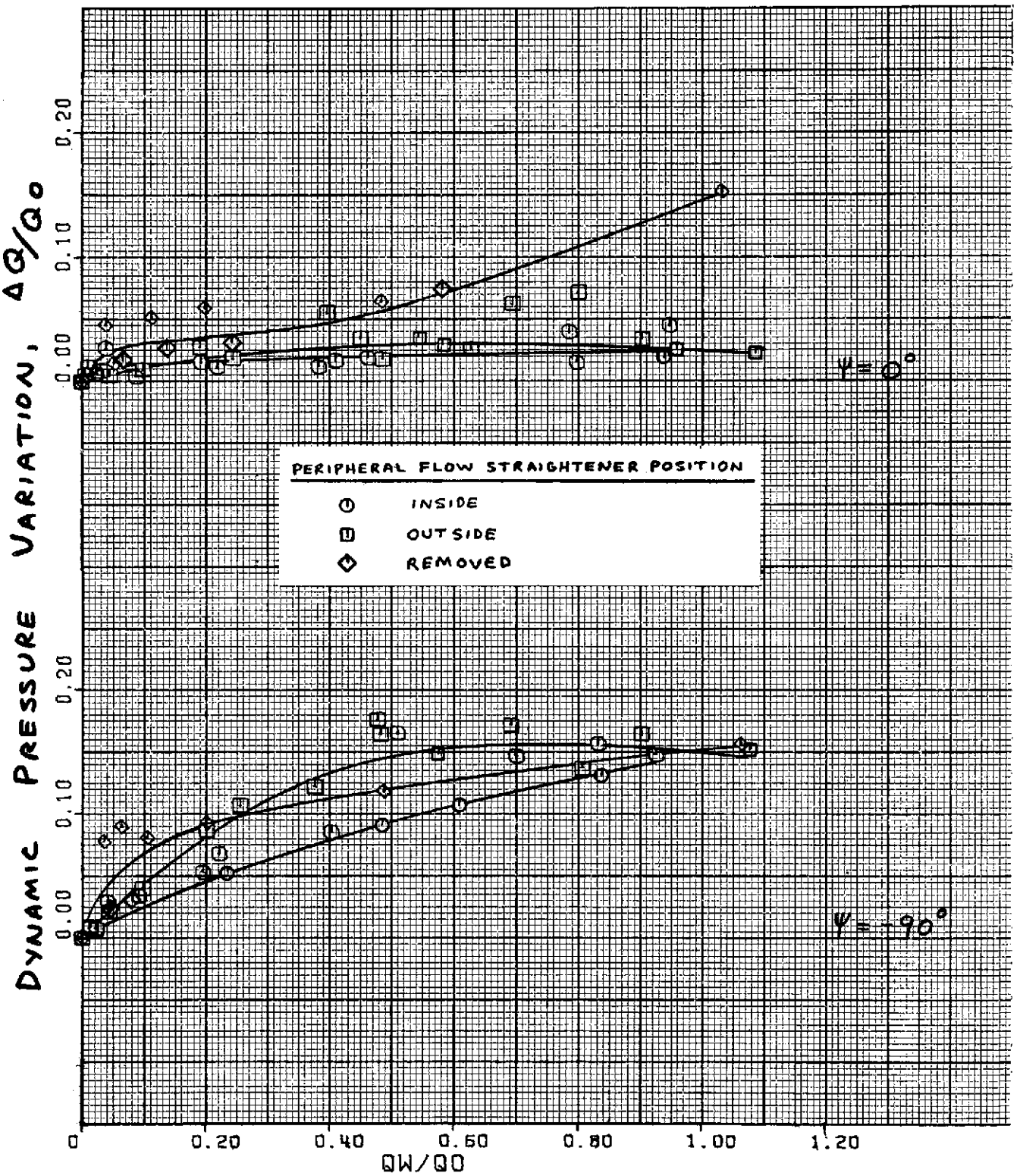

(b) Dynamic pressure variation; ψ = 0° and -90°.

Figure 10. - Continued.

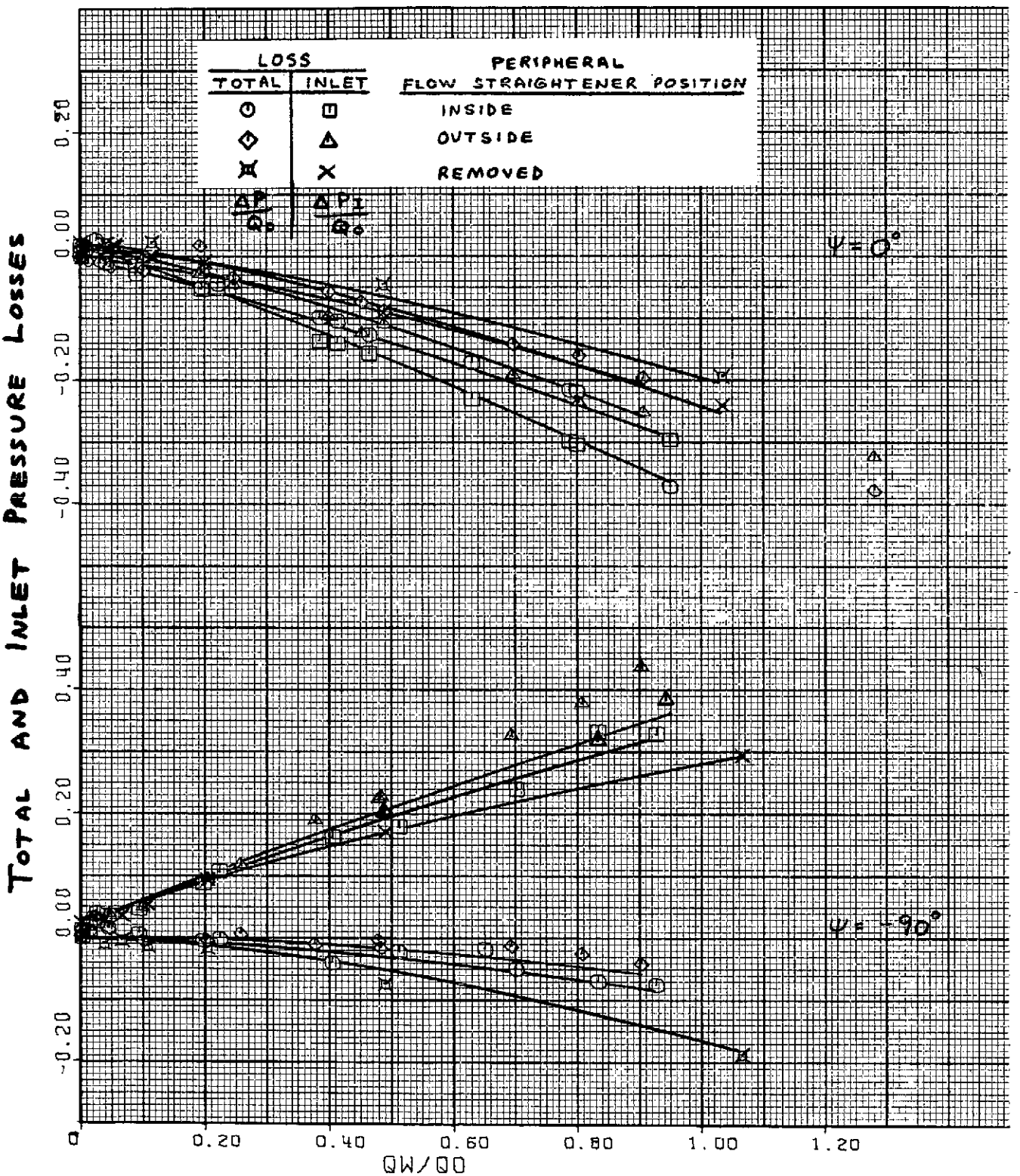

(c) Pressure losses; ψ = 0° and -90°.

Figure 10. - Concluded.

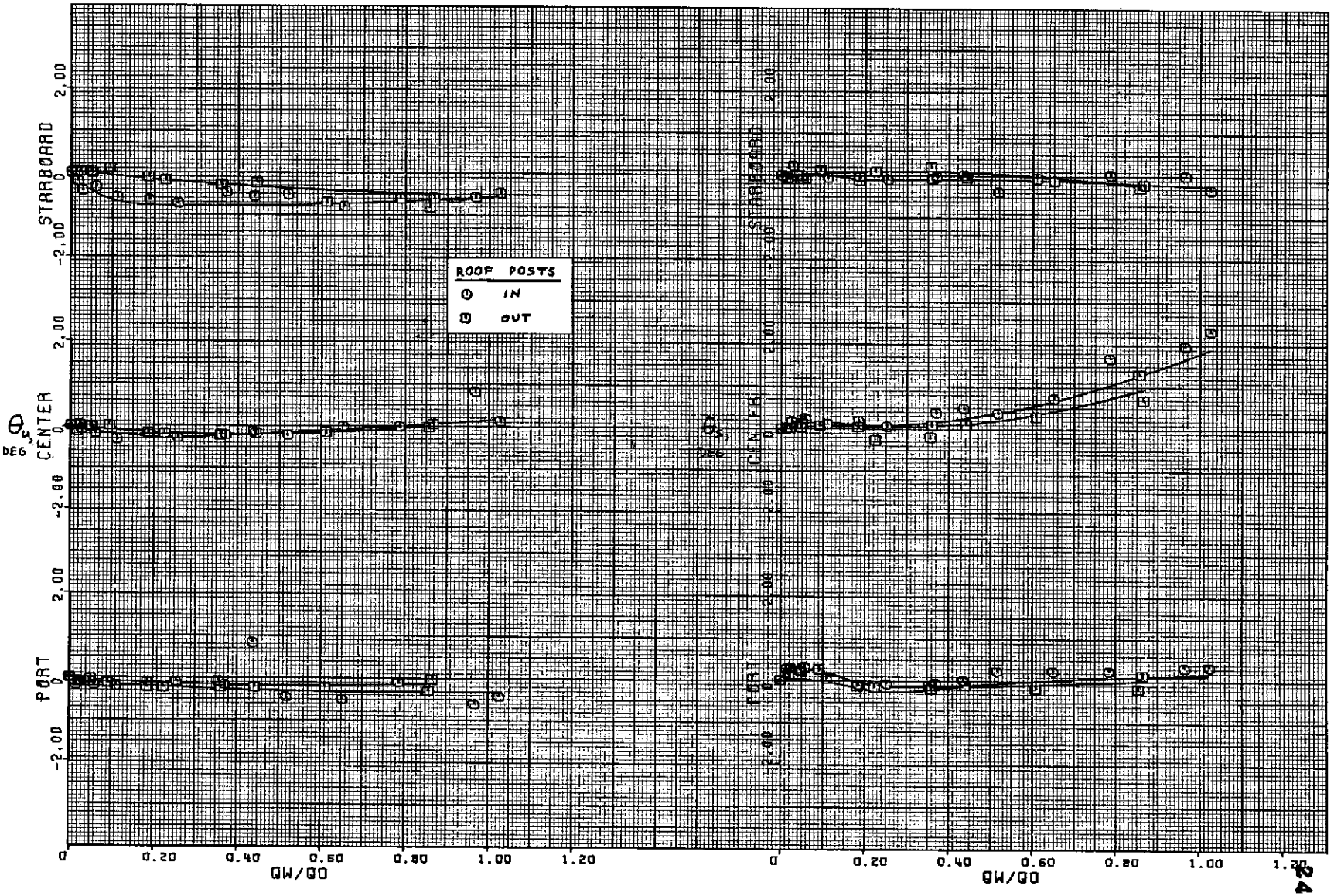

ϕ = 0°.
(a) Test section flow angularities.

Figure 11. - Effect of inlet roof posts with 58×203 cm (23×80 in) inlet, peripheral flow straighteners inside, 2.54×2.54 cm (1×1 in) contraction flow straighteners, area ratio 20 exit.

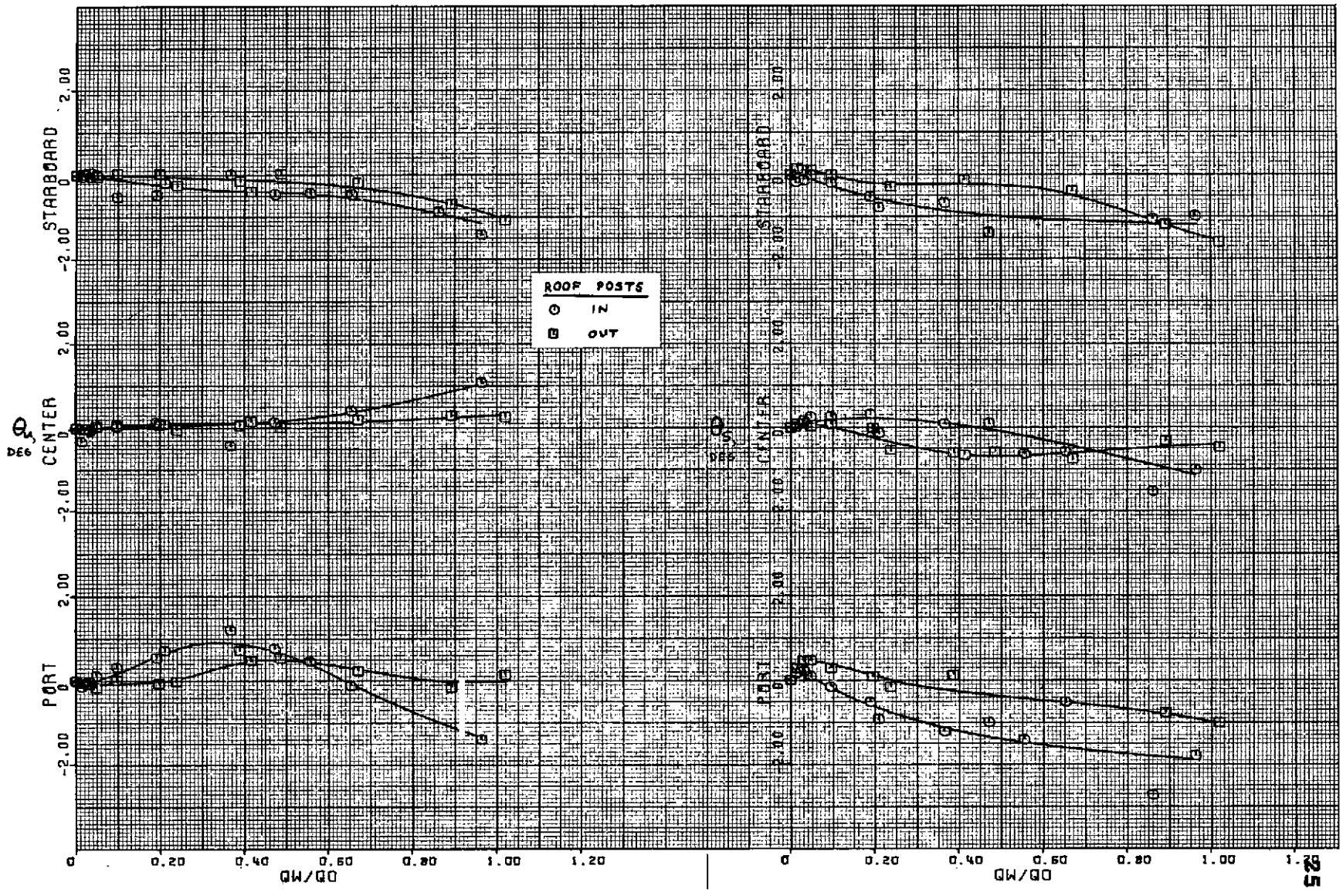

ψ = -90°.

(a) Test section flow angularities - continued.

Figure 11. - Continued.

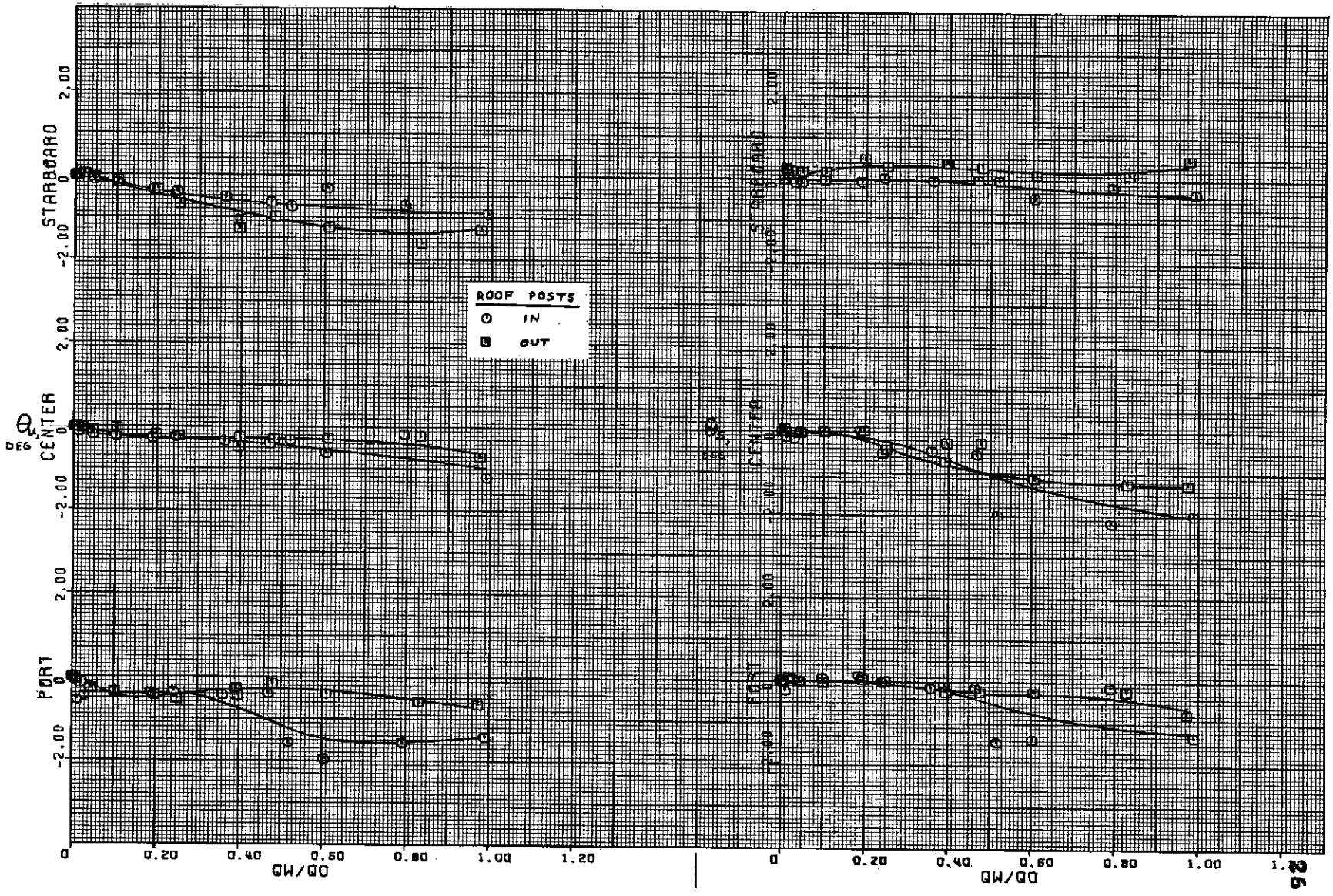

ψ = 180°.

(a) Test section flow angularities - concluded.

Figure 11. - Continued.

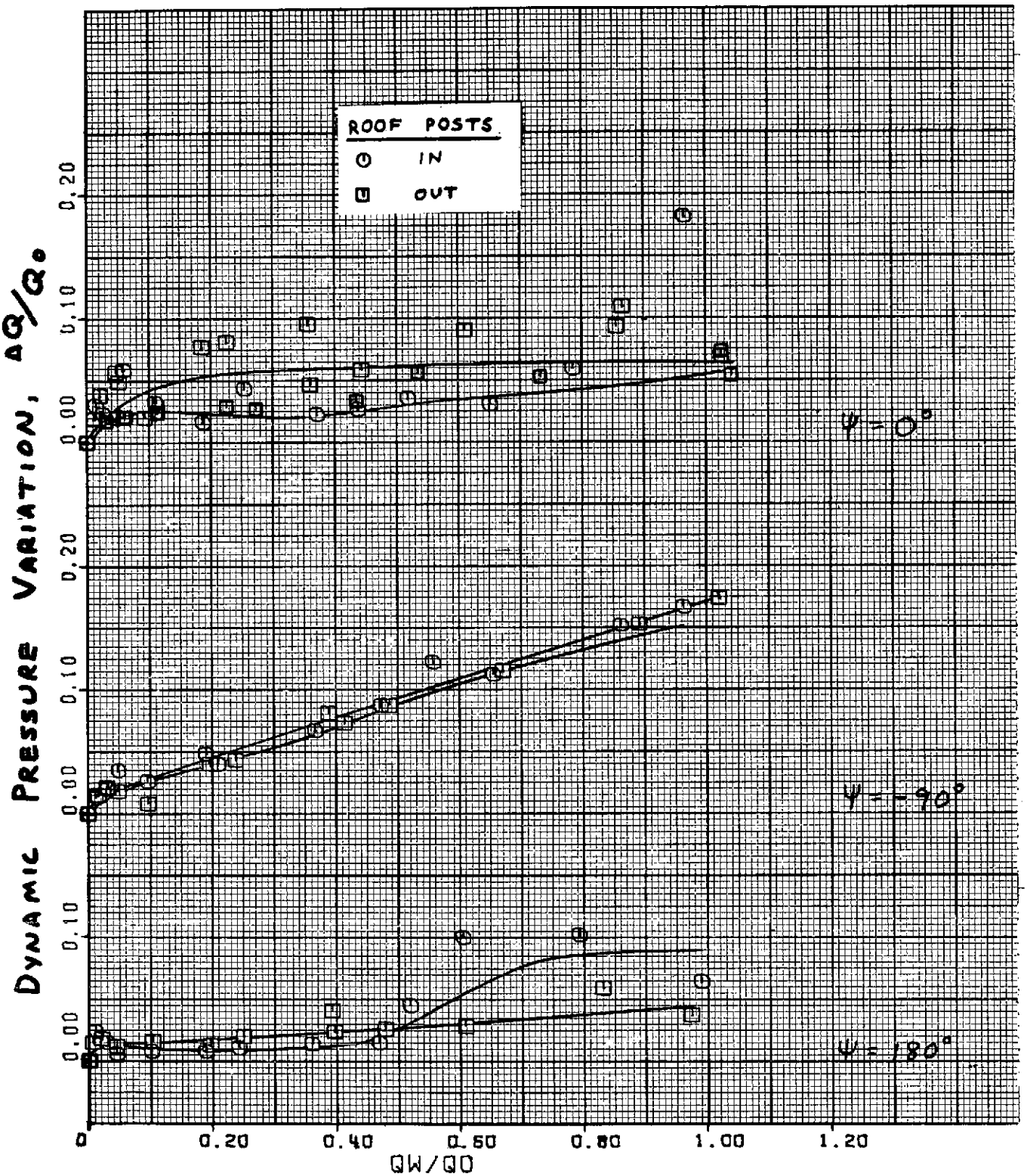

(b) Dynamic pressure variation; ψ = 0°, -90° and 180°.

Figure 11. - Continued.

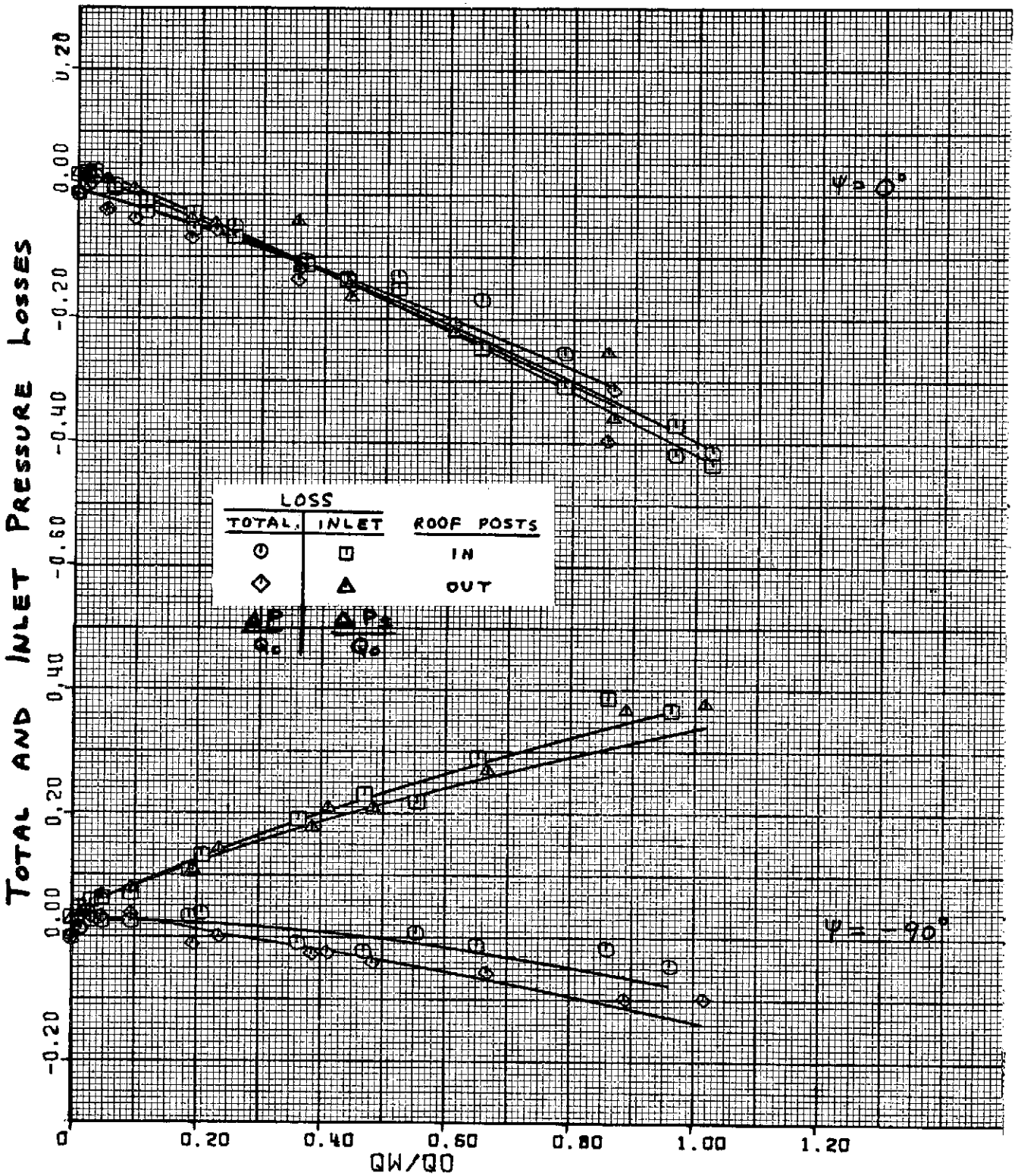

ψ = 0° and -90°.
(c) Pressure losses.

Figure 11. - Continued.

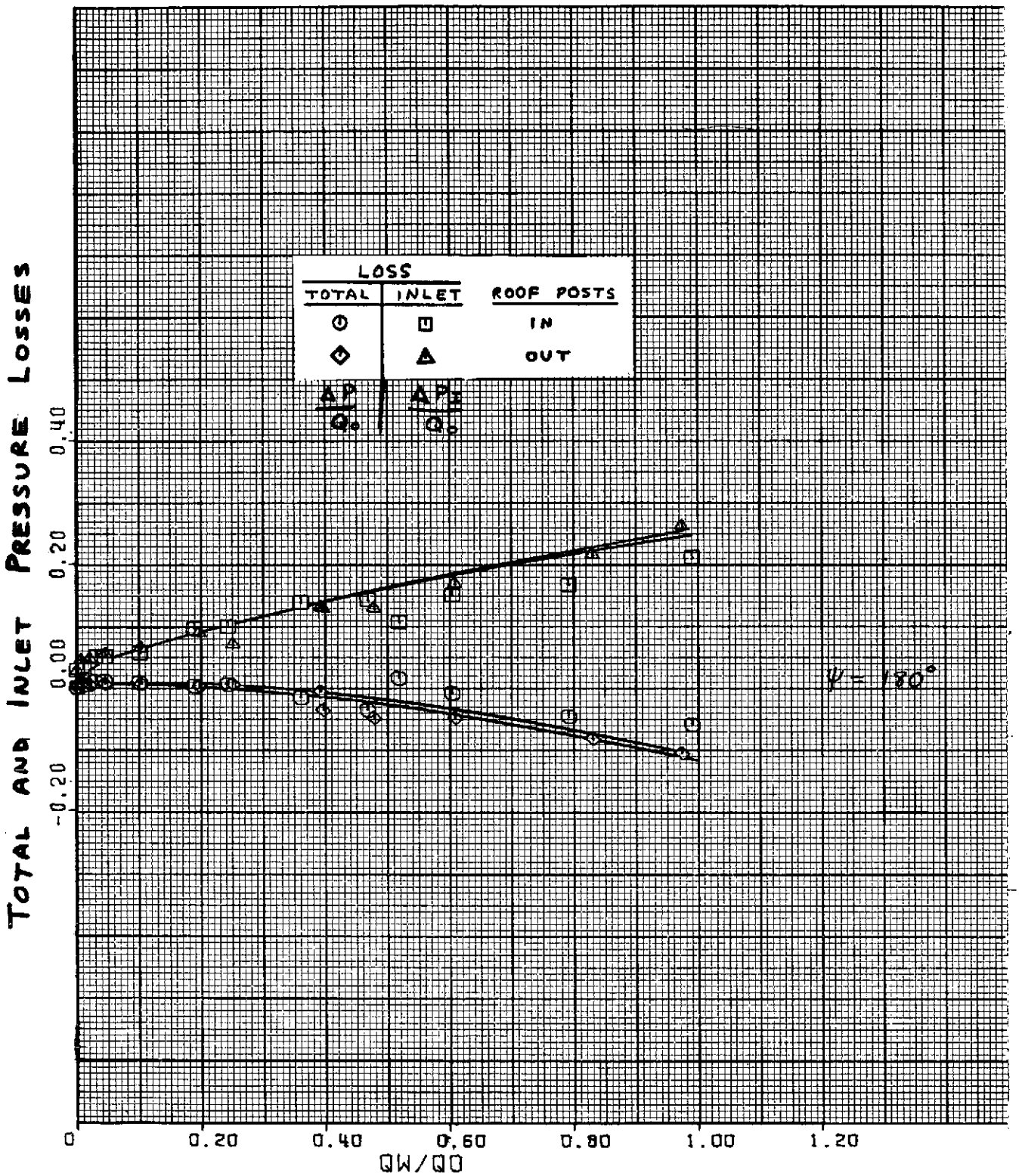

$\psi = 180°$.
(c) Pressure losses - concluded.

Figure 11. - Concluded.

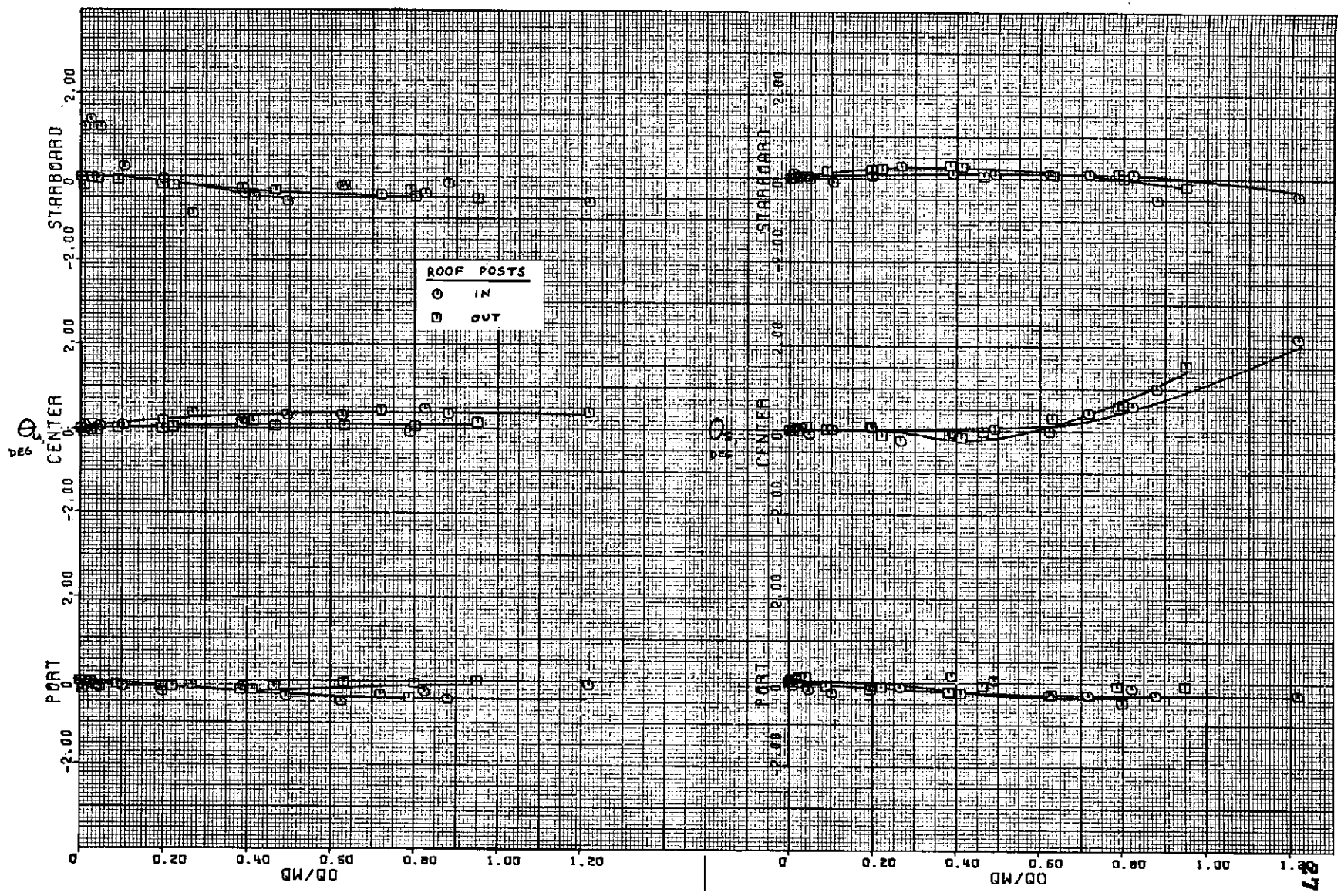

$\psi = 0°$.

(a) Test section flow angularities.

Figure 12. - Effect of inlet roof posts with 107×254 cm (42×100 in) inlet, peripheral flow straightener inside, 2.54×2.54 cm (1×1 in) contraction flow straightener, area ratio 20 exit.

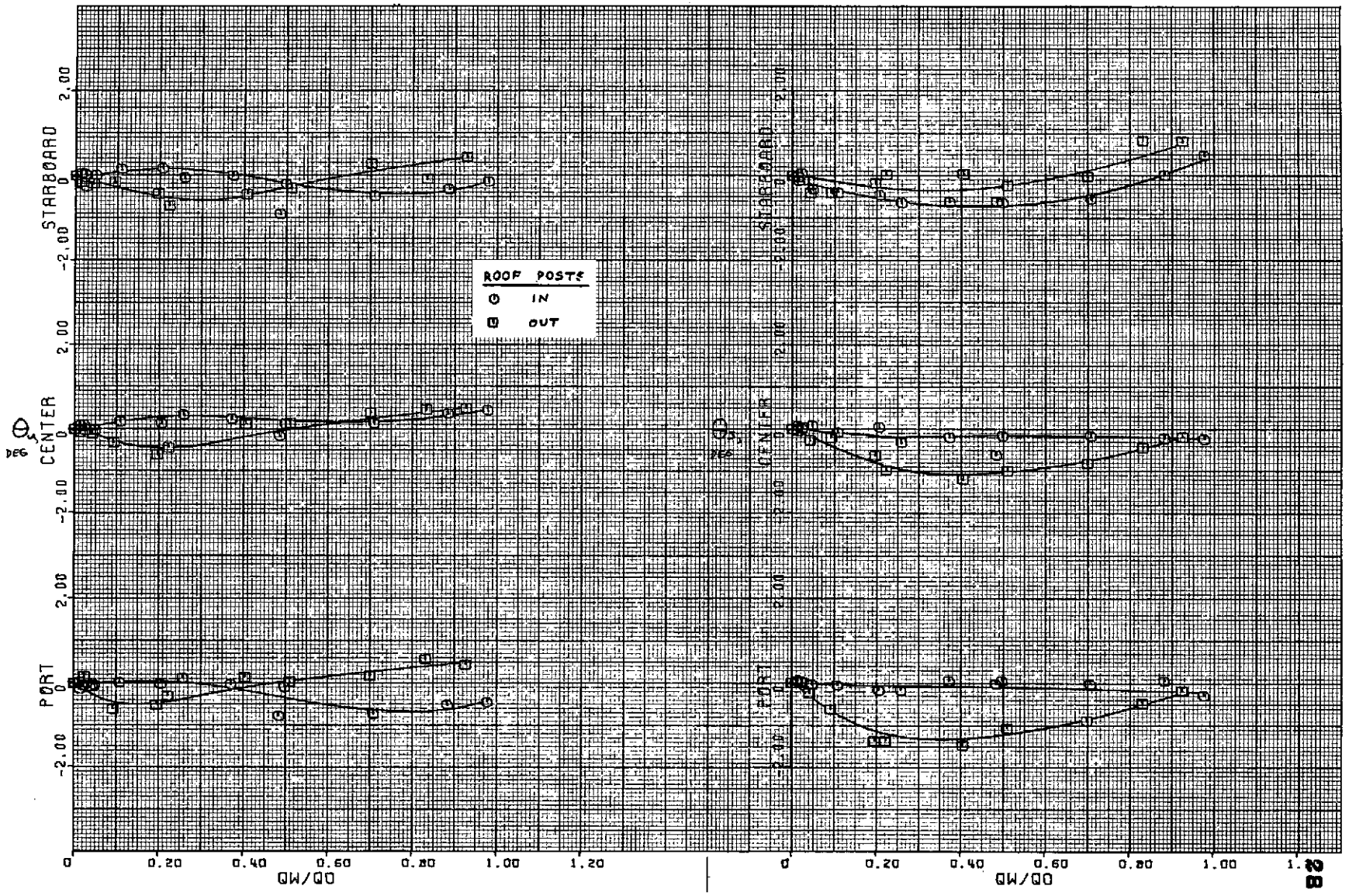

ψ = -90°.

(a) Test section flow angularities - concluded.

Figure 12. - Continued.

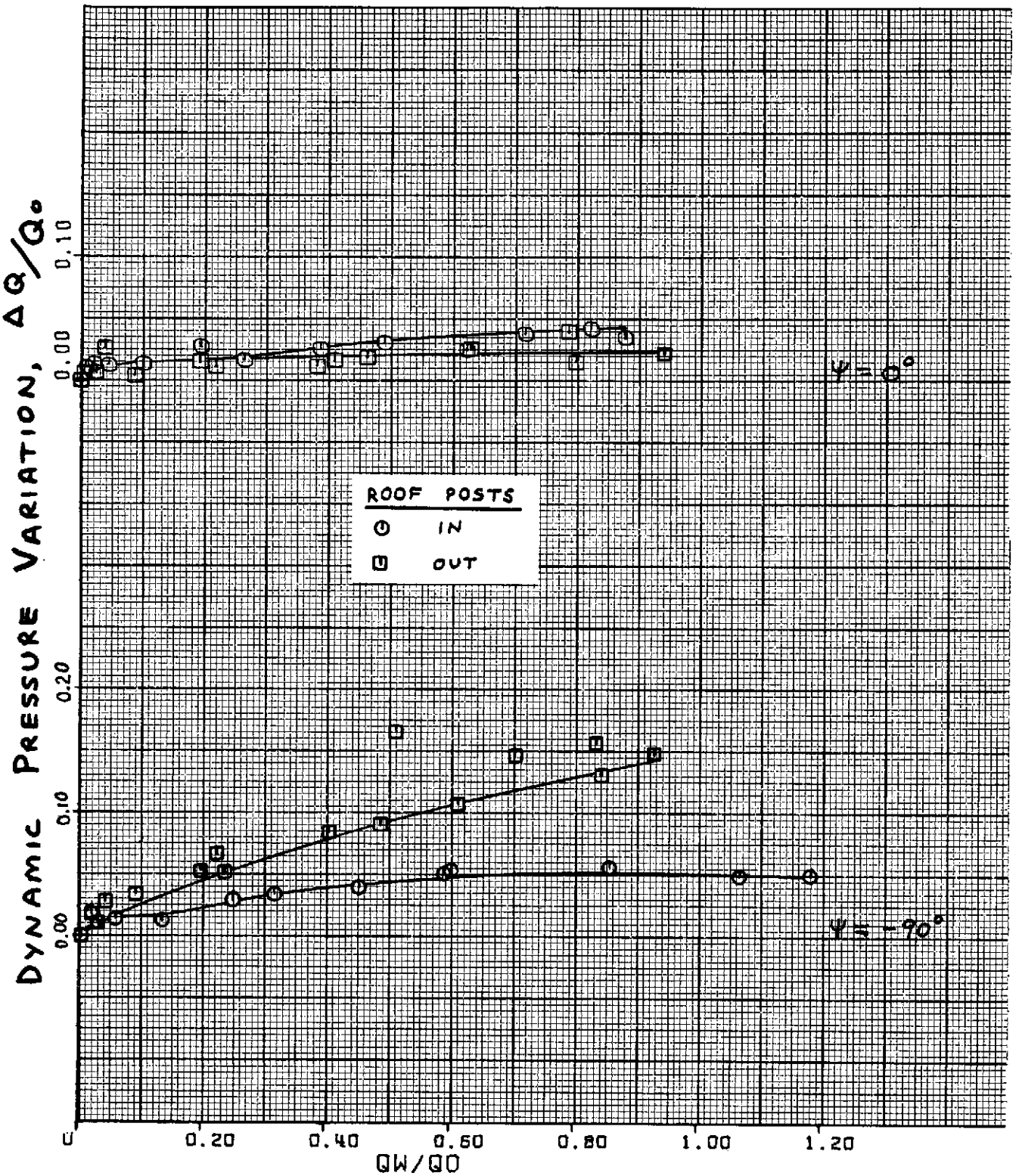

(b) Dynamic pressure variation; ψ = 0° and -90°.

Figure 12. - Continued.

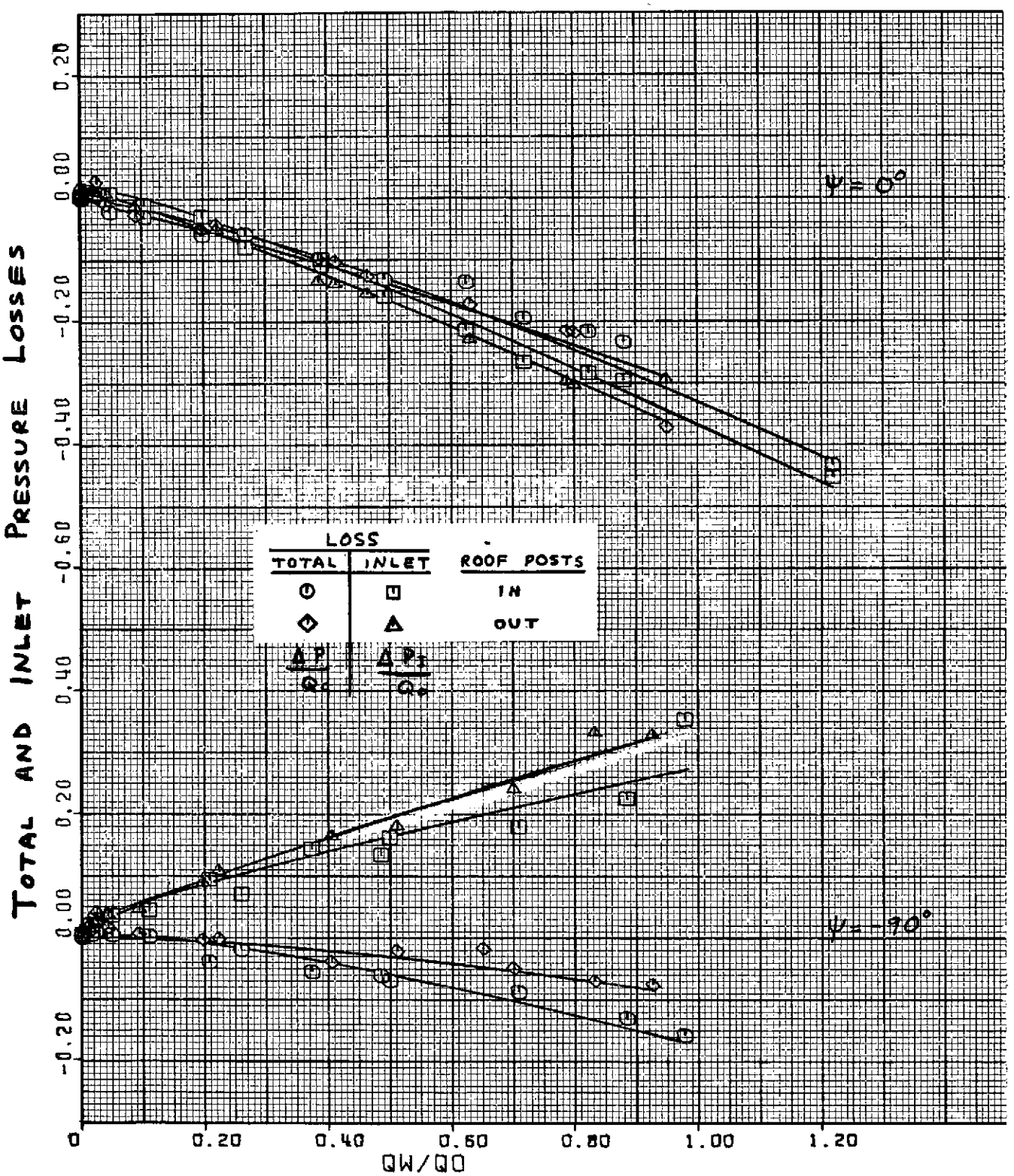

(c) Pressure losses; ψ = 0° and -90°.

Figure 12. - Concluded.

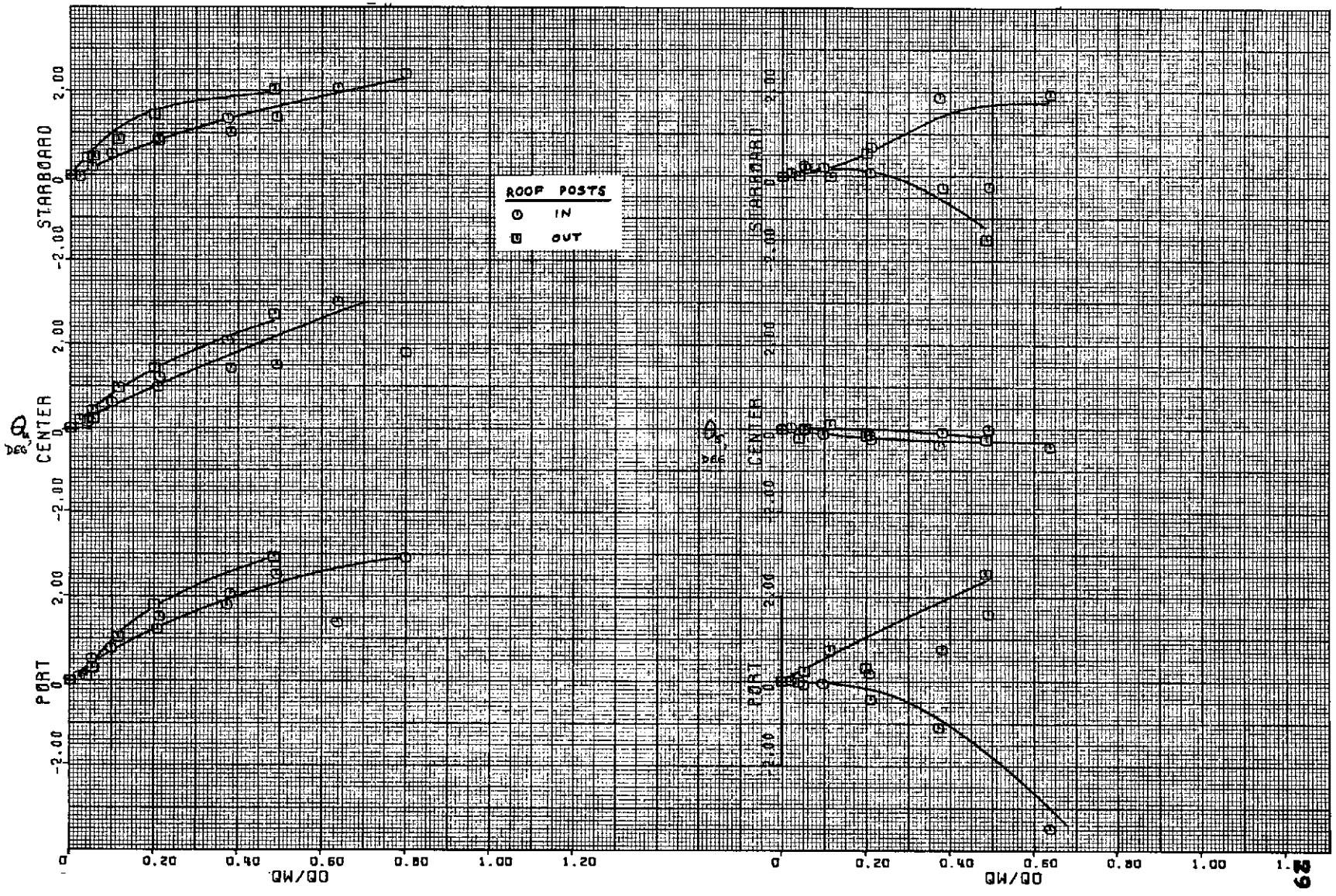

$\psi = 0°$.
(a) Test section flow angularities.

Figure 13. - Effect of inlet roof posts with 107×254 cm (42×100 in) inlet, peripheral flow straighteners removed, 2.54×2.54 cm (1×1 in) contraction flow straightener, area ratio 20 exit.

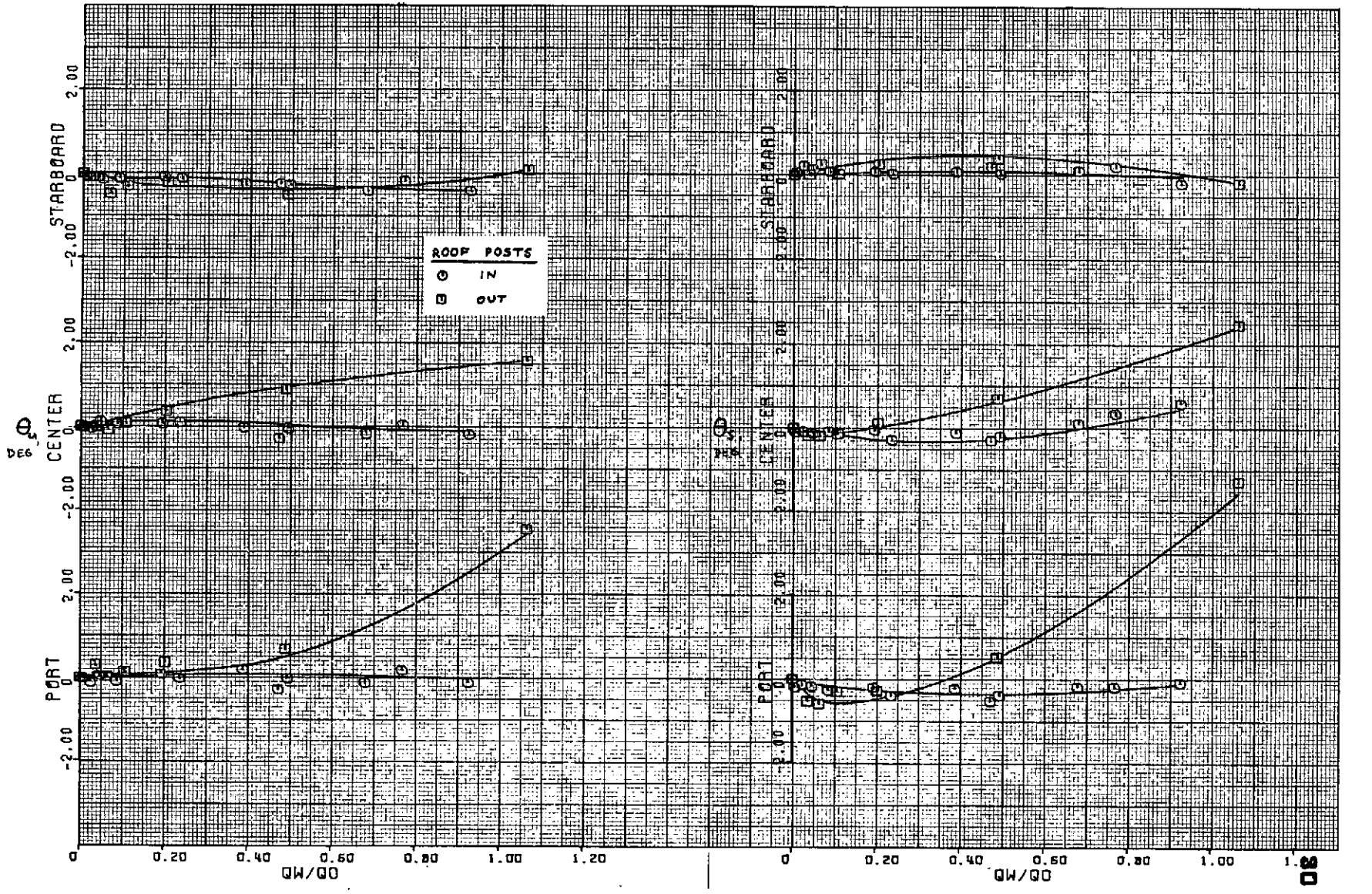

ψ = -90°.
(a) Test section flow angularities - continued.

Figure 13. - Continued.

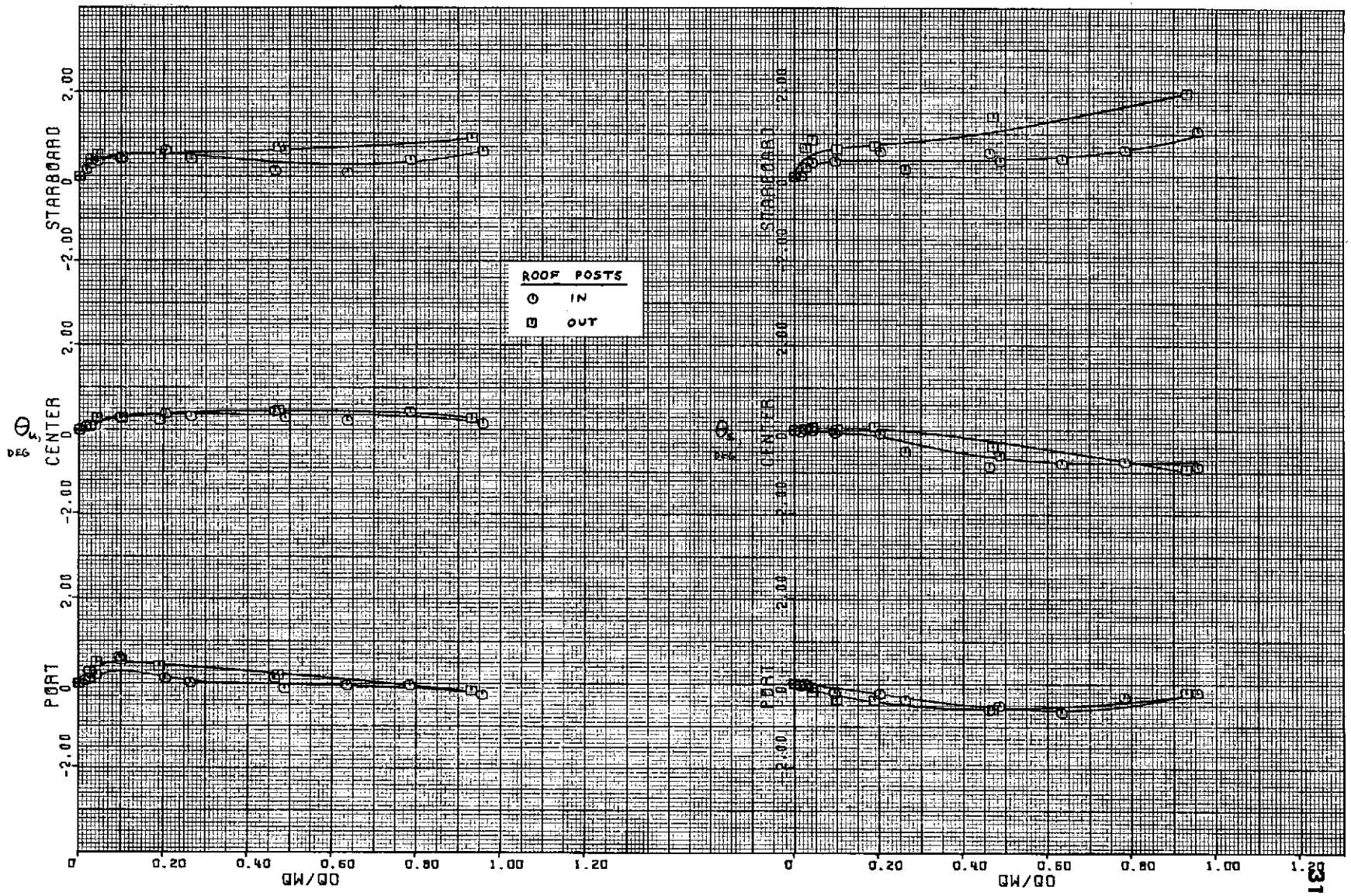

$\psi = 180°$.

(a) Test section flow angularities - concluded.

Figure 13. - Continued.

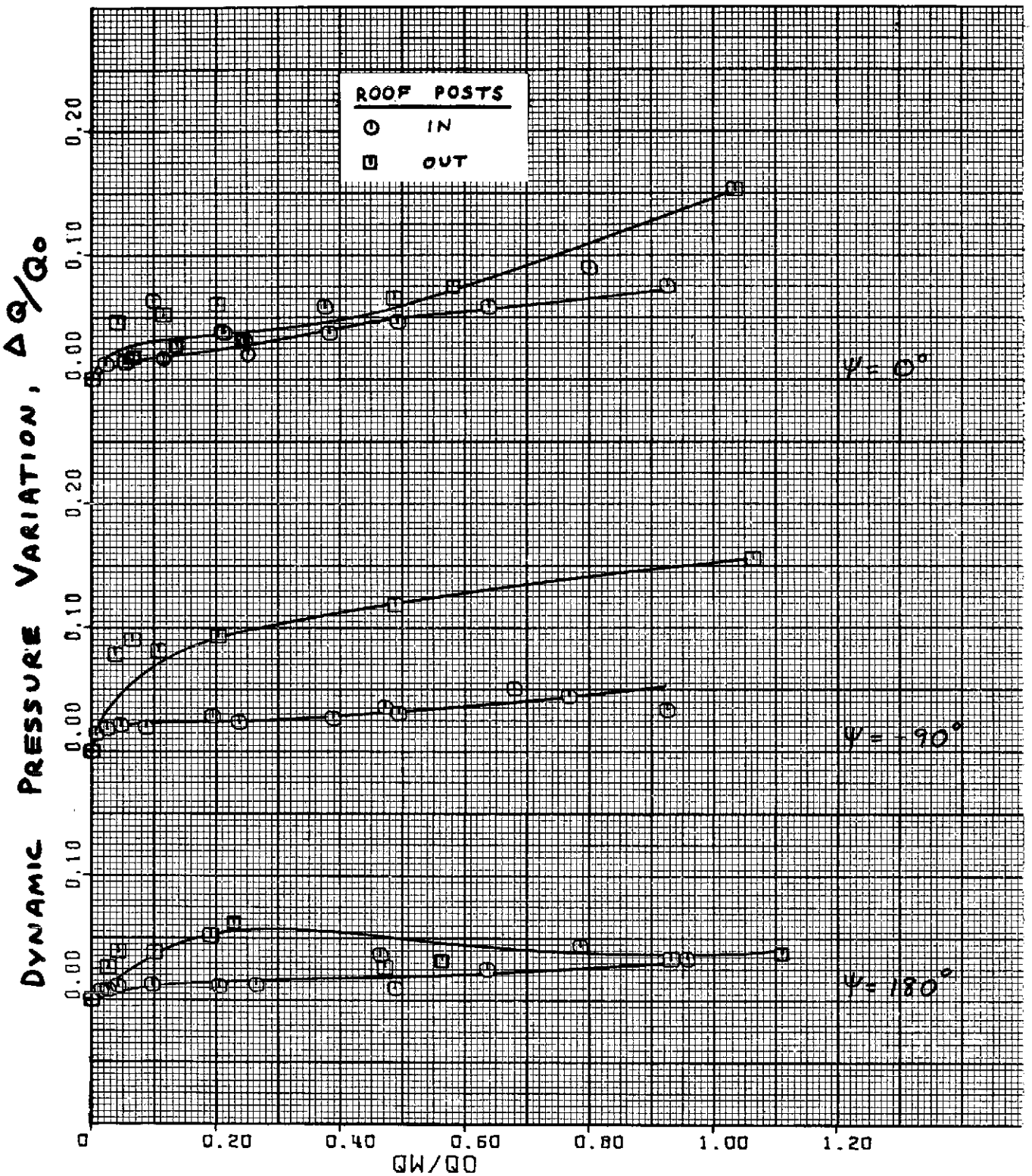

(b) Dynamic pressure variation; ψ = 0°, -90° and 180°.

Figure 13. - Continued.

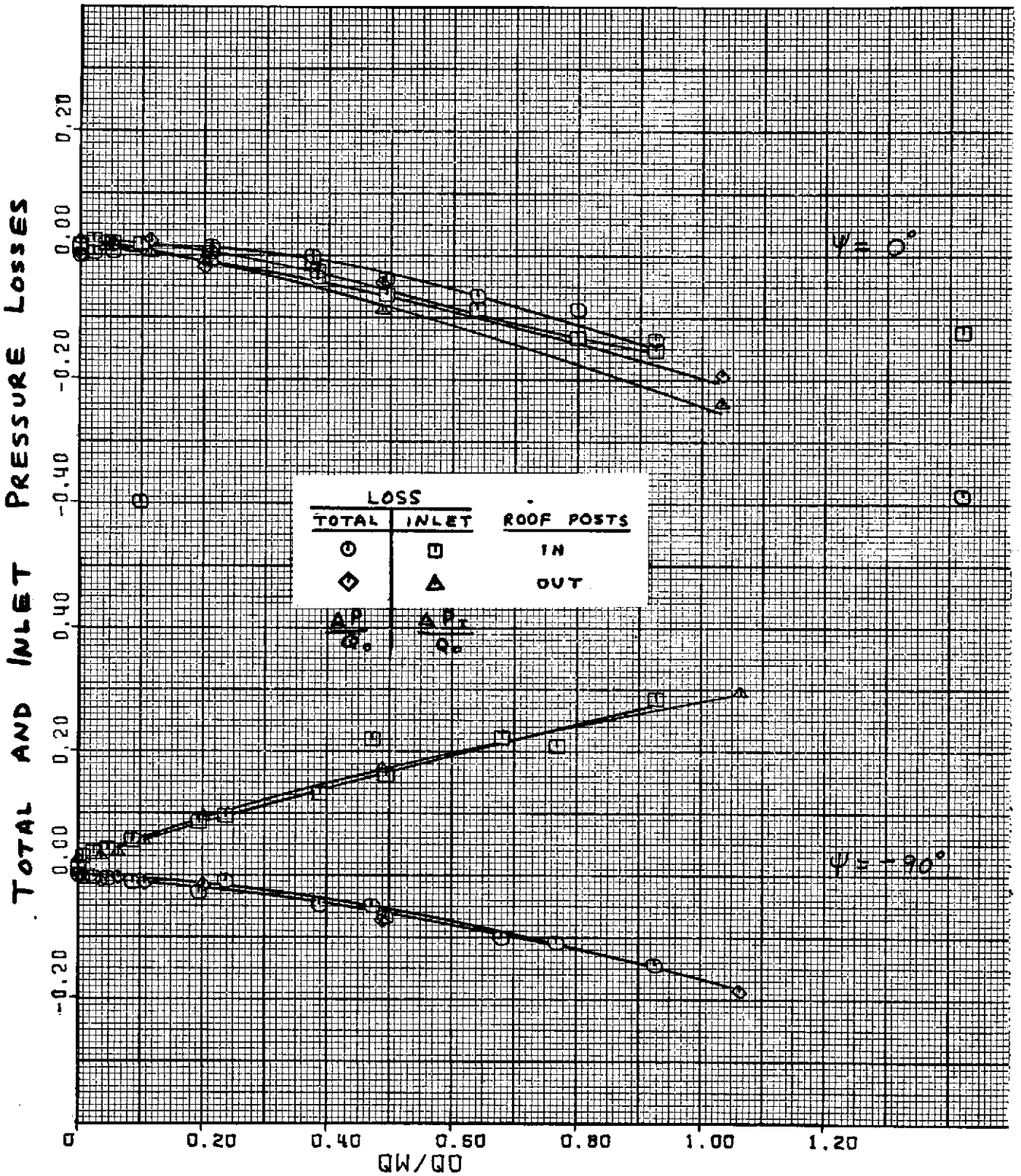

ψ = 0° and -90°.
(c) Pressure losses.

Figure 13. - Continued.

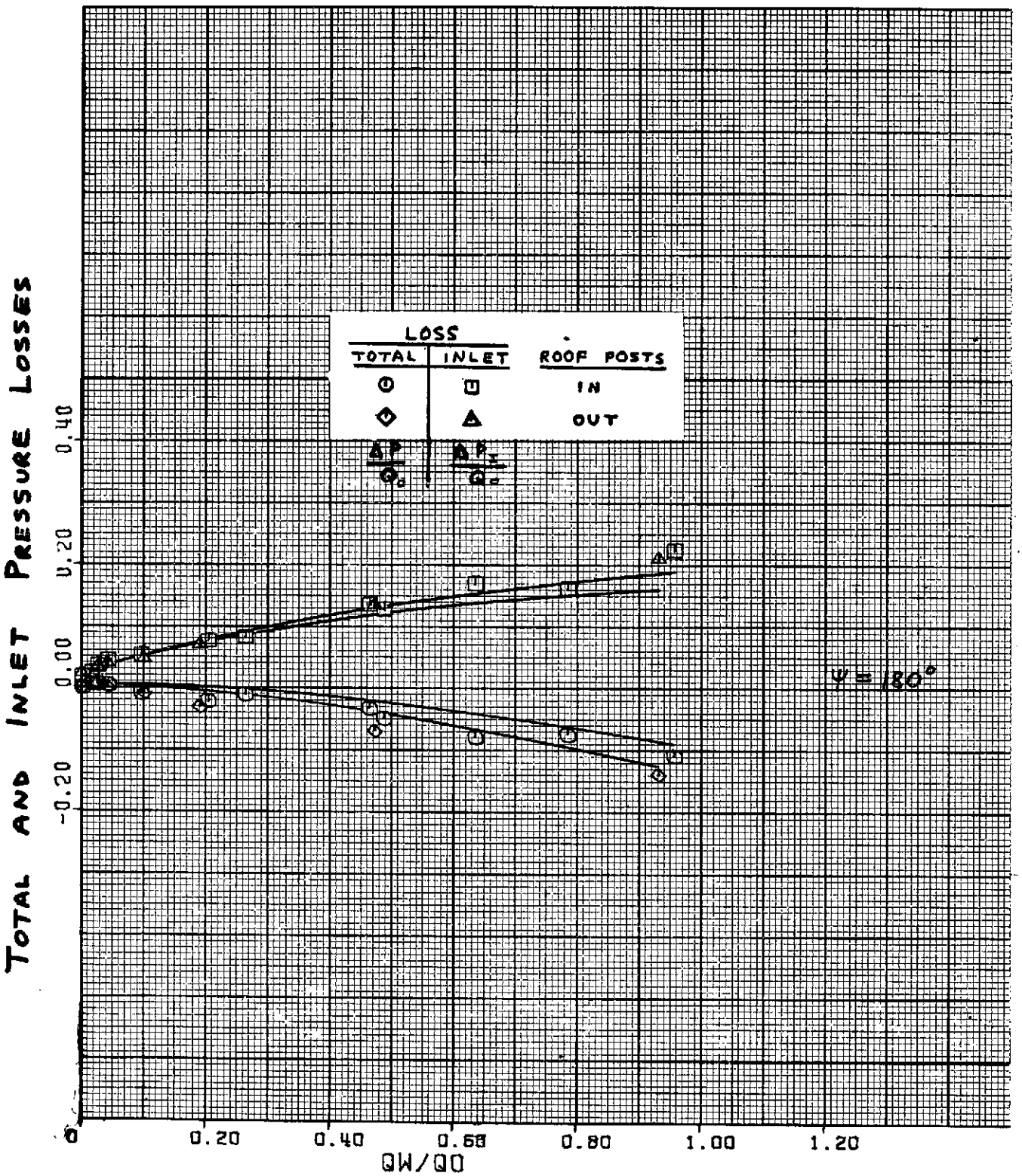

ψ = 180°.
(c) Pressure losses - concluded.

Figure 13. - Concluded.

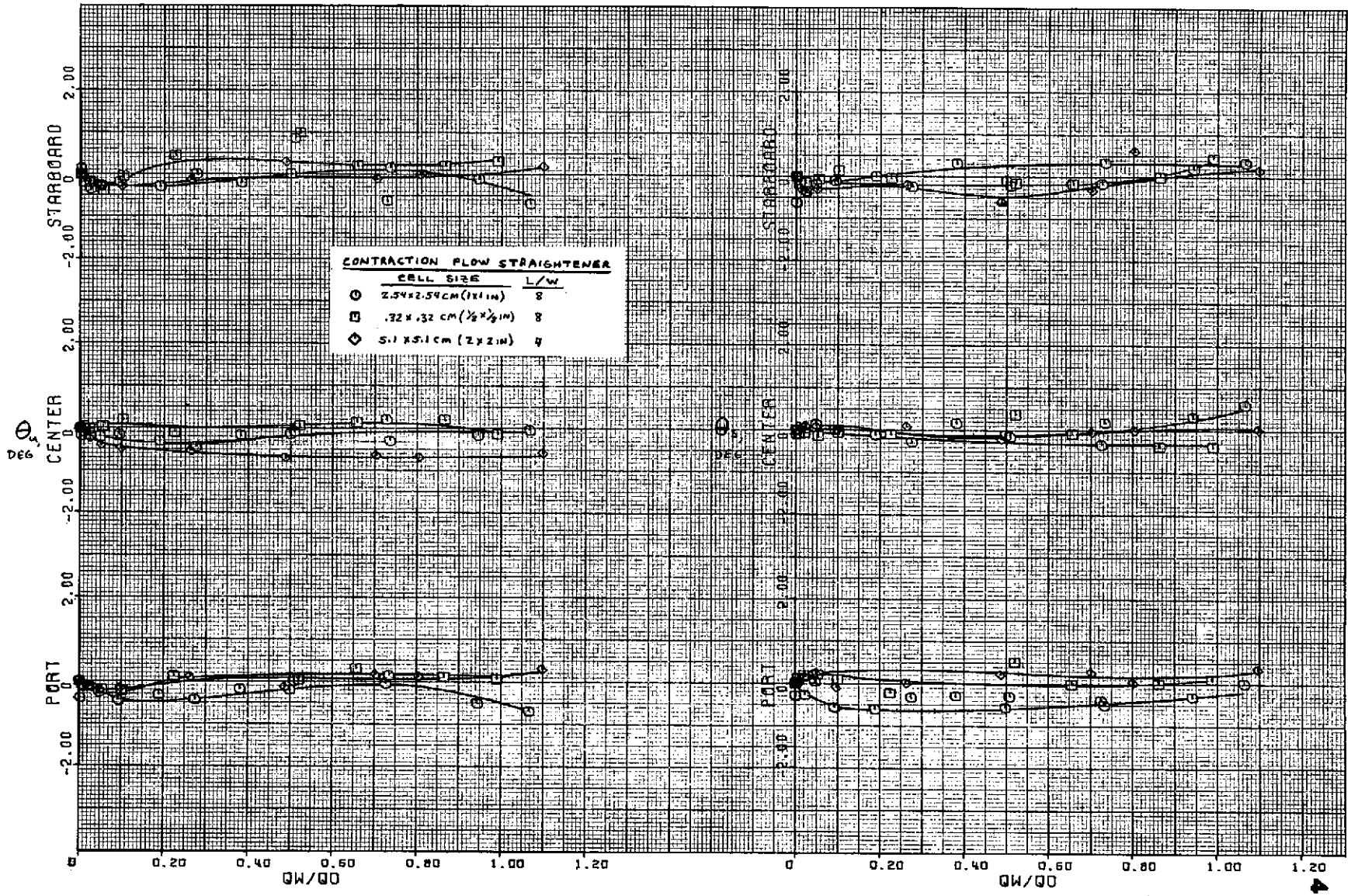

ψ = 0°.
(a) Test section flow angularities.

Figure 14. – Effect of contraction flow straightener size with 58×203 cm (23×80 in) inlet, roof posts in, front-only peripheral flow straightener, area ratio 20 exit.

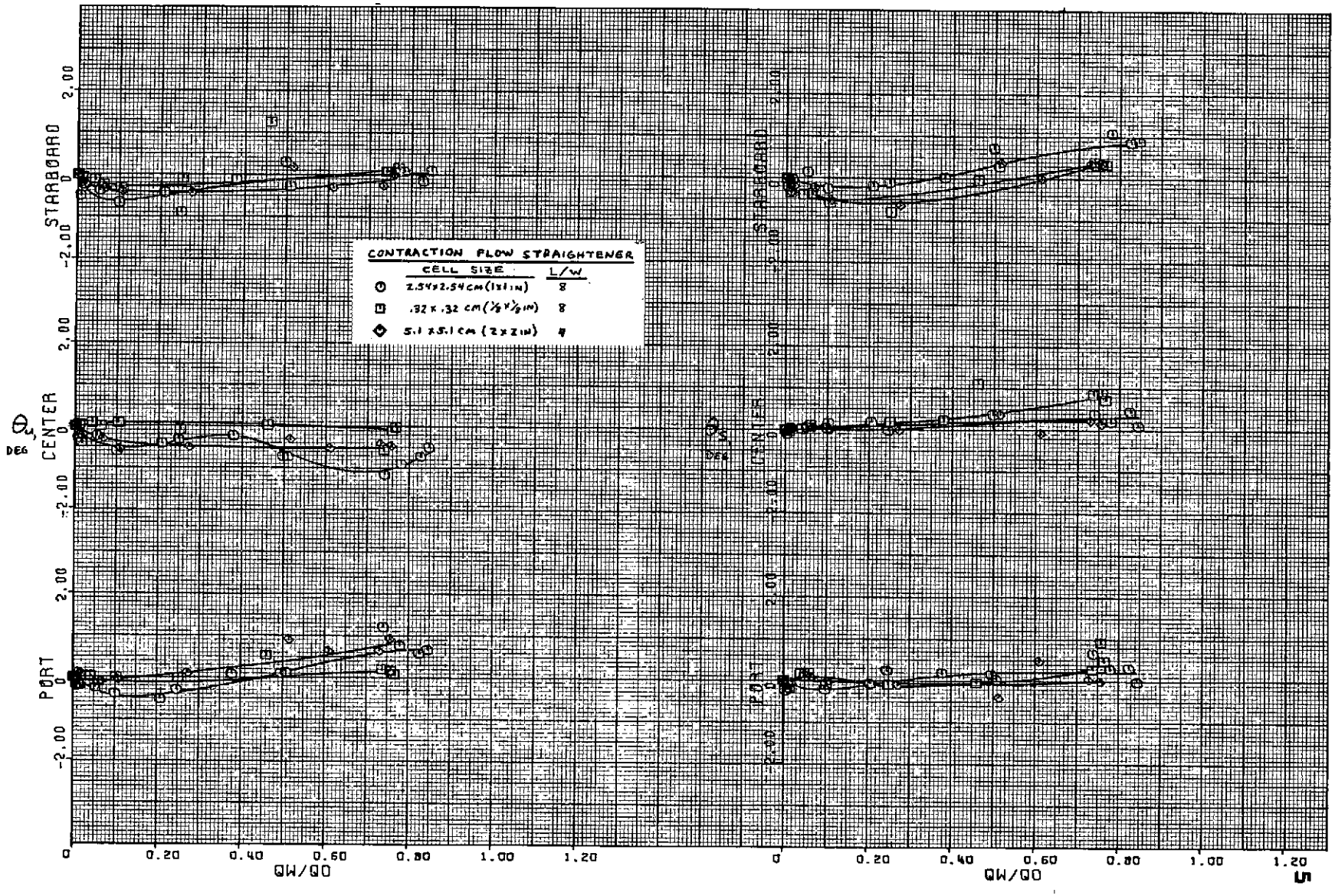

ψ = -22-1/2°.
(a) Test section flow angularities - continued.

Figure 14. - Continued.

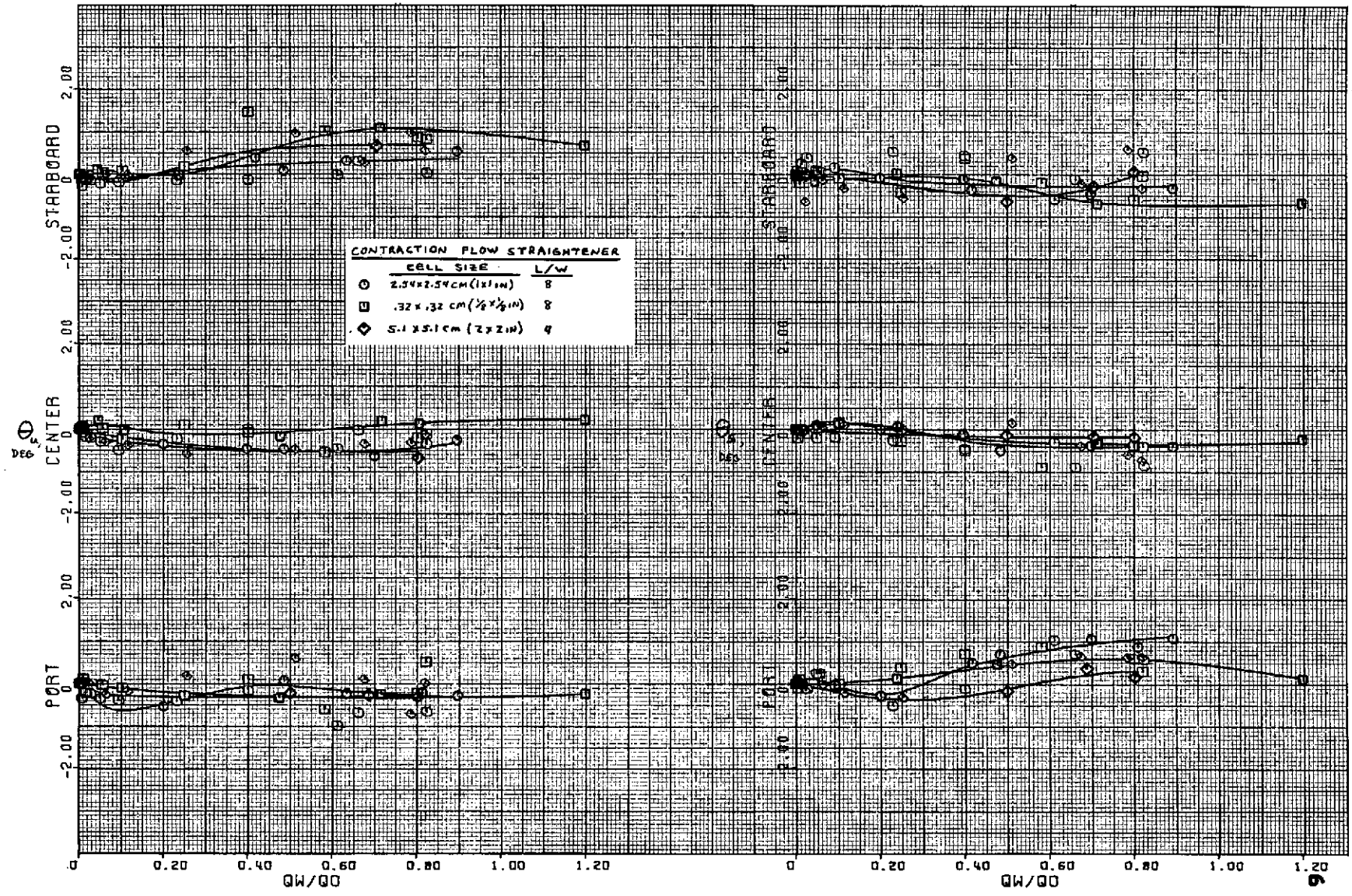

ψ = -45°.

(a) Test section flow angularities - continued.

Figure 14. - Continued.

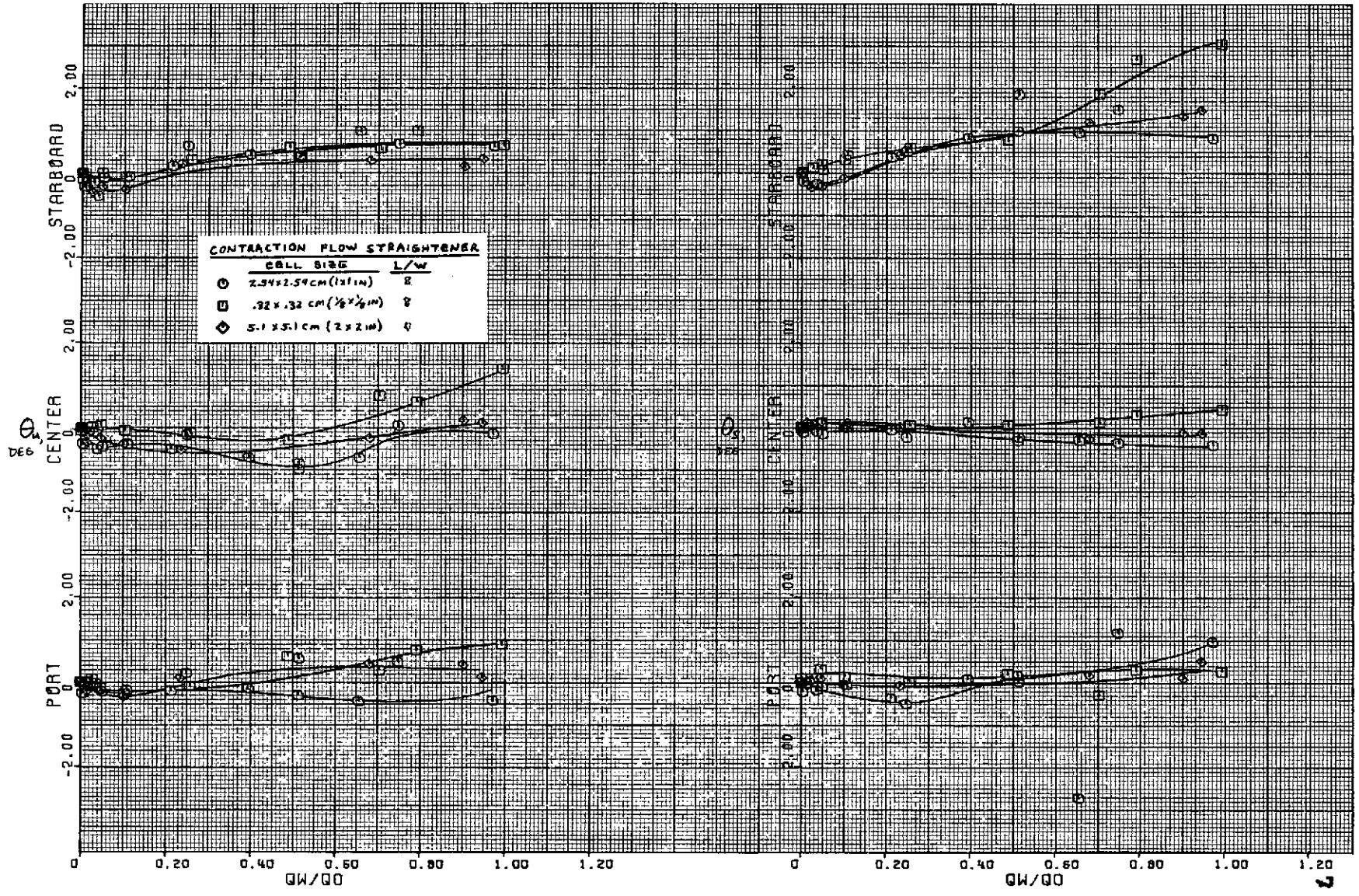

ψ = -67-1/2°.
(a) Test section flow angularities - continued.

Figure 14. - Continued.

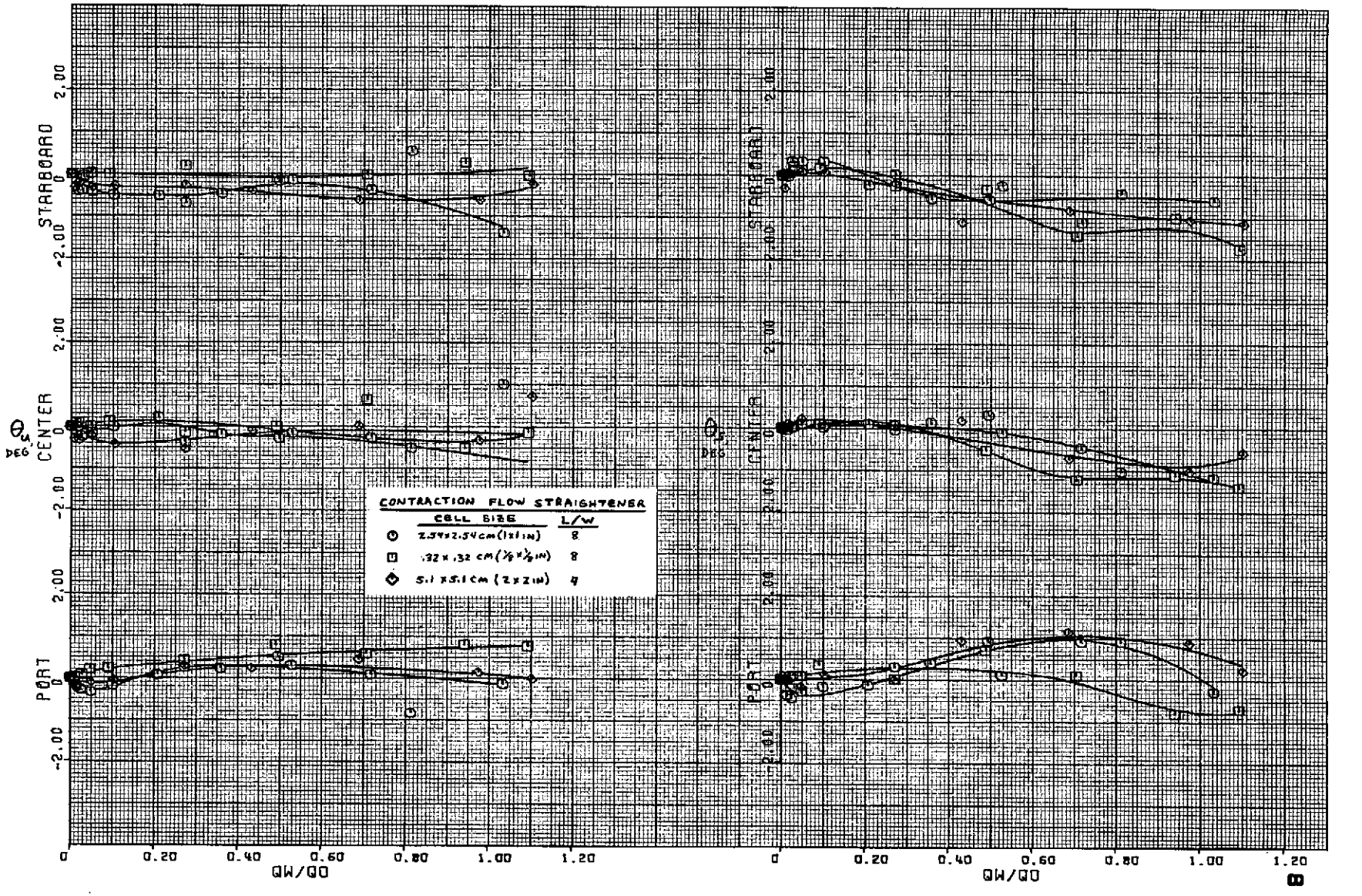

$\phi = -90°$.

(a) Test section flow angularities - continued.

Figure 14. - Continued.

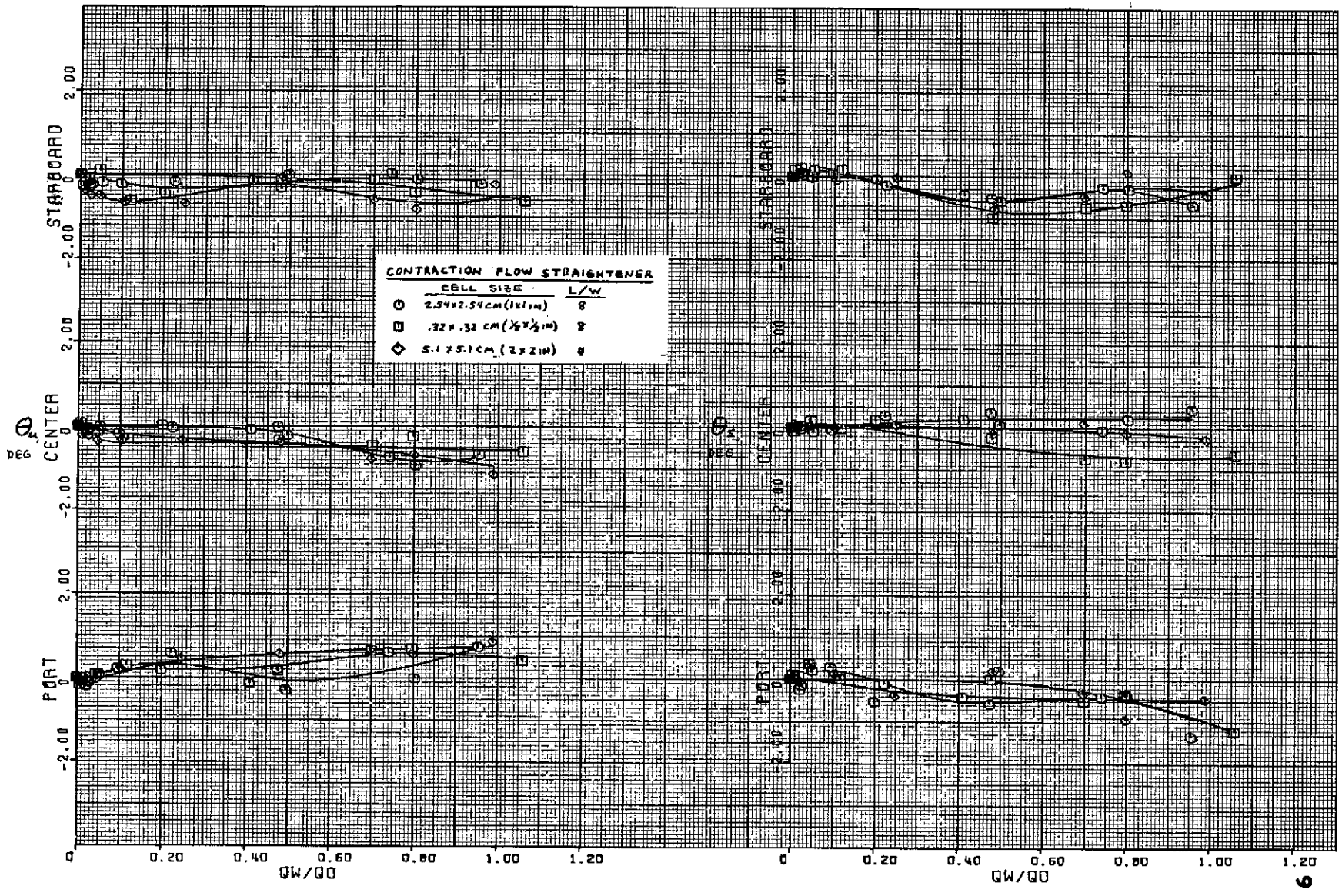

ψ = -112-1/2°.
(a) Test section flow angularities - continued.

Figure 14. - Continued.

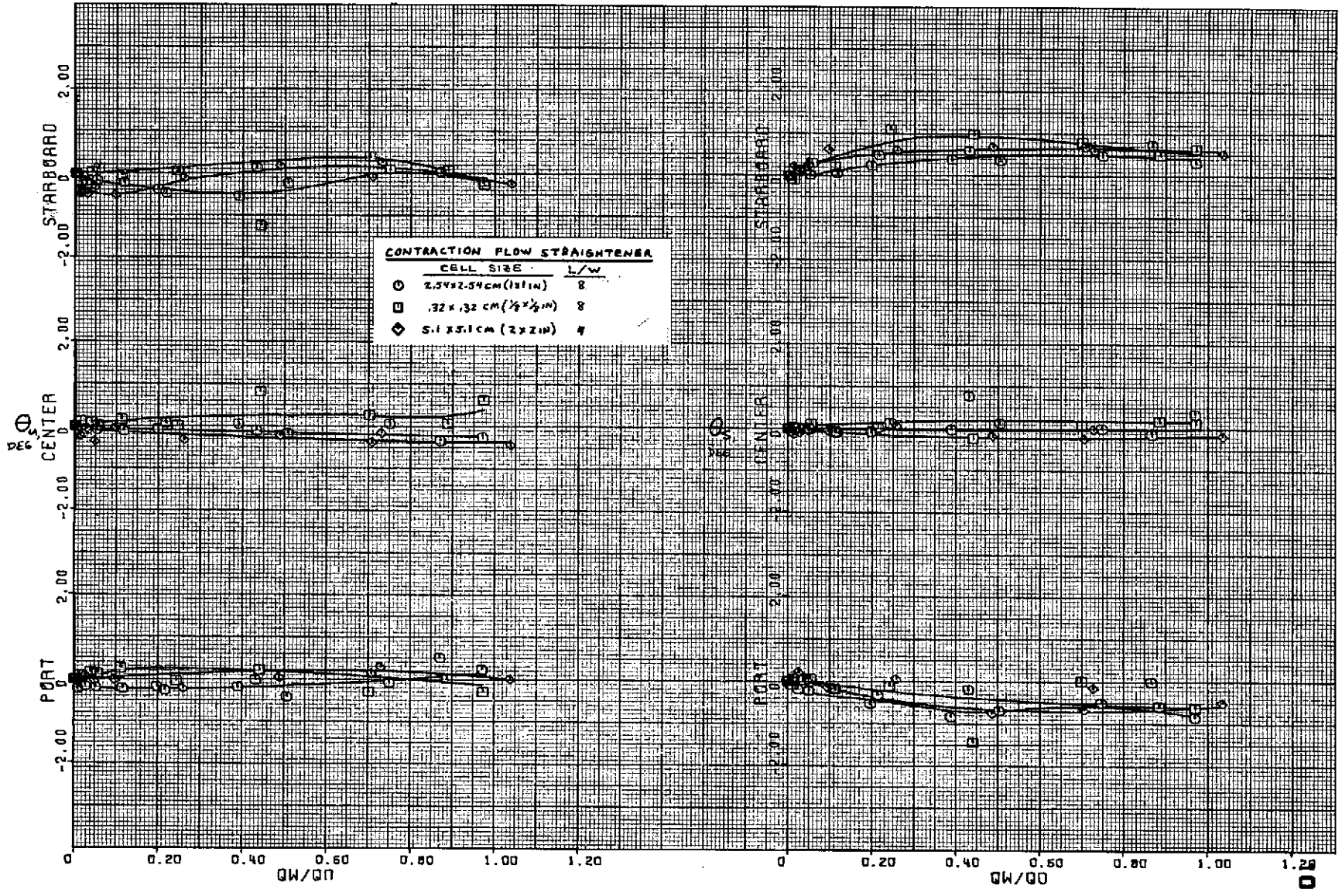

ψ = -135°.

(a) Test section flow angularities - continued.

Figure 14. - Continued.

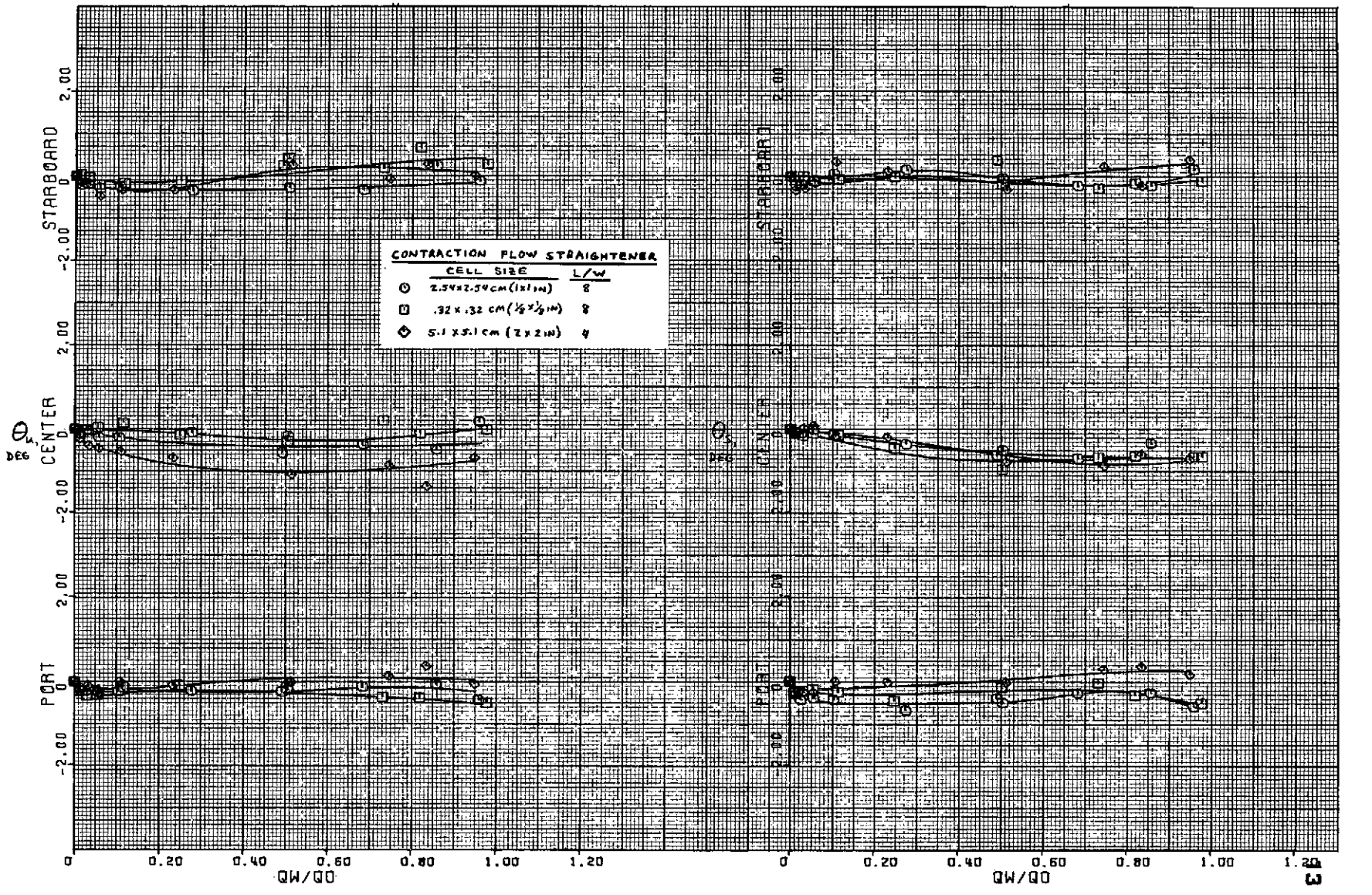

ψ = 157-1/2°.
(a) Test section flow angularities - concluded.

Figure 14. - Continued.

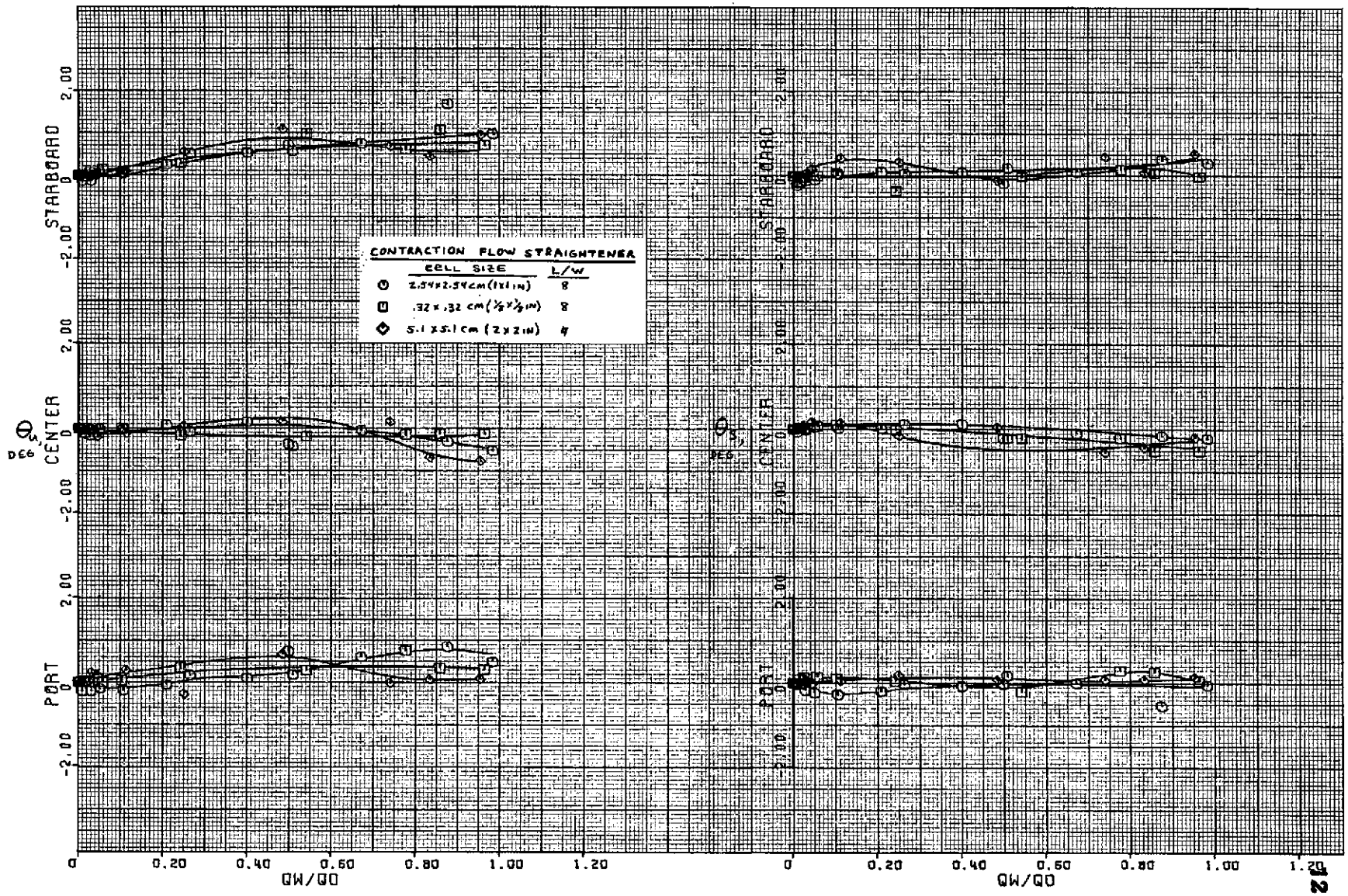

ψ = 180°.
(a) Test section flow angularities - continued.

Figure 14. - Continued.

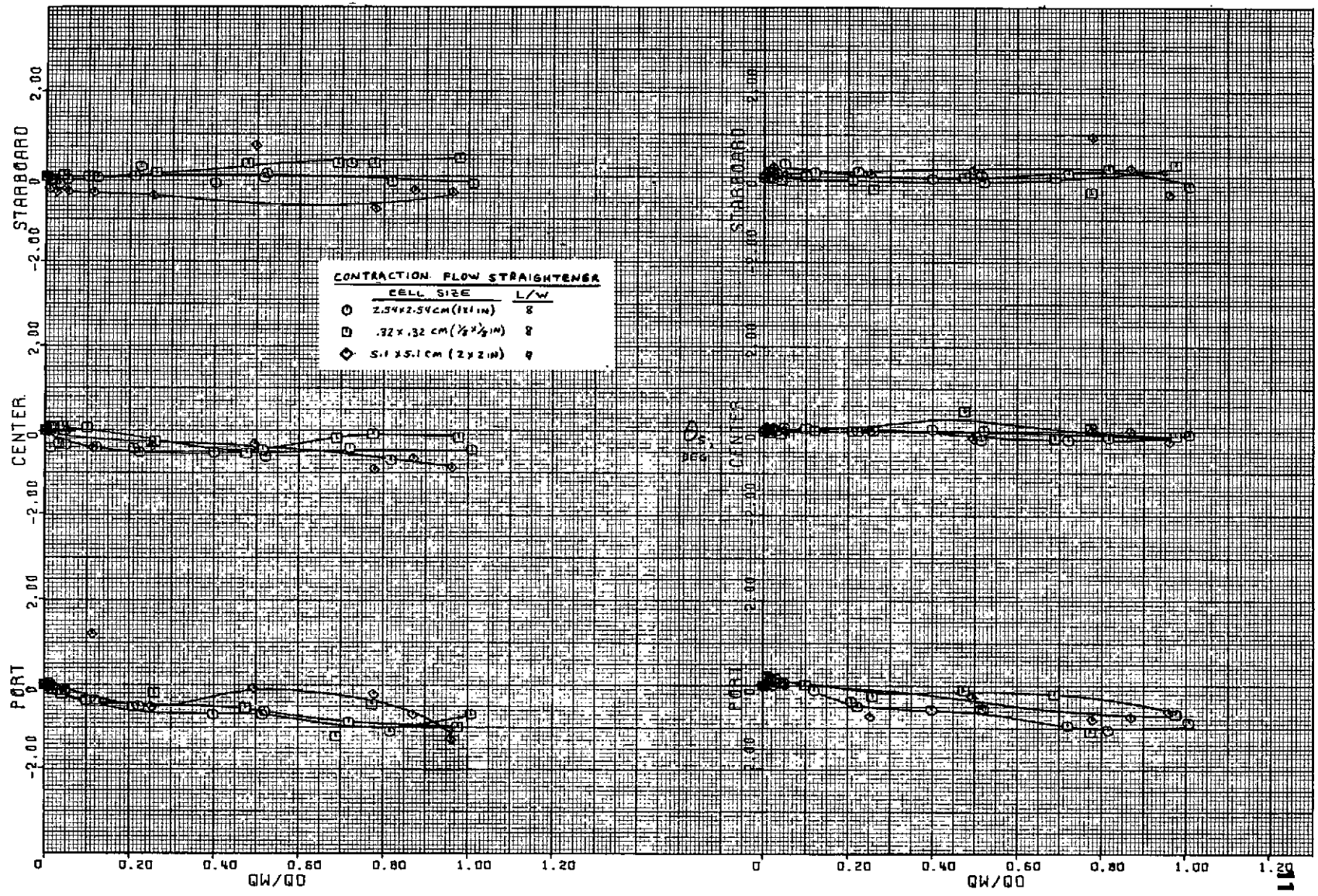

ψ = -157-1/2°.
(a) Test section flow angularities - continued.

Figure 14. - Continued.

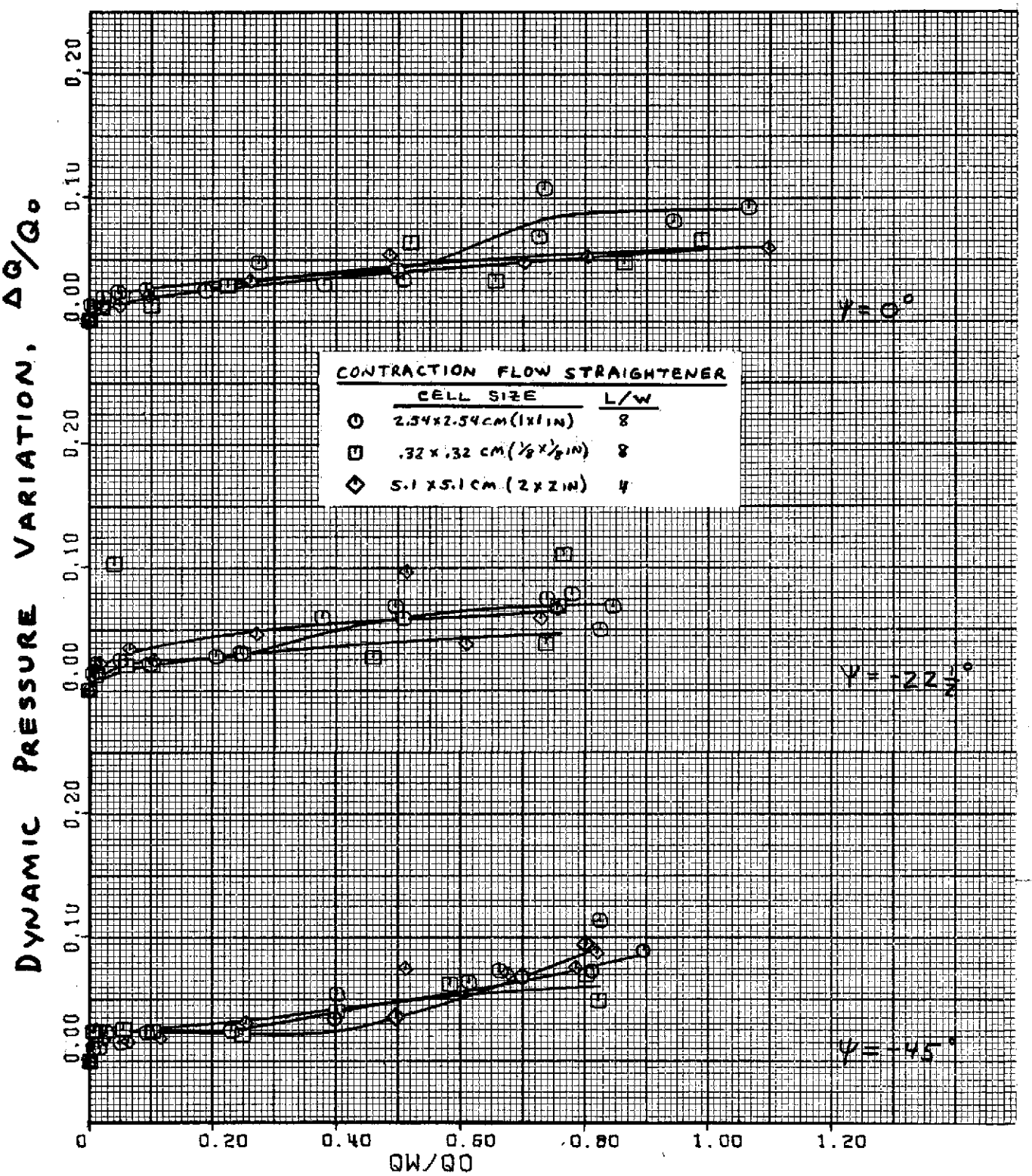

ψ = 0°, -22-1/2° and -45°.
(b) Dynamic pressure variation.

Figure 14. - Continued.

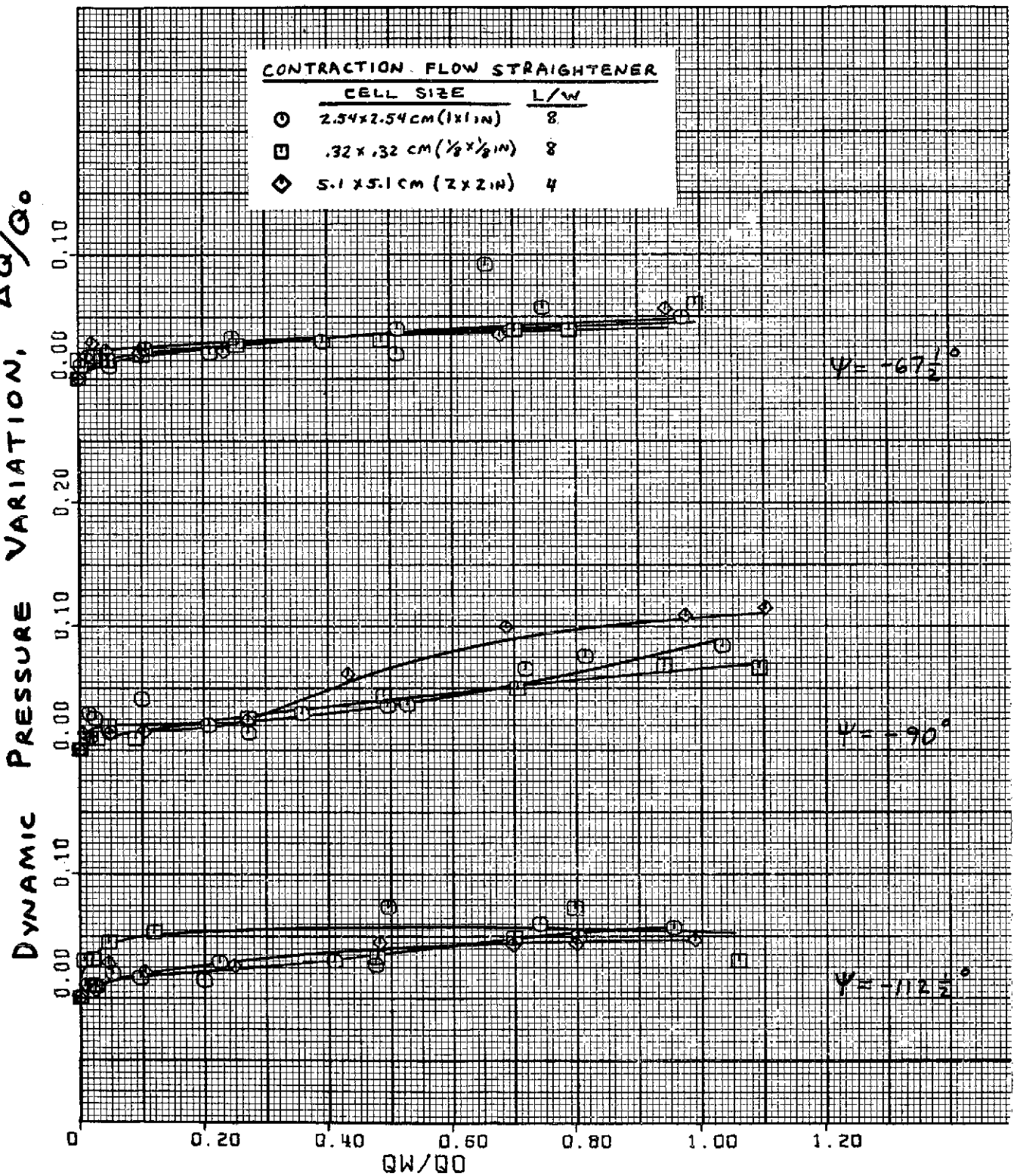

ψ =-67-1/2°, -90° and -112-1/2°.
(b) Dynamic pressure variation - continued.

Figure 14. - Continued.

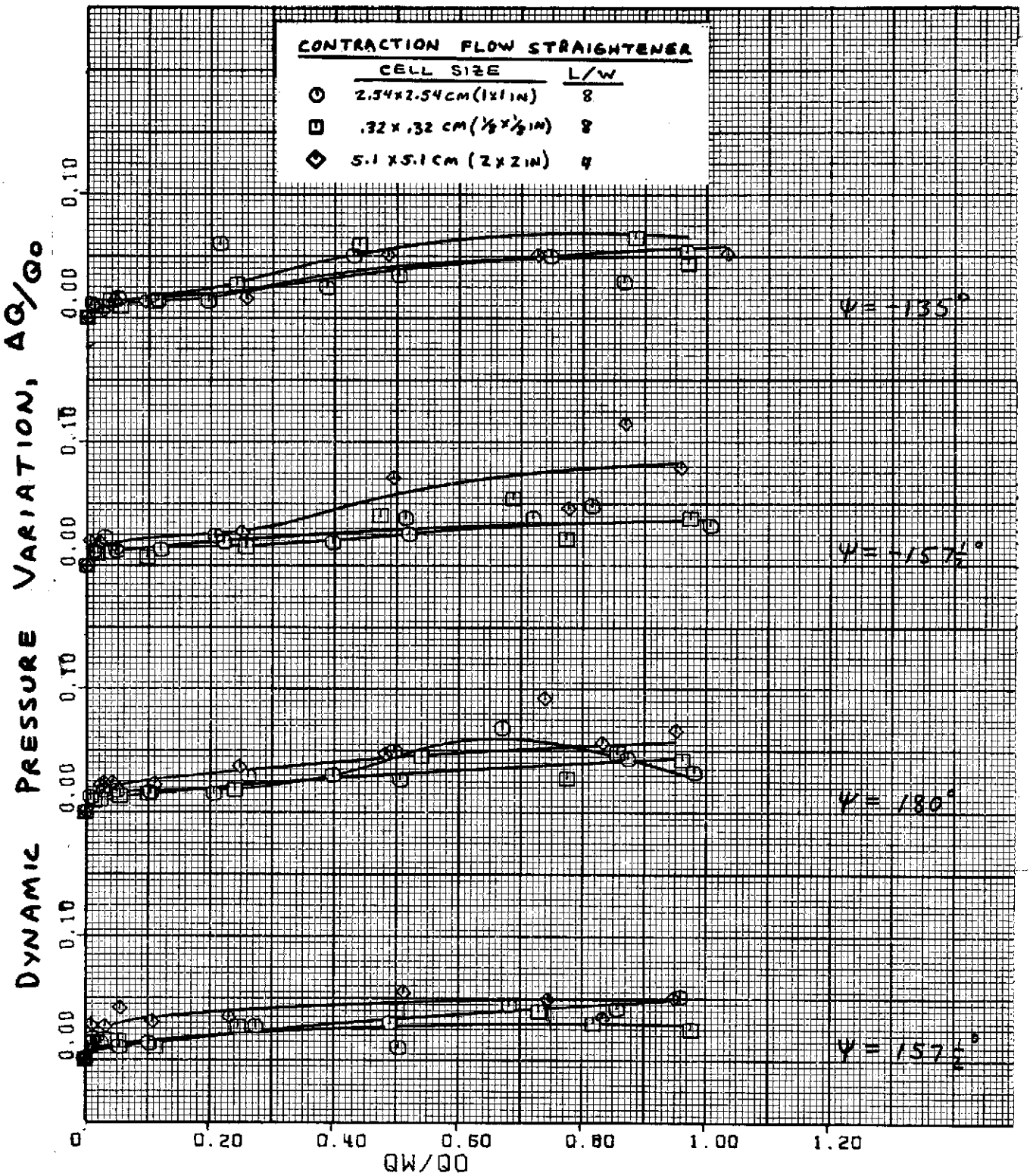

ψ = -135°, -157-1/2°, 180° and 157-1/2°.
(b) Dynamic pressure variation - concluded.

Figure 14. - Continued.

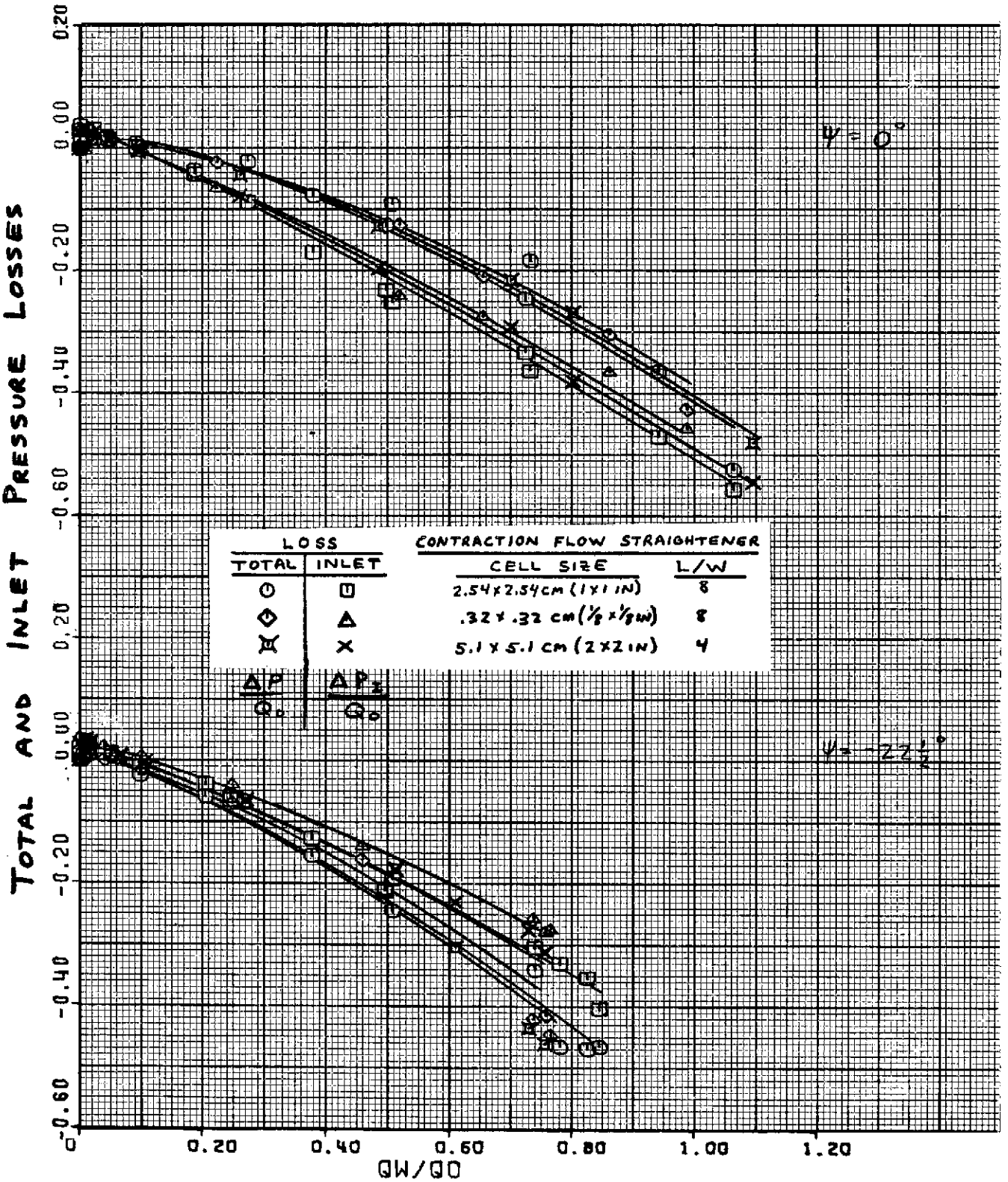

ψ = 0° and -22-1/2°.
(c) Pressure losses.

Figure 14. - Continued.

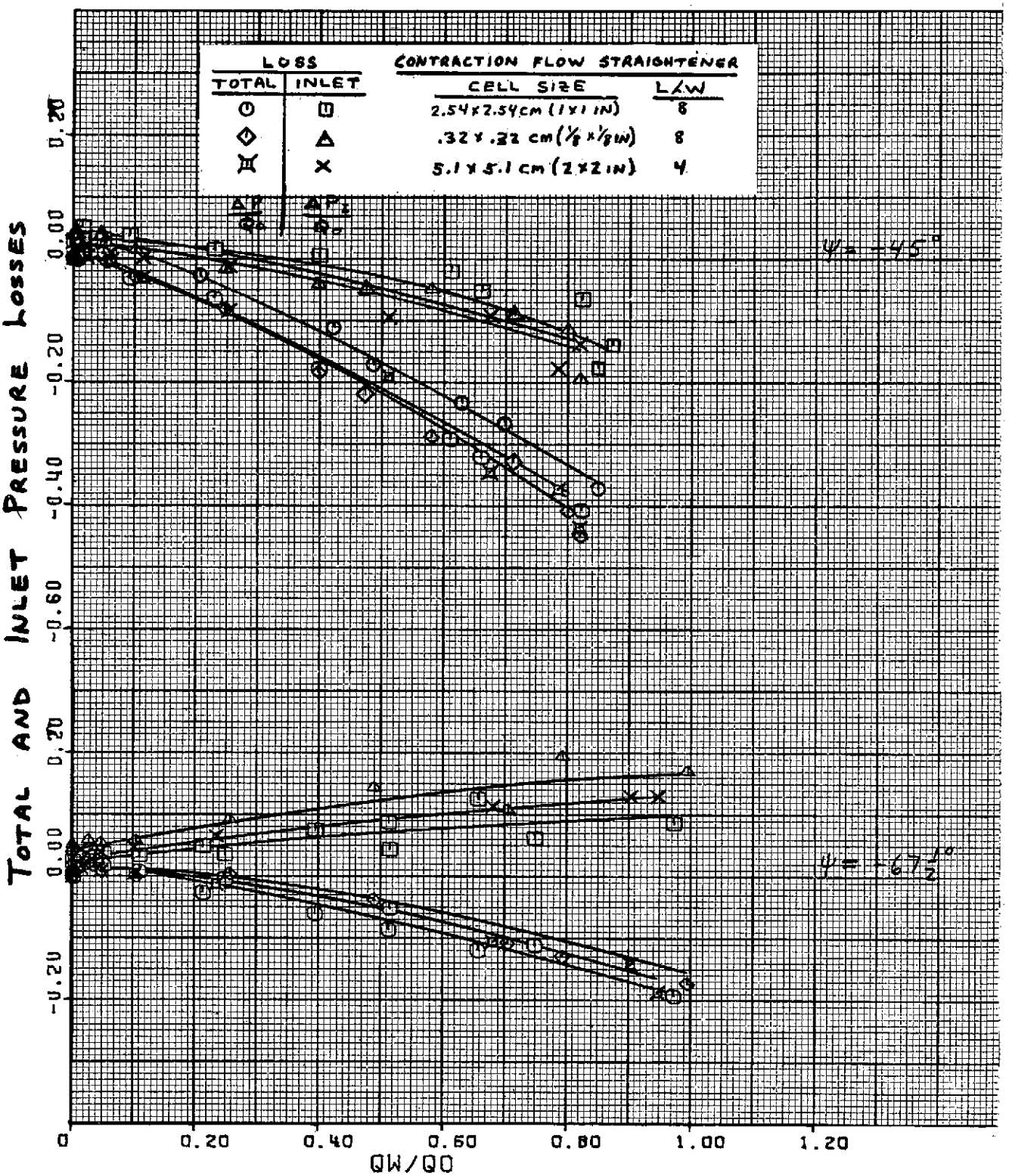

ψ = -45° and -67-1/2°.
(c) Pressure losses - continued.

Figure 14. - Continued.

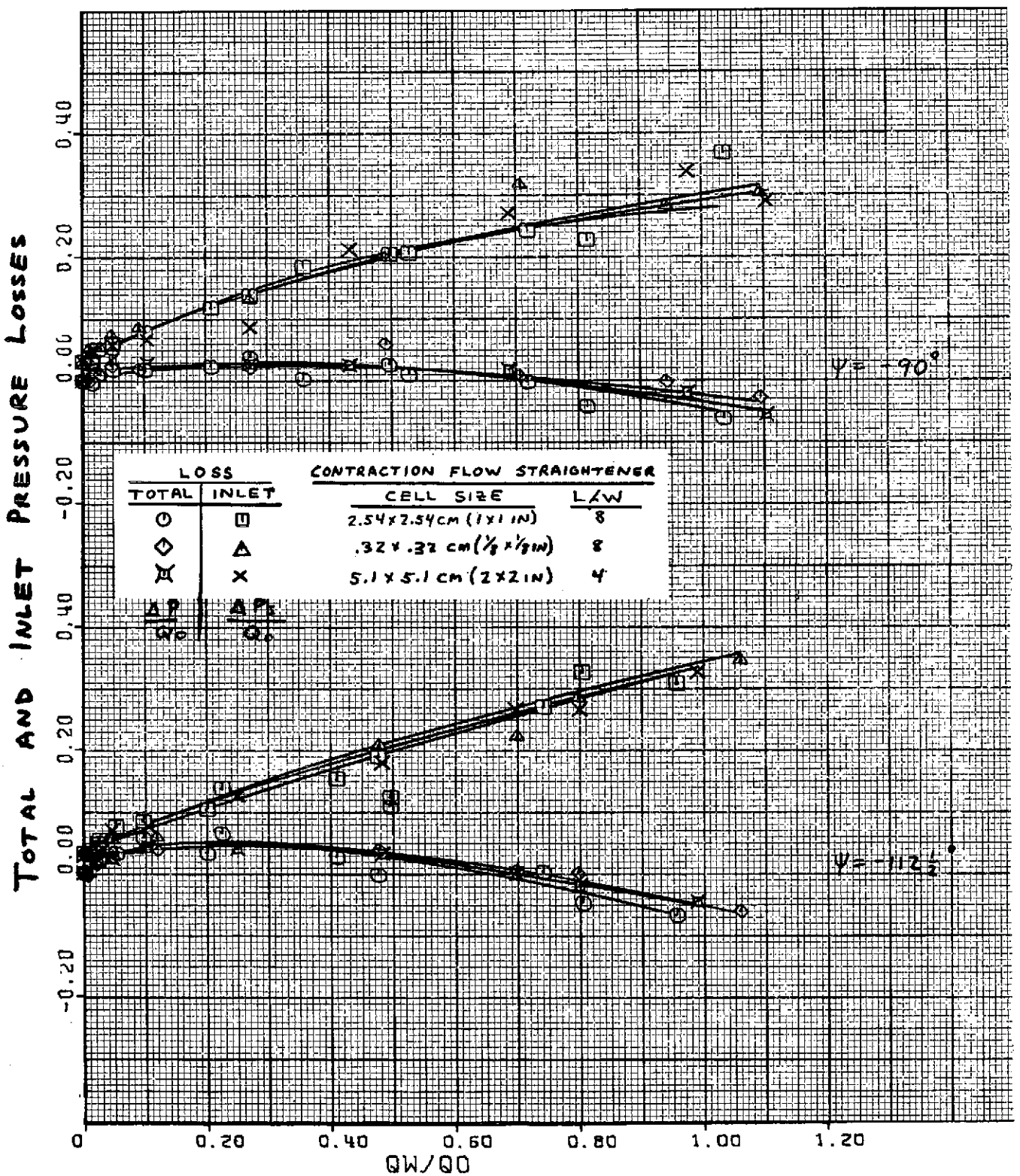

ψ = -90° and -112-1/2°.
(c) Pressure losses - continued.

Figure 14. - Continued.

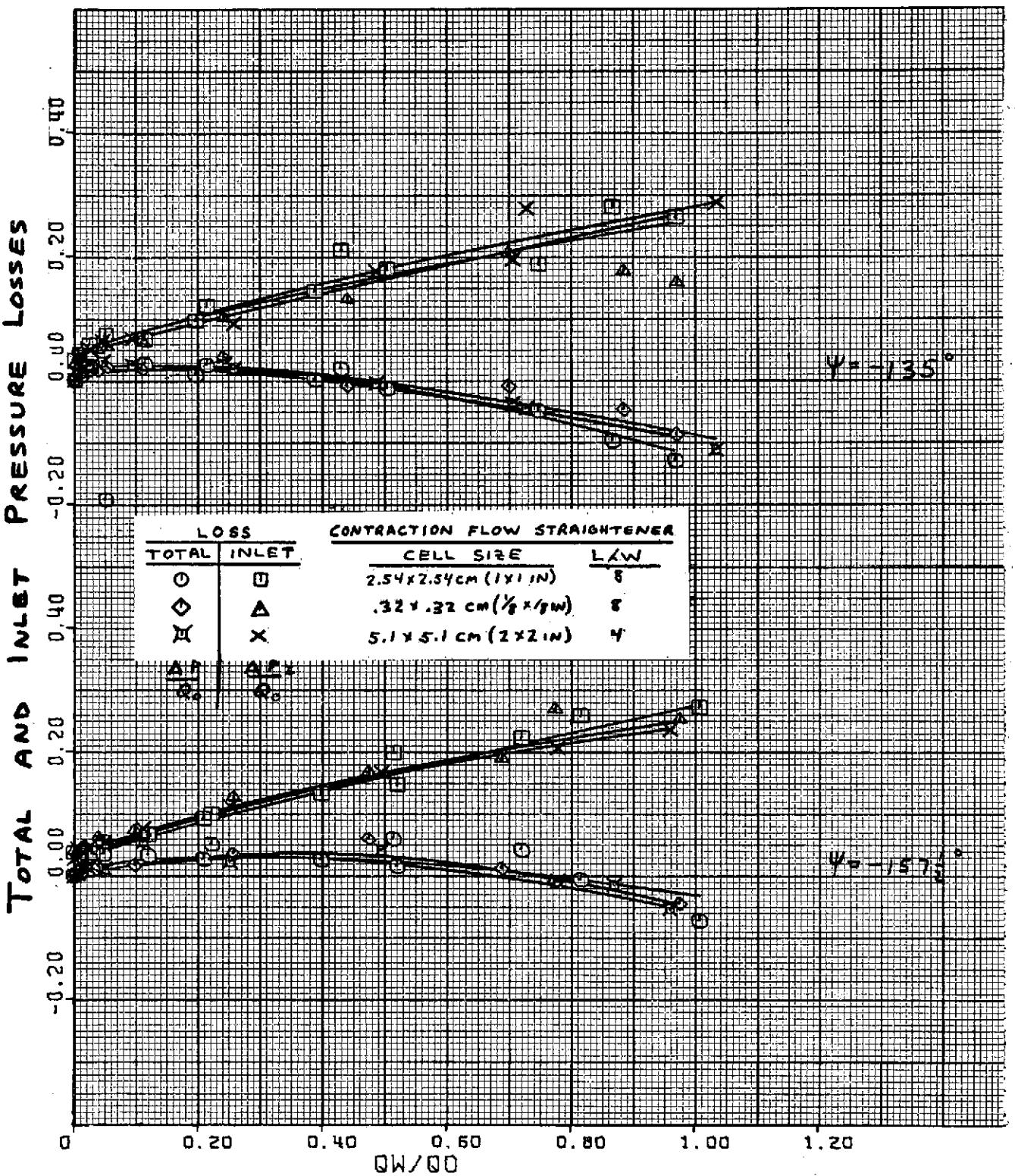

ψ = -135° and -157-1/2°.
(c) Pressure losses - continued.

Figure 14. - Continued.

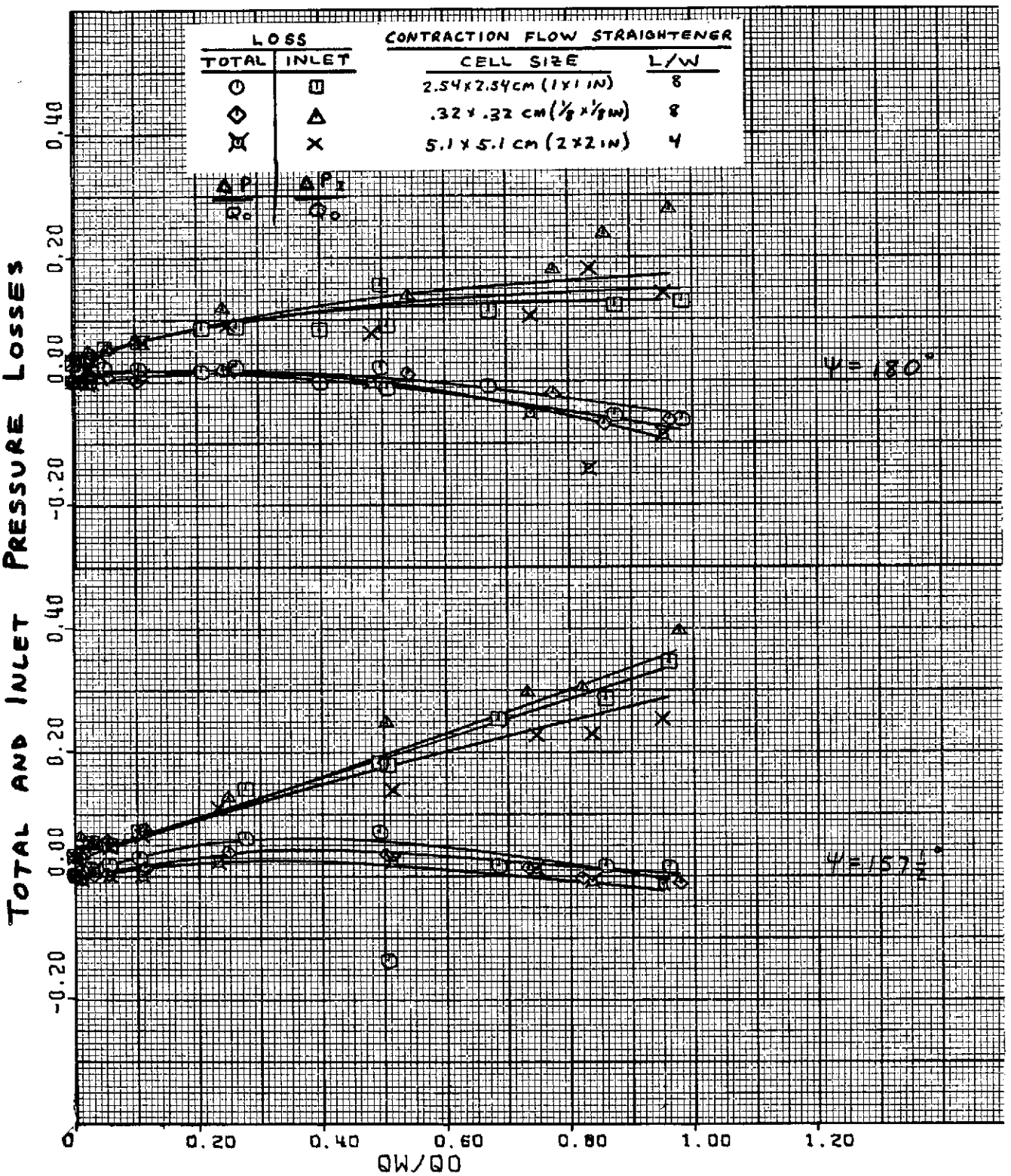

ψ = 180° and 157-1/2°.
(c) Pressure losses - concluded.

Figure 14. - Concluded.

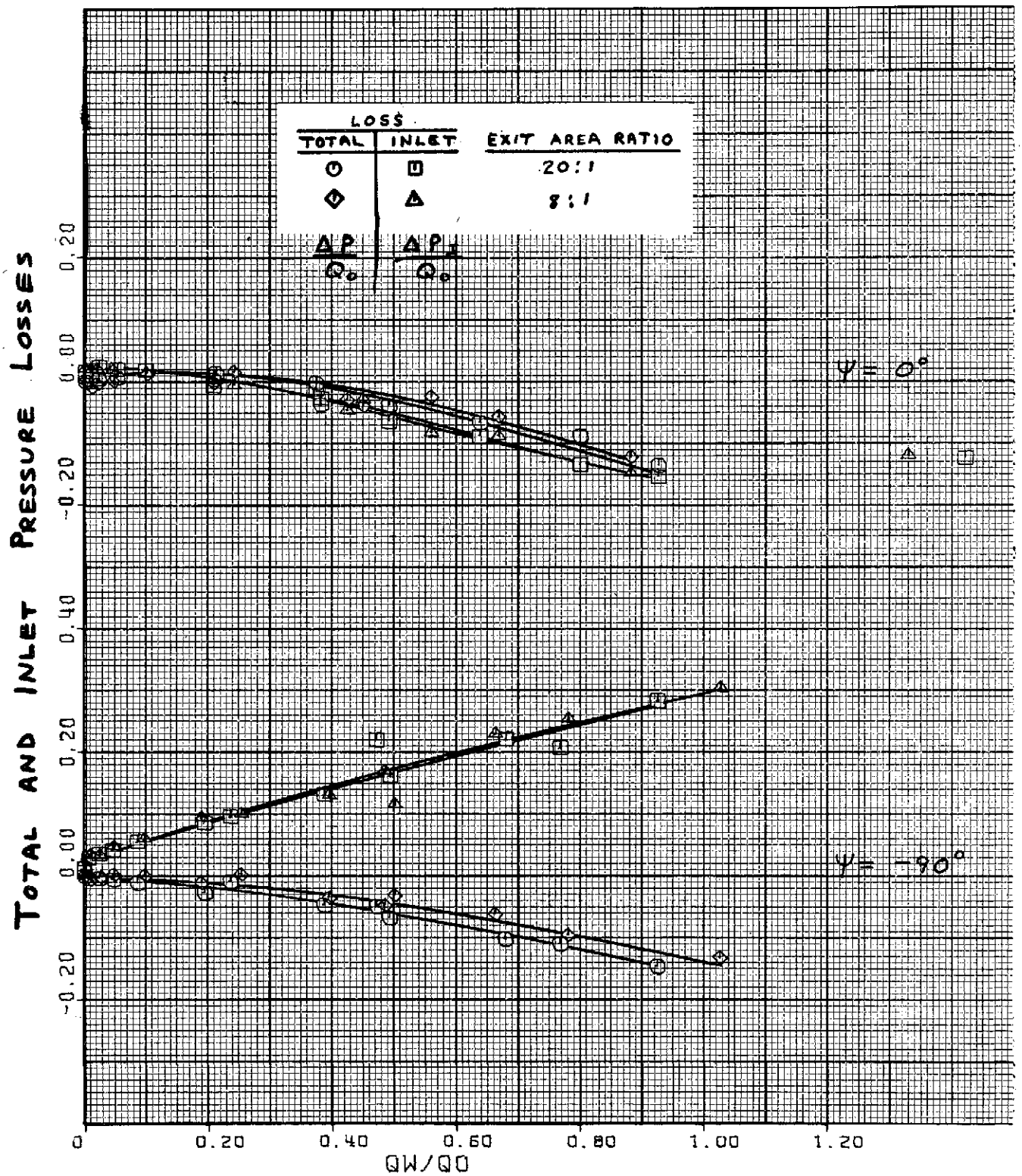

(a) $\psi = 0°$ and $-90°$.

Figure 15. - Effect of exit on pressure losses with 107×254 cm (42×100 in) inlet, roof posts in, peripheral flow straightener removed, 2.54×2.54 cm (1×1 in) contraction flow straightener.

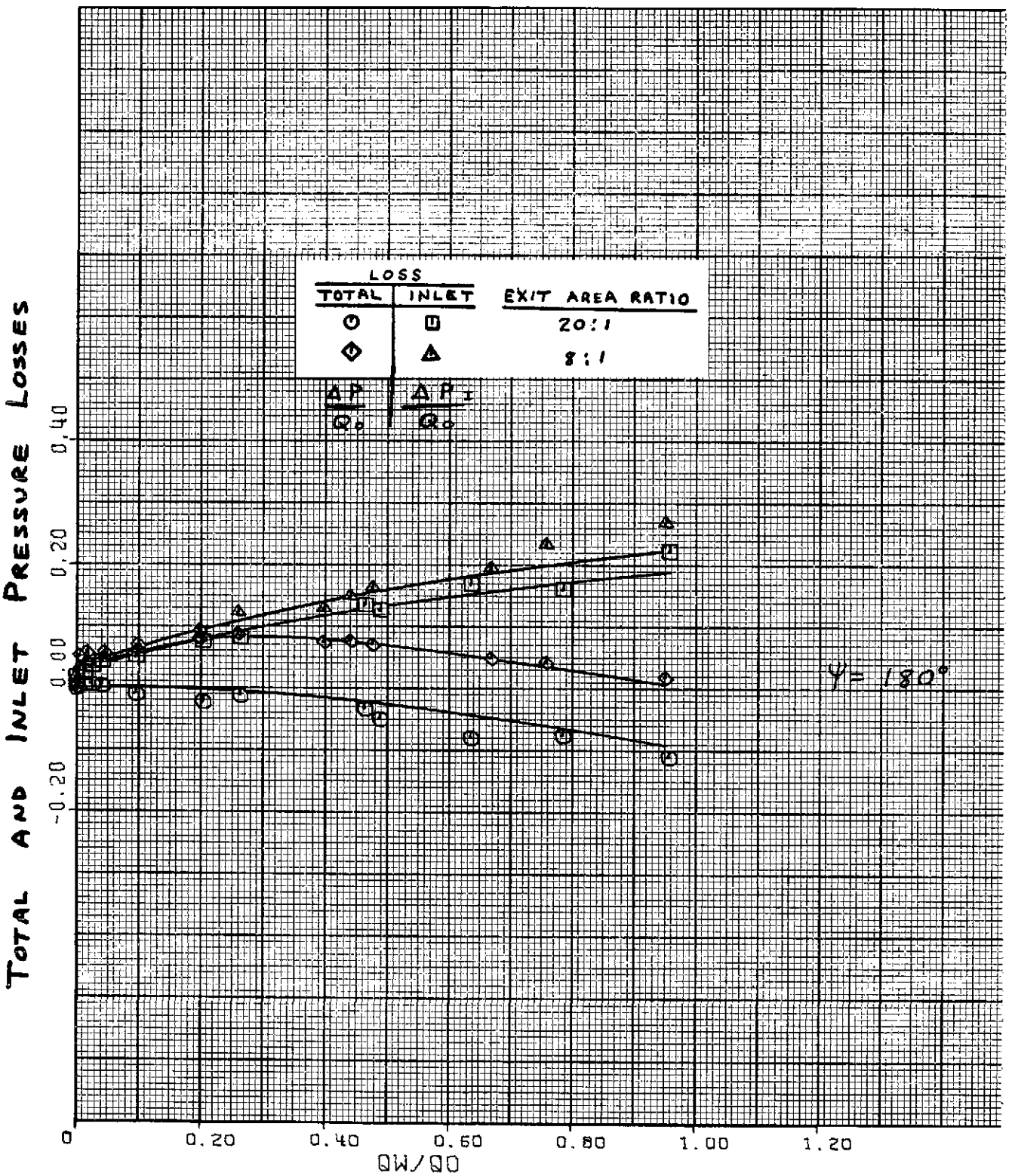

(b) $\psi = 180°$.

Figure 15. - Concluded.

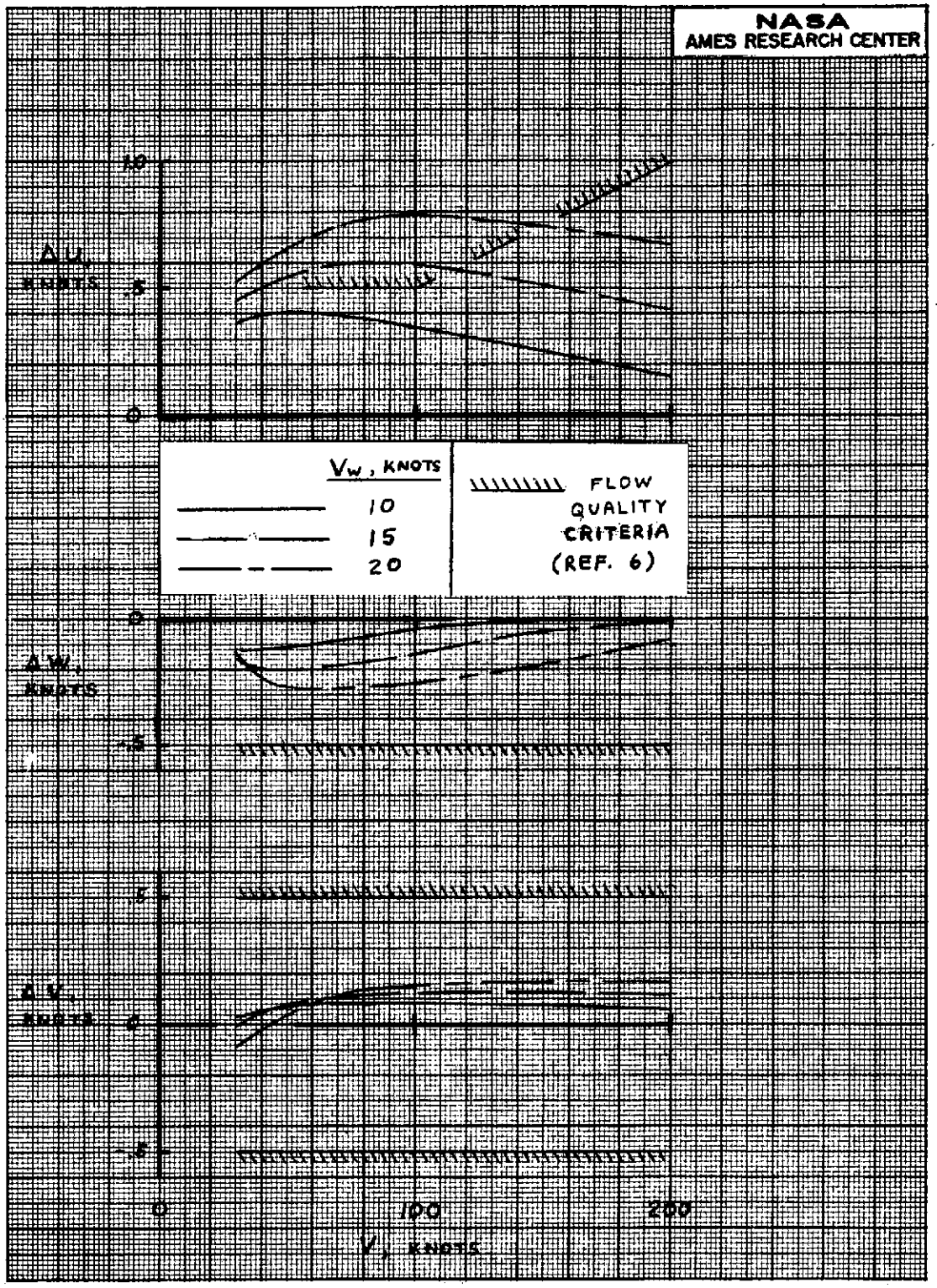

(a) Effect of wind magnitude at $\psi = 0°$.

Figure 16. - Flow quality evaluation for basic configuration: 58×203 cm (23×80 in) inlet, roof posts in, front-only peripheral flow straightener, 2.54×2.54 cm (1×1 in) contraction flow straightener, area ratio 20 exit.

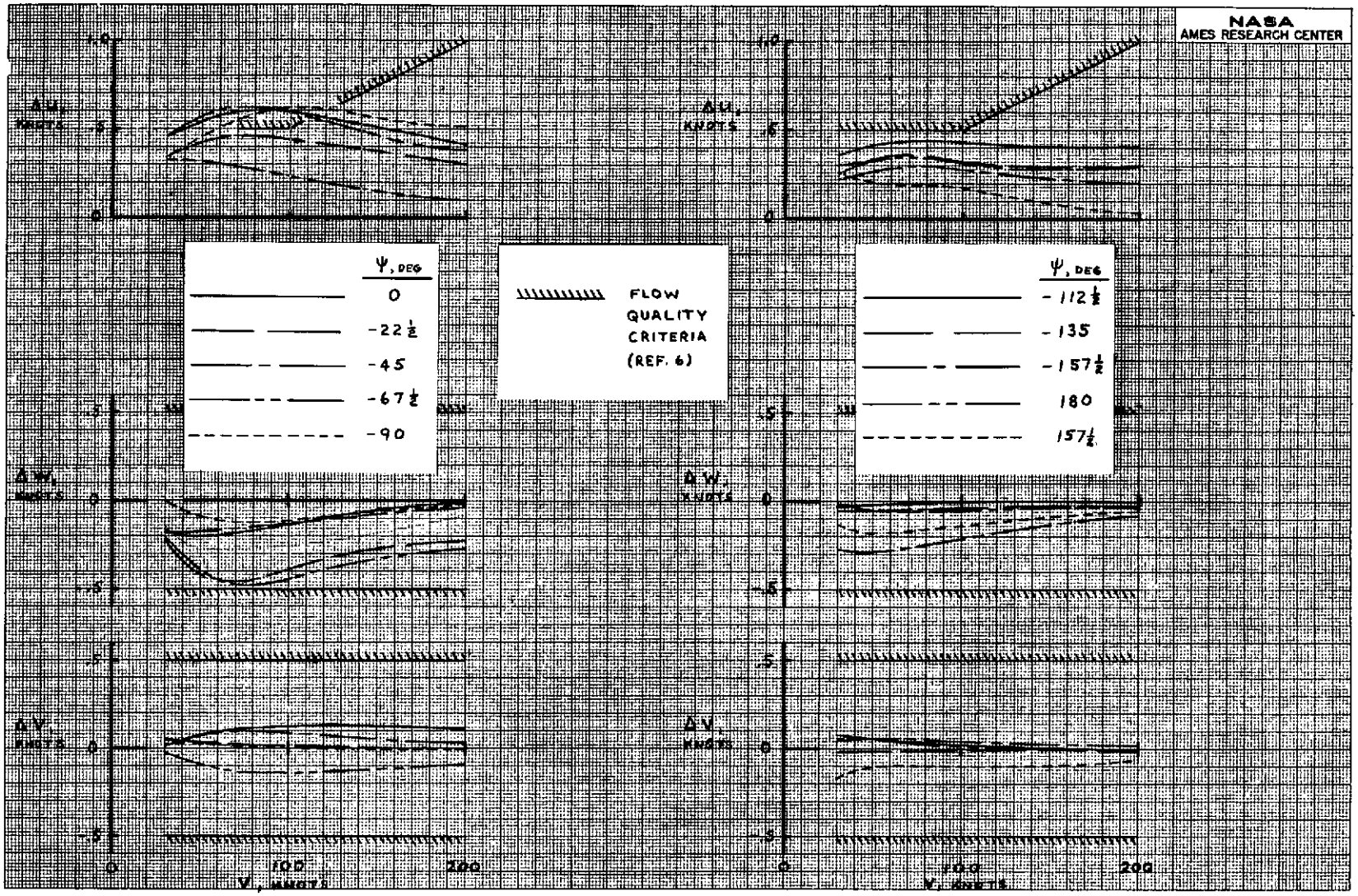

(b) Effect of wind direction at V_w = 15 knots.

Figure 16. - Concluded.